UNIVERSITY OF OKLAHOMA

GRADUATE COLLEGE

SYNTHESIS AND CHARACTERIZATION OF POLYNITRO-[2.2]PARACYCLOPHANES, A NOVEL XYLYLENE POLYMER, AND POLY(*p*-PHENYLENE SULFOXIDE)

A DISSERTATION

SUBMITTED TO THE GRADUATE FACULTY

in partial fulfillment of the requirement for the

degree of

Doctor of Philosophy

By

WARREN LEWIS DINGES

Norman, Oklahoma

1999

SYNTHESIS AND CHARACTERIZATION OF POLYNITRO-
[2.2]PARACYCLOPHANES, A NOVEL XYLYLENE POLYMER,
AND POLY(*p*-PHENYLENE SULFOXIDE)

A Dissertation

APPROVED FOR THE DEPARTMENT OF CHEMISTRY AND BIOCHEMISTRY

BY

ACKNOWLEDGMENTS

To characterize the last five to six years of my life as unusual, unplanned, and difficult would be an enormous understatement. Besides learning to hold on tight because it can be a rough ride, I've learned that much of the important, vital, and pithy experiences of life never find their way into an abstract, paper, or resume. They're most usually found and revealed over dinner, a drink, or a cup of coffee. So, it's those people with whom I have shared the good and the bad, the hilarious and the bitter experiences of the last few years that I simply want to say . . . Thanks.

It may sound really almost desperate, but my chemistry and academic pursuits have been one of the rare consistency of the past few years. Even if those Hofmann eliminations kept turning black and brown, the laws guiding them were fixed, and Avogadro wasn't changing his number to 7.02, at least not in our lab. So, I would most certainly like to thank Dr. Glatzhofer for holding down the chemistry constants as much as as possible, so I could finish what I came to Oklahoma to do. Few advisors have seen and dealt with the oddity and challenges of my stay at OU. Without his assistance, I would not be writing and defending this dissertation.

Much of this work and much of my understanding of chemistry and science comes from many other people, and I could not begin to rightfully claim this work and knowledge as solely my own. I can only hope that many of them may want to lay claim to it as a useful and solid contribution fitting what I have learned from them. So, I would like to thank my committee members, previous professors, and fellow group members.

Furthermore, I would also like to express my appreciation to the undergraduate researchers who worked on these projects. Adam Rush, Eric Uffman, and Yonathan Tilahun each contributed enormously to this work.

Beyond the lab and science, my closest friends and family have provided amazing support, encouragement, and even jabs as needed. To my mother, brother, and sister-in-law as well as my friends, Justan, Brian, Kortni, Jen, and the Yagmins, who have been around for years, I cannot begin to express my appreciation. You have listened long, laughed loudly, and made the last few years enjoyable.

My final acknowledgment has been left in this trailing place only because it is the one for which I most lack the words and methods to express my appreciation. Jason, whom I met almost five years to the week that I write this, has been my closest friend during these studies. At times, I fear that his role may best be characterized as collateral damage rather than shared life experiences. However, I think it most appropriate to simply say thanks for sharing an umbrella in the rain and storms. Hopefully, the next few years will have a bit sunnier weather.

TABLE OF CONTENTS

LIST OF TABLES

Table

LIST OF ILLUSTRATIONS

ABSTRACT

With the goal of better understanding previously documented, structurally related, exothermic decompositions of polynitro-paracyclophanes (polynitroPCP), two novel tetramethyl-tetranitro-[2.2]paracyclophanes and their related polymer were synthesized and characterized : 4,8,12,16-tetramethyl-5,7,13,15-tetranitro[2.2]paracyclophane (**45**) and 4,8,13,15-tetramethyl-5,7,12,16-tetranitro[2.2]paracyclophane (**46**), and poly(2,6-dimethyl-3,5-dinitro-*p*-xylylene) (**20**). These compounds and previously synthesized dinitro[2.2]PCP's were characterized by DSC thermal analysis techniques. Compounds **45**, **46**, and **20** decomposed exothermically at 314, 303, and 281 °C, respectively. The exothermic decompositions of the polynitroPCP's are not a product of the strain in the dimer [2.2]PCP members of this class, but rather a feature of the ethano bridge system. The elevation of the decomposition temperatures by 33 °C in the non-polymer polynitroPCP's is likely due to an attenuation of intermolecular nitro group interactions caused by intramolecular nitro group orientation restrictions. A smaller 10 °C decomposition temperature variation in the dinitro[2.2]PCP's follows a similar trend of likely nitro group orientation restrictions. The severely basic and nucleophilic conditions of the Hofmann elimination also proved incompatible to the synthesis of less methylated polynitroPCP's.

A novel polymer derived from these synthetic routes, poly(2,6-dimethyl-*p*-xylylene) (**21**), was synthesized and characterized. This amorphous, soluble polymer had the highest molecular weight of any literature reported xylylene polymer measured by

GPC (Mw = 150,500 and Mn = 60,510). The polymer **21** exhibited excellent thermal stability in helium and air. The onset of thermal decomposition in air (424 °C) was more than 100 °C higher than all non-fluorinated xylylene polymers. Excellent quality, free-standing, flexible films of **21** were cast from chloroform.

A less closely related polymer, poly(*p*-phenylene sulfoxide) (PPSX) (**18**) was synthesized by a novel homogenous oxidation of poly(*p*-phenylene sulfide) **17** with neat fuming nitric acid, fuming nitric acid in trifluoroacetic acid (TFA), and concentrated nitric acid in TFA. Several model compounds and modified reactions were studied which implicated a nitrogen oxide adduct as a major and required element in the selective oxidation to the polysulfoxide rather than the polysulfone. The intrinsic viscosity of the PPSX polymer was determined to be 0.274. PPSX was successfully fractionated yielding a high molecular weight polymer identified by GPC (Mw = 84,000 and Mn = 30,800). Multiple unitary and binary solvent systems were identified for PPSX, and clear, free-standing, flexible films were cast with plasticizer enhancement. Thermal analysis identified PPSX as an amorphous polymer with a decomposition temperature in air of 334 °C and in helium of 342 °C. The activation energies of the thermal decomposition of PPSX in air and helium were determined by the Friedman method to be 32 +/- 6 and 31 +/- 3 kcal/mol, respectively. PPSX successfully demonstrated the ability to chelate several metals in experiments intended to explore metal extraction applications.

Chapter One

Introduction

1.1 General Cyclophanes

Cyclophanes in their broadest sense are a widely diverse and extensively studied class of molecules. A cyclophane is most fundamentally defined as an aromatic hydrocarbon nucleus bridged by an aliphatic chain. The first synthesized cyclophane, [2.2]metacyclophane (**1**), was formed by Pellegrin in 1899 by a Wurtz coupling [1]. Several decades later Luttringhaus and others studied a class of cyclophanes which he referred to as *ansa* compounds: *ansa* is Latin for handle [2-4]. These *ansa* compounds (**2a** and **2b**) exhibited a unique form of optically active conformational isomerism referred to as atropisomerism. Atropisomers are stereoisomers resulting from restricted rotation about single bonds where the barrier to rotation is large enough to permit isolation of the isomers [5]. Depending on the chain (handle) length, the aromatic ring can rotate through the aliphatic chain racemizing the compound. When the chain is sufficiently short, there is

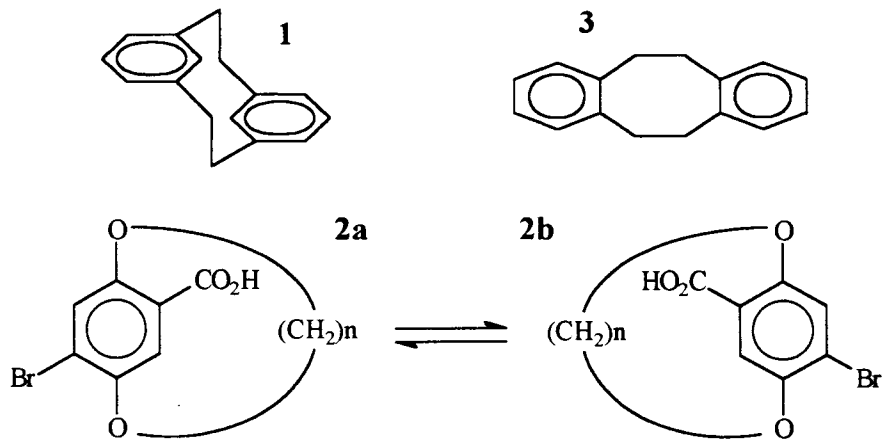

Figure 1. Early Cyclophanes

enough steric hindrance to allow for isolation of the separate enantiomers (**2a** and **2b,** n=10) at room temperature.

During the same time [2.2]orthocyclophane (**3**) was first synthesized, also by Wurtz coupling [6]. The final member of the doubly ethano-bridged cyclophanes, [2.2]paracyclophane, was first isolated in 1949 by Brown and Farthing by extraction of products from the pyrolysis of p-xylene [7]. Shortly thereafter Cram, a major contributor to the cyclophane field, published the first direct synthesis of [2.2]paracyclophane (**4**) [8] which was accomplished, again, using a Wurtz coupling, Figure 2.

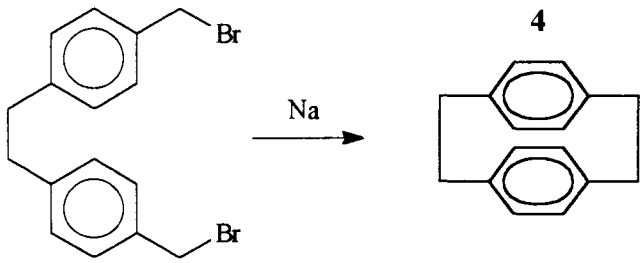

Figure 2 First Synthesis of [2.2]Paracyclophane

From those initial efforts the field of cyclophane chemistry has grown enormously. A variety of simple cyclophanes, [m.n]paracyclophanes, with varying bridge lengths were then synthesized [8]. Even the synthesis of the shortest bridged paracyclophane, [1.1]paracyclophane (**5**), was just recently published [9, 10]. This compound is unstable above -20 °C in solution. Multi-bridged and multi-layered cyclophanes as well as heterophanes further expanded the field of research. Cyclophane research now encompasses large macrocyclic host-guest compounds, metallophanes for studying conduction in organic materials, porphyrinophanes as models for biological enzymes,

polymeric cyclophanes, and molecular recognition based on crownophanes. Extensive reviews and monographs are available on these topics and cyclophanes in general [11-14].

1.2 [2.2]Paracyclophanes

As this research principally involved [2.2]paracyclophanes, this discussion will now be limited to that fundamental structure and the functionalized derivatives of [2.2]paracyclophanes (PCP's). The nomenclature used to identify cyclophanes has been adapted and modified through the years and now stands as a separate non-IUPAC system. The reviews and monographs as well as the included primary references listed above give much more detailed information regarding the naming of complex cyclophanes with heteroatoms, multiple bridges, and multiple decks. In the naming of [2.2]paracyclophane, the numbers within the square brackets define the length and number of bridges which are assumed to be saturated hydrocarbons. Hence, for [2.2]paracyclophane two ethano bridges are present. The "*para*" nomenclature, also non-IUPAC, simply specifies the attachment point of the bridges to the aromatic nucleus. The "cyclo" is meant to imply a benzene derivative with other arenes being explicitly defined such as naphthalenophane and thiophenophane as shown in Figure 3. Symmetry and equivalence of any aromatic rings is assumed unless specified; again, more complex rules apply where non-equivalence must be addressed.

The [2.2]paracyclophane system has also been subject to more reduced nomenclature rules because of its relative pervasiveness. For this dissertation, I will use the most common numbering system introduced originally by Cram [8, 15] with

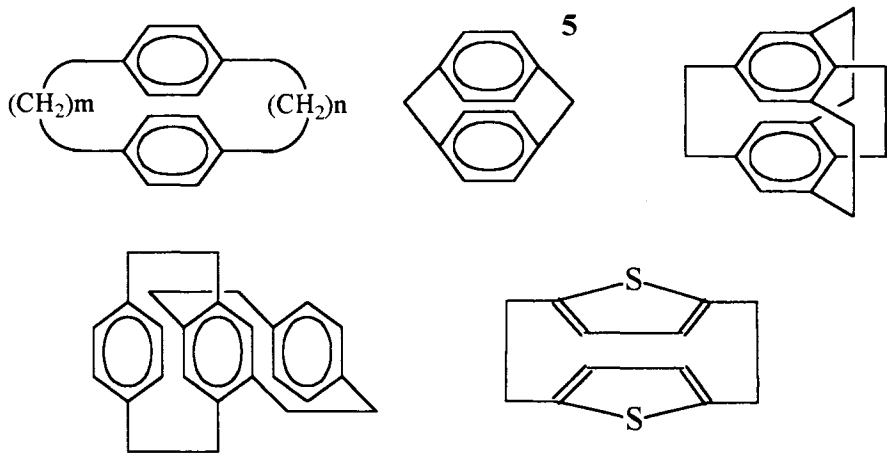

Figure 3 Varied Cyclophanes

modifications by Schubert [16]. In this system the carbons are numbered first across the longest bridge, then around the first ring, then across the second bridge and finally around the second ring as shown in Figure 4 for 4-nitro[2.2]paracyclophane (**6**). In cases of equal bridge length, numbering is started in order to give the lowest total substituent number.

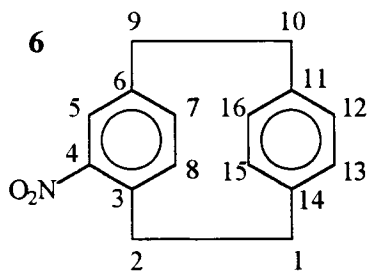

Figure 4 4-Nitro[2.2]PCP

The presence of multiple substituents does however, complicate the issue particularly in cases where restricted rotation creates atropisomers that are diastereomers, as is the situation with PCP. Ambiguity results from the two possible directions of numbering at the *ipso*-carbon junctures on the second (and subsequent) prochiral aromatic ring(s).

Cram's system dictates that, like the IUPAC system, numbering will proceed in the direction that gives the lowest total substituent numbering with all types of substituents being treated equally. Other systems arbitrarily define the direction of numbering to be spatially equal: clockwise for both (or all) rings. These other approaches become extremely ambiguous with higher cyclophanes. The four dinitro substituted PCP's are shown in Figure 5. Substitution on the ethano bridges is not addressed because this research did not involve such functionalization. The compounds **7** and **9** are both numbered as 4,13-dinitro[2.2]paracyclophanes, just as compounds **8** and **10** are both number as 4,12-dinitro[2.2]paracyclophanes. The rather extreme barrier to rotation that

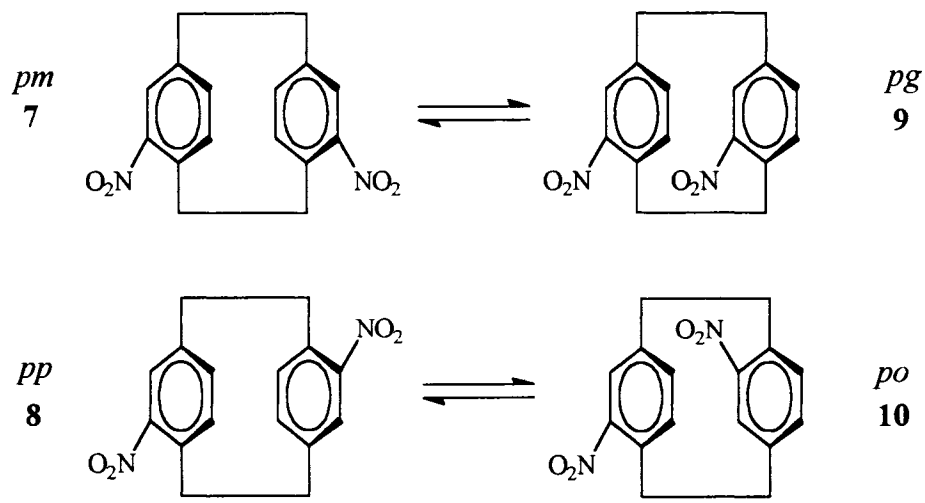

Figure 5 Dinitro[2.2]paracyclophanes

would interconvert these diastereomers allows for the separation and isolation of the atropisomers as compounds that behave different chemically. Thus, an additional system is needed to identify the atropisomers or rotational isomers. Cram used the terms *pseudo-geminal* (*pg*), *pseudo-ortho* (*po*), *pseudo-meta* (*pm*), and *pseudo-para* (*pp*), as attached to

the structures in Figure 5. The "*pseudo-*" prefix identifies the relative position of a substituent on the second PCP ring.

The final additional rule of nomenclature involves the differentiation of higher substituted atropisomers of PCP's [17-19]. In Figure 6, the two diastereomers of 4,7-dimethoxy-12,15-dinitro[2.2]paracyclophane (**11** and **12**) are shown. In these cases, the prefixes *anti* and *syn* are used to differentiate the atropisomers.

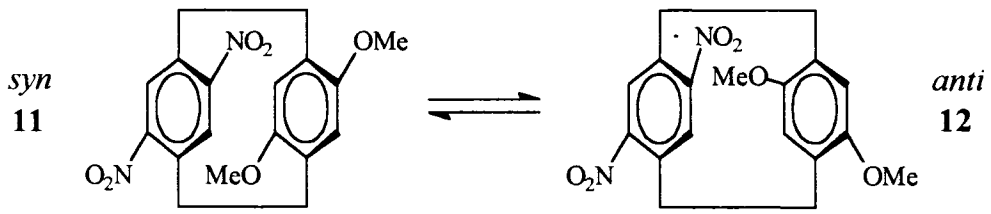

Figure 6 Dimethoxy-dinitro[2.2]PCP's

Currently, there is no adopted standard to name more uniquely substituted PCP such as the two atropisomers of 7-amino-4,12-dinitro[2.2]paracyclophane (**13** and **14**) in Figure 7. Most synthetic pathways to polysubstituted PCP's involve symmetric routes which either dimerize a xylylene or react equivalently on both arene halves producing symmetric PCP's. Hence, there has been a limited need for such expanded rules of nomenclature, because the products can be sufficiently identified with extant rules. In this work, disubstituted PCP's will be identified with the *pseudo* prefixes and tetra/octa substituted PCP's will be identified by the *anti/syn* prefixes where appropriate. In the few cases where ambiguous nomenclature may exist, the compounds will be identified graphically and referred to by number as was done above for compounds **13** and **14**.

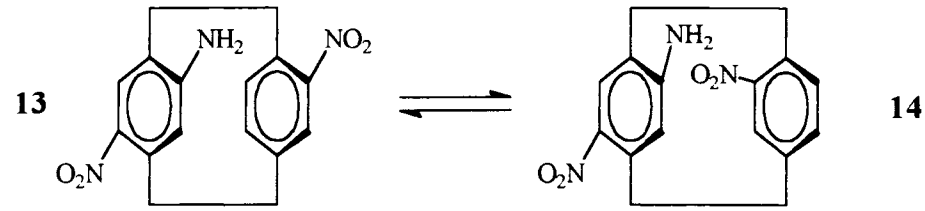

Figure 7 Amino-dinitro[2.2]PCP

As a final point on these nomenclature difficulties, they are a direct result of the prochiral nature of the substituted aromatic rings. Each of the substituted PCP aromatic halves represents a prochiral plane of symmetry perturbed asymmetrically by the other ring. The result of this mutual perturbation is diastereoisomerism. In cases where there is an additional vertical plane of symmetry through one of the rings (or handle) as is the case in mono-substituted PCP's like 4-nitroPCP (**6**) and the earlier *ansa* compounds (**2a** and **2b**), enantiomers result. These atropisomers, whether diastereomers or enantiomers, are only distinguishable to the extent that the rotational barrier to interconversion remains intact. Without the rotational barrier provided by the unique structural features of PCP, the many atropisomer pairs shown above would simply interconvert making the more difficult nomenclature issues moot.

The unique structural features of [2.2]paracyclophane are just one of the reasons that they are studied so extensively. There are three major fields of research directed towards the PCP and related systems. The first involves the study of the structural features and the stereochemical consequences of the hindered rotation. PCP provides a fairly easily accessible and chemically robust scaffold which can assist in a variety of stereoselective reactions [20-23]. Other work here in Professor Glatzhofer's laboratory

utilizes the PCP scaffold to direct stereoselective cyclopropanation reactions using a copper catalyst [24, 25] as in Figure 8.

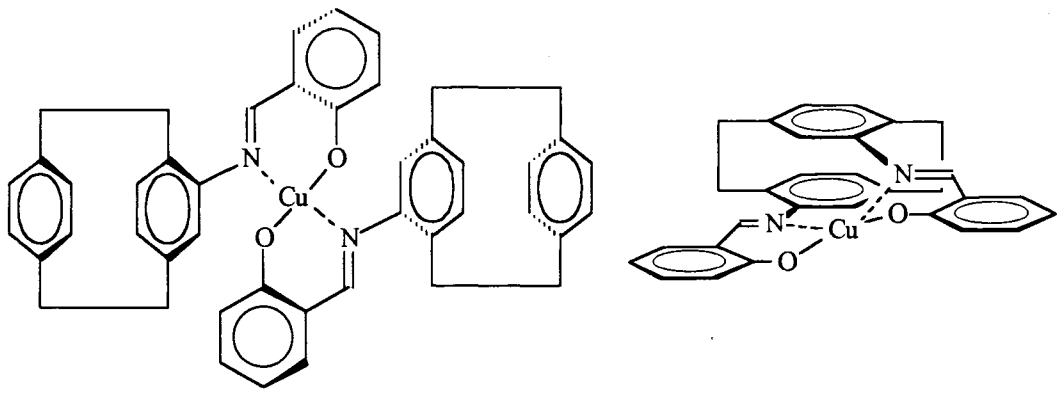

Figure 8 Metal Cyclophane Catalysts

The second major area of research in PCP fields addresses the electronic interactions of the aromatic rings which have been squeezed together. The normal van der Waals distance between two aromatic systems is approximately 3.4 Å [14]. This distance is reduced to between 2.75 and 3.09 Å for the aromatic carbons in PCP, see Figure 9 [14].

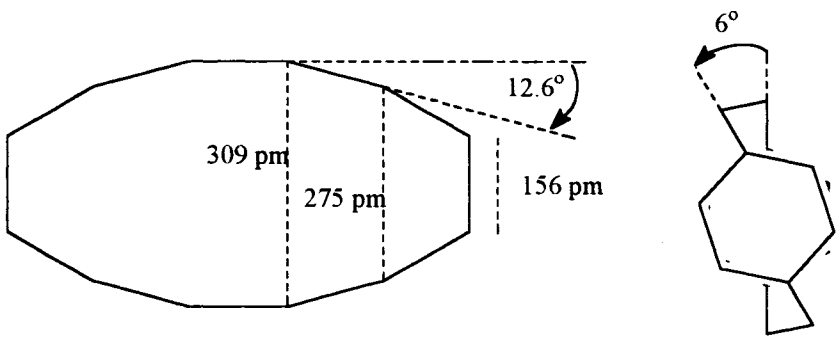

Figure 9 [2.2]Paracyclophane Distortion

The proximate result of this additional π-π interaction is a mixing of the orbitals of the two aromatic systems. These electronic effects can be seen in the electronic spectra, transannular substitution patterns during chemical reactions, and intramolecular charge-

transfer complexes of many PCP derivatives [11-14]. A specific example of the odd transannular substitution patterns is provided in Figure 10. In this case, electrophilic aromatic substitution is directed to the site across from the most basic π site in the already substituted ring almost to the complete exclusion of other positions [26].

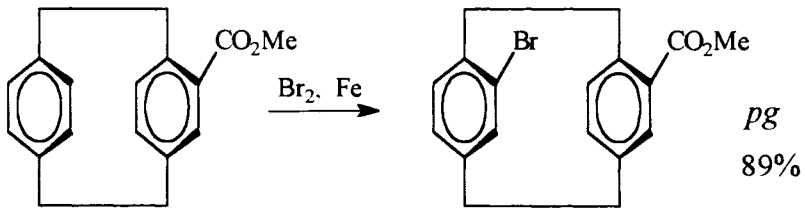

Figure 10 Bromination of a [2.2]PCP

The final major reason to study PCP's involves the rather extreme strain and distortion of the aromatic systems. As illustrated in Figure 9, the aromatic carbons of PCP do not lie in a plane as they do in a typical benzene ring. They are, in fact, pulled into a boat-like conformation with 12.6 degrees of distortion from planarity [14]. This systemic deformation produces a strain energy of approximately 32 kcal/mol, placing PCP into a class of highly strained molecules [14]. Cyclopropane has only 27 kcal/mol of strain energy. This potentially useful strain energy reserve as well the inherent structural features of the PCP system was the primary focus and impetus for my initial research into PCP's and polynitrated PCP's as energetic materials.

1.3 Energetic Materials

The term energetic materials is meant to include any substances that exhibit a significant energetic thermal decomposition typically producing large amounts of gaseous

products. This term is inclusive of primary explosives which initiate explosive chains, secondary explosives which are the working end of explosive chains, propellants which "burn" in rocket motors or guns, and blasting agents which are insensitive secondary explosives. The term energetic material applies to both the usually employed formulations and mixtures as well as the pure "explosive" compounds. Energetic materials are typically characterized by the usual physical parameters determined for most compounds such as melting point, heat of formation/combustion, and density. In addition, many other energetic material specific properties are assessed including heat of detonation, detonation velocity, detonation pressure, detonation temperature, temperature of decomposition, and sensitivity to shock, impact, fragment impact, friction, static discharge and heat. The working capacity of the energetic materials, generically referred to as brisance, is also determined by a variety of empirical methods. The foundations of explosive research has been laid in a generally more engineering rather than chemistry environment. This has necessitated the development and implementation of a large number of empirical test methods for the assessment of the specific properties of energetic materials. The more recent challenge to chemists and explosive engineers has been to bridge this gap between the ultimate output properties and the laboratory based rational design of explosive materials. Some general references on energetic materials and explosive engineering are included [27-31].

Explosive materials are broadly divided into inorganic and organic compounds. Inorganic explosives include ammonium nitrate, mercury fulminate, and sodium azide. The organic explosives are further subdivided into aliphatic and aromatic compounds. The

aliphatic explosives include both nitrate esters and nitramine based explosives such as nitroglycerin (NG), pentaerythritol tetranitrate (PETN), nitrocellulose, cyclo-1,3,5-trimethylene-2,4,6-trinitramine (RDX), and cyclo-1,3,5,7-tetramethylene-2,4,6,8-tetranitramine (HMX). The aromatic explosives are almost all nitro substituted benzene derivatives including 2,4,6-trinitrotoluene (TNT), picric acid, 1,3,5-triamino-2,4,6-trinitrobenzene (TATB). Some of these structures are shown in Figure 11.

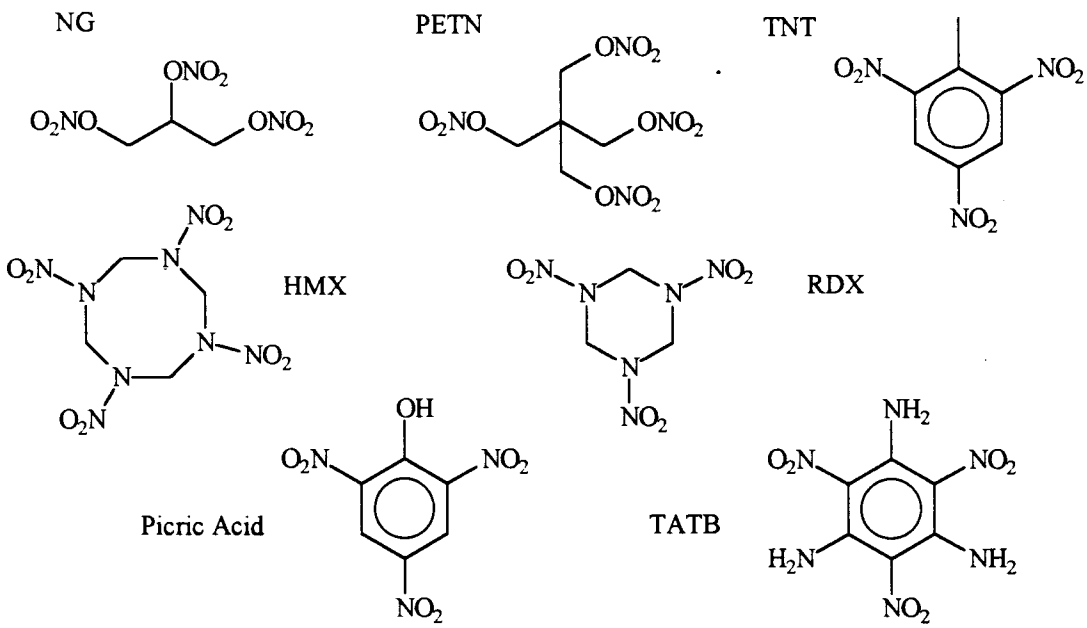

Figure 11 Common Explosives

In the process of synthesizing new explosives there are four main design parameters that provide a prediction of the output properties: oxygen balance, density, strain energy, and nitro bond length and orientation ($X\text{-}NO_2$). The importance of oxygen balance in explosives has its roots in the fundamental gaseous products of combustion or detonation. A general formula for an organic explosive can be written as $C_cH_hN_nO_o$.

Upon detonation or combustion, the explosive forms products according to some general rules:

1) All nitrogen forms N_2
2) All hydrogen is burned to H_2O
3) Any remaining oxygen burns carbon to CO
4) Any remaining oxygen burns CO to CO_2
5) Any remaining oxygen forms O_2
6) Nitrogen oxides are formed in trace quantities

The energy production and ability to do work of an explosive is inherently correlated to the production of these stable gaseous products. Oxygen balance serves as a measure of the balance between the fuel (hydrocarbons) and oxidizer (oxygen) in an explosive. Nitrogen does not figure into oxygen balance (OB) because it does not consume oxygen in significant quantities. OB and molecular weight (MW) is calculated as below in Equations 1 and 2 [28].

Explosive: $C_cH_hN_nO_o$

$$MW = 12.01c + 1.008h + 14.008n + 16o \quad (1)$$

$$OB\ (\%) = 1600 / MW\ [o - 2c - h/2] \quad (2)$$

OB is usually expressed as a percentage. Nitroglycerin, $C_3H_5N_3O_9$, has an OB of 3.5 % and is oxygen rich or slightly overoxidized. RDX, $C_3H_6N_6O_6$, has an OB of -21.6 % and is oxygen poor or moderately underoxidized. TNT, $C_7H_5N_3O_6$, has an OB of -74.0 % and is very underoxidized. TNT, a rather common explosive, even lacks enough oxygen to combust the carbon to carbon monoxide. An OB close to 0 % produces the highest energy and work, but sensitivity to impact also increases with increasing oxygen balance

[32]. An "ideal" explosive, meaning secondary explosive, propellant, or blasting agent, optimizes energetic yield by approaching an OB of 0 % without becoming "too" sensitive. Primary explosives are by their inherent nature designed to be sensitive so that they can initiate an explosive chain. They too, though, should have specific sensitivity to one source impetus such as percussion, heat (hot wire), friction, or spark, and remain relatively insensitive to others. It should be noted that the correlation of oxygen balance to sensitivity is a product of the molecular structure, not an intrinsic feature of oxygen content. There are inorganic explosives that have a high OB without being sensitive. Ammonium nitrate has an OB of 20 % and is extremely difficult to initiate.

Density (ρ) also has a very important role in the behavior of energetic materials. The shockwave pressure (called C-J pressure, P_{cj}) behind the detonation front is proportional to the density squared, as in Equation 3. The detonation velocity (D) is also directly proportional to density, as in Equation 4 [33].

$$P_{cj}\ (\text{kbar}) = 15.58\ N\ M^{0.5}\ Q^{0.5}\ \rho^2 \qquad (3)$$

$$D\ (\text{km/s}) = 1.01\ N^{0.5}\ M^{0.25}\ Q^{0.25}\ (1.00 + 1.30\ \rho) \qquad (4)$$

ρ - density (g/cm^3)
N - moles gaseous products per gram
M - average molecular weight of gaseous products (g/mol)
Q - heat of detonation (cal/g)

Many other properties, such as specific impulse and heat of detonation, are calculated with an inverse dependence on weight, further increasing the importance of density. Most output properties of energy or work depend on density to the second to fourth power. Some of the new designed explosives have been specifically synthesized to have an

increased density by building a symmetric, compact hydrocarbon framework. Figure 12 shows two designed explosives with high densities, 1,3,5,7-tetranitrocubane [34] and 1,3,5,7-tetranitroadamantane [35]. The polynitrated cubanes have a progressively

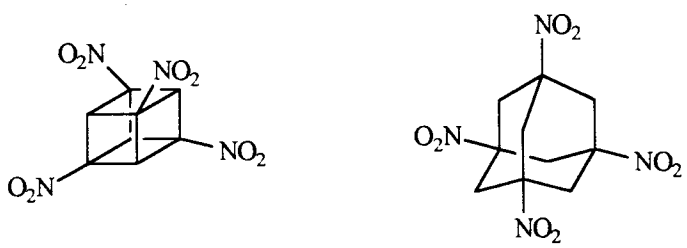

Figure 12 High Density Explosives

increasing density (g/cm^3): di-(1.66), tri-(1.74), tetra-(1.81), penta-(1.96), hexa-(1.68), nitrocubanes (Olah and Squire, 1991; Eaton et al, 1996) . The apparent anomaly in the density of 1,2,3,4,5,7-hexanitrocubane is caused by nitro group asymmetry and packing in the solid phase. The theoretical density of some organic explosives yet to be synthesized actually exceeds 2.0: hexanitrohexa-aza-adamantane 2.0-2.2 g/cm^3, octanitrocubane 2.0-2.1 g/cm^3, in Figure 13. For comparison Table 1 shows some densities, oxygen balances, detonation velocities, and heats of detonation for some common explosives [27, 28, 30, 31].

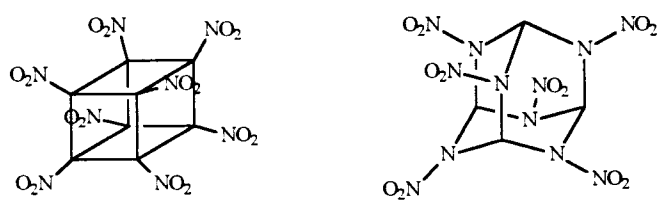

Figure 13 Theoretical High Density Explosives

Table 1. Common Explosive Properties

Explosive	Density g/cm^3	Oxygen Balance %	Det. Velocity* km/s	Heat of Det.** kcal/g
TATB	1.93	-55.9	7.35	2.83
HMX	1.90	-21.6	9.10	1.62
RDX	1.82	-21.6	8.75	1.62
PETN	1.76	-10.1	8.40	1.65
TNT	1.65	-74.0	6.90	1.41
NG	1.59	3.5	7.60	1.59

* Detonation Velocity at listed density

** Heat of Detonation calculated to the formation of liquid, not gaseous water

As briefly discussed earlier, molecular strain energy can act as potential energy reserve for energetic materials that is released upon detonation/combustion. However, there are no commercial explosives with a high degree of strain energy. Currently, the polynitrocubanes are the leading example of designed high strain energetic materials. The cubane nucleus has 157 kcal/mol strain energy that contributes directly to the heat of combustion and detonation in the polynitrated systems [36]. To the extent that the explosives remain kinetically stable, strain energy represents a "free" method of increasing the yields of energetic materials.

Nitro group bond length and orientation can also play a critical role in an explosive's output properties. The $X\text{-}NO_2$ bond is typically the weakest bond in an energetic material and its homolysis usually plays a major role in the decomposition pathways and initiation of the explosive [32]. This is particularly the case for nitroaliphatic (RNO_2), nitramine (R_2NNO_2), and nitrate esters ($RONO_2$) explosives, whose

homolytic bond dissociation energies (BDE, kcal/mol) are 60, 50, and 40, respectively [32]. Nitroaromatic compounds have BDE's of about 71 kcal/mol, which are only altered 1-4 kcal/mol by *ortho* methyl, additional nitro, and additional halogen-chalcogen substitution on the aromatic system [32]. This inherent bond stabilization of nitroaromatic compounds can provide a designed advantage by limiting lower energy decomposition pathways. There are other decomposition pathways that become more involved and even predominate in nitroaromatic decompositions. The nitro group can isomerize into a nitrite ester, anthranil compounds can form through reaction with *ortho* methyl groups, and benzofurazans can form through reaction with *ortho* amino groups, as shown in Figure 14.

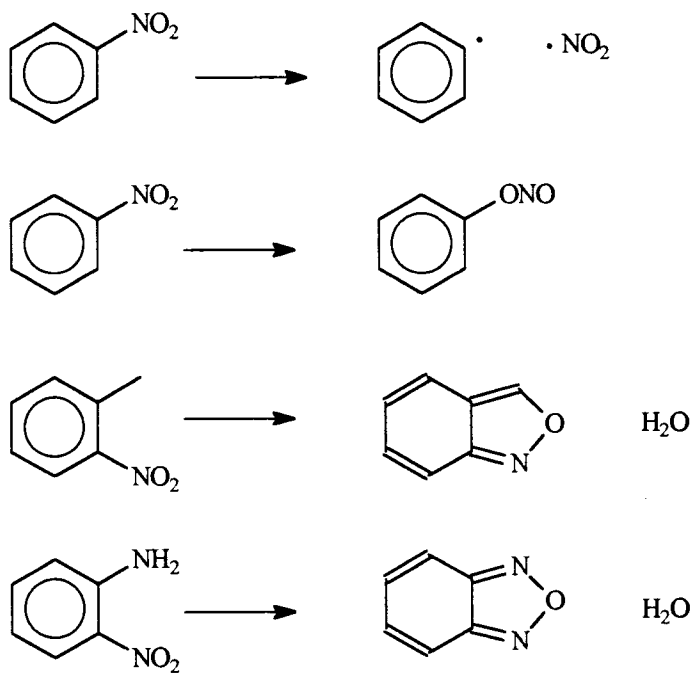

Figure 14 Nitroaromatic Decomposition Mechanisms

Each of these products then have a variety of decomposition pathways. The last two pathways in Figure 14 involving *ortho* substituents definitely predominate for most nitroaromatic explosives. They also contribute significantly to thermal instability and handling sensitization. These *ortho* substituent oxidation pathways all involve the formation of planar polycyclic aromatic compounds. An orientational or steric blocking of these pathways may provide a significant degree of stabilization to nitroaromatic explosives. A final point on the molecular design of explosives involves the packing of the compounds in the solid phase; something which is not easily predicted. The two polynitropolycyclic cage compounds in Figure 15 have almost identical densities [33]. Some general rules for predicting packing in the solid phase do appear to exist; particularly compact and symmetrical molecules have greater densities.

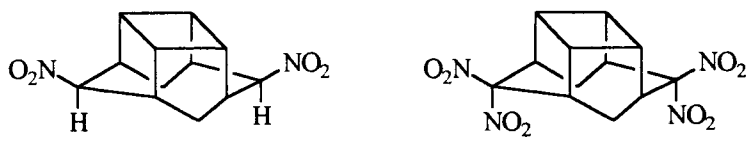

Density 1.75 g/cm^3 Density 1.76 g/cm^3

Figure 15 Polynitropolycyclic Cage Compounds

1.4 Polynitro[2.2]paracyclophanes

It may seem wholly obvious following the prior introduction, but the [2.2]paracyclophane nucleus is an ideal framework for the design of new energetic materials. Substitution of nitro groups on the aromatic sites forms nitroaromatic compounds which are generally the most kinetically stable explosives. Conceptually, the free rotation of the nitro groups could even be restricted through steric interactions that

would limit some of the lower energy decomposition pathways usually available to nitroaromatics. The PCP nucleus also contains an extra 32 kcal/mol of strain energy, yet it still retains relative stability. The compact and potentially symmetric nature of the PCP structure also has added design benefits related to the impact on density.

The first energetic decomposition of a polynitroPCP was documented by Dr. Mark Morvant and Scott Reid while working under the direction of Prof.'s Daniel Glatzhofer and Robert White [25]. The tetranitro PCP, *anti*-5,8,13,16-tetramethyl-4,7,12,15-tetranitro[2.2]paracyclophane (**15**) exhibited a significant energetic thermal decomposition at 308 °C. The tetrameric equivalent of **15** also exhibited a similar decomposition, but at 346 °C. The dimer and tetramer, *anti*-5,8,13,16,21,24,29,32-octamethyl-4,7,12,15,20,23,28,31-octanitro [2.2.2.2]paracyclophane (**16**) are shown in Figure 16. This unexpected energetic decomposition of **15** and **16** is particularly remarkable considering its extremely poor OB of -151.2 % for both. The compounds **15** and **16** even lack enough oxygen to stoichiometrically burn the hydrogen to water leaving a wholly unoxidized carbon residue after decomposition.

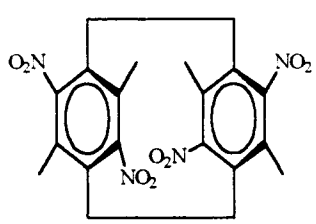

15

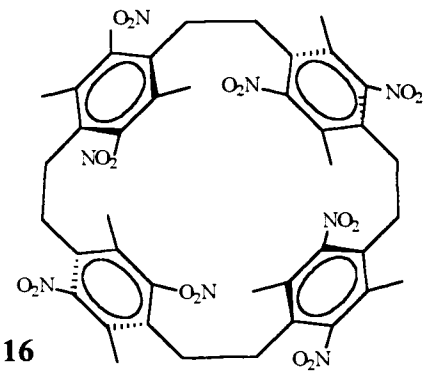

16

Figure 16 Compounds **15** and **16**

Prior to the synthesis and characterization of these compounds no other polynitroPCP's had exhibited such decomposition effects and only the dinitroPCP's **7**,**8**,**9** and **10** were known and isolated. The first two of the dinitroPCP's were synthesized and isolated by Cram and Allinger [37]. The final two, after correction on specific diastereomer identity, were isolated and characterized in 1969 [26]. Dr. Morvant provided a higher yield and more convenient synthetic and isolation procedure for the dinitroPCP's [25]. There are several mono- and dinitroPCP's known with many other substituents [17, 26, 37-39]. These initial synthetic successes along with the unexpected energetic decomposition provided the motivation to pursue the further synthesis and characterization of other polynitroPCP's. A better understanding of the reasons for these energetic decompositions and the application of these apparently novel mechanisms to the future design of energetic materials was sought. This goal was the initial and primary focus of my early research.

1.5 Energetic Polymers

Energetic polymers represent a large component of the explosives market. However, this representation is almost exclusively monopolized by the biopolymer derived nitrocellulose. The only other commercialized energetic polymers are nitrostarch, nitropoly(styrene) and poly(vinyl nitrate) (PVN) [40]. Polymers in general and their energetic counterparts are used as plasticizers and binders in energetic formulations. These formulations include primarily propellants of all types and putty or plastic explosives. Propellants whether in the form of small grains or poured and cast rocket motors have specifically designed shapes to optimize burn parameters. These polymer

explosive formulations are extruded and poured typically after being heated above a melting point. After cooling the polymer bound explosives should retain their shape over time without cracking. Such unwanted cracks in motors can produce an uncontrolled burn and catastrophic system failure. The break-down of a gelatinized dynamite made from nitrocellulose and nitroglycerin (NG) can result in sweating of the much more unstable NG. In addition to these more extreme difficulties with polymers in explosives, there is a general decreased efficiency when non-energetic polymers must be used in the formulations. The inherent fuel-rich nature of organic polymers must be balanced by additional oxidizer content. The non-energetic content of putty, plastic, or rubberized explosives typically is from 4-10 % [27, 28]. A wide variety of polymers are used in such applications including, poly(urethanes) (Estan 5702-F1), poly(styrene), fluoropolymers (Kel-F and Viton A), and poly(isobutylene). A variety of small molecules are also commonly added as lubricants and plasticizers.

An ideal energetic polymer such as nitrocellulose should be able to act as both a binder or elastomer and an energetic material, again without contributing detrimentally to the desired output energetic properties. Most previously synthesized energetic polymers exhibited unsuitable energetic properties. Some specific examples include: poly(nitroethylene) decomposes above 75 °C, poly(nitroindene) was too impact sensitive, and PVN (atactic) has poor mechanical properties [40]. The apparent absence of any other largely commercialized energetic polymer along with the potential benefits of such a polymer provided the original impetus for another major area of my research.

In an effort to produce such an energetic polymer, Dr. Glatzhofer reacted the

relatively insoluble poly(*p*-phenylene sulfide) (PPS) (**17**) or Ryton with fuming nitric acid [41] producing a soluble polymer. After significant characterization and study, it was determined that the nitric acid had in fact oxidized the sulfide to a sulfoxide without nitration of the aromatic system as in Figure 17. The explanation of this unexpected reactivity as well as the characterization of this relatively unknown polymer poly(*p*-phenylene sulfoxide) (PPSX) (**18**) became an additional focus of my research.

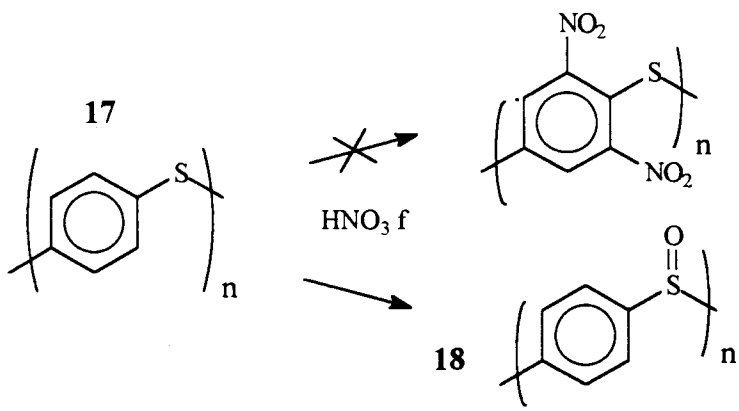

Figure 17 Synthesis of PPSX

1.6 Polyxylylenes

The final major field of study in my research involved polyxylylenes. Xylylene polymers are a fairly narrowly studied class of polymers that are closely related to [2.2]paracyclophanes [42]. The PCP's are usually the starting materials for the commercialized polyxylylenes using the Gorham process [43]. The term xylylene can be used interchangeably with quinodimethane and represents a dehydrogenated xylene as shown in Figure 18. The xylylene is generally a very reactive olefin system, although some such as 7,7,8,8-tetracyano-*p*-quinodimethane (TCNQ) are quite stable and isolable as also shown in Figure 18. Nomenclature for xylylenes remains fairly undecided and non-

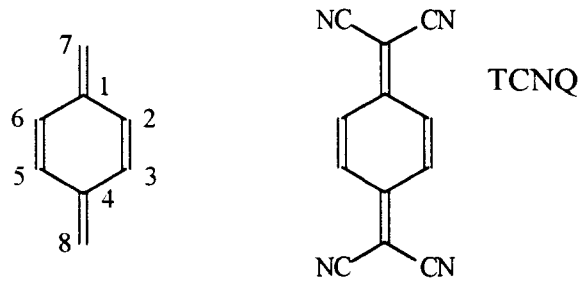

Figure 18 Quinodimethanes

IUPAC. Some authors prefer to maintain the α and α′ designation for substituents on the exomethylenes. This is a remnant of the equivalent nomenclature used in the parent xylene compounds and leaves ambiguity as to the numbering of substituents directly on the aromatic ring. The nomenclature that will be used here stems from the quinodimethane camp which numbers the aromatic carbons first, followed then by the exomethylene carbons as for TCNQ above. This research involves primarily *para* substituted xylylenes, but the *ortho* and *meta* compounds are known to a much lesser extent. Hence, the additional *para, ortho, meta* (*p, o, m*) needs to be added to the name. Alternatively, absolute numbering closer to IUPAC rules may be used: 1,4 for *para*, 1,3 for *meta*, and 1,2 for *ortho*. I will use the former system since poly(xylylene) itself is more descriptive of the polymer compounds when compared to the IUPAC preferred poly(1,4-phenylene-ethylene) instead of poly(*p*-xylylene).

There are several commercialized poly(xylylenes) marketed mostly by Union Carbide with most common applications being in the coatings and electronics industry [44, 45]. In general the polyxylylene polymers have excellent barrier properties to water and oxygen, high thermal stability, excellent electric insulator properties, and high chemical

inertness [42]. The single most difficult aspect of these polymers is their practical insolubility. They are typically only soluble in high boiling point solvents at high temperatures such as halobiphenyls, halonaphthalenes, and benzyl benzoate at temperatures from 150-300 °C. This lack of practical solubility necessitates expensive and wasteful vacuum pyrolysis/deposition of the polymers onto substrates. These substrate applications include semiconductor devices, capacitor dielectrics, and even valuable textiles and paper documents. Some common poly(xylylenes) are shown in Figure 19.

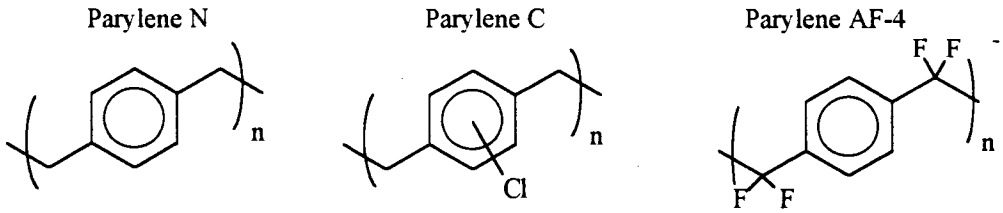

Figure 19 Common Poly(xylylenes)

Poly(*p*-xylylene), sold as Parylene N, is a general purpose barrier and electric insulator. Poly(chloro-*p*-xylylene), Parylene C, is a better oxygen and water barrier. Parylene AF-4, poly(7,7,8,8-tetrafluoro-*p*-xylylene) is used in more severe environmental conditions particularly because of its higher resistance to photodegradation [44, 45]. These commercial applications for xylylene polymers actually provide the single largest market for PCP and it's derivatives.

Many of the synthetic approaches to PCP's involve a xylylene intermediate that dimerizes to give the desired PCP, but the intermediate xylylene can also oligomerize and polymerize to give xylylene oligomers and polymers. In fact, the primary product in most PCP syntheses is an insoluble xylylene polymer. Just such a xylylene polymer was

produced by Morvant in his work to synthesize **15** and **16** above. This novel polymer, poly(2,5-dimethyl-3,6-dinitro-*p*-xylylene) (**19**) illustrated in Figure 20, like other polyxylylenes is insoluble, but it does uniquely exhibit a significantly exothermic decomposition [25].

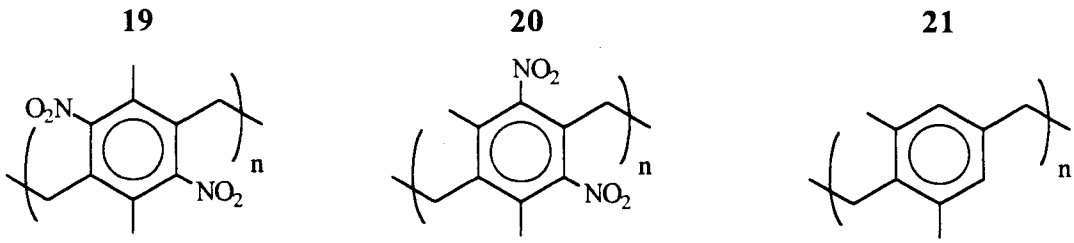

Figure 20 Novel Poly(xylylenes)

Hence, there is an obvious potential to additionally produce energetic xylylene polymers from the parallel effort to produce polynitroPCP's. This research did produce an additional insoluble energetic xylylene polymer, poly(2,6-dimethyl-3,5-dinitro-*p*-xylylene) (**20**). Additionally, a similar non-nitrated xylylene polymer, poly(2,6-dimethyl-*p*-xylylene) (**21**) was produced as shown in Figure 20. Fortunately, this polymer was uniquely soluble in a variety of common solvents producing excellent films upon evaporation.

Hence, the bulk of my dissertation research has been directed towards the synthesis and characterization of novel polynitroPCP's as energetic materials and the co-product poly(nitroxylylene) polymers as discussed in Chapter Two. Other significant efforts were focused on the synthesis and characterization of the novel, soluble poly(2,6-dimethyl-*p*-xylylene) as discussed in Chapter Three. The final chapter is directed at the synthesis and characterization of unexpected and novel poly(*p*-phenylene sulfoxide).

Chapter Two

Polynitro[2.2]paracyclophanes

2.1 Background

The synthetic approaches to [2.2]paracyclophanes (PCP's) and substituted PCP's are fairly varied. The original approach to ring closure using a Wurtz coupling required a narrow range of substituents [8]. However, the 1,6-elimination of a Hofmann type using an quaternary ammonium hydroxide salt allows a much greater diversity of substituents and has generally been the most widely applied synthetic approach. Other common routes include dithiacyclophanes which eliminate sulfur through a variety of methods and a unique Diels-Alder route to the reactive *p*-xylylene intermediate. There are several other more specific and much less commonly used routes that involve either 1,6-eliminations to form xylylenes or ring closure routes to directly form the ethano bridges. These general routes are shown below in Figure 21. Some general references to PCP synthesis [13, 14, 46, 47] as well as specific reaction types are provided [48-52].

The relative reactivity of the polynitroPCP precursors and our laboratory's prior successes guided my initial synthetic approaches to the 1,6-Hofmann elimination route or to the direct functionalization of an established PCP framework. This latter direct functionalization approach provided the first nitrated and dinitrated PCP's synthesized by Cram and others as previously discussed [26, 37]. While working in Dr. Glatzhofer's lab, Dr. Morvant experimented with the stepwise nitration of PCP and nitroPCP under a wide variety of conditions [25]. While Dr. Morvant's successes dramatically increased the yield

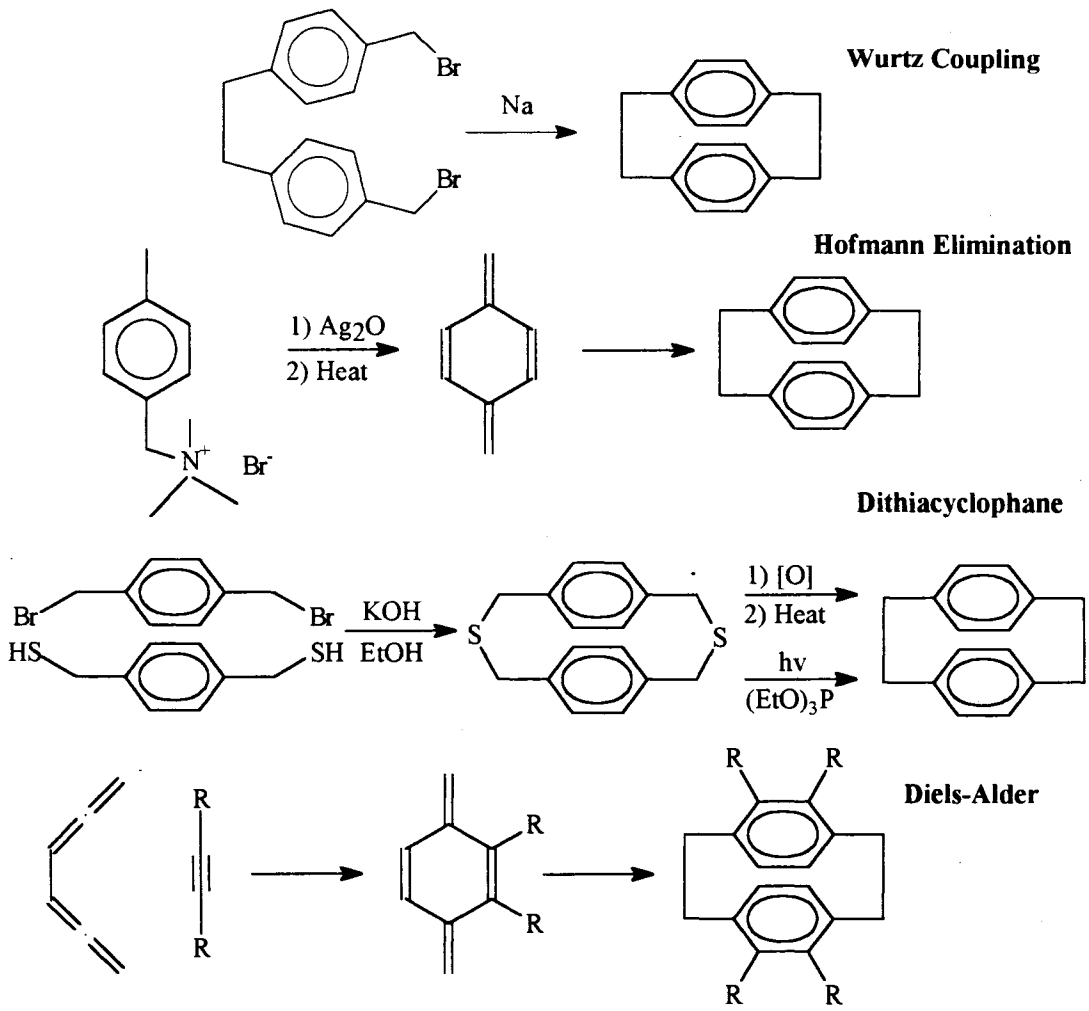

Figure 21 [2.2] Paracyclophane Synthetic Routes

of dinitroPCP's from prior literature syntheses, the prospects for extension of direct nitration to higher nitroPCP's seemed dubious; Dr. Morvant noted higher yields of presumptively phenolic oxidation side-products as the nitration conditions were made more severe. In a more hopeful approach, Dr. Morvant employed the 1,6-Hofmann elimination route to synthesize the first tetranitrated PCP, *anti*-5,8,13,16-tetramethyl-4,7,12,15-tetranitro[2.2]paracyclophane (**15**). Similarly, he synthesized the dinitroPCP's using the Hofmann elimination as shown in Figure 22. These combined successes in

synthesizing a tetranitrated PCP with blocking tetramethyl substituents and a dinitrated PCP which survived the quaternary ammonium hydroxide route, provided substantial hope of success in synthesizing parallel polynitroPCP's via the same routes.

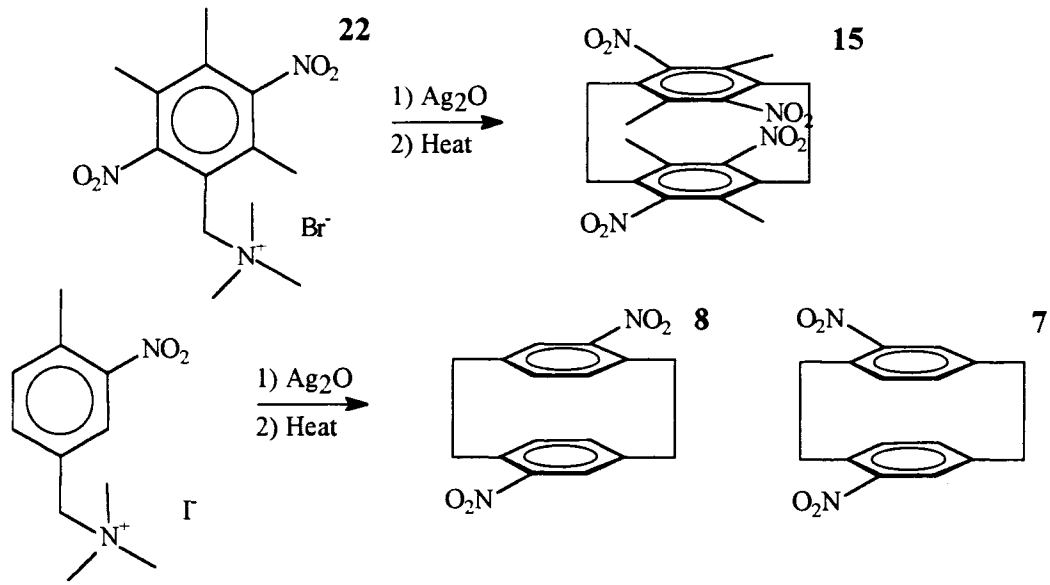

Figure 22 Previous PolynitroPCP Syntheses

With the intent of optimizing the energetic properties of the polynitroPCP's, synthetic targets were selected with higher oxygen balances. The primary goal was to remove the "extra" four methyl substituents on **15** improving the oxygen balance from -151 % to -124 %. The syntheses of three novel quaternary ammonium salts were devised as shown below. Compound **23**, N,N,N-trimethyl(4-methyl-2,5-dinitrobenzyl)ammonium bromide, was selected as the demethylated equivalent of compound **22**. Compound **24**, N,N,N-trimethyl(4-methyl-3,5-dinitrobenzyl)ammonium iodide, was chosen as a similar isomer of **23** which had a more direct synthetic route. Finally, compound **25**, N,N,N-

trimethyl(2,4,6-trimethyl-3,5-dinitrobenzyl)ammonium nitrate was selected as a target originally because of its analogous relationship to the other tetranitroPCP precursors (**22:23::25:24**). There was a further goal of investigating structure-activity relationships (SAR) of the isomeric tetranitroPCP's both with and without methyl substitutions. These

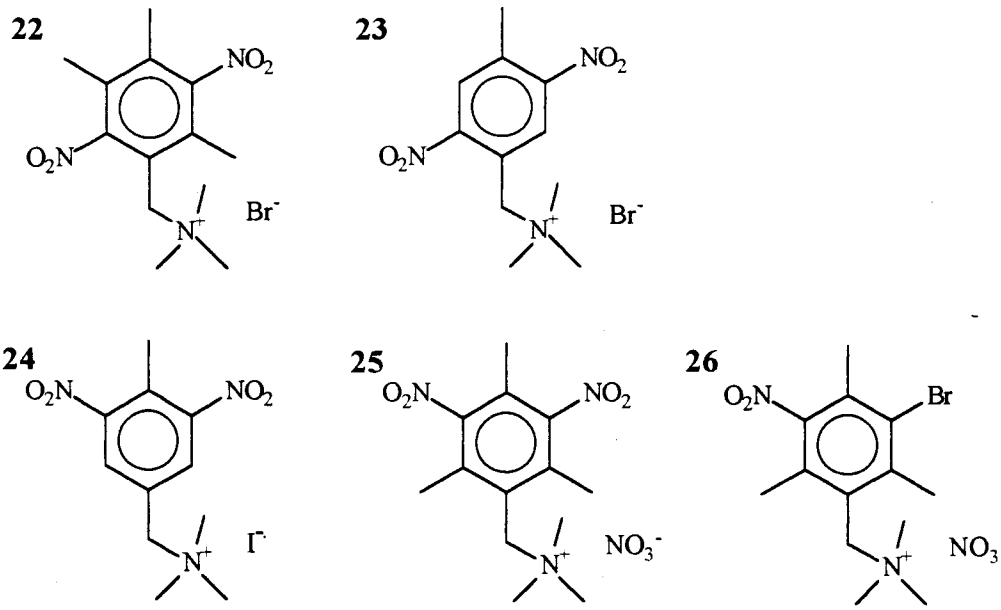

Figure 23 Novel Hofmann Salts

potential SAR insights could support the utility of the PCP framework as an unexplored control on nitro group rotation. These potential nitro group restricted rotations in the methylated compared to the non-methylated tetranitroPCP's may provide additional stabilization of the energetic materials. A final compound, N,N,N-trimethyl(2,4,6-trimethyl-3,5-benzyl)ammonium nitrate (**26**) was a serendipitous product from the synthesis of **25**.

2.2 Synthesis of N,N,N-trimethyl(4-methyl-3,5-dinitrobenzyl)ammonium iodide (24)

The synthetic route to the first of the quaternary ammonium salts proved to be both straight forward and high yield with a total percent yield from three steps of 80 %, as shown in Scheme 1. The commercially available starting material *p*-tolualdehyde was

Scheme 1

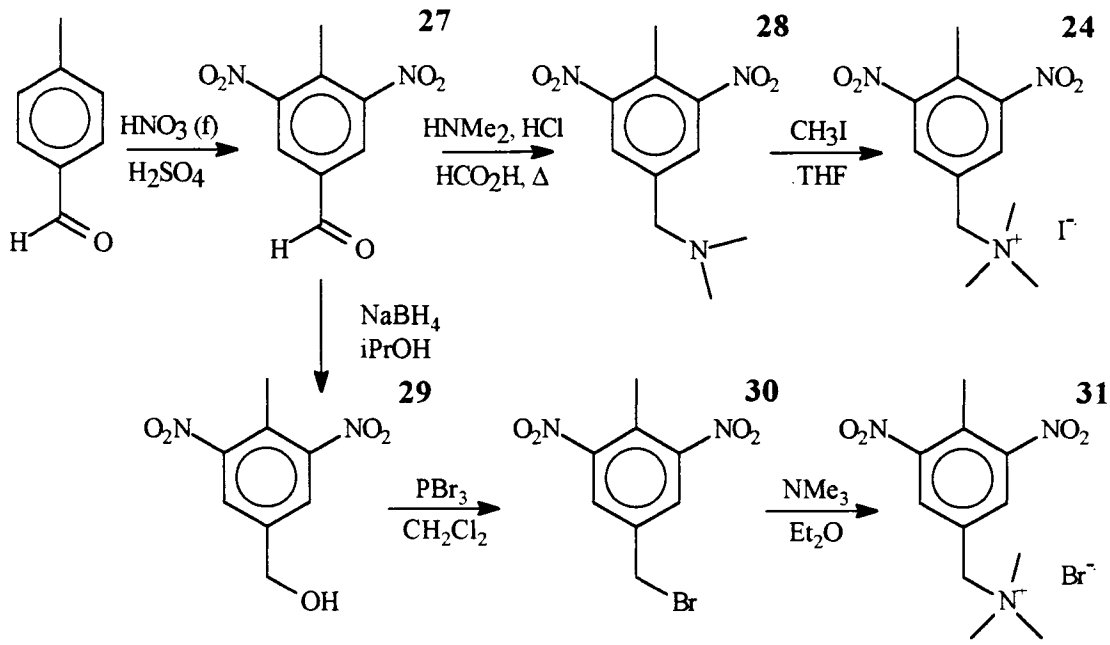

nitrated in a fuming nitric acid/sulfuric acid solution at room temperature for about six hours. Higher temperature reactions over shorter times produced significant amounts of the benzoic acid derived from **27** with a detrimental impact on yield. This nitration was a modification from literature of a similar mono-nitration of benzaldehyde [53], and *p*-tolualdehyde [54]. An attempt to use of concentrated nitric acid in place of fuming nitric acid produced an almost quantitative yield of the mono-nitrated benzoic acid (4-methyl-3-nitrobenzoic acid). With such a relatively high yield (88 %) and simple procedure, little

was required to further optimize this reaction. The next step involved an efficient reductive amination called the Leuckart-Wallach reaction in which **27** was aminated in formic acid using dimethylammonium chloride with an 88 % yield [55-58]. The reaction was complicated by the unavoidable side-product N,N-dimethylformamide (DMF). The product amine was never isolated because of the persistent DMF. Fortunately, the last reaction involved a precipitation that separates the DMF from the product. In the final reaction in Scheme 1, methyl iodide reacted with the amine **28** to form the quaternary ammonium salt, N,N,N-trimethyl(4-methyl-3,5-dinitrobenzyl)ammonium iodide(**24**) in high yield (94 %). The alternative lower pathway shown in Scheme 1 was the original synthetic route; but it proved to be much more difficult and much lower in yield. The sodium borohydride reduction produced the alcohol **29**, which was difficult to isolate even in moderate yields. The phosphorus tribromide halogenation proved to be quite messy producing a tarry highly noxious benzyl bromide **30**. The two poorly isolated intermediate products **29** and **30** were quite limiting to the final trimethylamine reaction which produced the quaternary ammonium bromide **31** in low overall yield. This alternative route was abandoned for the three-step, simple, high yield route reported above.

2.3 Synthesis of N,N,N-trimethyl(4-methyl-2,5-dinitrobenzyl)ammonium bromide(23)

The synthesis of this demethylated equivalent to Dr. Morvant's ammonium salt **22** was lower yield and longer than the other quaternary ammonium salt routes. Compound **23** was synthesized in four steps in an overall yield of 8 %, as shown in Scheme 2. The

Scheme 2

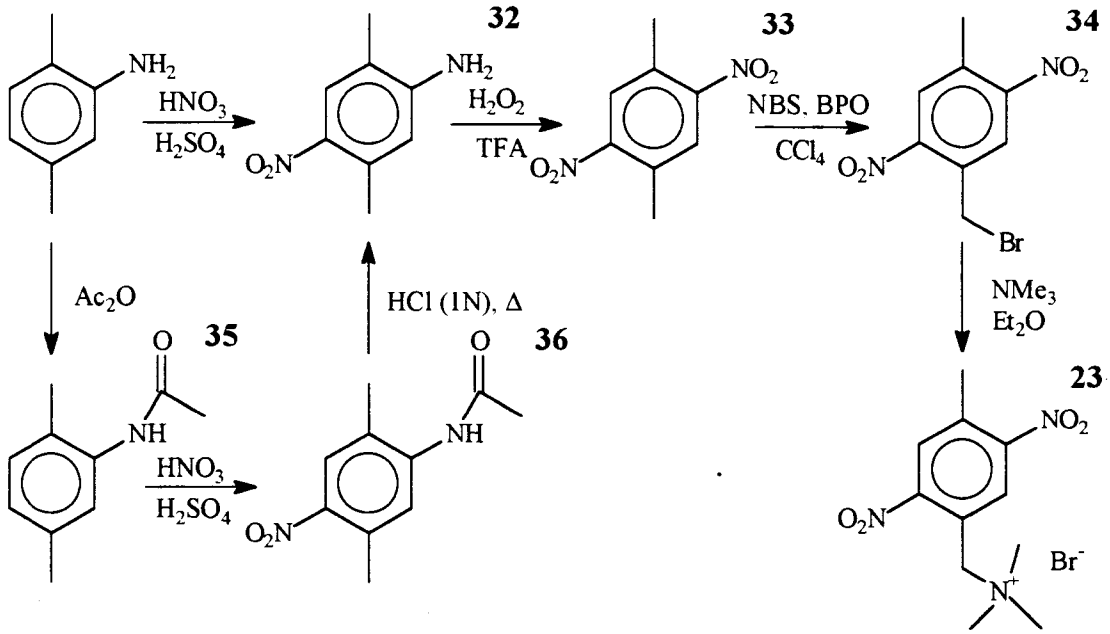

starting material, 2,5-dimethylaniline was directly nitrated in a mixed acid solution (nitric/sulfuric). The yield of the desired *para* nitration product, 2,5-dimethyl-4-nitroaniline, **32** was 53 %. The *ortho*-nitration product **32b** (*o/p* 0.379) was not immediately separated from the desired *para* nitration product **32**, because of its apparent oxidation and removal during the next step. The protection/deprotection route to the acetanilide **35** was initially explored as a way of ensuring *ortho/para* nitration of **36** [59] This side-route, while successful, proved unnecessary. Other work has demonstrated that direction nitration of anilines in acid solutions occurs *via* the aniline not the anilinium ion [60, 61]. The pertrifluoroacetic acid oxidation of **32** produced the desired **33** in 52 % crude yield and 36 % yield after recrystallization [62-64]. Other efforts were explored to obtain 1,4-dimethyl-2,5-dinitrobenzene through separation of the isomers after direct nitration of the parent xylene. While the first such separation was reported more than a

century ago [65-67], efforts using column chromatography in our laboratory were not successful, and they were subsequently left for the approach reported above. Free radical halogenation of **33**, with N-bromosuccinimide (NBS) in carbon tetrachloride using benzoyl peroxide (BPO) as an initiator afforded the benzyl bromide **34** in moderate yield (45 %) [68]. The remainder of the unreacted **33** (55 %) can be recovered after the next step. Similar halogenation reactions were run in benzene using NBS and azobisisobutyronitrile (AIBN) with somewhat lower yields. The carbon tetrachloride and BPO were selected and preferred based on availability and ease of separation of the NBS reaction byproducts. The final reaction in the synthesis of **23** uses gaseous trimethylamine to nucleophilically displace the bromine of **34** producing the product quaternary ammonium salt. The sub-atmospheric progressive generation of the trimethylamine was specifically designed in this work. This technique, explained in the Experimental section, helps to dramatically reduce both the release and waste of the very noxious and malodorous trimethylamine. The yield of **23** for this reaction was high (93 %). Furthermore, the unreacted **33** from the previous reaction was recovered (67 % recovered). The final yield of **23** through Scheme 2, increased from 8 % to 14 % when the recovery of **33** was taken into account.

2.4 Synthesis of N,N,N-trimethyl(2,4,6-trimethyl-3,5-dinitrobenzyl)ammonium nitrate (25) and N,N,N-trimethyl(2,4,6-trimethyl-3,5-benzyl)ammonium nitrate (26)

The last synthetic scheme for the quaternary ammonium salts actually produced two related compounds **25** and **26** in three steps each, as shown in Scheme 3. The

Scheme 3

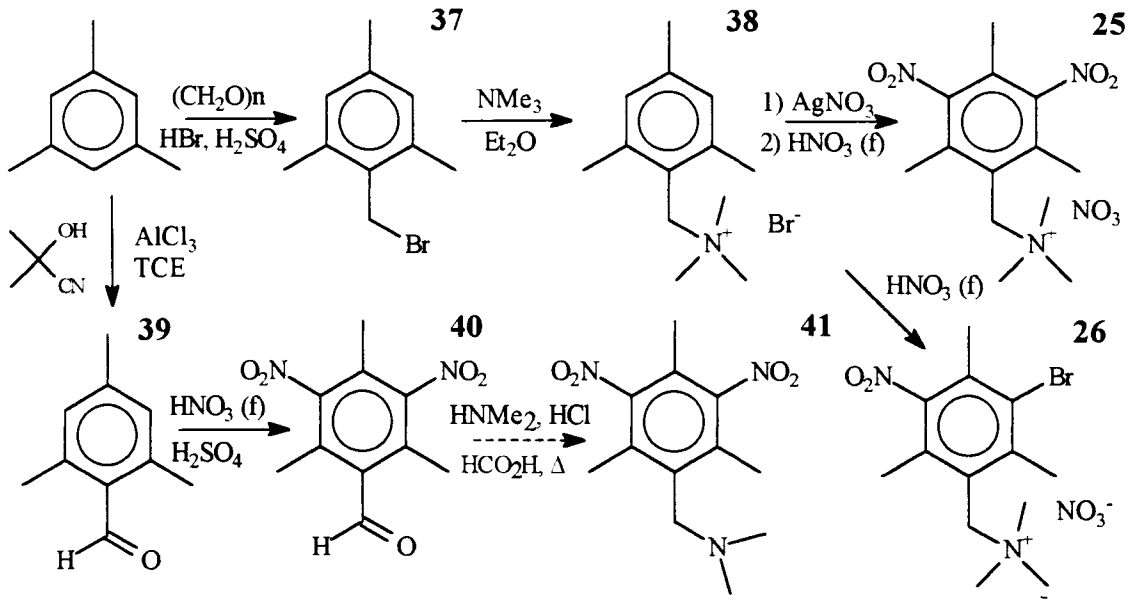

corresponding yields were 39 % and 73 % respectively. The convenient procedure for the bromomethylation of mesitylene was taken directly from the literature with a yield of 77 % [69, 70]. The bromomethylmesitylene **37** was then easily converted to the quaternary ammonium salt, N,N,N-trimethyl(2,4,6-trimethylbenzyl)ammonium bromide **38** in 95 % yield. This trimethylamine reaction was further improved beyond the sub-atmospheric progressive generation procedure discussed above in Section 2.3. Above, the trimethylamine was generated by the addition of aqueous hydroxide to solid trimethylammonium chloride in a partial vacuum. For this procedure, trimethylamine was generated by the addition of water to the loosely mixed sodium hydroxide pellets and solid trimethylammonium chloride, in a partial vacuum. This water addition procedure further simplified the trimethylamine generation by removing the transfer of a concentrated hydroxide solution. The direct nitration of **38** using fuming nitric acid initially produced a rather odd product, compound **26**. The quaternary ammonium bromide **38** reacts

quantitatively (99.5 %) with fuming nitric acid to produce the bromo-nitro derivative of **38**, presumptively through a nucleophilic aromatic substitution pathway. This reaction and the further characterization of **26** which exhibited a relatively unique rotational isomerism will be discussed in section 2.10. Compound **38** also reacted to produce **25** by being converted first to its nitrate salt by anion-exchange with silver nitrate. The quaternary ammonium nitrate then reacted with fuming nitric acid in a more expected manner producing **25** in 53 % yield. The alternative pathway shown in Scheme 3 was originally designed as a mimic of the previously successful approach taken in Scheme 1. This frustrating and less-than-successful pathway was a summer research project for undergraduate researcher Yonathan Tilahun. The first step, a Gattermann-like formylation to produce mesitaldehyde **39**, proceeded in unusually low yields despite the use of the acetone cyanohydrin reagent [71]. Other formylations using cyanides or dichloromethyl methyl ether proved even less successful [72, 73]. The subsequent nitration easily yielded the dinitrated mesitaldehyde **40**, but the following reductive amination to **41** proved quite impossible. Even stepwise imine formation followed by reduction failed. While the reductive amination failure could be explained by either electronic or steric effects of the *ortho* methyl groups, the success and brevity of the primary route shown in Scheme 3 provided a comforting solace for these early failures.

2.5 Hofmann Eliminations

The Hofmann eliminations on the multiple quaternary ammonium salts proved to be the most challenging aspect of this research. Prior experiences in our laboratory and in the

literature failed to indicate any fundamental difficulty with the Hofmann approach to the synthesis of polynitroPCP's. Difficulty was the most common characterization of the Hofmann approach to the lesser methylated polynitroPCP's.

The general Hofmann procedure detailed in the experimental section first generated the quaternary ammonium hydroxide salt from the quaternary ammonium halide [50]. This was accomplished by a precipitation based silver oxide exchange reaction. Silver oxide was slurried with the aqueous quaternary ammonium halide and stirred for about one to two hours. The desired quaternary ammonium hydroxide can then be separated from the silver halide and any unreacted silver oxide by vacuum filtration. The quaternary ammonium hydroxide aqueous solution was then pyrolyzed in a toluene filled reaction flask. The water layer was progressively removed using a Dean-Stark water separator. Subsequently, the quaternary ammonium hydroxide solution was pyrolyzed overnight. Most Hofmann routes to [2.2]PCP's produce 10-15 % PCP products, 80 % polymeric compounds, and 5-10 % miscellaneously organic products including benzyl alcohols, stilbenes, and unidentified compounds [50, 74]. This fundamental Hofmann procedure was modified in a variety of ways to better improve yields of the desired compounds. Specifically several solvents were substituted for toluene to modify the pyrolysis temperature: mesitylene, xylene, benzene, cyclohexane. As the quaternary ammonium nitrate salts **25** and **26** lacked a required halide counter ion, the silver oxide exchange reaction was replaced by an ion-exchange column. A progressive addition of the quaternary ammonium hydroxide solution was also substituted for the general biphasic pyrolysis. The goal of a dilution procedure by progressive addition was to limit the

formation of the polymer products [75].

The first quaternary ammonium salt synthesized through Scheme 1, N,N,N-trimethyl(4-methyl-3,5-dinitrobenzyl)ammonium iodide **24**, was the most extensively investigated compound. Ideally, **24** would have produced cyclophane **42**, 4,8,12,16-tetranitro[2.2]paracyclophane, as shown in Figure 24.

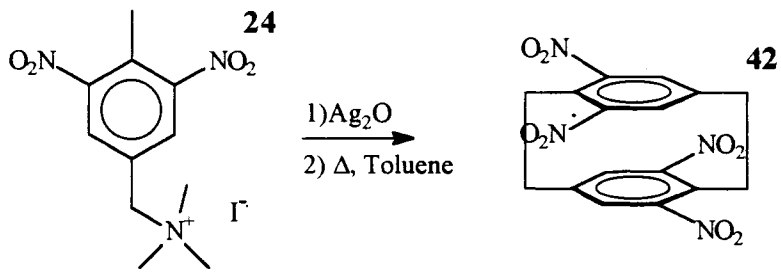

Figure 24 Synthesis of **42**

The general Hofmann procedure on **24** in fact produced two grossly identifiable substances: a brown tacky insoluble paste and a hygroscopic black/purple semi-crystalline solid soluble in polar solvents. The former brown paste was produced in greater amounts in higher temperature pyrolyses such as xylene and to a lesser extent in the lower temperature reactions. The latter black/purple solid was the solitary product of the lowest temperature cyclohexane pyrolysis. It was not observed in the xylene pyrolysis. The desired cyclophane **42** was not reproducibly synthesized; a single Hofmann procedure allowed isolation of less than 1 mg which was characterized only by proton NMR.

There are several possible explanations for the failure of the Hofmann elimination on compound **24**. Quaternary ammonium compounds are known to undergo several

rearrangements and nitro-compounds are known to be reactive to both nucleophiles and reducing agents. Some of the specific pathways are illustrated in Figure 25.

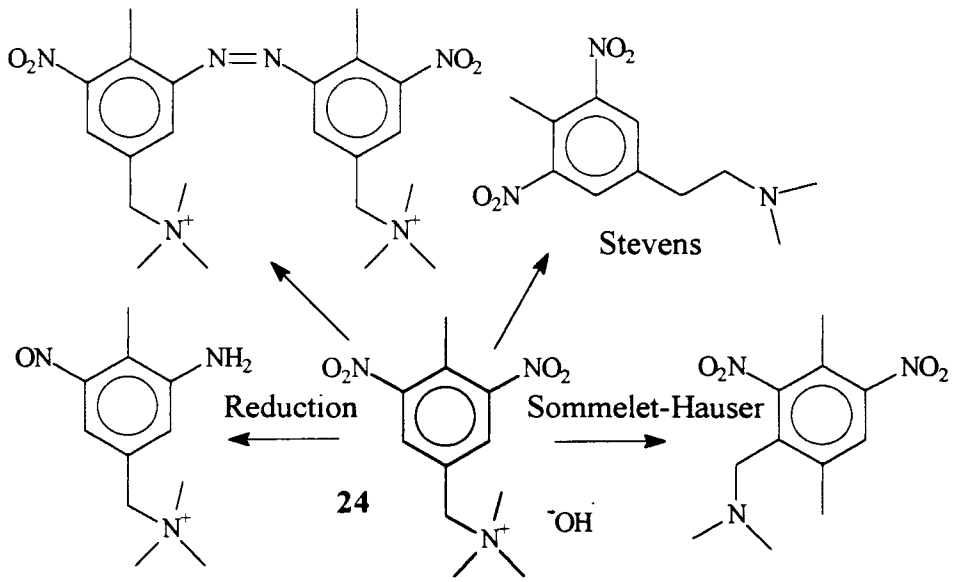

Figure 25 Potential Hofmann Side-Reaction

The Stevens rearrangement is generally thought to involve a nitrogen ylide, and hence requires a strong base, usually an alkyl lithium or sodium amide [76-78]. This rearrangement has not been documented on aryl nitro-compounds, and as such is probably not relevant to the Hofmann failure. Similarly, the Sommelet-Hauser rearrangement, which may normally compete with the Stevens rearrangement, also requires the use of strong bases which are incompatible with nitro-compounds [79-87]. The more likely explanations for the Hofmann failure may involve the reactivity of aryl nitro-compounds to nucleophiles as well as the confounding reduction of the nitro groups to nitroso, azo, azoxy, and amino compounds [88-94]. These possible reduction products are also graphically illustrated above in Figure 25. Nitro group reductions frequently complicate

nucleophilic aromatic substitution reactions, particular those involving alkoxides or hydroxide. These complications can be avoided or limited by introducing molecular oxygen which acts as a radical quencher blocking the electron reduction pathways [92, 93]. A similar approach was taken to assess the impact on the Hofmann reaction on **24**. Oxygen sparging during a Hofmann dilution procedure exclusively produced the dark black/purple product with no noticeable brown paste formed. This seemed to indicate that the brown paste was a result of nitro group reduction pathways which had been effectively blocked by the oxygen's presence. This supposition was further supported by a reaction of **24** with *t*-butoxide which is still capable of initiating reduction routes, but has a limited capacity for nucleophilic substitution routes. The exclusive product from the t-butoxide reaction was the usual brown paste product with no trace of the black/purple solid. Too many conclusions based on the texture and color of products should however, be avoided.

There are also many well documented reactions of aryl nitro-compounds through nucleophilic substitution forming anionic sigma complexes [95-97]. While possible on doubly deactivated aromatic systems, the sigma complexes tend to be formed and studied on triply deactivated systems such as trinitrobenzene. These nucleophilic substitution reactions occur quite rapidly at room temperature when the triply deactivated systems are exposed to oxoanions. In compound **24**, the additional deactivating effect of the benzyl trimethylammonio group in combination with the dinitro substitutions should be quite effective in activating the aromatic ring for nucleophilic substitution. The deactivating effect of the trimethylammoniomethyl group is documented to be about 70 % as strong as

the nitro group effect [98]. The likely nucleophilic substitution pathway for the hydroxide counter-ion of compound **24** is shown in Figure 26.

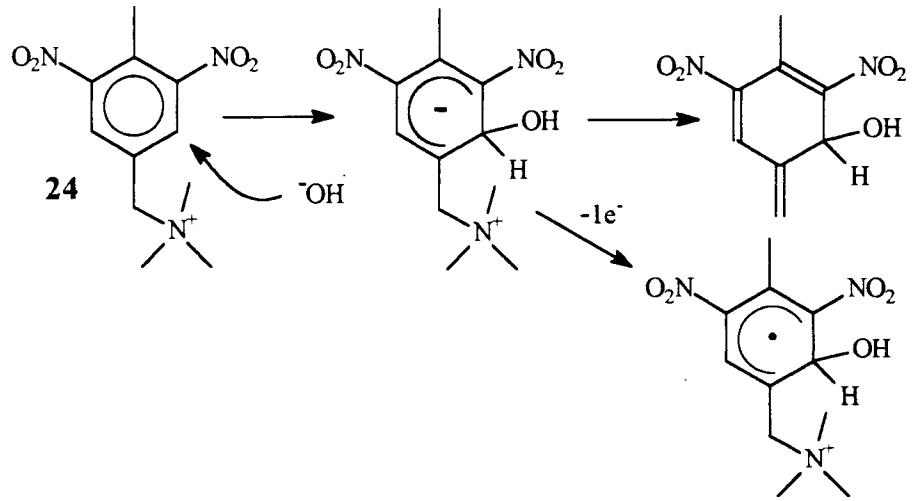

Figure 26 Hydroxide Sigma Complex Formation

The likely substitution of the hydroxide at the open aromatic site was chosen based on the relative stabilities of the sigma complex products. A simple semi-empirical molecular model confirmed the preference for the hydroxide attack at the open site, see Table 2 [99, 100].

Table 2. Sigma Complex Heats of Formation by PM3 (Kcal/mol)

	ΔH_f, OH^- *syn* attack	**ΔH_f, OH^- *anti* attack**
ipso	-1.79	-0.51
ortho	-20.48	-22.68
meta	-1.17	-6.10
para	-16.18	-15.16

The values given in Table 2 are defined according to the relative position to the trimethylammoniomethyl group. As the formation of the sigma complexes in nucleophilic substitution reactions is usually both endothermic and rate determining, the parallel to the actual sigma complex stabilities can be informative.

The dark black/purple color of the Hofmann product on **24** is consistent with the formation of a sigma complex. It should also be noted that the sigma complex in Figure 26 bears no molecular charge, and hence its formation in non-polar solvents from the charged quaternary ammonium hydroxide would be favored. The prominent smell of trimethylamine can also be noted during the Hofmann reaction on **24**. However, that smell and its parallel loss of trimethylamine is also present during the initial silver oxide exchange reaction. While a slight odor of trimethylamine is not uncommon during the exchange, the relative strength of the odor and likely greater loss of trimethylamine is unusual. A possible explanation for this gas evolution is also illustrated in Figure 26. This loss of trimethylamine forming a reactive dinitrotriene and possible oxidation-reduction pathways further complicate possible routes. The possible oxidation-reduction pathways are supported by the extreme difficulty in obtaining an NMR spectrum of the soluble black/purple solid in TFA or DMSO. When the dark black/purple solid isolated from the cyclohexane procedure was subjected to pyrolysis in toluene overnight, the brown paste resulted. Attempts to specifically identify the dark black/purple product were not successful. It was however, quite clear that the desired cyclophane **42** was not reproducibly produced in significant yields.

The Hofmann elimination on Compound **23** to form cyclophanes **43a** and **43b** produced a product similar to the one seen in the Hofmann reaction on compound **24**, see Figure 27. An ion-exchange resin (IER) was used to generate the quaternary ammonium hydroxide instead of the usual silver oxide exchange reaction. During the column based exchange a dark black band formed on the resin eventually stopping the column flow. No compounds could be removed from the column material. It was presumed that a similar sigma-complex formed with the equally undesirable effect.

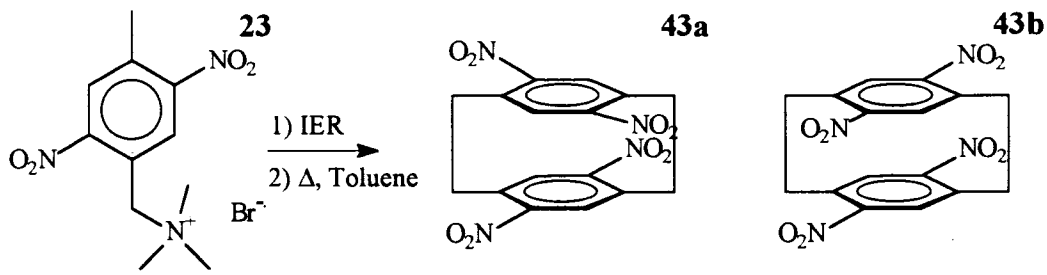

Figure 27 Synthesis of **43a** and **43b**

As it became quite clear that the Hofmann elimination route was incompatible with the triply deactivated aromatic systems with open sites, prospects for the Hofmann reaction of compounds **25** and **26** seemed much more hopeful. The synthetic approach detailed earlier in Scheme 3 produced two Hofmann salts that could produce polynitroPCP's. The Hofmann reaction on the bromo-nitro compound **26**, appears to have produced a cyclophane by mass spectral analysis, see Figure 28. The specific identification of cyclophanes **44a** and **44b** was not accomplished. As these products are only dinitrated and not a specific goal of this research, further efforts were to characterize

them were not made. The cyclophanes **44a** and **44b** may however, be quite useful for researchers interested in substituted PCP's as scaffolds for catalytic reactions.

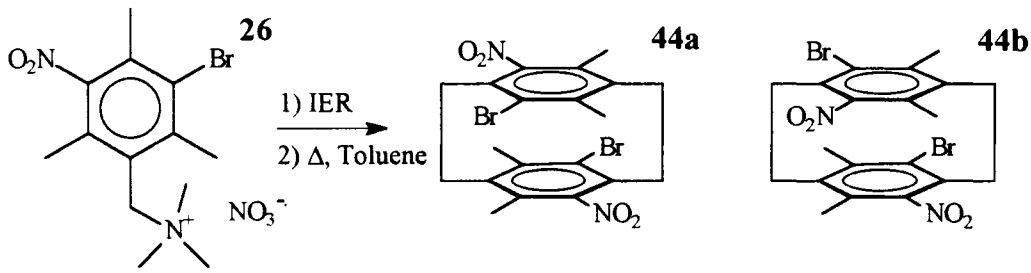

Figure 28 Synthesis of **44a** and **44b**

The final quaternary ammonium salt, **25**, yielded much better results, see Figure 29. Compound **25** was subjected to the ion-exchange resin modification of the Hofmann procedure without difficulty. The general features of the products and reaction were much more characteristic of Hofmann eliminations previously conducted in our laboratory and in the literature. The yield of insoluble, presumptively polymeric product was 67 %

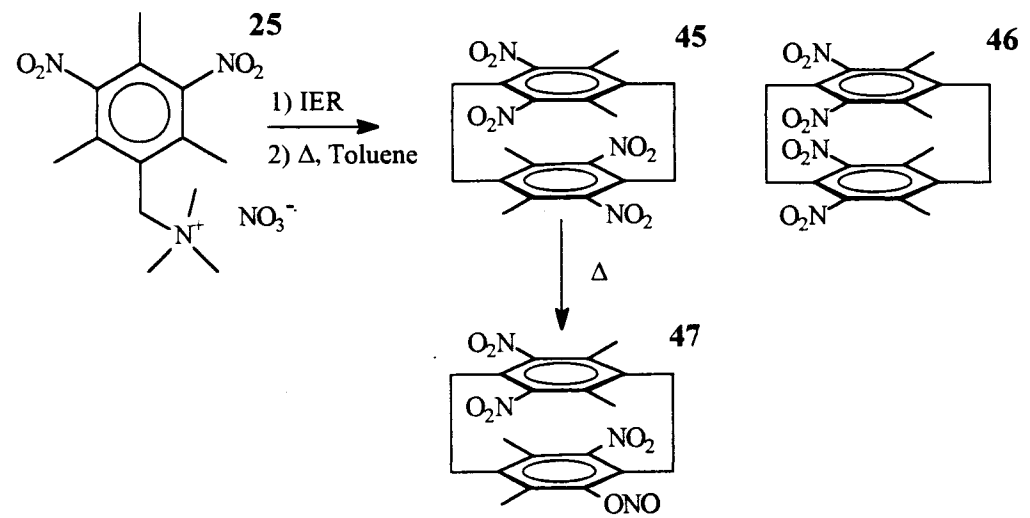

Figure 29 Synthesis of **45**, **46**, and **47**

with an additional 26 % yield of soluble unidentified organic products. The desired cyclophanes **45** and **46** were produced in 1 % yield in a ratio of about 3:1. The cyclophanes **45** and **46** were further separated by HPLC followed by mass spectral, ^{13}C NMR, ^{1}H NMR, and thermal analysis. The spectra for these compounds are presented in the appendices. Interestingly, the proton NMR spectrum of the crude mixture of **45** and **46** in benzene showed only two peaks, unlike the methylene chloride and chloroform spectrum which showed the more typical [2.2]PCP multiplets for **45** and separate peaks for **46**. The accidental degeneracy of the compounds in benzene is unique and inexplicable. The identification of compound **47** as the thermally rearranged nitrite ester of **45** was based on the proton NMR and the mass spectrum. As less than 1 mg of **47** was isolated, further specific confirmation of its identity was not possible.

2.6 Alternative Electrophilic Nitro Routes

As the prospect of directly synthesizing tetranitroPCP's lacking the aryl methyl substitutions seemed less likely, other synthetic routes were explored. As there are several tetrabromoPCP's available through fairly simple synthetic routes [101], it seemed quite appropriate to try to convert these bromo compounds via conversion to aryl lithiums to their related nitro compounds. Many aryl lithium compounds of PCP's are also known [102-106]. Two different electrophilic nitro sources were tried: dinitrogen tetroxide and a novel trialkylsilyl nitrate. These alternative routes are illustrated in Figure 30. A dinitrogen tetroxide route has been successfully employed by Eaton to synthesize penta- and hexanitrocubanes [107, 108]. The specific difficulty with this approach is that the aryl

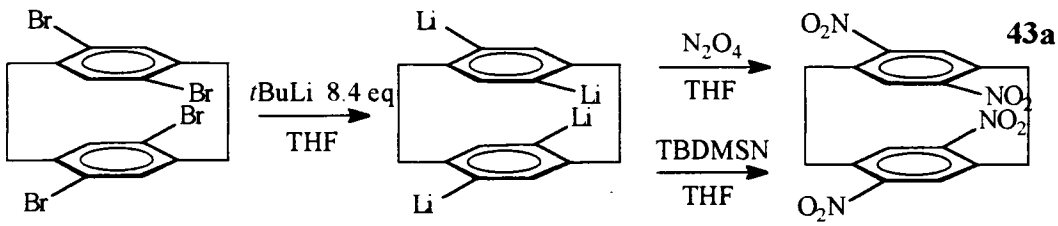

Figure 30 Alternative Electrophilic Routes

lithiums (and other organometallics) react with the intra and intermolecular nitro groups [109, 110]. Eaton controlled this by employing a melting interfacial reaction system. He however, produced relatively low yields (26 %) of a mononitro arene. A more successful route employed plumbanes rather than lithium reagents, which would have been well beyond the scope of this research. The reaction of dinitrogen tetroxide in tetrahydrofuran (THF) with tetralithioPCP's produced no identifiable products. With appropriate control of addition sequence, this route may provide polynitroPCP's.

The second alternative electrophilic nitro source was synthesized for this research. In an attempt to duplicate the more moderate reactivity of the alkyl nitrate compounds, but avoid the potentially troublesome alkoxide reaction byproducts, two trialkylsilyl nitrates were synthesized: trimethylsilyl nitrate (TMSN) and *t*-butyldimethylsilyl nitrate (TBDMSN). The former compound is a rare but effective nitrating reagent when used with boron trifluoride etherate in electrophilic aromatic nitrations [29, 111-114]. The latter reagent was synthesized in this work as the trimethylsilyl nitrate proved to be relatively unstable. The novel *t*-butyldimethylsilyl nitrate was much more stable and easily synthesized from the TBDMS chloride in an exchange reaction with silver nitrate. The

model reactions with phenyl magnesium bromide and phenyl lithium produced moderate yields of the corresponding aryl silanes, rather than the desired nitro compounds. This novel reagent may prove more useful with organometallic modifying agents such as TMEDA or copper, with Lewis acid catalysts, or with other solvents and reaction conditions. No further studies beyond the model reactions were attempted with TBDMSN.

2.7 Direct Nitration

The direct nitration of PCP and nitroPCP had previously produced moderate success for Dr. Morvant in the synthesis of the dinitroPCP's. The extension of this direct nitration route to yield trinitro and tetranitroPCP's has not been documented. While the previously documented difficulties and relatively low yields in synthesizing the dinitroPCP's seemed ominous, the potential benefits of the polynitroPCP's uniquely convergent nitration route provided some hope. As shown in Figure 31, pairs of the dinitroPCP's should each produce one of two trinitroPCP's, compounds **49** and **50**. The *meta* directed nitration of these compounds should then produce one of two tetranitroPCP's, **42** and **51** (enantiomers are not included). This convergent substitution pattern is due to the introduction of symmetry with progressive *meta* nitration. It should be noted that only the top route in Figure 31 has the mutual direction of both steric and electronic effects, while the lower route does have conflicting electronic and steric effects which might tend to produce other less symmetrical isomers. Fortunately, the *pp* and *po* dinitro[2.2]PCP's are produced in the greatest amount from the nitration of nitro[2.2]PCP. The stepwise rather

than direct dinitration of PCP produces the highest yields of the dinitroPCP's , as well as permits the isolation of the preferred dinitroPCP isomer(s).

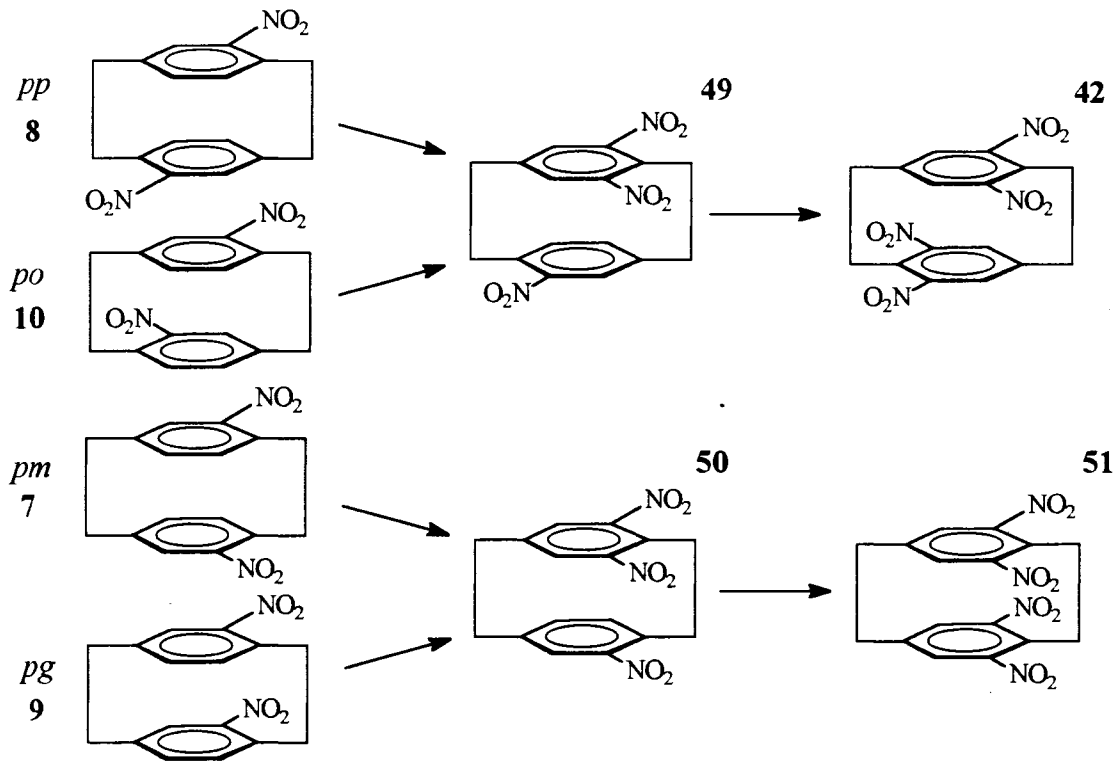

Figure 31 Direct Nitration Routes

The direct nitration of *pp*-dinitro[2.2]PCP **8** was attempted under a wide variety of conditions with mostly unsuccessful results: fuming nitric acid at 70 °C for 3 and 48 hrs, fuming nitric acid in TFA at 25 °C for 2 hrs; fuming nitric acid in acetic anhydride at 25 °C for 2 hrs; concentrated nitric acid at 70 °C for 48 hrs. The specific products from these reactions could not be identified. It is possible that the difficulty in direct nitration occurs from either oxidation to form phenolic compounds or from the formation of diene intermediates. The supposition of the phenolic compounds is based on the water solubility of the nitration products and the prior experiences of Dr. Morvant [25]. The remaining

non-water soluble material exhibits complex NMR signals that are most likely due to multiple asymmetric compounds. Other researchers have previously isolated diene products and skeletal rearranged products from the nitration of PCP's and other aromatic compounds [115-118]. Examples of potential products and pathways are given in Figure 32. The relative relief of PCP strain is presumed to be the primary source of this latter

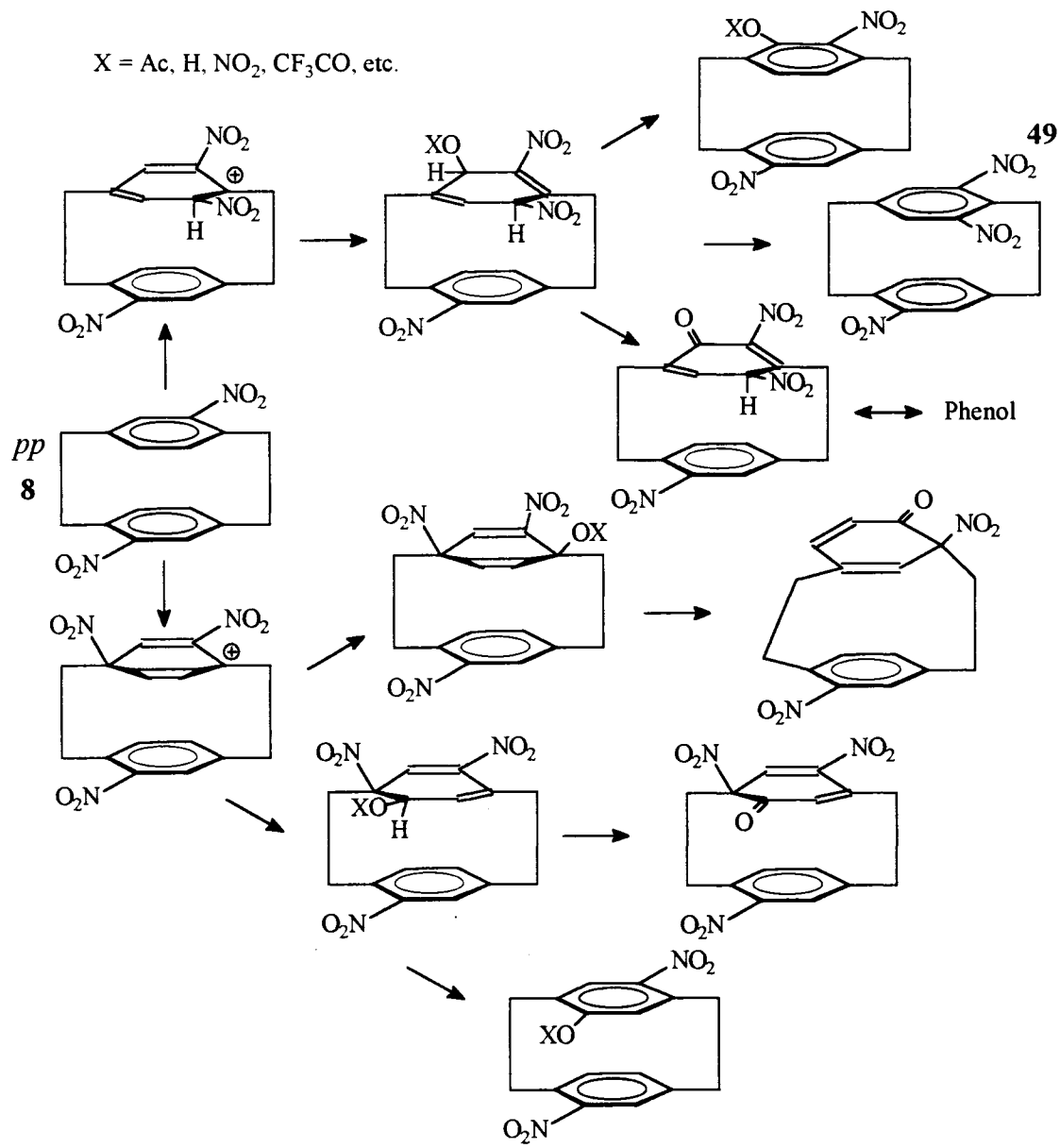

Figure 32 Direct Nitration Mechanisms

difficulty in the direct nitration routes. In related work Dr. Glatzhofer was able to synthesize 4,8,12-trinitro[2.2]PCP **49**, from the room temperature nitration of **8** in concentrated nitric acid over a several days. The identity of **49** was confirmed by proton NMR and mass spectral analysis. The direct synthesis of the other tetranitroPCP's has not been successful or reported elsewhere.

2.8 Vicarious Nucleophilic Substitution

A final alternative synthetic route to the tri and tetranitroPCP's was explored without success. Two vicarious nucleophilic amination reagents, 1,1,1-trimethyl- -hydrazinium iodide (TMHI) and 4-amino-1,2,4-triazole (ATAZ) were reacted with *pp*-dinitro[2.2]PCP **8** under literature conditions without identifiable products other than recovered starting material [119-123]. These reagents have been successful at mono-aminating nitrobenzenes, but they have not been applied to the PCP systems. As in Figure 33, the product amino-nitro-PCP's could then be oxidized to their respective nitro compounds. Both pertrifluoroacetic acid (pTFA) and the more mild sodium perborate (SPB) were successful in oxidizing amino[2.2]PCP to nitro[2.2]PCP in model studies

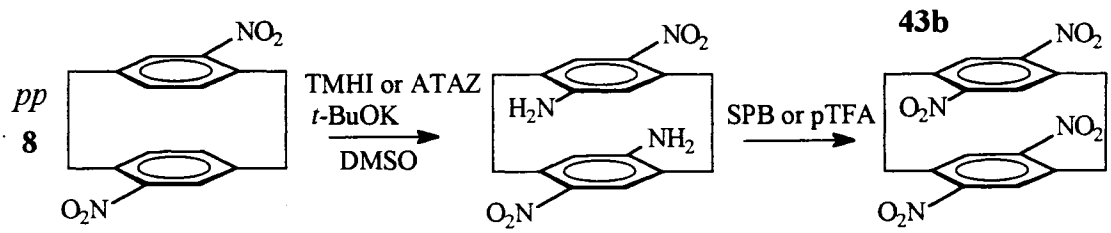

Figure 33 Vicarious Nucleophilic Substitution Route

[62-64, 124] and [125-127], respectively. There was not however, an opportunity to try these oxidations on the higher amino-nitroPCP's because of the lack of success with TMHI and ATAZ. The specific explanation for the initial failure of these vicarious nucleophilic substitution routes may be related to the relative susceptibility of deformed aromatic system to nucleophilic aromatic substitution; there is no literature precedent for such nucleophilic aromatic substitution reactions on PCP's.

2.9 Rotational Isomerism of N,N,N-trimethyl(3-bromo-2,4,6-trimethyl-5-nitrobenzyl)ammonium nitrate (26)

As previously discussed, compound **26** was synthesized in almost quantitative yield from N,N,N-trimethyl(2,4,6-trimethylbenzyl)ammonium bromide **38** by reaction with fuming nitric acid. The resultant compound **26** was intriguing both because of the unique mechanism of its synthesis and because of the rotational isomerism it exhibited. The hypothesized mechanism is shown in Scheme 4. The first nitration of **38** to yield N,N,N-trimethyl(2,4,6-trimethyl-3-nitrobenzyl)ammonium bromide **52** is likely to occur quite rapidly. The delay in the second nitration due to the doubly deactivated aromatic system of **52** provides the opportunity for the nucleophilic bromide ion to add to the aromatic ring. This bromide addition to **52** is displayed in Scheme 4 to occur at either of two less hindered *ipso*-methyl positions. The regioselectivity of this addition is preferred because of the stabilization of resultant anion. It should be noted that this addition produces a molecularly neutral species. Under non-oxidative conditions this first addition would not proceed, but rather reverse with loss of the bromide. However, in the unique oxidative

Scheme 4

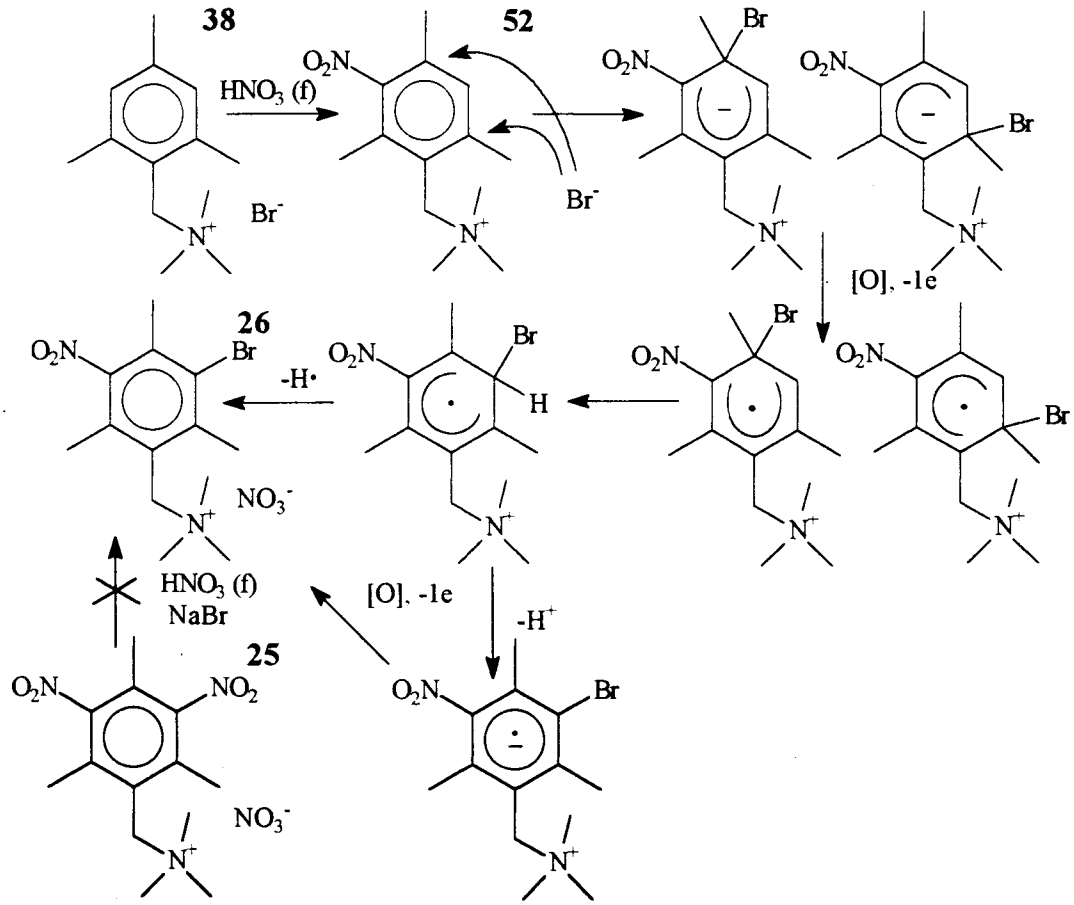

and nitrating environment of fuming nitric acid, oxidation of the sigma complex is possible and likely [95, 96]. The resultant sigma complex radical compounds now have an allowed [1,2] bromine shift pathway available. This shift is favorable both in terms of a decrease in steric strain of the sigma complex and an increase in electronic stabilization of the sigma complex radical. This resultant rearranged sigma complex radical can either lose a proton and then be again oxidized or directly lose a hydrogen atom both forming the product **26**. This mechanism is proposed primarily based on the lack of other reasonable routes. An attempt to form **26** from the dinitro compound **25** by reaction under identical conditions of fuming nitric acid with added sodium bromide produced only unreacted **25**. That

experiment eliminated the possible dinitration of **38** with secondary loss of a nitro group by nucleophilic aromatic substitution. Direct bromination of **38** through some unique electrophilic bromine species such as hypobromite seems even more remote. The evolution of dinitrogen tetroxide/ nitrogen oxide occurs during the reaction, which is consistent with an oxidation-reduction reaction in fuming nitric acid. It would be useful to mononitrate the nitrate salt of **38**, and then expose the isolated nitrate derivative of **52** to fuming nitric acid with sodium bromide. However, the activation of **52** for nucleophilic aromatic substitution by the combined ammonio and nitro groups is certainly plausible. Protonation of the nitro group in the acid medium may even further activate the system. The exceedingly high yield and combined experimental evidence provide strong support for the mechanism presented in Scheme 4.

The second unique aspect of **26** was the relatively unusual form of rotational isomerism that it exhibited. The trimethylammoniomethyl group of **26** is flanked by two *ortho* methyls which are further buttressed by flanking *meta* substitutions. The asymmetric *meta* substitutions (bromo and nitro) combined with the hindered rotation about the trimethylammoniomethyl-aryl axis creates two rotational enantiomers. While the specific use of the term atropisomerism is most accurately reserved for isomers that have been isolated at room temperature such as compounds **8** and **10** above, similar mesityl derived styrenes have been successfully isolated. The rota-enantiomers **26a** (aR) and **26b** (aS) and their rotational and symmetry interconversion are shown in Figure 34. The configurational nomenclature prefix "a" denotes axial chirality, which is a modification of the Cahn, Ingold, Prelog chirality rule [5].

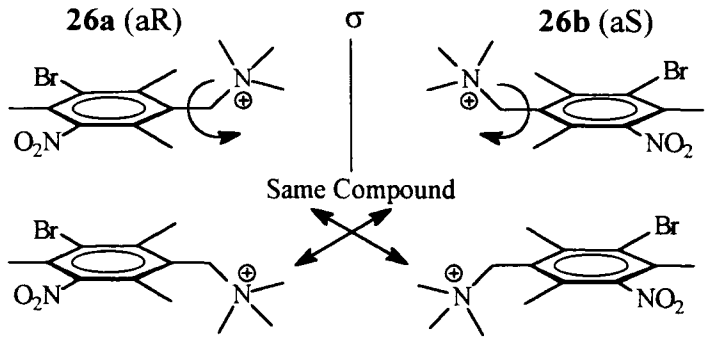

Figure 34 Rota-enantiomers **26a** and **26b**

This rotational isomerism of **26** was first identified by proton NMR. The two benzyl protons are diastereotopic; their substitution with deuterium would produce pairs of diastereomers. As such, NMR can differentiate their signals while the rotational barrier exists. The rotational barrier was studied in a variety of solvents and temperatures using both one and two dimensional techniques. The coupling constant of the benzyl protons was -14.7 +/- 0.3 Hz, which is a normal geminal benzyl proton coupling constant; the toluene methyl protons have a coupling constant of -14.5 Hz [128]. The benzyl protons showed a characteristic pair of doublets with second order features. This pair of doublets coalesced with increasing second order features into a first order singlet. The coalescence temperature, T_c in DMSO was 85 +/- 2 °C. This coalescence was not attained in methanol or acetone to their boiling points. The coalescence was fully reversal. The anisotropy of the two benzyl environments is inherently due to the rotational barrier. As that barrier is surpassed with increasing temperature, the averaged signal difference of those environments also decreases, and they coalesce to a single signal. The determination of the rotational barrier energetic parameters was complicated by the second order features

of the spectra. These second order features are inherently caused by the small difference in the environment anisotropies reflected by the chemical shifts relative to the coupling constant between those environments. Specifically, the difference in chemical shifts was about 30.6 Hz and the coupling constant was 14.7 Hz, producing a $\Delta\delta/J$ of 2.1, clearly less than the value of 10 where only first order spectra result. In the case of two coupled nuclei (AB) with a $\Delta\delta/J < 10$, the doublet center frequencies are not at the actual doublet resonance frequencies. The difference in chemical shift in an AB system must in this case be calculated using Equation 5 [128].

$$\Delta\delta = [(\nu_4 - \nu_1)(\nu_3 - \nu_2)]^{1/2} \qquad (5)$$

$\Delta\delta$ - Chemical shift difference (Hz)

ν_n - Frequency of AB Peak (Hz)

These second order features prohibit a simple line width analysis to determine the rotational barrier energetics [129]. However, Equation 6 can be used to get a fairly accurate value for change in Gibbs free energy of activation [128].

$$\Delta G^{\ddagger} = 19.14\ T_c\ (9.97 + \log_{10} T_c/\Delta\delta) \qquad (6)$$

T_c - Coalescence Temperature (K)

$\Delta G^{\ddagger}$ - Gibbs free energy of activation (J/mol)

Alternatively, for coupled AB systems a more specific equation that includes the coupling constant J in Hz may be used as in Equation 7 [130].

$$\Delta G^{\ddagger} = 19.14\ T_c\ (10.32 + \log_{10}(T_c/(\Delta\nu^2 + 6J^2)^{1/2})) \qquad (7)$$

Using this Equation 6, the $\Delta G^{\ddagger}_{298}$ for the rotational barrier was calculated at 75.7 kJ/mol, while Equation 7 gives an activation energy of 76.7 kJ/mol. This is a sizeable energy of

activation and should allow isolation of the rota-enantiomers at room temperature, but not too much above that [5]. This rotational barrier is on the same scale as other mesityl styrenes and mesityl fluorenes, as shown in Figure 35 [5, 130-136].

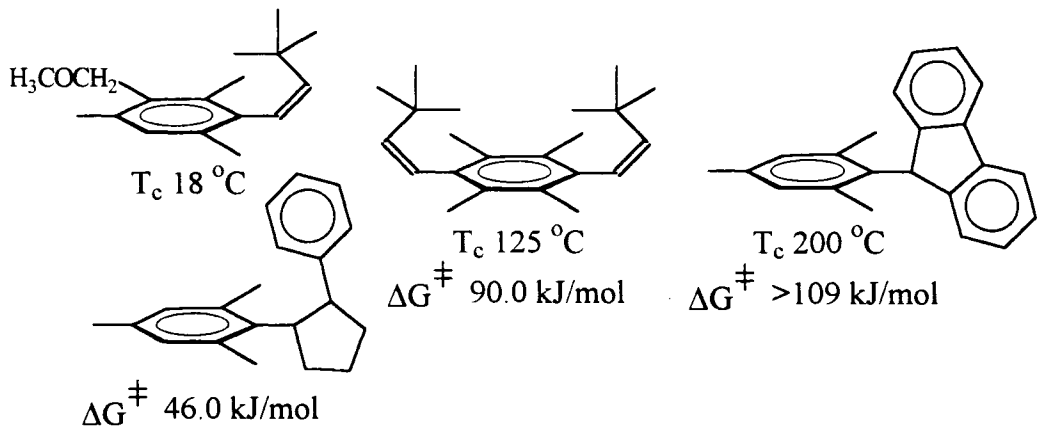

Figure 35 Other Rotational Atropisomer Barriers

The relative assignment of the benzyl protons is possible through the use of two dimensional NMR techniques. The anisotropy of the *meta* nitro group is presumed to be the major differential influence on the benzyl protons. The relatively vertical geometry of the nitro group with respect to the aromatic ring would place both the nearest *ortho* methyl group and the closest benzyl proton in the shielding cone of the nitro plane current. This placement in the shielding cone of the nitro group would cause a relative upfield shift of both the nearest *ortho* methyl group and the nearest benzyl proton. These relative configuration assignments were confirmed by NOESY 2D NMR, as shown in Figure 36. The downfield benzyl protons were closest in space to the downfield *ortho* methyl protons and vice versa for the upfield pairs, as identified by crosspeaks in Figure 36.

Compound **26** was crystallized from acetonitrile forming small needles. The molecule itself has a fairly typical structure. Several views are shown in Figure 37. The unit cell containing eight ion pairs is shown in Figure 38. The rota-enantiomers **26a** and **26b** pair in the unit cell with each other **26a** to **26a** and vice versa in an equivalent stacked arrangement. The pairs also then share the same hemi-cell with a flipped pair of the same enantiomer. Furthermore, the charged portions of the molecules are layered in the crystal in parallel faces of the unit cell; both the nitrate and ammonio groups are near parallel external faces of the unit cell. The aromatic rings form stacked, but offset, *pi* facial columns that extend through the smallest dimension of the unit cells. These columns are best visualized in Figure 39. There also appears to be a mild bonding interaction between the aryl bromine and a neighboring nitro oxygen with a distance of 3.14 Å.

2.10 Thermal Analysis of PolynitroPCP's

The thermal analysis of the new tetranitroPCP's and the trinitroPCP provided insight into likely decomposition processes. As previously discussed, nitroaromatic compounds can decompose by a variety of reaction pathways. As Figure14 on page 16 illustrates, the more common decomposition pathways are aryl-nitro bond homolysis, nitro-nitrite isomerism, and reaction with *ortho* substituents forming anthranil/benzofurazan compounds [32]. The predicted dominant reaction pathways in the condensed phases at lower temperatures and pressures are clearly the reactions with *ortho* substituents. The aryl-nitro bond homolysis pathway dominates at higher temperatures and pressures as well as gas phase decomposition, which frequently determines shock sensitivity characteristics.

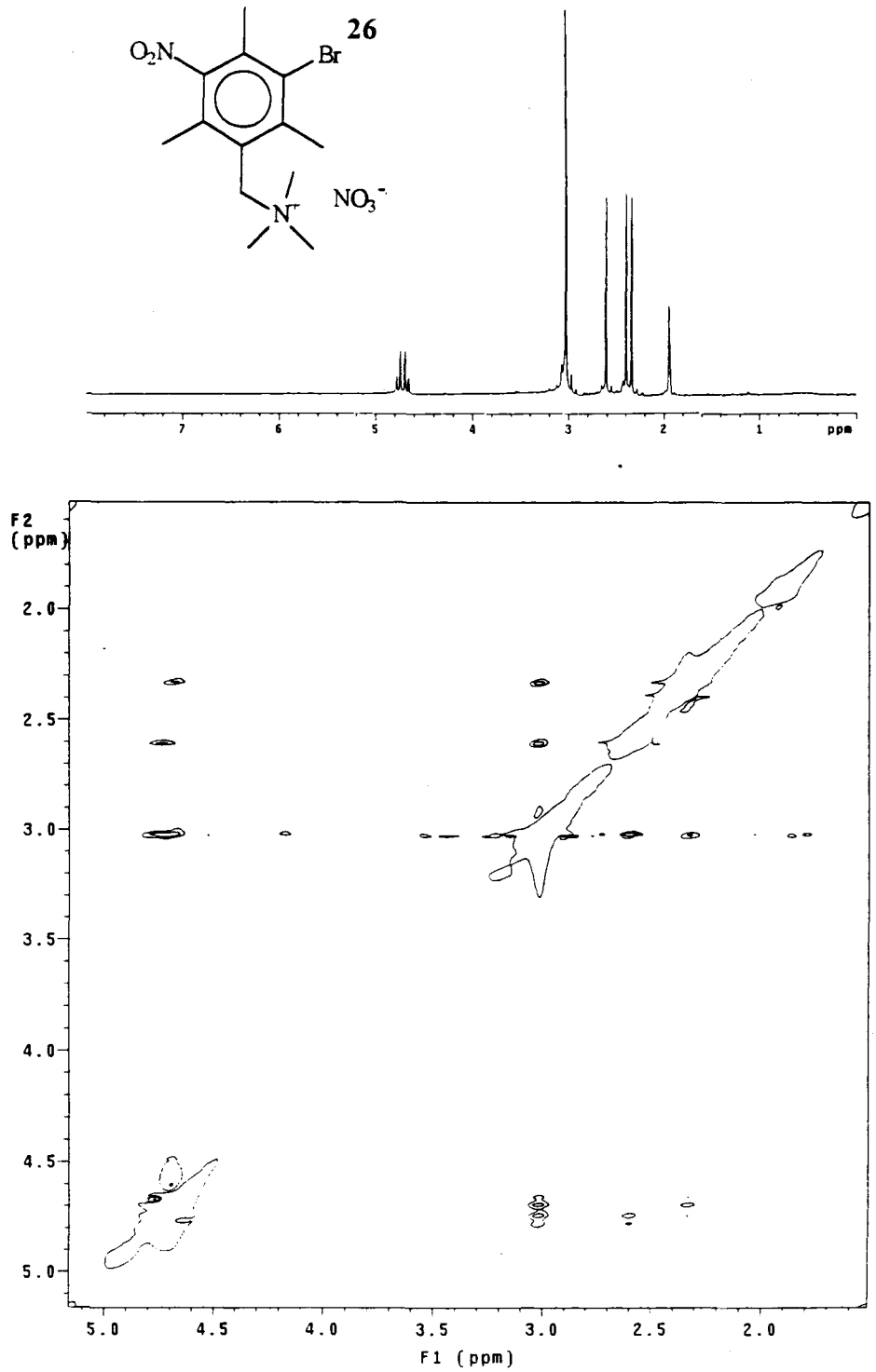

Figure 36 NOESY 2D NMR of Compound **26**

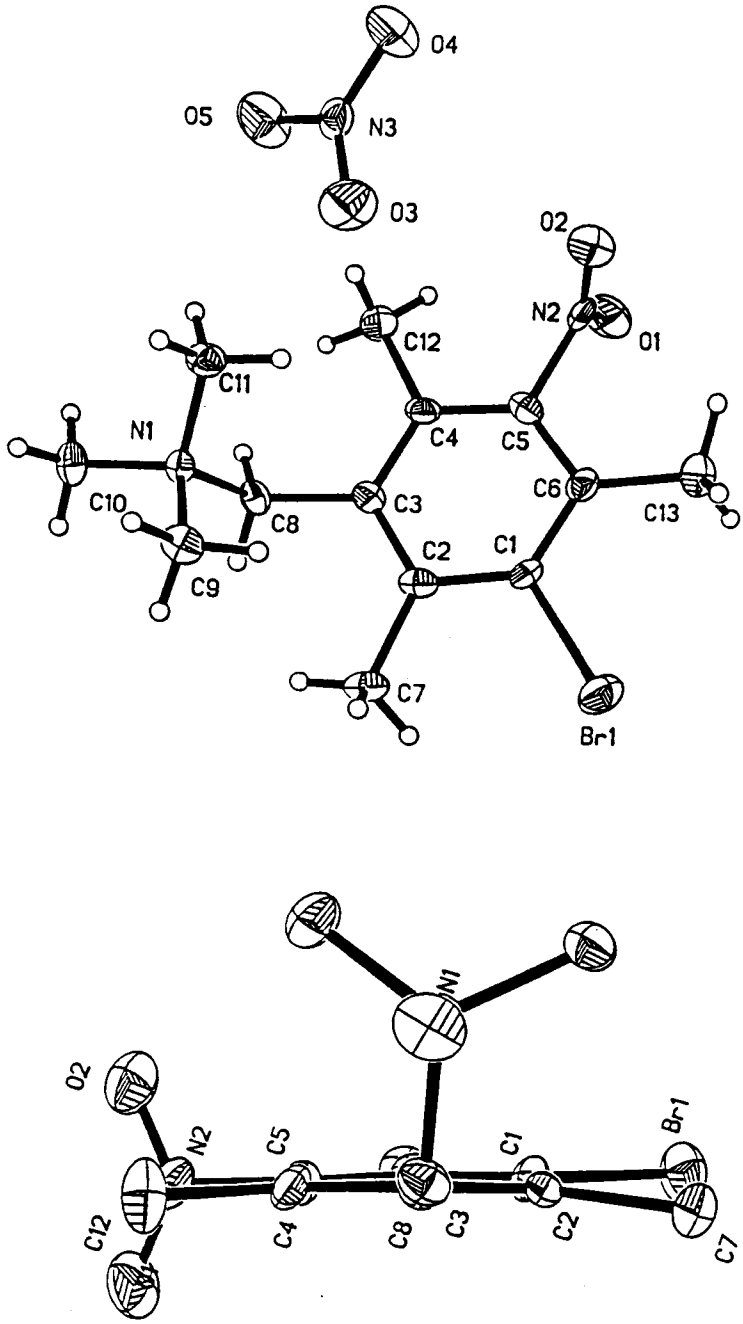

Figure 37 X-ray Crystal Structure of Compound **26**

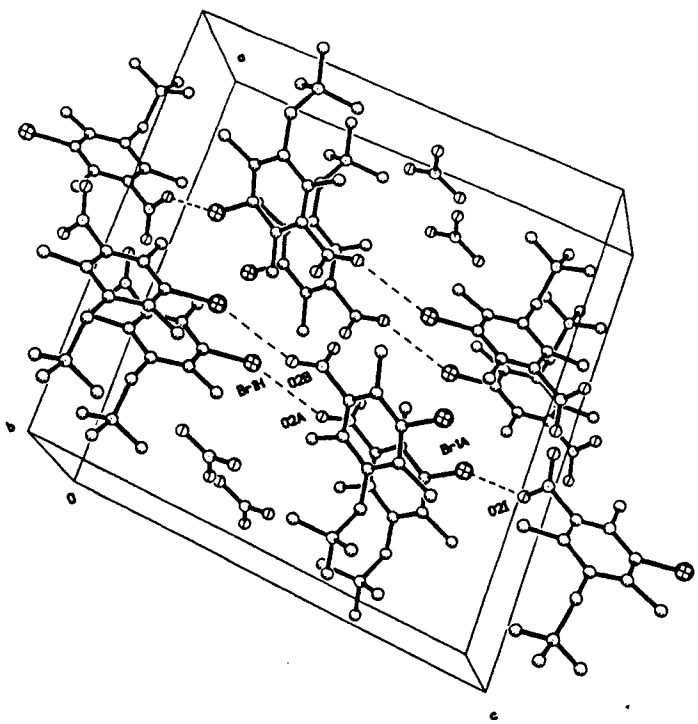

Figure 38 X-ray Crystal Structure Showing Unit Cell of Compound **26**

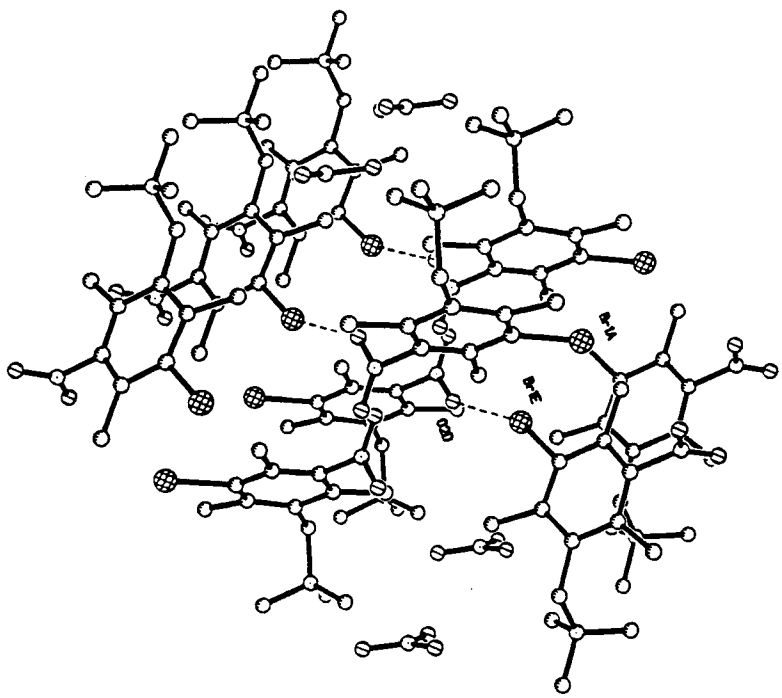

Figure 39 X-ray Crystal Structure Showing Aryl Stacking of Compound **26**

Impact sensitivity is determined by a mixture of the two. The specific role of nitro-nitrite bond homolysis is a clearly lacking area of current knowledge, but most prior work shows it to be of lesser importance. Despite these fairly well determined general principles, the relative importance of intra versus intermolecular interactions in these decomposition pathways is not known. This has a strong bearing on the design of energetic materials, which tends to focus by necessity on the intramolecular issues. The intermolecular issues remain a fairly unknown black box of decomposition importance.

Due to the limited quantities of novel cyclophane materials, thermal characterization was restricted to analysis by Differential Scanning Calorimetry (DSC). For comparison, cyclophanes **15** and **16** previously synthesized by Dr. Morvant were also re-analyzed. Interpretation of DSC decompositions of energetic materials can be difficult. This is primarily due to the evolution of gaseous products that can in essence sweep away heat that would have been recorded on the thermogram. In DSC a small amount of material (1-10 mg) is sealed within an aluminum pan. Typically, this pan is then heated in an small oven. The heat flow is constantly determined by comparison to a mutually heated reference pan. Besides the expected calibration issues both in terms of absolute temperature and heat flow, it is also quite important to maintain effective thermal contact of the sample and any reaction products with the pan and the underlying thermocouple. In the case of energetic materials, the gaseous products produced on decomposition lower the experimental heats of reaction determined by DSC. Heats of detonation or explosion are best determined from bomb calorimetry determined heats of combustion/formation combined with analysis of decomposition byproducts [27, 28]. It should be again noted

that the actual heats of detonation can vary drastically based on the conditions of initiation, pressure, confinement, temperature, moisture content, particle size, etc. The heat of decomposition determined by DSC can be viewed as a lower limit to the heat of detonation. Comparisons of heats of decomposition determined by DSC should be made with extreme caution when there are differences in oxygen balance, chemical structure, decomposition pathways, and ratios of gaseous products. However, DSC can accurately determine the temperature of specific thermal transitions for energetic materials.

All of the tetranitroPCP's and their related polymers as well as the trinitroPCP exhibited strong exothermic decompositions without melting. These decompositions are a unique feature of these polynitrated systems. A similar exothermic decomposition is not seen in dinitrodurene (1,2,4,5-tetramethyl-3,6-dinitrobenzene) [25]. The unique reactivity of these compounds cannot be attributed alone to the molecular structure of the strained PCP system, as the related polymers also exhibit the decomposition as well as the unstrained tetrameric compound **16**. It seems more likely that the exothermic decompositions are a feature of the dinitroaromatic system in the context of an accessible reactive pathway whether through PCP ring opening or polymer chain cleavage. The PCP system does however, impart some unique reactivity to the compounds. The onset temperatures for decomposition are listed with the related compounds in Figure 40. The tetranitro[2.2]PCP decomposition temperatures showed some interesting trends when compared to the polymeric compounds. The compounds **15** and **45** each share equivalent spatial relationships of the methyl and nitro groups on each half of the molecule (bisecting plane passing along the ethano bridge C-C bonds). The difference in the decomposition

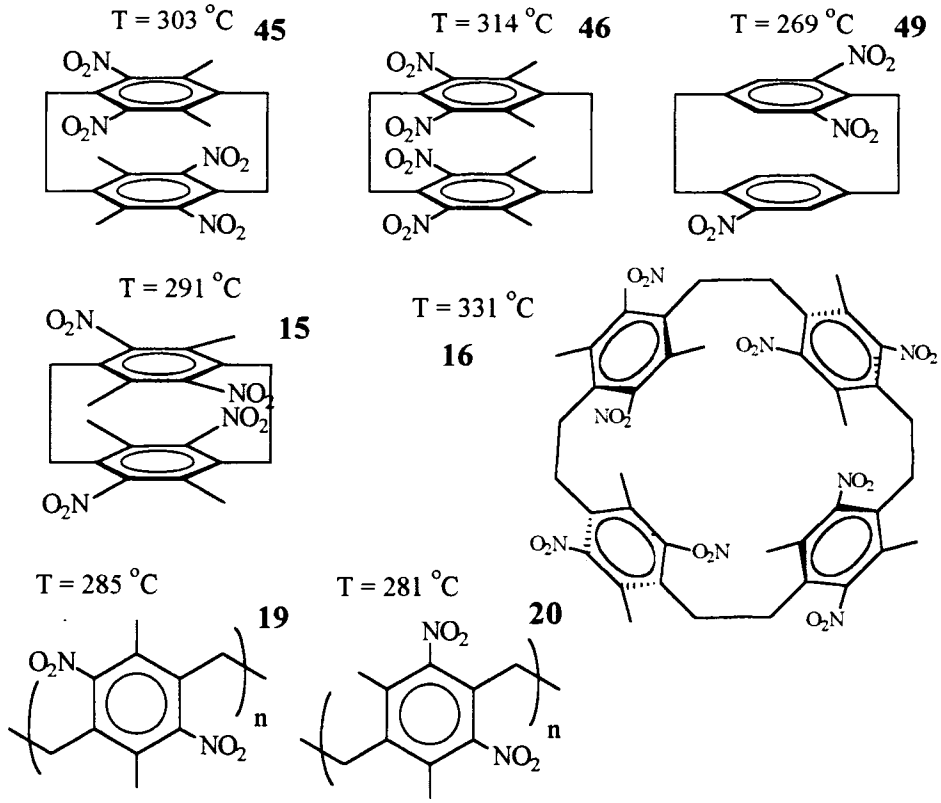

Figure 40. Thermal Decompositions of the PolynitroPCP's

temperatures (12 °C) can only be explained by the relative torsion of the PCP aromatic rings. In compound **15**, an increased twist of the two opposed aromatic rings decreases the steric interactions of both halves of the PCP system. In compound **45**, the increased twist would increase steric interactions on one side and decrease them on the other. This proposed, preferred increase in twist is confirmed in the X-ray structure of **15**, which shows a torsion of the ethano bridges of an average 11.9° [25], compared to the 6° for [2.2]PCP [14]. Compound **46** has a clearly more crowded steric environment with two sets of stacked nitro groups. This increased sterically crowded arrangement seems to delay the decomposition of **46** to the highest temperature (314 °C) of the tetranitro-

tetramethyl[2.2]PCP's. This delay in decomposition could be due to either preferential orientation of the nitro groups so that intramolecular pathways are limited or a relatively more planar orientation of the stacked nitro groups so that intermolecular pathways are limited. This latter interpretation seems more likely particularly when the even higher decomposition temperature (331 °C) of the tetrameric, unstrained **16** is considered. However, a strong conclusion based on intermolecular interactions should not be made without related crystal structure for these compounds. Even the current X-ray structures available for compounds **15** and **16** probably do not accurately reflect the intermolecular distances and interactions involved in the decomposition reactions because those crystals contain included toluene not present in the DSC analyzed solid [25]. However, the unusually higher decomposition temperature for compound **16** is not consistent with a requisite intramolecular nitro group stacked interaction.

The four dinitro[2.2]PCP's have relatively lower decomposition temperatures preceded by a normal melting point: *pg*-**9**-275 °C, *po*-**10**-275 °C, *pm*-7-270 °C, and *pp*-**8**-265 °C. These decomposition temperatures are only slightly higher than TNT's (260 °C) decomposition temperature which is also preceded by a melting point. The relative importance of intermolecular forces has been demonstrated in TNT; TNT vapor shows no decomposition until 301 °C [31]. Among the dinitro[2.2]PCP's, the more sterically crowded compounds **9** and **10** decomposed at slightly higher temperatures relative to the less crowded compounds **7** and **8**. This slight delay in decomposition temperatures of these related compounds can be rationalized again with similar intermolecular and intramolecular interactions. Compounds **9** and **10** have nitro groups which are on the

same side of the [2.2]PCP framework, and hence they can sterically interact forcing a more planar nitro group orientation. Compounds **7** and **8** have nitro groups which are on opposites sides and can adopt a more vertical orientation. The more vertical rather than the more planar orientation may allow a greater intermolecular interaction lowering the decomposition temperature. The collectively lower decomposition temperatures of the dinitroPCP's relative to the tetranitroPCP's can also be explained in terms of the steric environments of the nitro groups. All of the dinitroPCP's would be expected to have more vertically oriented nitro groups relative to the tetranitroPCP's. The single trinitroPCP **49** had a decomposition temperature (269 °C) in the same region as the dinitroPCP's. This would be expected in the context of the less crowded nitro group that is alone on one half of the PCP framework like compounds **7** and **8**.

The two related polymers also each exhibited a significant exothermic decomposition without any obvious melting or glass transition temperature. The polymer **19** derived from the same reaction that produced compounds **15** and **16** decomposed at 285 °C. The similar polymer **20** derived from the same reaction that produced compounds **45** and **46** decomposed at 281 °C. The shape and form of the decompositions of the two polymers **19** and **20** are qualitatively similar. The decomposition temperatures of both polymers were lower than their polynitro[2.2]PCP equivalents by about 6 °C for **19** and 22 °C for **20**. These lower decomposition temperatures can again be explained by either intramolecular or intermolecular pathways, dependent upon the nitro-group orientations which are more limited in the nitro[2.2]PCP equivalent compounds. Both of the polymers **19** and **20** are related to a poly(dinitro-*p*-xylylene) literature reported equivalent which

was synthesized by directly nitrating the parent poly(*p*-xylylene) PPX. While not specifically characterized beyond elemental and general decomposition analysis, the soluble dinitroPPX also exhibited an exothermic decomposition like **19** and **20** but with the sensitivity of PETN or RDX and the power of TNT [137]. This indicated that this exothermic decomposition of the dinitroPPX's is a general feature of their structure.

The heats of decomposition of the polynitroPCP derivatives are listed in Table 3. These values were determined by DSC, and the TNT heat of decomposition as determined on the same instrument under similar conditions is included for comparison. The relative ordering of these heats of decomposition is difficult to explain. The relatively higher heats of decomposition for the polymers can be explained by their greater amounts of carbonaceous residue remaining. This residue may tend to increase the experimental heat of decomposition by retaining more heat relative to the gaseous decomposition products produced preferentially by the other compounds. This difficulty underscores the

Table 3. Heats of Decomposition by DSC (kJ/g)

#	Compound	ΔH_{dec}
45	4,8,12,16-tetramethyl-5,7,13,15-tetranitro[2.2]paracyclophane	2.29
46	4,8,13,15-tetramethyl-5,7,12,16-tetranitro[2.2]paracyclophane	2.04
20	poly(2,6-dimethyl-3,5-dinitro-*p*-xylylene)	2.09
15	*anti*-5,8,13,16-tetramethyl-4,7,12,15-tetranitro[2.2]paracyclophane	2.09
16	*anti*-5,8,13,16,21,24,29,32-octamethyl-4,7,12,15,20,23,28,31-octanitro[2.2.2.2]paracyclophane	1.90
19	poly(2,5-dimethyl-3,6-dinitro-*p*-xylylene)	3.30
TNT	2,4,6-trinitrotoluene	1.56

limitations of DSC for the determination of heats of decomposition when variable gaseous products are produced. For rough comparison the heat of detonation of TNT under typical conditions is 5.40 kJ/g [27]. Heats of detonation and decomposition can vary quite significantly depending on the explosive and conditions. TNT's heat of detonation is one of the lower heats of detonation of the common commercial explosives primarily because of its poor OB. It should be noted that heat of detonation is not absolutely correlated to desired explosive properties. The work of an explosive is done by the expanding gases not necessarily the heat to detonation. This heat of detonation primarily serves as a localized source of energy to propagate the reactions that liberate the desired gaseous products. In that context, a high heat of reaction is not a sole beneficial end-goal.

Another useful predictive measure of explosive properties is the production of gaseous products per gram [29]. As calculated based on the oxygen balance, TNT produces 33.8 mmol/g, and for all of the compounds in Table 3 that number is 22.5 mmol/g. This value is directly related to the specific impulse of an explosive, which is defined as the total thrust per unit weight over the combustion period. The specific impulse combined with a high combustion temperature are the most specific designable features of an explosive. Typically, the specific impulse has optimized by maintaining an oxygen balance near 0 % and a large positive heat of formation, however, the compounds above produce lower molecular weight gaseous products (N_2 and H_2O) at relatively high temperatures due [29]. In apparent contradiction to this desired positive heat of formation, polymer **19**'s heat of formation was experimentally measured in this work by bomb calorimetry to be large and negative: -2502 kJ/mer or 11.27 kJ/g. All of these

surprisingly energetic compounds in Table 3 seem to act as a stable store of gaseous products which are liberated upon decomposition which is initiated by the structural features of the carbon framework of the polynitroPCP's or their related polymers. The relatively high decomposition temperatures are fundamentally due to the unique steric environment of the aryl-nitro group orientations through intermolecular interactions.

2.11 Summary and Conclusions

This work has been successful in synthesizing two novel tetramethyltetranitro-[2.2]PCP's and their related xylylene polymer. All of these compounds exhibited an exothermic decomposition at relatively high temperatures. These unique, higher temperature exothermic decompositions are not solely a result of the strained PCP framework. The unique features of the PCP system or the extended polymer chain do provide reaction pathway(s) for decomposition that are not easily accessible to equivalent dinitrated aromatics. These pathways are most likely related to ethano bridge bond scission uniquely available to these PCP and related polymer systems. The hindered environment of the tetramethyltetranitro[2.2]PCP's does delay the decomposition temperature by up to 33 °C, but this hindrance may be more based on limitations of intermolecular rather than intramolecular interactions. The specific mechanism of this raising of the decomposition temperature is most likely due to hindered nitro group mobility which limits intermolecular interactions, but further work is needed to confirm this. The unnecessary strain energy of the [2.2]PCP system would however, contribute beneficially to the energy liberated during decomposition.

The synthetic schemes reported for the quaternary ammonium salts do provide efficient and simple synthetic routes to compounds **23**, **24**, **25**, and **26**. However, the Hofmann eliminations to produce the ultimately desired tetranitro[2.2]PCP's suffered from zero or unusually low yields. The most likely cause for the failure of the first two Hofmann eliminations is the inherent reactivity of the triply deactivated quaternary ammonium salts to nucleophilic substitution. Other synthetic routes to the tetranitro[2.2]PCP's lacking the detrimental methyl substitutions will most likely require fundamentally different approaches. These deactivated aromatic compounds are most stable to electrophiles and acids rather than the nucleophiles and bases required during the Hofmann elimination. The unusually low yields of the successful Hofmann elimination are most likely due to the adverse steric environment that may tend to produce more polymer rather than dimer from the likely xylylene intermediate. There is a potential to increase these yields somewhat through modification of the reaction conditions using dilution principles or phenothiazine-like radical traps.

Several other more unique synthetic strategies were attempted without significant success. The synthesis of a novel nitrating reagent *t*-butyldimethylsilyl nitrate was accomplished, but the immediate application of this compound to this work was not successful. Other prior work has successfully employed the related, but less stable trimethylsilyl nitrate to electrophilic aromatic nitrations using Lewis acid catalysts.

This work also succeeded in characterizing an uncommon rotational isomerism in a novel quaternary ammonium salt which was synthesized through a novel mechanism. The rotational barrier interconverting the rota-enantiomers indicated that the compounds

should be isolable at room temperature. Beyond a simply Quixotic interest, this salt or other similar derivatives should be able to provide insight into the 1,6-Hofmann elimination mechanism. The posited xylylene intermediate which has a plane of symmetry should provide an exclusively racemic cyclophane product. However, an enantiomeric excess in the cyclophane products would support other more complex mechanisms.

2.12 Experimental

General Methods. All starting materials and solvents were acquired commercially and used without further purification unless stated otherwise. **New Compounds** are marked by an asterisk * in their experimental section. All instrumentation, hardware, and software employed for this research are detailed in Appendix D.

4-Methyl-3,5-dinitrobenzaldehyde (27). A 1L Erlenmeyer flask was filled with concentrated sulfuric acid (400 mL) and placed in an ice bath on a stir plate with a stir bar added. A single aliquot of fuming nitric acid (250 mL) was added to the sulfuric acid, which warmed to approximately 50 °C upon addition. The acid solution was stirred until the temperature decreased to 5 °C. A 100 mL separatory funnel was then filled with *p*-tolualdehyde (54.68 g, 0.4553 mol). The *p*-tolualdehyde was added dropwise to the chilled, stirred acid solution while maintaining the reaction solution between 10-12 °C There was a significant evolution of a brown gas and heating upon addition of the aldehyde. After complete addition taking approximately one hour and 15 minutes, the ice bath was removed and the homogenous clear yellow solution was stirred at room temperature for an additional five hours. The solution was then dumped onto crushed ice

(1L) in a 2L beaker. The precipitated pale yellow-white solid was isolated by vacuum filtration. The crude product was then dissolved in acetone and methylene chloride (4:1, 800 mL total) and stirred overnight in a 1L Erlenmeyer flask covered with foil over anhydrous sodium sulfate and potassium carbonate. After gravity filtration, the filtrate was reduced on a rotary evaporator to give 4-methyl-3,5-dinitrobenzaldehyde (**27**) a yellow-white solid (84.44 g, 88 %): mp 112-113 °C; ^{1}H NMR (300 MHz, $CDCl_3$) δ 10.08 (s, 1H), 8.48 (s, 2H), 2.67 (s, 3H); ^{1}H NMR (300 MHz, DMSO) δ 10.08 (s, 1H), 8.70 (s, 2H), 2.55 (s, 3H); ^{13}C NMR (75 MHz, $CDCl_3$, decoupled) δ 186.9, 152.2, 135.4, 132.9, 127.1, 15.4.

N,N-dimethyl(4-methyl-3,5-dinitrobenzyl)amine (28)*. The starting material, 4-methyl-3,5-dinitrobenzaldehyde (**27**) (10.29 g, 49.00 mmol, 1 eq) and dimethylammonium chloride (24.57 g, 3013 mmol, 6.1 eq) were added to a 250mL round bottom flask. Formic acid (88 %, 75 mL) was then added. The reaction flask was set-up with a heating mantle, water jacketed condenser, and stir bar. The reaction mixture was heated to a gently reflux solvent for 68 hours. The condenser was removed to allow a portion (40 mL) of the reaction solvent (mostly formic acid) to boil off. The heating mantle was removed so that the solution could cool to room temperature. The reaction solution was transferred to a 1L beaker with methylene chloride (300 mL), deionized water (100 mL), and a stir bar. Potassium carbonate was added to the vigorously stirred beaker solution until the water layer tested to a pH of >10 with litmus paper. A significant amount of carbon dioxide evolves during the neutralization procedure. The biphasic solution was transferred to a 1 L separatory funnel. The organic layer was removed. The aqueous

layer was extracted with methylene chloride (100mL). The combined organic layers were dried over anhydrous sodium sulfate, gravity filtered, and reduced by rotary evaporation. The product, a light brown tarry solid not unlike peanut butter in appearance (13.55 g), was analyzed. The product was a mixture of the desired N,N-dimethyl(4-methyl-3,5-dinitrobenzyl)amine (**28**) and a side-product dimethylformamide (DMF). The yield of **28** (11.25 g, 96 %) was calculated by ^{1}H NMR ratio to DMF. Further isolation was not performed because the next reaction completely separated the target compound from the confounding and persistent DMF. ^{1}H NMR (300 MHz, DMSO) δ 8.14 (s, 2H), 7.95 (s, DMF), 3.54 (s, 2H), 2.89 (s, DMF), 2.73 (s, DMF), 2.43 (s, 3H), 2.18 (s, 6H); ^{1}H-NMR (300 MHz, $CDCl_3$) δ 8.00 (s, DMF), 7.96 (s, 2H), 3.50 (s, 2H), 2.95 (s, DMF), 2.87 (s, DMF), 2.53 (s, 3H), 2.26 (s, 6H).

N,N,N-trimethyl(4-methyl-3,5-dinitrobenzyl)ammonium iodide (24)*. The starting material, N,N-dimethyl(4-methyl-3,5-dinitrobenzyl)amine (**28**), as a tarry mixture with DMF impurity (13.55g total, 11.25 g **28**, 47.03 mmol **28**, 1 eq) was dissolved in THF (150 mL) in a 250 mL round bottom flask with a stir bar and septum. Methyl iodide (3.5 mL, 56 mmol, 1.2 eq) was added to the reaction flask with stirring. The solution was stirred at room temperature overnight. The product, N,N,N-trimethyl(4-methyl-3,5-dinitrobenzyl)ammonium iodide (**24**) a yellow powder, precipitates from the THF solution and is isolated by vacuum filtration. The product was rinsed with two 25 mL portions of THF, and dried under vacuum overnight giving a final yield of 16.84 g, 94 %. mp 184-205 °C progressive darkening, 210 °C charring, 218 °C oil ; ^{1}H NMR (300 MHz, DMSO) δ 8.45 (s, 2H), 4.71 (s, 2H), 3.07 (s, 9H), 2.51 (s, 3H); ^{13}C NMR (75 MHz, DMSO,

decoupled) δ 156.4, 137.1, 133.8, 129.7, 70.9, 57.6, 19.7; MS-FAB in 3NBA for $C_{11}H_{16}N_3O_4$-254 + I, m/e (rel intensity) 255 (18), 254 (100, M+), 238 (10), 154 (29), 137 (16), 136 (20).

2,5-Dimethyl-4-nitroaniline (32). A 500 mL round bottom flask was filled with concentrated sulfuric acid (250 mL) and placed on a stir plate with a stir bar added. The starting material, 2,5-dimethylaniline (12.3 g, 0.102 mol) was added dropwise to the reaction flask over ten minutes. Following addition of the aniline, the reaction slurry was stirred at room temperature for 1.5 hours to dissolve the anilinium salt which formed during the addition. Concentrated nitric acid (10 mL, 1.6 eq based on 70 % HNO_3) was added dropwise to the solution over five minutes with rapid stirring. During the addition the reaction solution warmed slightly to 35 °C. The reaction was stirred at room temperature for two hours. During the reaction a sodium hydroxide solution was prepared by dissolving pellets (400 g, 10 mol) in deionized water to a total volume of 500 mL. This base solution was chilled in a freezer to about 10 °C. The acid reaction solution was dumped on crushed ice (1L). This acid/ice slush was poured slowly into the sodium hydroxide solution in a 2 L beaker with vigorous stirring. The final pH of the combined solution tested to >12 and the temperature was near 25 °C. This aqueous solution was then extracted 10 times with 200 mL portions of methylene chloride. The combined organic extracts were then dried over anhydrous sodium sulfate, gravity filtered, and reduced by rotary evaporation to yield a red-brown tarry product (12.3 g). The total yield of the desired 2,5-dimethyl-4-nitroaniline (**32**) and side product 2,5-dimethyl-6-nitroaniline **32b** was 73 %. The yield of **32** alone was 53 % determined from ^{1}H NMR. The ratio of

ortho to *para* substitution was 0.379. Extensive isolation and analysis of the product was not attempted due to the conditions and results of the next reaction. ^{1}H NMR (400 MHz, $CDCl_3$) δ 7.93 (s, 1H, **32**), 7.07 (d, J = 9 Hz, 1H, **32b**), 6.53 (d, J = 9 Hz, 1H, **32b**), 6.45 (s, 1H, **32**), 5.10 (br, 2H, **32b**), 4.18 (br, 2H, **32**), 2.53 (s, 3H, **32**), 2.39 (s, 3H, **32b**), 2.17 (s, 3H, **32b**), 2.13 (s, 3H, **32**).

1,4-Dimethyl-2,5-dinitrobenzene (33). The starting material, a tarry mixture of 2,5-dimethyl-4-nitroaniline (**32**) and 2,5-dimethyl-6-nitroaniline **32b** (16.46 g, 99.06 mmol total, 1 eq total, 71 mmol **32**) was dissolved in trifluoroacetic acid (TFA) (170 mL) in a 250 mL beaker. Hydrogen peroxide 30 % aq. (57.4 g, 495 mmol, 5 eq) was mixed with 75 mL TFA in a 125 mL Erlenmeyer flask and stirred for 10 minutes. The starting material solution and the peroxide solution were combined in a 500 mL round bottom flask equipped with a stir bar and a water condenser. The solution autocatalytically heated to about 50 °C. The reaction was allowed to stir under self-heating for 2.5 hours at which point it had cooled to room temperature. The solution was then dumped into crushed ice (250 mL) with deionized water (500 mL). An orange solid precipitated upon dumping into the ice-water. The product solid was isolated by vacuum filtration and subsequently vacuum dried overnight at room temperature. The product was dissolved in methylene chloride/diethyl ether (200 mL, 1:2). The organic solution was washed with saturated sodium carbonate (100 mL), separated from the aqueous layer, dried over anhydrous sodium sulfate, gravity filtered, and reduced by rotary evaporation. The crude product (9.53 g, 49 % based on mmol total) was a mixture of the desired product, **33** (52 % crude yield by ^{1}H NMR based on 71 mmol **32**) and the isomer **32b**. The crude product was then

recrystallized in absolute ethanol to give 5.00 g of pure **33** by ^{1}H NMR (36 % based on 71 mmol **32**). Recrystallization byproducts were not isolated further. ^{1}H NMR (300 MHz, $CDCl_3$) δ 7.92 (s, 1H), 2.62 (s, 3H); ^{1}H NMR (300 MHz, DMSO) δ 8.13 (s, 1H), 2.51 (s, 3H).

1-Bromomethyl-4-methyl-2,5-dinitrobenzene (34)*. The starting material, 1,4-dimethyl-2,5-dinitrobenzene (**33**) (4.76 g, 24.2 mmol, 1 eq) was placed in a 250 mL round bottom flask with a stir bar, heating mantle, water condenser, septum, and drying tube. Freshly recrystallized N-bromosuccinimide (NBS) (8.63 g, 48.5 mmol, 2 eq) was added to the flask which was filled with carbon tetrachloride (200 mL). Benzoyl peroxide (BPO) (0.589 g, 2.4 mmol, 0.1 eq) was added. The flask was heated to reflux solvent for 19 hours. At that point, the reaction solution was vacuum filtered to remove the NBS byproducts. The resultant organic layer was washed 10 times with 100 mL portions of a saturated sodium carbonate solution mixed with equal parts deionized water. The final washed organic layer was separated, dried over anhydrous sodium sulfate, and reduced by rotary evaporator. The product (5.65 g) was 53 % **34** and 47 % starting material **33** by ^{1}H NMR. Further isolation was not attempted as the next reaction easily separates the compounds. The yield of **34** by ^{1}H NMR was 45 %. The product **34** is a mild lachrymator and the use of gloves for all handling is recommended. ^{1}H NMR (300 MHz, $CDCl_3$) δ 8.16 (s, 1H, **34**), 8.01 (s, 1H, **34**), 7.92 (s, 1H, **33**), 4.80 (s, 2H, **34**), 2.68 (s, 3H, **34**), 2.62 (s, 3H, **33**).

N,N,N-trimethyl(4-methyl-2,5-dinitrobenzyl)ammonium bromide (23)*. The combined product (3.57 g, 50 % **34**, 6.49 mmol **34**, 1 eq) containing the bromomethylated **34** and the non-reactive **33** was placed in a 250 mL side-arm, round bottom flask with septum and stir bar. The reaction flask was filled with anhydrous diethyl ether (150 mL). A 125 mL side-arm Erlenmeyer flask was charged with trimethylammonium chloride (3.15 g, 33.0 mmol, 5 eq). The Erlenmeyer flask was capped with a septum and attached to the reaction flask via tygon tubing with an intervening potassium hydroxide (pellets) drying tube. The entire system was then evacuated via needle cannulation through the reaction flask. The vacuum was removed a minute or so after the diethyl ether began to boil. Sodium hydroxide 5N (8.1 mL, 41 mmol, 6.3 eq) was added in 2 mL portions at ~5 minute intervals to the Erlenmeyer flask through the septum by syringe. Trimethylamine gas was seen evolving with resultant precipitation of product in the reaction flask. Typically, two more short (10 s) evacuations were performed through the reaction flask septum. The progressive evacuations were balanced with slow addition of the sodium hydroxide to maintain the entire apparatus at slightly below atmospheric pressure as indicated by distension of the septa. This apparatus and addition method maintained relatively tight control on the evolution of the noxious and malodorous trimethylamine gas. After the final addition of sodium hydroxide, the reaction flask was stirred overnight under the trimethylamine atmosphere. The crude precipitated product **23**, a tan solid, was isolated by simple vacuum filtration with two subsequent washes of 25 mL portions of anhydrous diethyl ether. The product N,N,N-trimethyl(4-methyl-2,5-dinitrobenzyl)ammonium bromide **23** was vacuum dried at room temperature and analyzed

giving 2.01 g, 93 % based on 6.5 mmol **34**. The non-reactive 1,4-dimethyl-2,5-dinitrobenzene (**33**) was recovered from the filtrate by simple rotary evaporation (1.19 g, 67 % recovered based on 1.79 g **33**). mp 150-165 °C progressive darkening, 180 °C oil ^{1}H NMR (300 MHz, DMSO) δ 8.47 (s, 1H), 8.37 (s, 1H), 4.91 (s, 2H), 3.08 (s, 9H), 2.64 (s, 3H).

Bromomethylmesitylene (37), 1-bromomethyl-2,4,6-trimethylbenzene. The starting material, mesitylene (52.17g, 0.4340 mol, 1 eq), was placed in a 500 mL round bottom flask with a stir bar, water condenser, and heating mantle. Paraformaldehyde (13.23 g, 0.4406 mol (CH_2O), 1 eq) was added to the flask which was filled with glacial acetic acid (400 mL). Hydrobromic acid (50 mL) 48 % solution in water was added to the reaction flask which was heating at 74 °C for 3.5 hours. The warm reaction solution was dumped directly onto crushed ice (1 L). A white precipitate, **37**, formed immediately. The product was isolated by vacuum filtration and washed with 3 portions of deionized water (50 mL ea). The bromomethylmesitylene was vacuum dried at room temperature yielding 71.51 g, 77 %. It should be noted that bromomethylmesitylene is a persistent and extreme lachrymator. Use of gloves and a fume-hood for all handling is strongly encouraged. mp 41-42 °C (lit. mp 46-47 °C) [70] ; ^{1}H NMR (300 MHz, $CDCl_3$) δ 6.87 (s, 2H), 4.58 (s, 2H), 2.39 (s, 6H), 2.28 (s, 3H).

N,N,N-trimethyl(2,4,6-trimethylbenzyl)ammonium bromide (38)*. The starting material bromomethylmesitylene **37** (4.36 g, 20.5 mmol, 1 eq) was placed in a 150 mL side-arm Erlenmeyer flask with septum and stir bar. This reaction flask was filled with anhydrous diethyl ether (100 mL). A 50 mL side-arm Erlenmeyer flask was charged with

trimethylammonium chloride (10.2 g, 107 mmol, 5 eq) and sodium hydroxide pellets (5.35 g, 134 mmol, 6.3 eq). The Erlenmeyer flask was capped with a septum and attached to the reaction flask using tygon tubing with an intervening potassium hydroxide (pellets) drying tube. The entire system was evacuated via needle cannulation through the reaction flask. The vacuum was removed a minute or so after the diethyl ether began to boil. Deionized water (10 mL) was added dropwise over 30 minutes to the trimethylammonium chloride/sodium hydroxide Erlenmeyer flask through the septum by syringe. Trimethylamine gas was seen evolving with resultant precipitation of product in the reaction flask. Typically, two more short (10 s) evacuations were performed through the reaction flask septum. The progressive evacuations were balanced with slow addition of the water to maintain the entire apparatus at slightly below atmospheric pressure as indicated by distension of the septa. This apparatus and water addition to the combined solids maintained even tighter control on the evolution of the trimethylamine gas. After complete addition of the water, the reaction flask was stirred overnight under the trimethylamine atmosphere. The crude precipitated product **38**, a white powder, was isolated by simple vacuum filtration with two subsequent washes of 25 mL portions of anhydrous diethyl ether. The product N,N,N-trimethyl(2,4,6-trimethylbenzyl)ammonium bromide **38** was vacuum dried overnight at 80 °C and analyzed giving 5.31 g, 95 %. mp 211 °C softening with contraction 221-267(end) °C light browning to caramelized oil; ^{1}H NMR (300 MHz, DMSO) δ 7.01 (s, 2H), 4.59 (s, 2H), 3.03 (s, 9H), 2.40 (s, 6H), 2.25 (s, 3H); ^{1}H NMR (300 MHz, $CDCl_3$) δ 7.00 (s, 2H), 4.89 (s, 2H), 3.44 (s, 9H), 2.52 (s, 6H), 2.30 (s, 3H); MS-FAB in NBA for $C_{13}H_{22}N$-192 + Br, m/e (rel intensity) 193 (21, M+1),

192 (100, M+), 191 (2), 176 (4), 145 (3), 134 (14),133 (97), 132 (14), 119 (4), 117 (3), 115(2).

N,N,N-trimethyl(2,4,6-trimethyl-3,5-dinitrobenzyl)ammonium nitrate (25)*. The starting material, N,N,N-trimethyl(2,4,6-trimethylbenzyl)ammonium bromide **38** (8.19 g, 30.0 mmol, 1 eq), was dissolved in dry acetonitrile (200 mL) in a 250 mL Erlenmeyer flask with a stir bar. Silver nitrate (5.1 g, 30 mmol, 1 eq) powder was added to the flask. The flask was covered with foil and stirred for two hours. The insoluble powder changed in appearance (silver nitrate exchanged for silver bromide). The reaction solution was vacuum filtered to remove the precipitated silver bromide. The N,N,N-trimethyl(2,4,6-trimethylbenzyl)ammonium nitrate solution was reduced by rotary evaporation. The intermediate nitrate salt (7.31 g, 96 %, 28.8 mmol) was transferred to a 250 mL round bottom flask with a stir bar and ice bath. Fuming nitric acid (40 mL) was added dropwise to the powder with vigorous stirring while maintaining the temperature below 5 °C. After complete addition of the fuming nitric acid, the solution was allowed to warm to room temperature. After five hours at room temperature, the fuming nitric acid solvent was removed by low pressure rotary evaporation using a vacuum pump without heating. The yellow, wet solid was dissolved in dry acetonitrile (15 mL). Diethyl ether (100 mL) was added to precipitate the desired product. The N,N,N-trimethyl(2,4,6-trimethyl-3,5-dinitrobenzyl)ammonium nitrate **25** was collected by vacuum filtration and vacuum dried at room temperature. The yield of **25** was 5.47 g, 16.0 mmol, 55 % based on the nitrate salt, and 53 % based on **38**. mp 190 °C yellowing 241-242 °C decomp; ^{1}H NMR (400 MHz, CD_3CN) δ 4.68 (s, 2H), 3.06 (s, 9H), 2.42 (s, 6H), 2.21 (s, 3H).

N,N,N-trimethyl(3-bromo-2,4,6-trimethyl-5-nitrobenzyl)ammonium nitrate (26)*. Fuming nitric acid (50 mL) was placed in a 100 mL round bottom flask with a stir bar and ice bath. The acid was chilled to 0 °C. The starting material, N,N,N-trimethyl(2,4,6-trimethylbenzyl)ammonium bromide **38** (10.01 g, 36.78 mmol, 1 eq), was added with rapid stirring. There was a significant evolution of a brown gas upon addition. After complete addition of **38**, the solution was allowed to warm to room temperature. After five hours at room temperature, the fuming nitric acid solvent was removed by low pressure rotary evaporation using a vacuum pump without heating. The resultant oil was dissolved in dry acetonitrile (25 mL). The acetonitrile solution was stirred over excess solid potassium carbonate for one hour, and filtered. The acetonitrile solution was dried over anhydrous magnesium sulfate for one hour, gravity filtered, and reduced in volume by rotary evaporation. The yield of N,N,N-trimethyl(3-bromo-2,4,6-trimethyl-5-nitrobenzyl)ammonium nitrate **26** was 13.84 g, 99.5 % based on **38**. mp 210 °C yellowing 222-224 melt with decomp; ^{1}H NMR (400 MHz, CD_3CN) δ 4.79 (d, J = 15 Hz, 1H), 4.63 (d, J = 15 Hz, 1H) 3.02 (s, 9H), 2.60 (s, 3H), 2.39 (s, 3H), 2.33 (s, 3H); ^{13}C NMR (125 MHz, CD_3CN, decoupled) δ 153.2, 144.4, 132.9, 131.1, 129.4, 127.0, 63.7, 53 8. 24.4, 19.9, 16.4; MS-FAB in 3NBA for $C_{13}H_{20}N_2O_2Br$, m/e (rel intensity) 317 (6, M+2),315 (5, M+).

N,N,N-trimethyl(2,4,6-trimethyl-3,5-dinitrobenzyl)ammonium nitrate (25) reaction with sodium bromide in fuming nitric acid. The starting material **25** (75 mg, 0.22 mmol, 1 eq) was combined with sodium bromide (93 mg, 0.91 mmol, 4 eq) in a 10 mL round bottom vial with a stir bar and septum. The vial was filled with fuming nitric acid (5

mL) and stirred at room temperature for 4.5 hours. The fuming nitric acid was removed by low pressure rotary evaporation using a vacuum pump without heating. The resulting solid was triturated with acetonitrile (5 mL). The trituration vacuum filtrate was dried over anhydrous magnesium sulfate, filtered, and reduced by rotary evaporation. The product, a yellow/white solid, was identified by proton NMR as recovered starting material (66 mg, 88 % recovered). ^{1}H NMR (400 MHz, CD_3CN) δ 4.68 (s, 2H), 3.06 (s, 9H), 2.42 (s, 6H), 2.21 (s, 3H).

General Hofmann elimination procedure. The quaternary ammonium halide (10.0 mmol, 1 eq) was dissolved (or slurried in the case of limited solubility) in deionized water (75 mL) in a 125 mL Erlenmeyer flask with a stir bar. Freshly precipitated silver oxide (10.0 mmol, 1 eq) as a wet paste was added to the Erlenmeyer flask. The slurry was stirred at room temperature for approximately one hour. The silver oxide was previously prepared from mixing solutions of potassium hydroxide (1.12 g, 20.0 mmol, 2eq) dissolved in water (30 mL) and silver nitrate (3.40 g, 20.0 mmol, 2 eq) dissolved in water (30 mL). The gray-black silver oxide immediately precipitated. It was isolated by vacuum filtration followed by three water (10 mL ea) rinses. After one hour of stirring, the quaternary ammonium hydroxide solution was filtered by vacuum filtration to remove the precipitated silver halide and excess silver oxide. The aqueous quaternary ammonium hydroxide filtrate was transferred to a 1L round bottom reaction flask which had been previously filled with toluene (500 mL). The reaction flask was fitted with a stir bar, heating mantle, Dean-Stark water separator, and water condenser. The reaction flask was heated at a gentle reflux until the water had been completely removed, approximately one

to two hours. The reaction flask was further heated at reflux for an additional eight hours. After the eight hours, the precipitate (mostly polymer) formed during the reaction was separated by vacuum filtration. The filtrate was reduced by rotary evaporator to produce the primary small molecule products in approximately 10-15 % yield based on xylylene equivalents.

Modified Hofmann elimination procedures.

Dilution procedure. This modification involved the progressive addition of the quaternary ammonium hydroxide solution (75 mL) to the refluxing toluene reaction flask. This procedure required the use of an addition funnel placed on the top of a second air or water condenser. A two-neck 1L reaction flask was required instead of the prior single-neck flask. The dropwise addition of the quaternary ammonium hydroxide solution was adjusted, so that no visible water remained in the reaction flask during the procedure. This modified addition took approximately four hours. The final toluene reaction solution was heated for an additional six hours.

Alternative solvents. Toluene was substituted with mesitylene, xylene, benzene, and cyclohexane. Any solvent that is not water-miscible, less dense than water, and forms a low-boiling point azeotrope with water may be used.

Ion-exchange resin. The quaternary ammonium hydroxide salt was generated by the use of an anion-exchange resin, Dowex 550A OH. This modified procedure was required when the quaternary ammonium counter ion was not a halide. Specifically, compounds **25** and **26**, both nitrates, required the procedure. The Dowex hydroxide resin (4 meq OH/g) (80 meq OH, 8 eq) was slurried in excess deionized water, and stirred for 30 minutes.

The resin was packed into a chromatography column. The quaternary ammonium salt (10 mmol, 1 eq) was dissolved in a water/acetonitrile solution (100 mL, 1:1). The quaternary ammonium salt solution was loaded and percolated through the column using an additional 100 mL of water/acetonitrile (1:1). Complete elution was confirmed by testing the eluent with litmus paper pH (< 8) The quaternary ammonium hydroxide solution was transferred to the reaction flask for a general Hofmann elimination procedure.

Oxygen sparging. The dilution Hofmann procedure above was modified to include the use of oxygen gas bubbled through the silver oxide exchange reaction and in the toluene during the dropwise addition of the quaternary ammonium hydroxide solution. A moderate oxygen flow rate (>10-15 bubbles/s) through a frit was maintained throughout the entire reaction.

Hofmann elimination on N,N,N-trimethyl(4-methyl-3,5-dinitrobenzyl)ammonium iodide (24). The starting material compound **24** (3.85 g, 10.1 mmol, 1eq) was treated according to the dilution procedure modification of the general Hofmann elimination. Sodium hydroxide was used in place of potassium hydroxide. The silver oxide exchange reaction lasted 1.5 hours, and dropwise addition of the resulting quaternary ammonium hydroxide solution took two hours. There was a noticeable aroma of trimethylamine during the exchange reaction and a color change to a deep red/brown. During the thermolysis, a dark brown/purple solid precipitated from the toluene. The pasty solid (0.996 g) was isolated by vacuum filtration. The filtrate was reduced in volume to give a small amount of a yellow/white solid (0.001 g). Trituration of the solid in a soxhlet extractor with toluene produced a small amount of starting material **24**, identified by ^{1}H

NMR and MS-FAB (M+, 254) in accordance with its synthesis above. No other identifiable compounds could be separated from the solid extract. The small amount of soluble material isolated from the original toluene filtrate showed a trace of the presumed cyclophane product **42**, 4,8,12,16-tetranitro[2.2]paracyclophane. The synthesis of the product **42** was not reproducible. The primary purple/brown solid could be separated into a brown powdered material, which was wholly insoluble in all tested solvents, and a dark purple solid which was hygroscopic and soluble in water, DMSO, TFA, and acetone. The solid was separated by trituration with acetone followed by vacuum filtration. ^{1}H NMR (300 MHz, Acetone) δ 7.83 (m, 1H), 7.44 (m, 1H), 3.79 (m, 1H), 3.03 (m, 1H); ^{1}H NMR (300 MHz, C_6D_6) δ 7.69 (m, 1H), 7.39 (m, 1H), 3.59 (m, 1H), 2.88 (m, 1H); ^{1}H NMR (300 MHz, $CDCl_3$) δ 7.73 (m, 1H), 7.41 (m, 1H), 3.74 (m, 1H), 3.00 (m, 1H).

Hofmann on N,N,N-trimethyl(4-methyl-3,5-dinitrobenzyl)ammonium iodide (24) with oxygen sparging. The starting material **24** (4.83 g, 12.7 mmol) was treated according to the oxygen sparging modification of the general Hofmann procedure. After the dropwise addition over 1.5 hours and the subsequent overnight thermolysis, the insoluble purple/brown solid had the same appearance as the other similar unsuccessful reaction on **24**. Inspection of the product by ^{1}H NMR showed no discernible compounds.

Hofmann on N,N,N-trimethyl(4-methyl-3,5-dinitrobenzyl)ammonium iodide (24) in Xylene. The starting material **24** (10.04 g, 26.4 mmol) was treated according to the dilution procedure modification of the general Hofmann elimination with the use of xylenes instead of toluene. The product from the reaction was completely insoluble and brown in appearance (3.95g).

Hofmann on N,N,N-trimethyl(4-methyl-3,5-dinitrobenzyl)ammonium iodide (24) in cyclohexane. The starting material **24** (4.10 g, 10.8 mmol) was treated according to the general Hofmann procedure with the use of cyclohexane instead of toluene. A semi-crystalline dark purple solid formed during the reaction and was isolated by filtration (1.71 g). The solid appeared identical to the solid produced from the more standard toluene procedure. The solid was wholly soluble in polar protic solvents. There was no brown insoluble material formed at the lower temperature of the cyclohexane. The semi-crystalline dark purple solid (0.701 g) was heated overnight at reflux in toluene/water (50 mL, 4:1) in a 50 mL round bottom flask with a water condenser and stir bar. The primary product from the second pyrolysis was a brown insoluble paste.

Reaction of N,N,N-trimethyl(4-methyl-3,5-dinitrobenzyl)ammonium iodide (24) with potassium *t*-butoxide. The starting material **24** (2.10 g, 5.51 mmol, 1 eq) was added to *t*-butanol/toluene (250 mL, 1:4) in a 250 mL round bottom flask with a stir bar, heating mantle, and water condenser. Potassium *t*-butoxide (0.74 g, 6.6 mmol, 1.2 eq) was added with an immediate color change upon addition (brown). The reaction was stirred at room temperature for two hours. The reaction was heated at reflux overnight A brown precipitate (0.671 g) was isolated by vacuum filtration. No product could be identified by ^{1}H NMR in the toluene/t-butanol solvent.

Hofmann on N,N,N-trimethyl(4-methyl-2,5-dinitrobenzyl)ammonium bromide (23). The starting material **23** (1.56 g, 4.67 mmol, 1eq) was treated according to the ion-exchange resin modification of the general Hofmann procedure above. After dissolving **23** in the water/acetonitrile solvent, it was loaded onto the prepared Dowex column. The

column turned from its previous light tan color to a dark black as the starting material migrated down. The column dramatically decreased in volume flow rate leaving a dark band fixed on the top one-fourth. No material could be isolated from the column eluent.

Hofmann on N,N,N-trimethyl(3-bromo-2,4,6-trimethyl-5-nitrobenzyl)ammonium nitrate (26). The starting material **26** (2.81 g, 7.44 mmol) was treated according to the ion-exchange resin modification of the general Hofmann procedure above. After dissolving **26** in the water/acetonitrile solvent, it was loaded onto the Dowex column and eluted through the column without difficulty. The Hofmann also proceeded without obvious black/brown material production. The pyrolysis produced an insoluble tan/yellow powder (0.505 g) and a soluble yellow/orange solid (1.18 g) after removal of the toluene by rotary evaporation. The total yield of product was 89 % (based on xylylene, 7.44 mmol). The crude soluble product was characterized: MS-DIP 12 eV for $C_{10}H_{10}BrNO_2$-255/257, m/e (rel intensity) 273 (2), 255 (100, M+), 257 (97, M+2), 243 (2), 241 (2), 240 (9), 238 (10), 212 (2), 210 (2), 159 (3), 131 (6), 118 (3), 106 (1), 103 (1); ^{1}H NMR (400 MHz, $CDCl_3$) δ 5.22 (s, 1H), 2.54 (s, 2H), 2.35 (s, 2H), 2.24 (s, 2H), 2.07 (s, 2H); ^{13}C NMR (100 MHz, $CDCl_3$, decoupled) δ 170.6, 151.3, 140.7, 132.7, 129.7, 127.7, 126.9, 60.9, 20.8, 20.6, 19.4, 14.1. Further purification was attempted using semi-preparative HPLC (Chloroform/Toluene, 1:1; 2 mL/min). The soluble product (0.44 g) was dissolved in chloroform (1.5 mL). The only significant fraction separated by HPLC analysis was again further analyzed by ^{1}H NMR and ^{13}C NMR. The spectra matched that of the crude product reported above with lesser baseline impurities. The integration ratios changed slightly in the proton spectrum. MS-DIP 12 eV for $C_{10}H_{10}BrNO_2$-255/257, m/e

(rel intensity) 317 (2), 315 (2), 258 (5), 257 (100, M+2), 255 (94, M+), 240 (13), 238 (12), 212 (3), 210 (3), 199 (2), 197 (2), 159 (3), 131 (4), 118 (3); ^{1}H NMR (400 MHz, $CDCl_3$) δ 5.22 (s, 3H), 2.55 (s, 5H), 2.36 (s, 5H), 2.25 (s, 5H), 2.08 (s, 5H); ^{13}C NMR (100 MHz, $CDCl_3$, decoupled) δ 170.7, 151.3, 140.7, 132.6, 129.9, 127.7, 127.0, 61.1, 21.0, 20.8, 19.6, 14.4. Another mass spectrum more clearly indicated a likely cyclophane product: MS-DIP 12 eV for $C_{20}H_{20}Br_2N_2O_4$-510/512/514, m/e (rel intensity) 514 (11, M+4), 512 (22, M+2), 510 (7, M+), 273 (7), 258 (10), 257 (100), 255 (96), 240 (14), 238 (11). Specific assignment and identification of the likely products as *anti*-4,12-dibromo-5,7,13,15-tetramethyl-8,16-dinitro[2.2]paracyclophane **44a** or the *syn* isomer **44b** (or the **45a** and **45b** isomers) was not accomplished.

Hofmann on N,N,N-trimethyl(2,4,6-trimethyl-3,5-dinitrobenzyl)ammonium nitrate (25) yielding 4,8,12,16-tetramethyl-5,7,13,15-tetranitro[2.2]paracyclophane (45)* and 4,8,13,15-tetramethyl-5,7,12,16-tetranitro[2.2]paracyclophane (46)*. The starting material **25** (5.07 g, 14.7 mmol, 1 eq) was treated according to the ion-exchange resin modification of the general Hofmann procedure above. After dissolving **25** in the water/acetonitrile solvent, it was loaded onto the Dowex column and eluted through the column without difficulty. The Hofmann also proceeded without obvious black/brown material production. The pyrolysis was reduced in time to four hours. After the pyrolysis, an insoluble tan/yellow powder was separated by vacuum filtration and vacuum dried (2.19 g). The primary filtrate was reduced by rotary evaporation to yield a yellow/tan solid crude product(1.10 g). The crude product was triturated with acetone (2 mL). A fine light tan powder, a mixture of cyclophanes **45** and **46**, was separated by vacuum

filtration (79.8 mg). The trituration filtrate was reduced by rotary evaporation to yield a mixed unidentifiable product (0.863 g). The products **45** and **46** (51.1 mg total in 2.5 mL CH_2Cl_2) were further purified and separated by semi-preparative HPLC (methylene chloride, 500 µl/injection, 2 mL/min). After combining the multiple injection fractions, the cyclophanes **45** and **46,** and possibly **47** were characterized (18 mg **45**, 7 mg **46**, 1 mg **47**). The compound **47** was tentatively identified as the nitrite ester isomer of **45**, 4,8,12,16-tetramethyl-5-nitrato-7,13,15-trinitro[2.2]paracyclophane The yield based on xylylene was: 1 % total **45**, **46**, and **47**, 67 % insoluble polymeric material, 26 % soluble organic material, for a total of 94 % combined products. **45:** MS-DIP 12 eV for $C_{20}H_{20}N_4O_8$-444, m/e (rel intensity) 445 (4, M+1), 444 (100, M+), 223 (2), 222 (61), 205 (3), 192 (2); ^1H NMR (300 MHz, $CDCl_3$) δ 3.57 (m, 1H), 3.22 (m, 1H), 2.32 (s, 3H); ^1H NMR (300 MHz, CD_2Cl_2) δ 3.55 (m, 1H), 3.21 (m, 2H), 2.30 (s, 6H); ^{13}C NMR (75 MHz, CD_2Cl_2, decoupled) δ 149.7, 143.4, 133.9, 124.6, 29.7, 27.7, 16.7. **46:** MS-DIP 12 eV for $C_{20}H_{20}N_4O_8$-444, m/e (rel intensity) 444 (100, M+), 222 (84), 207 (49), 160 (13); ^1H NMR (300 MHz, $CDCl_3$) δ 3.49 (s, 1H), 3.43 (s, 1H), 2.38 (s, 3H); ^1H NMR (300 MHz, CD_2Cl_2) δ 3.48 (s, 1H), 3.39 (s, 1H), 2.37 (s, 3H); ^{13}C NMR (75 MHz, CD_2Cl_2, decoupled) δ 144.1, 133.9, 125.8, 31.1, 28.7, 16.6. **45** and **46:** (3:1) ^1H NMR (400 MHz, C_6D_6) δ 2.56 (s, 2H), 1.84 (s, 3H). **47:** 428 (9), 427 (100), 222 (26), 206 (5), 205 (35), 192 (4), 189 (3), 188 (8), 176 (4), 161 (8), 159 (7), 148 (3), 146 (4), 133 (3), 132 (6), 86 (4), 84 (5), 49 (3); ^1H NMR (300 MHz, $CDCl_3$) δ 4.05 (m, 1H), 3.54 (m, 2H), 3.44 (m, 2H), 3.19 (m, 2H), 3.09 (m, 1H), 2.55 (s, 3H), 2.31 (s, 3H), 2.92 (s, 3H), 2.13(s, 3H).

***t*-Butyldimethylsilyl nitrate (48)*.** The starting material *t*-butyldimethylsilyl chloride (0.41 g, 2.7 mmol, 1 eq) was dissolved in dry THF in a (7 mL) in a 10 mL round bottom vial with a stir bar and Teflon cap. Powdered silver nitrate (0.96 g, 5.6 mmol, 2 eq) was added to the stirring solution. The reaction vial was stirred overnight in the dark. The *t*-butyldimethylsilyl nitrate was isolated by vacuum filtration to remove the silver chloride and unreacted silver nitrate followed by rotary evaporation to remove the solvent. The yield determined from NMR was 0.40 g, 83 %. TBDMSN slowly produces nitrogen dioxide as it decomposes to the di-*t*-butyldimethylsilyl ether. **48:** ^{1}H NMR (400 MHz, $CDCl_3$) δ 0.98 (s, 3H), 0.41 (s, 2H).

Chapter Three

Poly(2,6-dimethyl-*p*-xylylene)

3.1 Background

As discussed in Section 1.6 and illustrated in Figure 19, there are several commercialized *p*-xylylene polymers with primary applications in the electronics and coatings industries [44, 45]. The xylylene class of polymers can be best characterized as chemically inert, relatively insoluble, electrically resistive, and thermally stable [42].

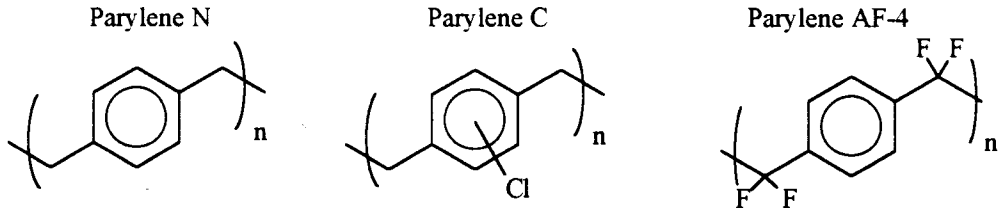

Figure 19 Common Poly(xylylenes)

While the excellent barrier properties of the class provide the primary advantage for coating applications, the required, wasteful vacuum vapor deposition limits many applications where film and spin coating might be more efficient. There are also numerous literature examples of xylylene polymers that have never found a place in the commercial market. Some of these poly(xylylenes) (PPX) are listed in Figure 41 [42, 43, 138-149]

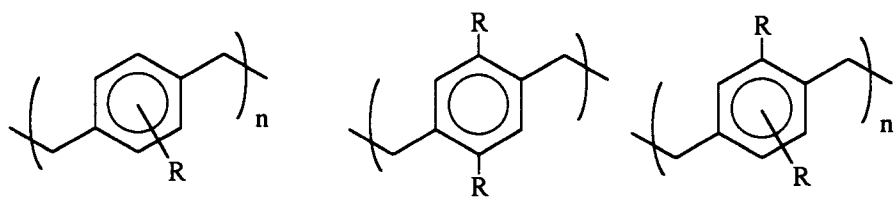

R = H, methyl, ethyl, i-propyl, n-butyl, phenyl, acetyl, cyano, fluoro, chloro, or bromo

R = methyl, ethyl, methoxy, chloro, bromo, or hydroxy

R = ethyl or nitro

Figure 41 Known Poly(xylylenes)

There are also many PPX derivatives with substitutions primarily on the aliphatic portion, such as the commercialized Parylene AF-4 in Figure19 [42]. As this work did not involve such substitutions, they will not be discussed here. The interest in those aliphatic substituted polymers is focused primarily on the parent xylylene rather than the resultant PPX polymer. The phenyl substituted poly(*p*-xylylene), (PPPX) was soluble in common organic solvents at room temperature. PPPX was, hence, the first poly(xylylene)(PPX) to be characterized by common organic techniques [143]. Gel permeation chromatography (GPC) determined the molecular weights, Mn = 8,700 and Mw = 55,000 versus poly(styrene). PPPX was also characterized by ^{1}H and ^{13}C NMR. PPPX did form freestanding films, but the relatively low molecular weights limited the film properties. The alkyl substituted PPX's are progressively more soluble with increasing chain length: 2-methyl-PPX is soluble in hot toluene, 2-ethyl-PPX is soluble in 1,1,2,2-tetrachloroethane at room temperature, and 2-*n*-butyl-PPX is soluble in chloroform at room temperature [43].

The PPX polymers are also generally characterized as highly crystalline (50-70 %) with poly(*p*-xylylene) itself exhibiting multiple crystalline phases [44, 150, 151]. This crystallinity and associated melting points however, decrease with increasing side chain bulk: T_m for PPX 400 °C, T_m for methyl-PPX 205 °C, T_m for ethyl-PPX 165 °C [43]. The PPX's also usually have a glass transition temperature T_g which follows the same trend: 80, 55, 25 °C for H-, methyl-, ethyl-PPX, respectively [43]. The phenyl substituted PPX is a completely amorphous polymer [143]. The ethyl-PPX has been reported to be both crystalline and amorphous depending on synthetic method [143].

The primary synthetic method to prepare the commercialized Parylenes employs the vacuum vapor deposition polymerization known as the Gorham process [42, 43]. The PCP dimer of the desired polymer is pyrolyzed in a vacuum furnace to form the xylylene monomers in the gas phase. These monomers then condense and polymerize on the target surface forming a growing diradical chain. The resultant polymer film is solvent-free, linear, highly crystalline, and high molecular weight. Persistent chain-end free radicals can frequently be measured in the resultant films by ESR spectroscopy. These radicals are protected by the highly crystalline environment, but gradually disappear after exposure to air [43, 152]. Previously, molecular weights have been determined by ESR based end-group analysis and by viscometry for the less common soluble PPX's [143, 152]. The initial molecular weights of the Gorham process films are about M_n = 10,000, but this number changes drastically with time; the actual composition and molecular weights of these later crosslinked and terminated films is difficult to assess [152]. There are many other synthetic methods that produce the non-commercialized PPX polymers. All of the previously discussed methods for synthesizing PCP derivatives also produce polymeric and oligomeric products that are usually discarded without further analysis. This same windfall polymer from a Hofmann elimination produced the novel poly(2,6-dimethyl-*p*-xylylene) **21** which is the focus of this chapter.

3.2 Synthesis of Poly(2,6-dimethyl-*p*-xylylene) (21)

The synthetic approach to the novel poly(2,6-dimethyl-*p*-xylylene) **21** was a serendipitous outcome of the synthesis of the related quaternary ammonium salts **25** and

26 as in Scheme 3. The common intermediate in that synthesis, compound **38**, was the starting material for a general Hofmann elimination in toluene that produced **21**. The Hofmann elimination on **38** (26.8 g) produced high yields of organic products, 87 % based on xylylene. There was a small amount of presumably high molecular weight insoluble product which was not analyzed further (0.80 g, 6 %). After solvent removal the polymer **21** was precipitated by addition of diethyl ether and then isolated by vacuum filtration (1.83 g, 14 %). The filtrate was then reduced, redissolved in toluene, and subsequently triturated with methanol to produce a lower molecular weight polymer (2.23 g, 17 %). The filtrate from the second precipitation and filtration was reduced producing an organic oil (6.42 g, 49 %). The total percent yield of **21** from the starting materials through Scheme 3 following three steps was 10 %.

The three general soluble products from the Hofmann elimination were extensively analyzed. Despite these efforts using column chromatography, GC-MS, ^{1}H NMR, ^{13}C NMR HPLC, recrystallization, and sublimation, the low molecular weight non-polymeric organic compounds could not be identified. The low molecular weight polymer was also analyzed by GPC. The molecular weight distribution of this second polymer fraction was distinctly bimodal with M_n = 892, M_w = 10,100, and PD = 11.3. This second polymer fraction did not produce free standing films from chloroform. In contrast to the other products the first, high molecular weight polymer fraction produced excellent, clear, flexible films from chloroform. The characterization of this polymer **21** will be discussed in the next section.

3.3 Characterization of Poly(2,6-dimethyl-*p*-xylylene) (21)

The novel polymer **21** was characterized by a wide variety of instrumental techniques. The molecular weight distribution analysis of **21** by GPC gave the highest and narrowest molecular weight distribution of any xylylene polymer analyzed by GPC: Mn = 60,510, Mw = 150,500, PD = 2.49 compared to poly(styrene) standards in toluene. This high molecular weight explains the excellent film properties of **21**. Several thin and thick films of **21** were prepared by simple solvation in chloroform. Air evaporation of the chloroform solution on a glass slide produced a flexible film within 15 minutes. Further drying decreases the flexibility with a related increase in film rigidity.

The structure of **21** was analyzed by a variety of NMR spectroscopic methods. The specific structure of the polymer **21** was not exactly certain. As illustrated in Figure 42, the starting quaternary ammonium hydroxide can conceptually eliminate by two pathways producing either *para*- or *ortho*-xylylene. Each of these xylylenes can then dimerize, oligomerize, and polymerize with other xylylenes. It was presumed with the hope of simplicity that one of the pathways would significantly predominate yielding products that were fairly homogeneous in their source xylylene. This hope was supported by the prior results of Dr. Morvant and others. In Morvant's work to produce cyclophanes **15** and **16** from **22** as in Figure 22, there were no *ortho*- or *meta*- xylylene derived products identified. In a similar durene derivative, a Hofmann elimination did produce some *ortho*-xylylene products, but at dramatically lower levels. As in Figure 43, the *ortho*-xylylene product was isolated in approximately 100 times lower yield than the *para*-xylylene product [18]. Interestingly, the polymer of Longone and Chow, an isomer of **21** was not

soluble. Significant concentrations of an *ortho*-xylylene have only been seen in systems in which only the elimination pathway is available [42, 153-155].

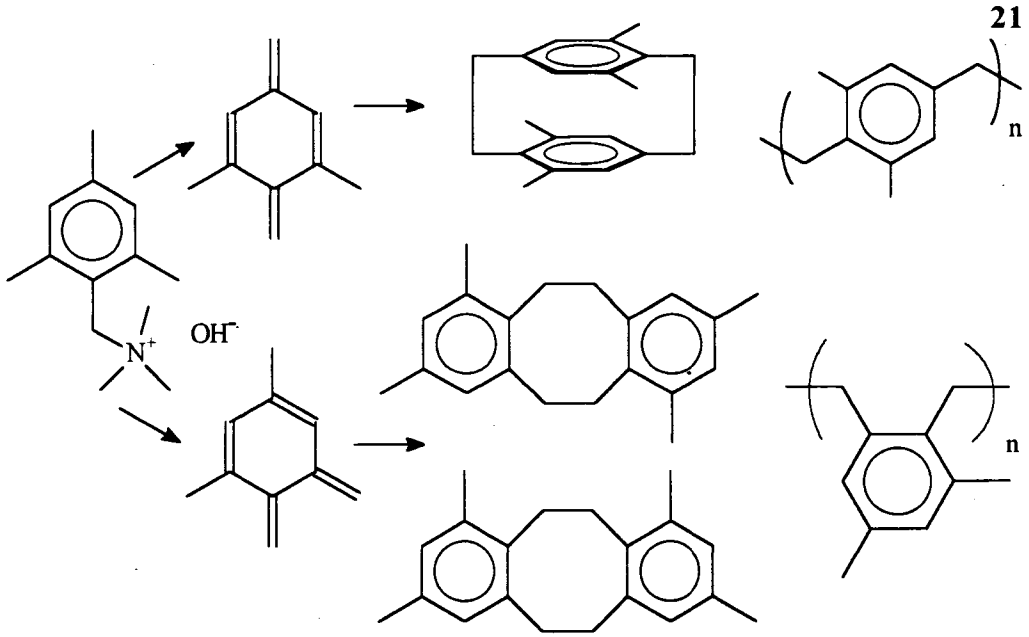

Figure 42 Xylylene Routes for **38**

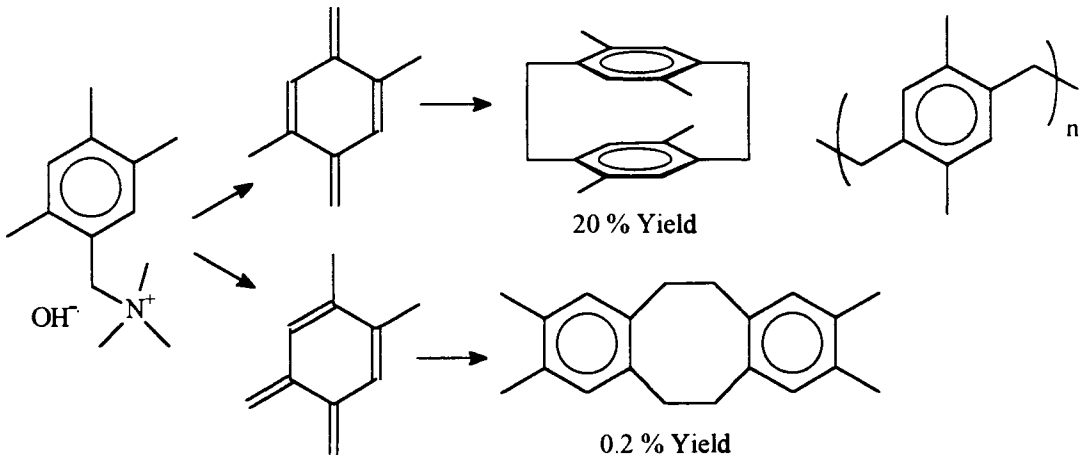

Figure 43 Related Xylylene Routes

The standard 1D proton NMR spectrum of **21** in d-chloroform showed broad peaks in the appropriate aromatic, methylene, and methyl regions with fitting integration ratios. There was however, some anisotropy evidenced by broad multiplicity of the methylene and methyl regions. Conceptually the multiplicity could be due to different monomer composition (*para-* and *ortho*-xylylene), different diads of the repeat units (head-to-tail, head-to-head, tail-to-tail), rotational atropisomerism, or combinations of these. To investigate these possibilities and specifically identify the polymer structure, 2D NMR techniques and variable temperature NMR were employed. After limited NOE effects were observed in a 2D NOESY experiment, a similar rotating frame 2D experiment called ROESY proved more successful. The identifiable crosspeaks in Figure 44 clearly show a spacial relationship of each methyl environment with a single aromatic environment. It was critical that neither methyl peak showed a broad, double spacial relationship to both of the aromatic peaks as would be expected in the *ortho*-xylylene structure. Hence, from the ROESY experiment, **21** appears to be the *para*-xylylene structure. The ^{13}C NMR also showed expected chemical shift environments, but again there were multiple environment anisotropies which could not be immediately explained. In efforts to explore possible conformational contributions to the anisotropies, a variable temperature proton NMR experiment was performed in d_6-benzene. In this solvent the broad multiplicities coalesced into the expected three broad peaks. There were no changes in the proton spectrum from room temperature to 90 ^0C. It should also be noted that as both possible xylylenes are 1,2,3,5-tetrasubstituted benzenes, the IR spectrum could not provide a simple confirmation of the structure. Based on the absence of a temperature dependent

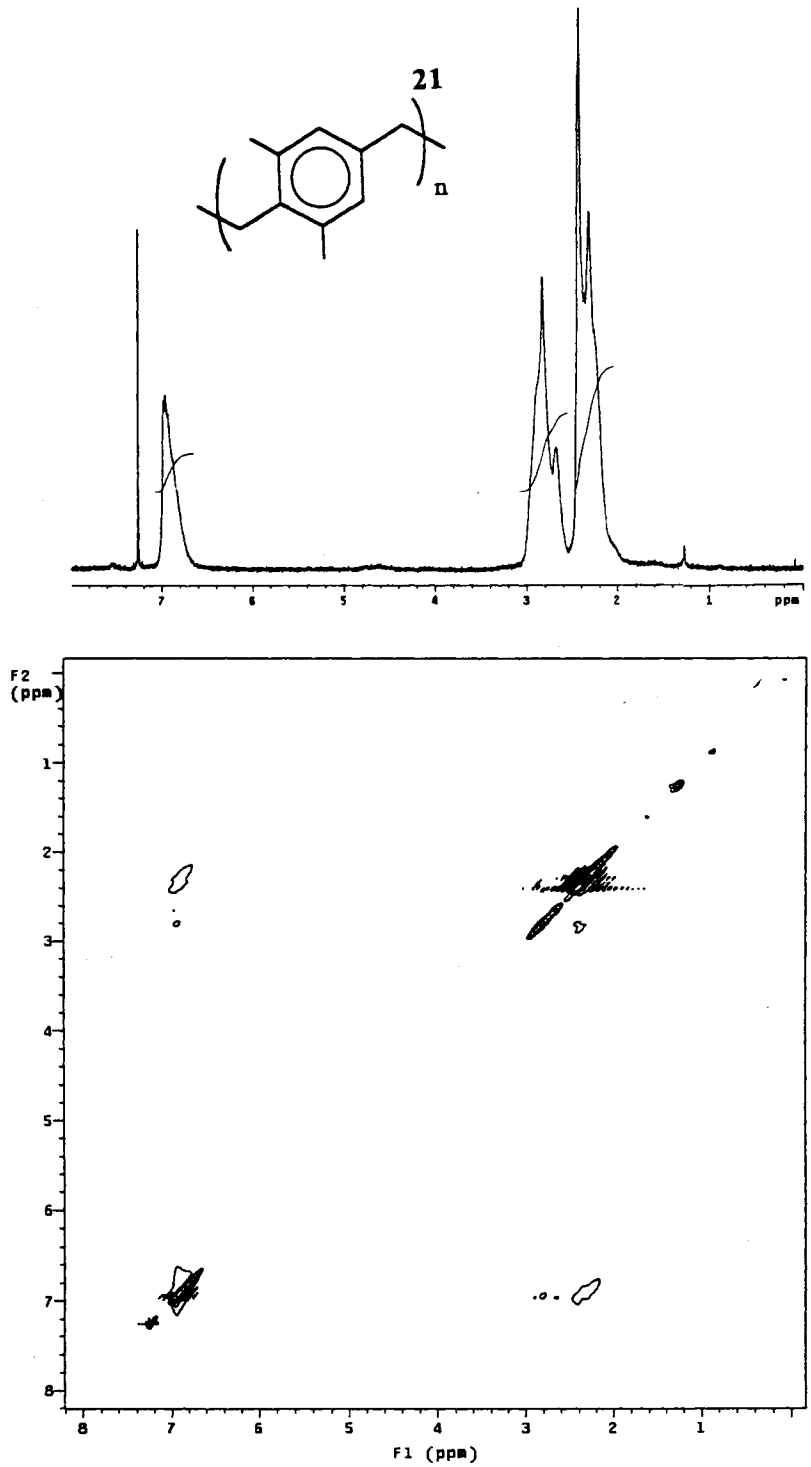

Figure 44 ROESY 2D NMR of **21**

anisotropy and the results of the ROESY experiment, **21** can be identified as poly(2,6-dimethyl-*p*-xylylene) in a mixed head-to-tail and head-to-head arrangement, see Figure 45.

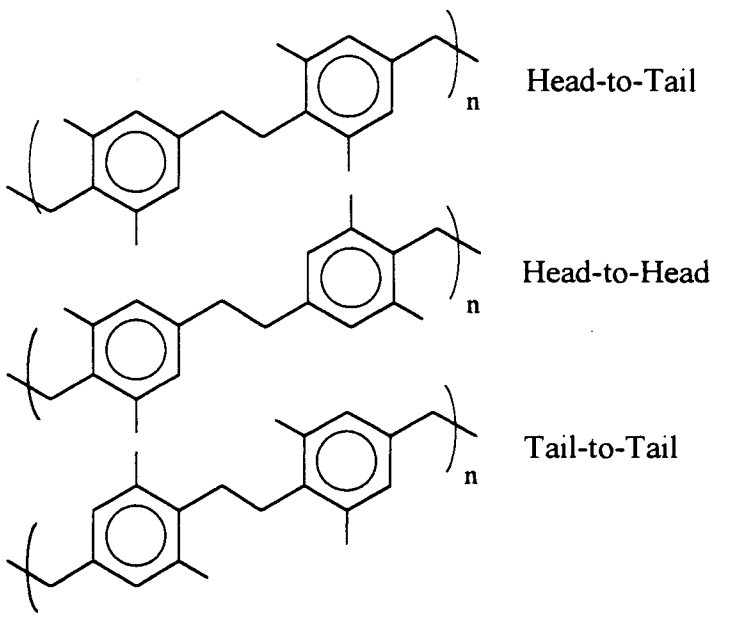

Figure 45 Diads of Polymer **21**

The predominance of the head-to-tail diad is concluded based on likely steric effects on the polymerization. Furthermore, the ROESY experiment also showed a single methylene-methyl crosspeak spacial relationship, as would be expected with the predominance of the head-to-tail diad, but the head-to-head diad crosspeak could be barried below the detection limit. An explanation for the predominance of head-to-tail reactivity can be posited based on the steric environment of the flanking *ortho* methyl groups which might block tail-to-tail polymerization but allow head-to-tail and head-to-head reaction. Later identification of the small molecule oligomers and dimers (PCP's) would provide further support for the head-to-tail diad predominance.

As many applications of the PPX polymers are dependent upon the thermal stability, several thermal techniques were applied to **21**. Initial TGA analyses of the polymer films indicated a significant amount of residual chloroform solvent. The films retained this solvent despite vacuum drying (12.8 wt% retention) and vacuum oven drying at 80 °C (6.6 wt% retention) for 24 hours. Only vacuum drying at 150 °C for 24 hours was successful in removing the entrapped solvent. There was a significant decrease in the flexibility and an increase in the rigidity of the films as the solvent was removed, indicating a plasticizing effect of the residual solvent. The TGA thermogram of **21** in air is displayed in Figure 46. The decomposition was only mildly affected by the use of helium rather than air (onset of 442 vs. 424 °C). The thermal decomposition in air exhibited a two step process which is common to the PPX's. The DSC analysis of **21** as illustrated in Figure 47, showed an absence of crystallinity and glass transition temperature. The single non-reversible endothermic peak at 164 °C is solvent evaporation from the pan. The sample was film deposited into the pan with only vacuum oven drying. The absence of this endothermic transition was verified in a fully dried sample run later. The odd initially exothermic form followed by endothermic form of the decomposition was reproducible. The DSC decomposition onset temperature of 396 °C is slightly lower than the weight losing decomposition evident on the TGA. A potential two step process of initiating chain scission followed by depolymerization and evaporation could possibly explain the slight onset temperature variability as well as the unusual shape of the DSC thermogram.

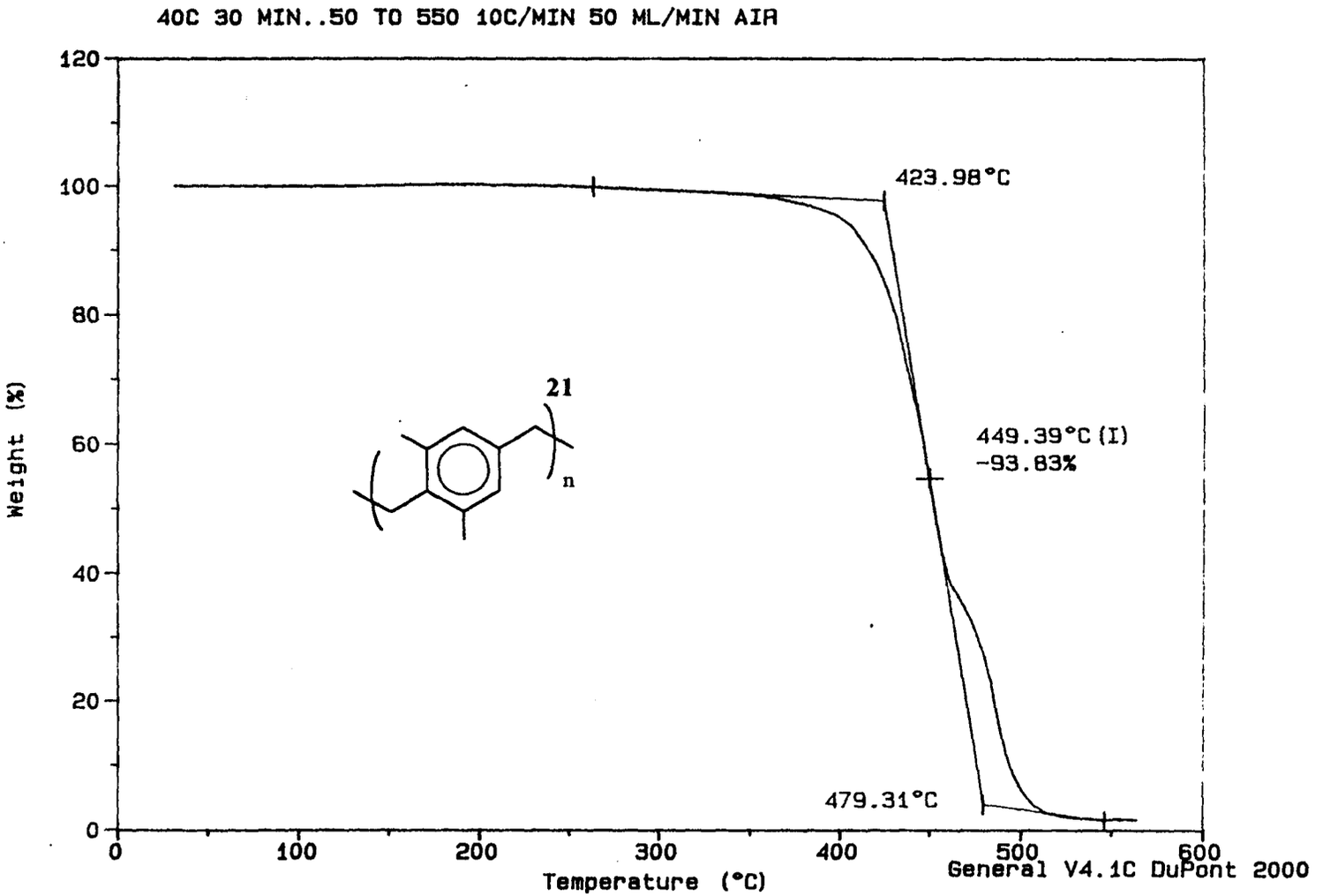

Figure 46 TGA of Poly(2,6-dimethyl-*p*-xylylene) (**21**) in Air

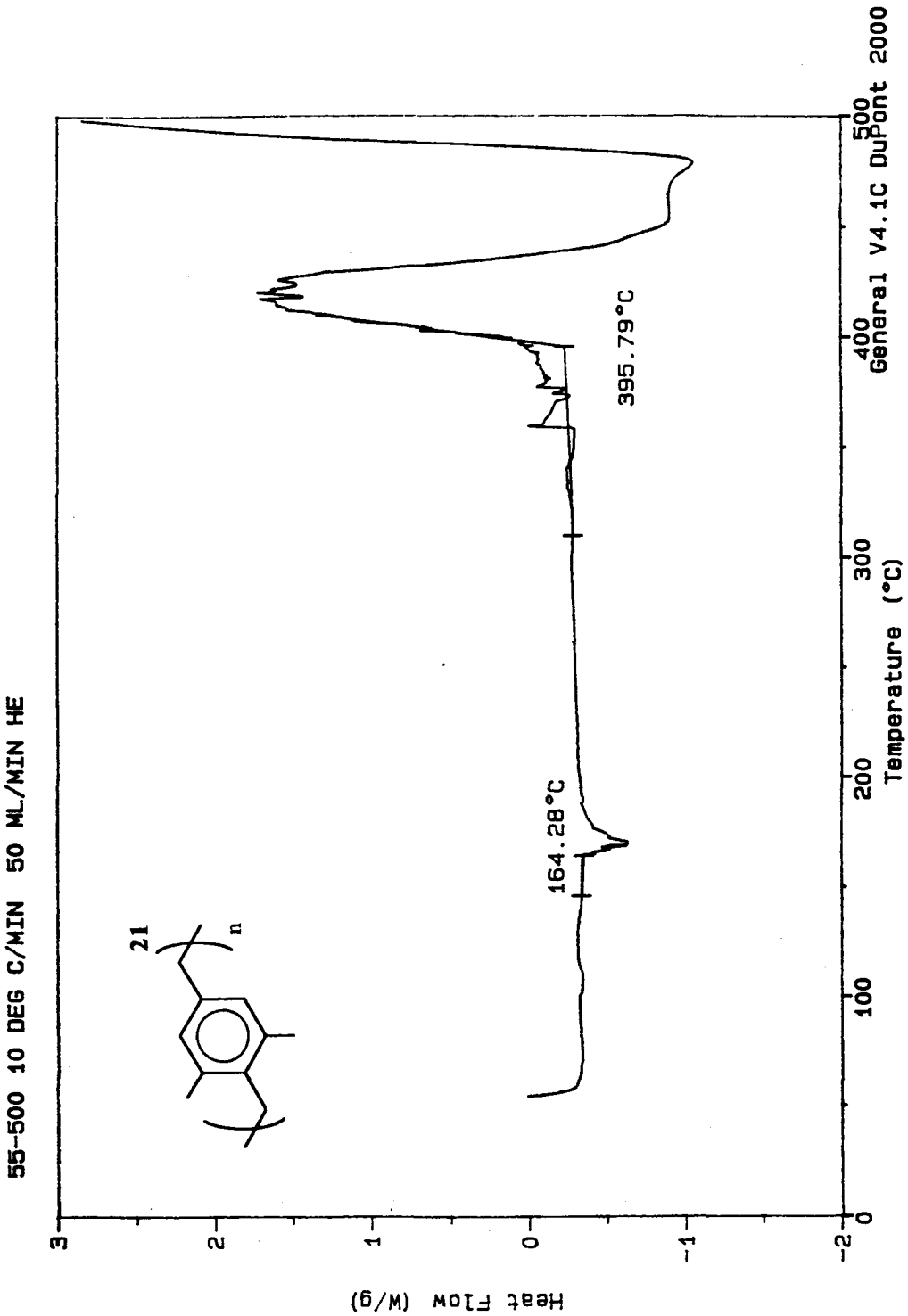

Figure 47 DSC of Poly(2,6-dimethyl-*p*-xylylene) (**21**)

Compared to other PPX polymers, these thermal analyses were quite promising for the thermally extreme applications of the polymer. For comparison the thermal properties of the commercialized PPX's polymers are listed in Table 4 [45].

Table 4. Poly(*p*-xylylene) Thermal Characteristics (°C)

Polymer	T_{Dec}, Inert	T_{Dec} Air	T_m	T_g
Poly(2,6-dimethyl-*p*-xylylene)	442	424	NA	NA
Poly(*p*-xylylene)	450	270	400	80
Poly(chloro-*p*-xylylene)	500	270	290	80
Poly(7,7,8,8-tetrafluoro-*p*-xylylene)	530	500	500	95
Poly(dichloro-*p*-xylylene)	500	320	270	110

The novel polymer **21** clearly has some unique thermal features. It's thermal stability in an inert atmosphere is in the same range as all of the other PPX's. However, the more important thermal decomposition temperature in air is dramatically (>100 °C) higher than all of the other PPX's except the fluorinated Parylene AF-4. The presumed decomposition mechanism in air has been previously reported to potentially involve the formation of peroxy radicals at the aliphatic carbons [45]. The formation of these peroxy species also causes a small weight gain in the TGA prior to the decomposition onset. This pre-decomposition weight gain is not seen in the TGA decomposition of **21**. This absence of a pre-decomposition weight gain and the dramatically higher decomposition temperature strongly support the possibility of a unique decomposition pathway for **21**. A similar absence of pre-decomposition weight loss and high decomposition temperature is

also seen in Parylene AF-4. There is a similar and small 20-30 °C difference in the decomposition temperatures in air and inert gas for both **21** and Parylene AF-4, demonstrating a significantly smaller role of oxygen in the decomposition initiation. The absence of crystalline and glass phases for **21** does however, potentially limit its barrier and mechanical properties [42, 43, 156]. The barrier properties have been related to the crystallinity of the PPX's, and the mechanical properties are strongly dependent on polymer phases. The solvent retention properties of **21** do tend to support the possibility that an amorphous polymer may serve as an efficient barrier film. Furthermore, the elastomeric and elongation at break properties of the alkyl substituted PPX's have shown some potential utility (>200 % for 1-2 mil films) [43].

3.4 Summary and Conclusions

The novel polymer poly(2,6-dimethyl-*p*-xylylene) **21** was easily synthesized in moderate yields (10 %) from mesitylene. The polymer **21** is the highest and narrowest molecular weight *p*-xylylene polymer to be characterized by GPC (Mn = 60,510, Mw = 150,500, PD = 2.49), and possibly by ESR end group analysis. The polymer's structure was assessed by the use of one and two dimensional NMR techniques as well as variable temperature NMR. In the normal trend of other *p*-xylylene polymers, **21** exhibited high thermal stability in an inert atmosphere with a weight loss decomposition temperature of 442 °C. More uniquely, **21** decomposed in air at 424 °C, more than 100 °C higher than any other non-fluorinated *p*-xylylene polymer. Only the fluorinated Parylene AF-4 exhibits such a high decomposition temperature in air. The polymer also failed to exhibit a

crystalline melt or glass transition temperature on cycled DSC experiments which was unusual for symmetrically substituted *p*-xylylene polymers. In a similar trend of uniqueness, **21** was completely soluble in common organic solvents such as chloroform, toluene, benzene, and methylene chloride. Strong, flexible, free-standing films of **21** were cast from chloroform. These films retained significant quantities of the chloroform solvent which seemed to act as a plasticizer. The retained solvent can be fully removed from the films by vacuum heating (150 °C).

While the amorphous poly(2,6-dimethyl-*p*-xylylene) **21** may have some limited mechanical properties due to the absence of crystallinity, the potential benefits from its high thermal stability in air, excellent film properties, and unique solubility bode well for its ultimate utility. The *p*-xylylene class of polymers usually exhibit excellent electric resistance, and the related alkyl derivatives follow that same trend. While the barrier properties of **21** have not been assessed, similar alkyl-*p*-xylylenes exhibit excellent barrier properties. Further investigations into these more application-oriented properties of electrical resistance and barrier features as well as reaction yield optimizations are certainly justified.

3.5 Experimental

General Methods. All starting materials and solvents were acquired commercially and used without further purification unless stated otherwise. **New Compounds** are marked by an asterisk * in their experimental section. All instrumentation, hardware, and software employed for this research are detailed in Appendix D.

Hofmann on N,N,N-trimethyl(2,4,6-trimethylbenzyl)ammonium bromide (38). The starting material **38** (26.8 g, 98.6 mmol, 1eq) was treated according to the general Hofmann elimination procedure as described in Section 2.12. The Hofmann was scaled proportionally using a 300 mL total volume for the quaternary ammonium hydroxide solution in toluene (2.5 L) in a 3 L flask. Otherwise, the general procedure was followed. After cooling to room temperature following the pyrolysis a small amount of insoluble product that was isolated by vacuum filtration (0.800 g). The primary reaction filtrate was then reduced by rotary evaporation to a sticky gel. This gel was triturated with diethyl ether (400 mL) producing a white stringy solid (1.827 g). This solid was isolated by vacuum filtration. The second filtrate was reduced by rotary evaporation and redissolved in toluene (75 mL). The second dissolved product was triturated with methanol (150 mL) producing a second polymeric solid (2.23 g) which was isolated by vacuum filtration. The third filtrate was dried over anhydrous magnesium sulfate, vacuum filtered and reduced by rotary evaporation producing a yellow oil (6.42 g). The combined products (11.3 g) were 87 % yield based on exclusively xylylene products (98.6 mmol). The first insoluble product (0.800 g) was not analyzed further. The second product (1.83 g), the high molecular weight **21**, was analyzed by GPC, ^{1}H NMR, ^{13}C NMR, ROESY 2D NMR IR, TGA, and DSC. The third product (2.23 g), a bimodal low molecular weight polymer was analyzed by GPC and ^{1}H NMR. The fourth product mixture (6.42 g) could not be separated or identified despite extensive attempts using spectroscopy, chromatography, recrystallization, and sublimation. The interesting and novel polymer poly(2,6-dimethyl-*p*-xylylene) **21*** was isolated in 14 % yield (1.83 g) based on xylylene (98.6 mmol). **21**: GPC

in toluene relative to PS std (r^2=0.991), Mw 150,500, Mn 60,510 PD 2.49; ^{1}H NMR (400 MHz, $CDCl_3$) δ 6.9 (br, 1H), 2.8 (br, 2H) 2.3 (br, 3H); IR-film (cm^{-1}, strg, mod, wk) 3009m, 2955s, 2928s, 2864m, 2733w, 1473s, 1457s, 1377w, 1217m, 1143w, 1031m, 854s, 756s, 668w.

Chapter Four

Poly(*p*-phenylene sulfoxide)

4.1 Background

As discussed in Section 1.5 and illustrated in Figure 17, the relatively unknown polymer, poly(*p*-phenylene sulfoxide) (PPSX) **18**, was synthesized in Dr. Glatzhofer's laboratory as a serendipitous product from the novel homogeneous reaction of fuming nitric acid with the engineering polymer, poly(*p*-phenylene sulfide) (PPS) **17** [41]. While the initially intended product, poly(dinitro-*p*-phenylene sulfide) was not formed, the polymer **18** proved to be completely soluble in some common solvents and binary solvents. Compared to other aryl sulfur polymers this facile solubility was quite unique and permitted extensive characterization. The majority of the work on PPSX was conducted by undergraduate researcher Adam Rush and summer undergraduate research fellow Eric Uffman. Their hard work on the sometimes tedious characterization of a polymer was invaluable.

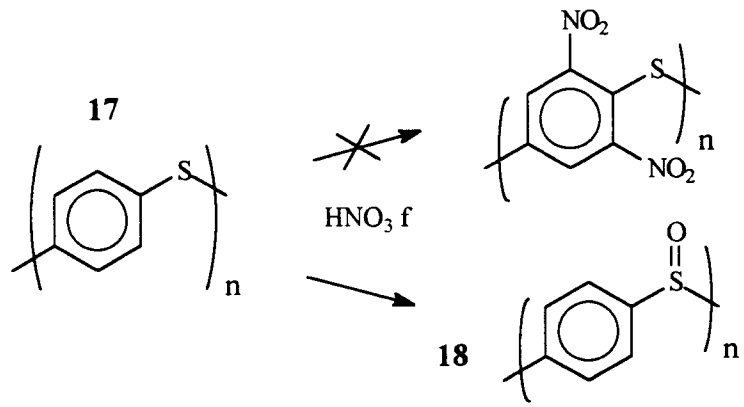

Figure 17 Synthesis of PPSX

There are two well studied classes of aryl sulfur polymers: poly(aryl sulfide) and poly(aryl sulfone) [157-159]. Both of these polymer classes are used as engineering plastics in applications requiring high thermal stability and relative chemical and corrosion resistance. Specific tuning or designing of the desired thermal and physical properties is possible for these polymers by incorporating various aryl groups and changing the molecular weight distribution. In practice, the higher molecular weight poly(aryl sulfones) also incorporate aryl ether moieties, poly(aryl ether sulfones), to achieve reasonable solubility and thermal characteristics [159, 160]. All of these polymer classes are typically injection molded at higher temperatures (>200-250 °C). These sulfide and sulfone polymers are virtually insoluble at temperatures less than 175 °C and widely soluble in solvents at 250-300 °C [157, 159]. The poly(aryl sulfides) are also used as curable molded resins which crosslink in an irreversible thermal cure [161]. The specific polymers poly(*p*-phenylene sulfide) PPS or Ryton® and poly(*p*-phenylene sulfone) PPSO are both highly crystalline with thermal stabilities in air extending beyond 500 °C [157, 159]. Replacement of the phenyl groups with larger aryl groups or substituted phenyl groups dramatically decreases the crystallinity and thermal stability of these polymers. Hence, the polymers, PPS and PPSO with the related poly(phenyl ether sulfone) are the major commercialized products. As a side note the abbreviations PPS and PPSO have been previously used in literature and commerce to represent their respective phenylene sulfide and sulfone polymers, so PPSX was selected as a less than ideal abbreviation for poly(*p*-phenylene sulfoxide).

Beyond the homogenous polymers, PPS and PPSO, several groups have studied and patented processes and modifications that partially alter the oxidation states of the aryl sulfur polymers in a heterogenous manner [162-178]. Typically the starting material, PPS, is oxidized or treated by an oxidizing agent that is either stoichiometrically or surface/interface limited by the inherent insolubility of PPS. Some of the oxidants that are reported in literature include nitric acid, hydrogen peroxide, peroxy acids, ozone, and various hypochlorites. Some of the surface/interface limiting conditions include reacting the oxidant with powdered, fiber, and laminar PPS. The products from all of these oxidizing treatments are clearly heterogenous and insoluble. They have generally been characterized by elemental analysis or less frequently by some surface vibrational or electronic spectroscopic technique. Most of these studies reported the ability to control the approximate and average oxidation states of the polymer repeat units over the continuum from sulfide to sulfoxide to sulfone. Generally, these studies reported improved thermal stability, greater chemical resistance, or greater crosslinking potential concurrent with an increase in oxidation state to the point of sulfur-oxygen equivalence. These improved properties were the primary motivation or benefit of the oxidizing treatment. Some of these groups that used nitric acid as an oxidant either presumed or measured nitro group introduction into the PPS/PPSX/PPSO polymer backbone. A single patent reported the production of a soluble polymer product from the reaction of PPS with nitric acid in methane sulfonic acid (1:5) at 0 °C [162]. The precipitated product was analyzed by IR which qualitatively demonstrated the presence of nitro and sulfoxide groups. There was no further characterization reported in the patent. Several other

patents also claim invention or synthesis of the fundamental PPSX structure without providing any specific characterization beyond elemental analysis. In each of these cases the product is not soluble and most likely heterogeneous [164, 167-170, 172, 173, 175, 176, 178]. Unfortunately, there are no peer-reviewed publications outside of this patent focused work that provide any further insight into or characterization of PPSX.

Other than these limited reports of heterogenous, PPSX-like polymers, there has been only one other reported main-chain sulfoxide polymer. This polymer illustrated in Figure 48, poly(*p*-phenoxyphenyl sulfoxide) was synthesized by the oxidation of the parent poly(aryl ether sulfide) with hydrogen peroxide in chloroform [179]. The product sulfoxide polymer was soluble and fully characterized by IR, ^{1}H NMR, TGA, DSC, and viscometry. The analysis of the sulfoxide polymer demonstrated thermal stability equivalent to the related sulfide and sulfone polymers, and an amorphous structure only matching the related sulfone polymer. The amorphous sulfoxide and related sulfone could be drawn into fibers from melts, but no other mechanical properties were assessed.

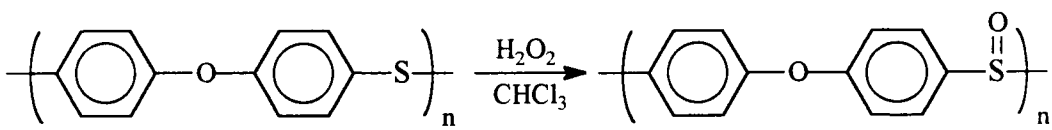

Figure 48 Poly(*p*-phenoxyphenyl sulfoxide)

At least three other groups have successfully synthesized side-chain or end-group sulfoxide polymers as substrate-bound sulfoxide reagents [180-182]. These polymers, as illustrated in Figure 49, provide a recyclable sulfoxide reagent employed as a sulfonium ylide, Swern oxidation reagent, or an acid halide oxidation reagent. The three

poly(styrene) derived polymers are supported as insoluble Merrifield resin-like systems. The poly(ethylene glycol) (PEG) derived polymer is soluble, providing greater recycling and higher yields compared to the related insoluble poly(styrene) system. As these insoluble side-chain and soluble end-capped sulfoxide polymers were designed as supported reagents, their relatively minor sulfoxide portions were not analyzed as novel sulfoxide polymers.

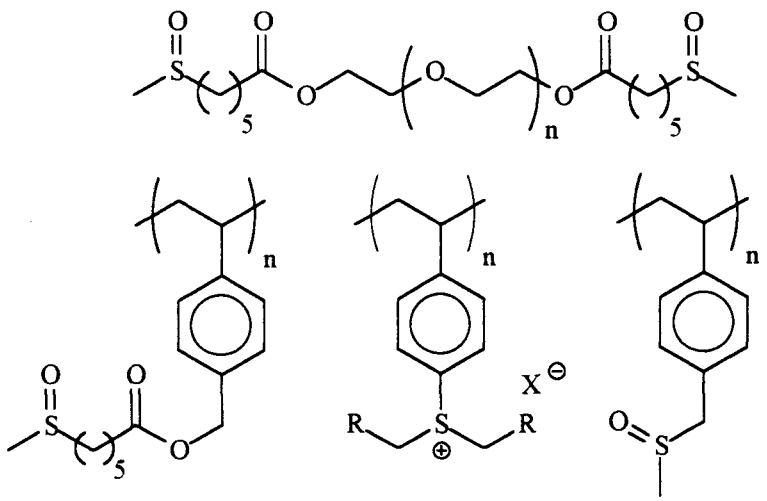

Figure 49 Sulfoxide Polymers

While a complete discussion of the electric and photoelectric properties of organic polymers is well beyond the scope of this dissertation, the potential importance of any conjugated organic polymer almost requires a brief introduction [158]. There are several conjugated organic polymers that are soon approaching commercial applications as light emitting diodes, optoelectronic devices, flexible conductors, and polymer electrolytes [183-186]. Some of the fore-runners in this field include poly(thiophene) derivatives, poly(phenylene vinylene), poly(phenylene oxide), poly(acetylene), poly(pyrrole),

poly(aniline), and PPS [158]. While a conjugated *pi* system is not specifically required, virtually all polymer conductors have such a system with the possible exclusion of polymer electrolytes [158]. The mobility of charge carriers along a polymer chain is also hindered by orientational requirements created by this conjugated *pi* system [187]. Greater flexibility as well as poly-functionality (two lone pairs versus one double bond) improves conduction [187]. Solubility simplifies device construction and improves any required dopant distribution [158, 187]. A homogenous solid phase structure also improves conduction; for polymers this typically means that the regular irregularity of amorphous polymers is preferred to the junctions created at the crystallite borders of crystalline polymers [188, 189]. Finally, the band gap defined by the HOMO-LUMO gap of the polymer or doped polymer should ideally be tunable to a variety of applications [158, 187]. Such a tunable nature has recently been defined in variably oxidized thiophene oligomers [190]. From this brief introduction it should be clear that PPSX may be ideally suited as an addition to the growing conducting polymer field. PPSX has a fully conjugated main-chain with a flexible tetrahedral sulfoxide linker between the phenyl rings. The polymer is both soluble and amorphous with the added potential of a tunable band gap. The HOMO-LUMO gap may be potentially adjusted by partial oxidation or reduction along the polymer as well as variable dopant interaction with the sulfoxides.

4.2 Synthesis of poly(*p*-phenylene sulfoxide) (PPSX) (18)

A vast array of synthetic approaches is available to synthesize sulfoxides. Most of these methods involve the oxidation of the parent sulfide compounds. Some recent and

broad reviews are available on this chemistry [191-193]. The most difficult challenge in the oxidation of sulfide to sulfoxides is preventing the overoxidation to the corresponding sulfone. This has most typically been controlled by limiting reaction time, temperature, and reagent quantity. Nitric acid was first reported as a sulfoxide forming oxidizing reagent more than a century ago in the oxidation of dibenzyl sulfide [194]. Since that early work, many researchers have expanded and specified the reactivity of nitric acid in the production of sulfoxides. In our laboratory, the solubilization of PPS by stirring in fuming nitric acid was initially thought to involve primarily nitration following the typical genre of nitric acid in organic chemistry. After extensive product characterization, it became clear that not only was the expected nitration absent, but rather the whole polymer oxidation deactivated the PPSX effectively protecting it from nitration. The initial success with fuming nitric acid provided a starting point from which the synthesis of PPSX was explored and optimized.

A typical PPSX synthesis involved simply pouring the powdered PPS starting material into stirring fuming nitric acid. The reaction warmed mildly upon addition with a significant amount of NO_2 gas being liberated. After 5-10 minutes the reaction mixture becomes homogenous, clear, and orange. After a total reaction time of 30 minutes, the reaction was quenched by pipetting or pouring into water. The crude PPSX was isolated by vacuum filtration. The PPSX was also typically further purified by dissolving in trifluoroacetic acid (TFA) and reprecipitating in water. The purified PPSX retained significant amounts of water after filtration. This residual water was usually removed by washing the purified PPSX with acetone several times and vacuum oven drying for at least

two days. Yields typically exceeded 88 %. Time and temperature changes to this standard reaction were explored. Temperatures ranging from 0 to 42 °C resulted in an equivalent PPSX product. Higher temperatures produced partial overoxidation to the sulfone product: 54 °C gave 5.8 % sulfone and 65 °C gave 6.3 % sulfone, as determined by proton NMR. Longer reaction times extending to 48 hours conducted at room temperature failed to produce any overoxidation.

As fuming nitric acid is a fairly expensive solvent, several other reagents and modifications of this initial procedure were studied. Identical reaction conditions in concentrated rather than fuming nitric acid failed to produce a homogenous product. After filtration to remove the residual insoluble material, the soluble polymeric product was analyzed by proton NMR (40 % yield). The soluble fraction contained a small amount of underoxidized sulfide monomers (< 2 %). Clearly concentrated nitric acid was not an appropriate substitute reagent and solvent. A mixed concentrated nitric acid reagent with a solvent of sulfuric acid (1:4 vol:vol) under similar reaction conditions produced a fully dissolved product in comparable yields of 71 %. However, the product was partially overoxidized to sulfone (3 %). A second mixed acid reaction using excess fuming nitric acid with acetic acid as a solvent (1:2 vol:vol) failed to produce a fully soluble product. The soluble portion was identified as also containing underoxidized sulfide monomers (5 %). A third mixed acid reaction using excess fuming nitric acid with TFA as a solvent (1:10 vol:vol) successfully produced only PPSX without overoxidation or underoxidation in high yields (95 %). This reaction became the primary synthetic technique used to synthesize PPSX.

As a final step to reduce the PPSX synthetic cost the excess fuming nitric acid/TFA reaction was further modified by limiting the fuming nitric acid to stoichiometric quantities (1:1 PPS monomer:HNO_3). This reaction successfully produced exclusively PPSX. At this point the single most expensive portion of the reaction was still the fuming nitric acid. Excess, concentrated nitric acid was substituted for fuming nitric acid using TFA as a solvent (1:3 vol:vol). This reaction successfully produced exclusively PPSX. A final synthetic modification using excess concentrated nitric acid with a stoichiometric quantity of TFA (1:1 PPS:TFA) failed to produce a completely soluble product. The soluble material contained underoxidized sulfide monomers (5 %).

Several alternative oxidants were assessed for their ability to produce PPSX from PPS. As solubility of the desired PPSX appeared to be quite important, alternative oxidants and solvents were selected based on ability to dissolve PPSX and a cost less than concentrated nitric acid. Peroxytrifluoroacetic acid (pTFA) was reacted with PPS producing an insoluble white powder. This powder was identified as the wholly overoxidized PPSO polymer by IR spectroscopy. The spectra demonstrated the absence of PPS and PPSX equivalent peaks and the presence of sulfone characteristic peaks: stretches at 1328, 1293, and 1164 cm^{-1} and a strong scissoring at 640 cm^{-1} [195]. The identity of PPSO was also confirmed by direct oxidation of PPSX with pTFA in TFA producing the equivalent insoluble white powder and corresponding IR spectrum. A sodium hypochlorite solution in TFA was also investigated as a potential oxidant. The sodium hypochlorite reaction primarily produced an insoluble product. A small amount (17 %) of soluble product was identified by NMR as PPSX with a small degree of

overoxidation (<1 %). Another hypochlorite reaction using calcium hypochlorite in a binary solvent of TFA and methylene chloride (1:2 vol:vol) produced only 3 % of a soluble PPSX product which again showed a small degree of overoxidation. The insoluble reaction products from the two hypochlorite reactions were not analyzed.

The three finalized reaction methods to synthesize PPSX produce the polymer with ease and in high yields. The original method using just fuming nitric acid can be supplemented with the use of limited quantities of either fuming or concentrated nitric in a solution of TFA. Other oxidants produced low or absent yields of PPSX typically with overoxidation to the sulfone.

4.3 Characterization of poly(*p*-phenylene sulfoxide) (PPSX) (18)

The PPSX polymer was characterized by a wide variety of instrumental techniques. The proton NMR spectrum of PPSX provided a number of conundrums throughout the research. Initially, the simplicity of the proton NMR spectrum provided a challenge. in the face of the expected nitration. The proton spectrum showed one singlet at 7.9 ppm. Interestingly, the peak demonstrated a downfield migratory aptitude that was eventually explained by residual water content. In actuality the reference frequency of the TFA solvent moved relative to the fixed PPSX signal. This was confirmed using an inner reference tube with direct addition of water to the external tube. All chemical shifts of PPSX spectra reported in this dissertation have been adjusted to the upfield frequency of 7.9 ppm. Several synthetic methods produced either underoxidation or overoxidized PPSX products. These products both produced characteristic pairs of doublets indicative

of the sulfone and sulfide diads. The sulfur diad doublets were significantly upfield at 7.63 and 7.53 ppm. One of the sulfone diad doublets was buried in the shoulder of the PPSX peak and the other was at 8.15 ppm. The carbon NMR spectrum showed the expected two peaks at 148.1 and 129.1 ppm. The IR spectrum of PPSX was distinct from both PPS and PPSO. The IR spectrum contained several peaks representative of sulfoxides and *para*-disubstituted benzenes: sulfoxide stretches at 1095s and 1046s cm^{-1}; para-disubstituted benzenes 823m and 811m cm^{-1}; sulfoxide scissoring 564s and 534m cm^{-1} [195]. Low molecular weight mass spectroscopy techniques were not applicable to PPSX, but attempts were made to characterize PPSX using matrix-assisted laser desorption ionization mass spectroscopy (MALDI-MS). There was no response using a variety of a matrices, deposition solvents, and ionizing metals. Elemental analysis was conducted on PPSX as well as PPS and PPSX for comparison. The results of the elemental analysis are presented in Table 5. All of the elemental compositions followed the expected trends with increasing oxidation at sulfur. The initial low sulfur content was maintained throughout the series, but with a progressive decrease in magnitude. The introduction of a small amount of nitrogen with the nitric acid oxidation was most likely due to a small amount of nitration. The PPSO was synthesized by pTFA oxidation of the analyzed PPSX which explains the similar nitrogen and likely nitro group content. The most common end-groups and variable linkers are chlorobenzenes, phenols, and N-methyl-2-pyrrolidones [196]. The constant chlorine content is indicative of chlorobenzene end-groups and any phenol end-groups would most likely be dinitrated by the fuming nitric acid. Overall, the elemental analysis matched the theoretical composition, but the

Table 5. Elemental analysis of PPS, PPSX, and PPSO *

Compound	C	H	Cl	N	O	S
PPS**	66.09 (66.63)	3.59 (3.73)	0.12 (0)	<0.05 (0)	5.01*** (0)	25.14 (29.64)
PPSX**	55.05 (58.04)	3.08 (3.25)	0.13 (0)	0.52 (0)	14.89 (12.89)	22.66 (25.82)
PPSO**	50.96 (51.42)	2.79 (2.88)	0.11 (0)	0.52 (0)	20.69 (22.83)	21.99 (22.87)

* Results given as actual(theoretical)
** All polymers derived from Aldrich Mn10K
***Calculated by difference from other components

difficulties presented by the heterogeneity of macromolecular systems complicated the issue. There is also the potential that incomplete charring during the sulfur analysis produced a less-than-complete sulfur response.

Several PPSX properties unique to polymeric systems were also assessed. Specifically, gel permeation chromatography (GPC) was performed on the different PPSX samples prepared according to either the excess fuming nitric acid in TFA procedure or the original fuming nitric acid procedure. The PPS samples were obtained from either Phillips Chemical or Aldrich Chemical with molecular weights previously assigned or estimated by meltflow analysis of the PPS: Aldrich samples were identified as Mn 10K, Poise 1400, Poise 500, Poise 275; the Phillips samples were identified as PR09 (Mw 50,000), GR01 (Mw 50,000, but branched), E2080 (80,000) [196]. Fractionation was also conducted on the Aldrich Poise 1400 sample. The parent PPSX sample was fractionated into four molecular weight fractions by a combination of precipitation and solvation techniques. The fractions were identified as the Highest (23 %), Medium

(53 %), Low (2 %), and Lowest (4 %) molecular weights. All of the primary samples as well as the fractionated samples were analyzed using GPC. The GPC was run in a binary solvent system of *m*-cresol and chlorobenzene (1:10, wt:wt). The molecular weights were calculated relative to poly(styrene) (PS) standards. The GPC results are presented in Table 6.

Table 6. GPC of PPSX samples

Sample	Mw	Mn	PD
Phillips PR09*	30,800	12,500	2.46
Phillips GR01**	56,900	18,600	3.07
Phillips E2080**	63,200	16,000	3.95
Aldrich Mn10K*	22,600	9,750	2.32
Aldrich Poise 275*	39,100	14,700	2.66
Aldrich Poise 500*	42,000	14,700	2.86
Aldrich Poise 1400**	68,700	19,800	3.47
Poise 1400 Highest**	84,000	30,800	2.72
Poise 1400 Medium**	73,000	27,300	2.67
Poise 1400 Low**	26,600	5,300	5.04
Poise 1400 Lowest**	24,500	5,900	4.17

*GPC relative to PS std ($r^2 = 0.9992$):
**GPC relative to PS std ($r^2 = 0.9987$):

The GPC results followed the expected molecular weight trends for the polymers with increasing meltflow values. The Aldrich Mn10K polymer had the narrowest distribution of all of the polymers, but also the lowest absolute molecular weight. The progressive increase in molecular weight paralleled by an increase in polydispersity (PD) would be expected for the PPS stepgrowth polymerization run to various stages of completeness.

PPS is typically synthesized by reacting 1,4-dichlorobenzene with sodium sulfide in N-methyl-2-pyrrolidone. The Phillips GR01samples is branched by the use of 1,3,5-trichlorobenzene in addition to the usual 1,4-dichlorobenzene [196] which causes an effective increase in number averaged molecular weight without a paralleling increase in weight average molecular weight. The fractionation of the Aldrich's Poise 1400 sample effectively separated the polymer into the highest available molecular weight PPSX polymer. While this fractionation was far from optimized, it clearly demonstrated that higher molecular weight fractions can definitely be separated from the original polydispersed PPSX samples. There was a significant variability (+/- 5 %) in the GPC data on repeated runs. However, this relatively minor variability did not impact any of the conclusions drawn above.

A fairly extensive viscometry study was conducted on PPSX derived from the Aldrich PPS samples. For each of these polymers, the inherent viscosity was determined using an Ubbelohde viscometer in *m*-cresol. It was during the cleanup between viscometry runs that the potential for binary solvent systems was first recognized. Rinsing the viscometer with methylene chloride did not produce precipitation. Inherent viscosity is a concentration independent property of polymer solutions that is frequently used to estimate molecular weight. The inherent viscosity is determined by dividing the reduced viscosity (also called Viscosity ratio) by the concentration in (g/dL) [197]. The inherent viscosity extrapolated to zero concentration is defined as the intrinsic viscosity. Intrinsic viscosity is considered a molecular weight and concentration independent property of a polymer. The inherent viscosities of the Aldrich derived PPSX samples are presented in

Table 7. The correlation coefficient (r^2) for a linear regression of inherent viscosity versus the natural logarithm of weight average molecular weight was 0.985.

Table 7. PPSX inherent viscosities in *m*-cresol

Sample	η_{inh}(dL/g)	Mw	Mn
Aldrich Mn 10K	0.263	22,600	9,750
Aldrich Poise 275	0.343	39,100	14,700
Aldrich Poise 500	0.379	42,000	14,700
Aldrich Poise 1400	0.461	68,700	19,800

A more involved study was conducted to determine the intrinsic viscosity of PPSX. Intrinsic viscosity is determined by extrapolating the reduced or inherent viscosity of multiple samples to zero concentration. For the intrinsic viscosity study, the Aldrich Mn10K derived PPSX was used. The results are presented in Figure 50. The intrinsic viscosity clearly retains a odd discontinuity at lower concentrations. This discontinuity is most likely due to normal errors induced at the lower polymer concentrations. In these lower concentrations the relative viscosity was only 1.12 or less with an absolute time difference of less than 11 seconds. The higher concentrations are much more precise. The correlation coefficient (r^2) for a linear regression of the seven highest concentrations versus their reduced viscosities was 0.882. The intrinsic viscosity was determined by extrapolation to zero concentration: 0.274. The same value but with higher error was determined when all of the data were included: 0.274 and $r^2 = 0.564$ respectively.

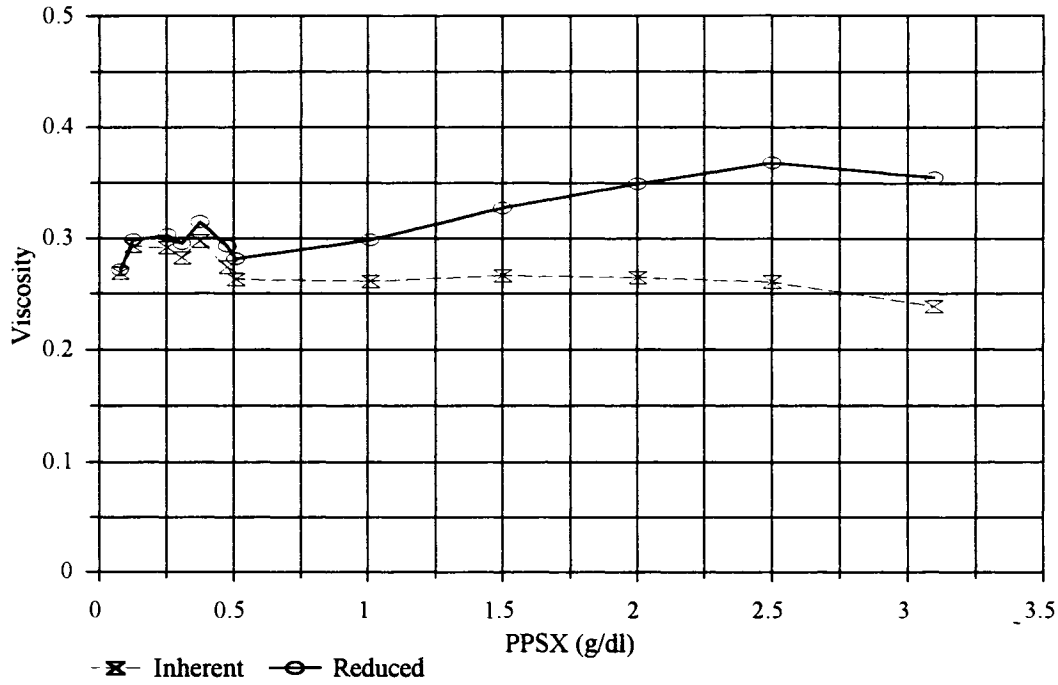

Figure 50 Viscosity of PPSX in *m*-Cresol

As the solubility of any polymer is critical to many applications, the diversity of available solvents and the properties of films cast from these solvents were assessed. The primary solvents for PPSX were somewhat limited: TFA, *m*-cresol, and fuming nitric acid. Phenol and concentrated nitric acid were marginal solvents, and concentrated sulfuric acid initially dissolved PPSX, but later reacted producing a green solution and precipitate. There are many well characterized sulfoxide adducts with phenols, other hydroxyl compounds, and nitrogen oxides [192]. These adducts have formed the basis for the spectroscopic characterization of the stereochemistry and conformational mobility of sulfoxides. Clearly, the formation of these solvated adducts must be important to the solubility of PPSX in *m*-cresol, TFA, and fuming nitric acid. In a parallel extension of the adduct formation principle for the solubility of PPSX, several binary solvent systems were

identified. These binary solvents were grossly assessed. A pre-dissolved solution of PPSX in *m*-cresol was diluted with progressive quantities of a second solvent. Precipitation frequently occurred with the highly polar secondary solvents presumably because of their disruption of the PPSX adducts (N,N-dimethylformamide (DMF) and nitromethane in *m*-cresol; dimethylacetamide and DMF in TFA). The successful binary solvents included: methylene chloride, chloroform, 1,2-dichloroethane, chlorobenzene, nitrobenzene, toluene, benzene, xylene, mesitylene, cumene, *n*-propylbenzene, bromonaphthalene, dimethylacetamide , and TFA in *m*-cresol; methylene chloride, 1,2-dichloroethane, and benzene in TFA. Generally, haloalkanes, aromatics, and haloaromatics with some additional polar solvents worked well as the second solvent in binary system with *m*-cresol or TFA.

The quality of films cast from these solvents varied enormously. There were no free-standing films successfully cast from any TFA solution, and low boiling point binary systems produced uniformly poor to absent films. The best films were cast from the highest molecular weight PPSX (Phillips E2080), which was used for the film casting experiments. A concentrated *m*-cresol solution (PPSX 1 g/ 25 mL) produced a fair film which remained brittle. The best films were cast from this *m*-cresol solution with added propylene carbonate plasticizer or binary solvents of the *m*-cresol stock solution with cumene or *n*-propylbenzene. Cumene is *i*-propylbenzene. Propylene carbonate added to the cumene/*m*-cresol binary system also produced a good film. These better films were transparent, flexible, and fairly durable.

The final major area of PPSX characterization involved extensive thermal analysis using thermogravimetric analysis (TGA) and differential scanning calorimetry (DSC). As both PPS and PPSO are known for their thermal stability, the potential for a similar utility of PPSX directed the investigation into thermal stability. Initial TGA analyses conducted on the Phillips PR09 derived PPSX seemed to show a consistent onset of decomposition with significant weight loss at about 334 °C in air and 342 °C in Helium. The relatively small difference between the decomposition temperature in air and helium is somewhat

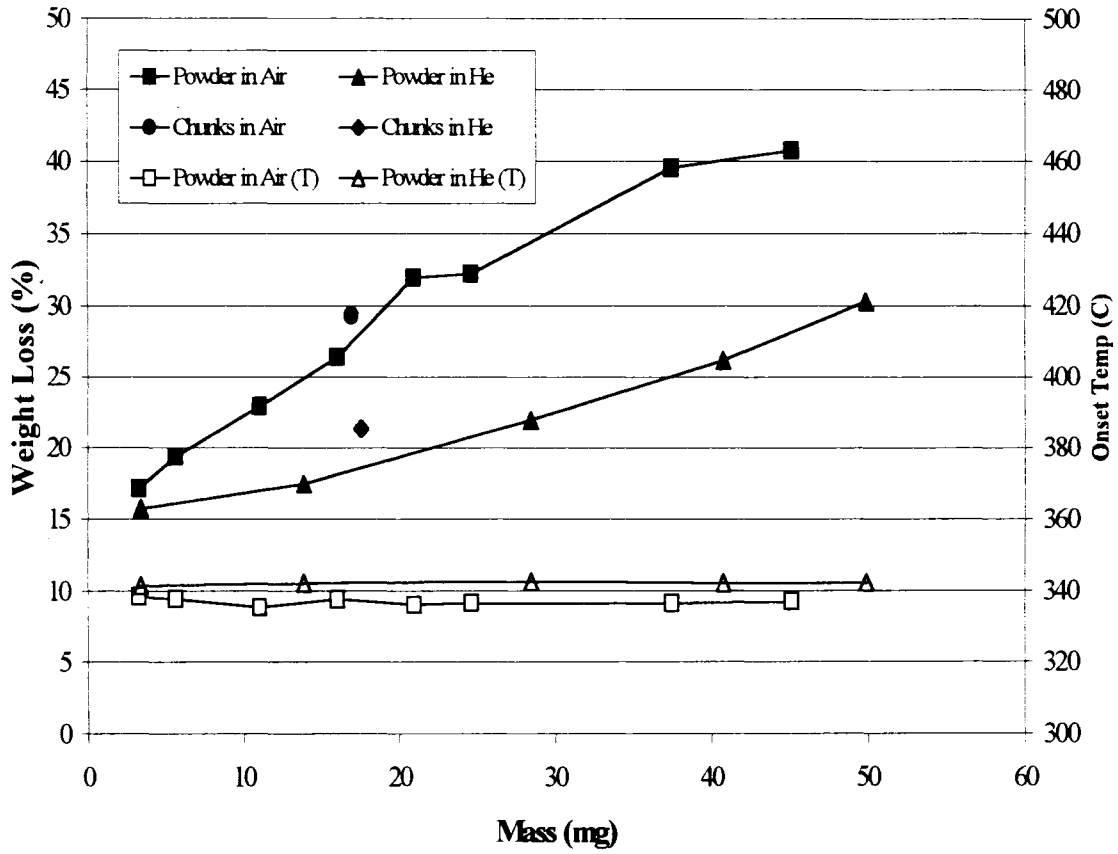

Figure 51 Mass Dependent PPSX TGA Decomposition

unique and most likely indicates an only marginal involvement of air (oxygen) in the initiation of the decomposition process [198]. The percentage of this weight loss seemed to vary significantly from a low of 16-17 % to a high of 41-42 %. It became clear that the weight loss was strongly dependent on the amount of sample analyzed during the TGA. Figure 51 illustrates the TGA weight loss dependence on the initial sample mass in both air and helium. As previously mentioned, the onset temperatures remained constant. It also seemed reasonable that the form of the PPSX sample would impact the weight loss. As also illustrated in Figure 51, large PPSX chunks (about 4.2 mg each) produced greater weight loss than the equivalent weight powder. This sample mass dependence is best explained by localized heating effects that balance a likely crosslinking cure that limits weight loss with a volatilizing decomposition that increases weight loss. A maximal weight loss experiment was conducted by heating a large sample of PPSX in an oven at 350 °C for 30 minutes and a second sample at 420 °C for 95 minutes. The product from the thermolysis experiments was a brittle carbonaceous solid with a porous fibrillar structure. The percentage weight loss was 41 % and 53 %. A loss of all sulfoxide moieties corresponds to a weight loss of 39 % and a loss of all sulfoxides and hydrogens corresponds to a weight loss of 42 %. The decomposition of PPSX likely involves the scission of the sulfoxide aryl C-S bond liberating SO. The SO may also remove hydrogens with its departure. The residual aryl rings can then undergo coupling or further decomposition. This pattern of decomposition has been verified in mass spectroscopy of aryl sulfoxides, and the potential crosslinking has been seen in the oxidation and subsequent decomposition of poly(aryl sulfides) [192, 198]. The production of SO, SO_2,

SOH, and diphenyl sulfide was also confirmed by pyrolysis-GC/MS in this work.

An expanded analysis of the decomposition kinetics of PPSX was conducted using variable heating rates with TGA. There are a variety of thermal analysis methods for determining kinetic parameters for reactions in general and polymer decomposition in specific. An excellent discussion and derivation of these methods are provided in another dissertation from the University of Oklahoma [199]. The method involves a modification of the Arrhenius equation. The Arrhenius equation is presented in Equation 8 and the relevant Friedman modification in Equation 9.

$$-dc/dt = A \cdot e^{-(Ea/RT)} \cdot C^n \qquad (8)$$

$$(-1/w_o)(dw/dt) = A \cdot e^{-(Ea/RT)} \cdot f(w/w_o) \qquad (9)$$

The desired kinetic parameters are the activation energy (E_a), reaction order (n), and the pre-exponential or frequency factor (A), which has been interpreted as a frequency of volatilization for polymer decompositions [200]. There are several key assumptions of the Friedman method modification of the Arrhenius equation. First, the concentration (c) is assumed to be proportional to the residual weight fraction (w/w_o) or a function of residual weight fraction ($f(w/w_o)$). This assumption is valid if the decomposition involves a single reactant of relatively constant molecular weight decomposing through a consistent mechanism. There is a strong implication that neither requirement is met with the PPSX decomposition particularly in light of the sample mass dependence of the TGA weight loss and the documented mass spectral decomposition pathways of aryl sulfoxides. Equation 9 is further modified by taking the natural logarithm of both sides producing Equation 10.

$$\ln\{(-1/w_o)(dw/dt)\} = \ln\{A\} + \ln\{f(w/w_o)\} - E_a/RT \quad (10)$$

Equation 10 matches the more common derivations of the Arrhenius equation from which kinetic parameters are determined. With the assumption that the function of the residual weight fraction, $f(w/w_o)$, is constant over a reasonably broad temperature range, a simple linear equation results. For the Friedman method multiple TGA thermograms are collected at varying heating rates. The values for Equation 10 are calculated at early w/w_o (residual weight fractions) across the thermograms. Using Equation 10, a plot of $\ln\{-(w_o)^{-1}(dw/dt)\}$ versus 1/T at the different residual weight fractions has a slope of $-E_a/R$ and an intercept of $\ln\{A*f(w/w_o)\}$. The frequency factor (A) and the reaction order can then be obtained by assuming that $f(w/w_o)$ has a direct exponential dependence on the reaction order, as in Equation 11. This assumption also produces Equation 12 by substituting and taking the natural logarithm of both sides of the intercept.

$$f(w/w_o) = [(w - wf)/w_o]^n \quad (11)$$

$$\ln\{A \cdot f(w/w_o)\} = \ln\{A\} + n \cdot \ln\{(w-w_f)/w_o\} \quad (12)$$

A second plot of the $\ln\{A \cdot f(w/w_o)\}$(the intercepts) versus $\ln\{(w-w_f)/w_o\}$ will have a slope of n and an intercept of $\ln\{A\}$. Hence, all three desired kinetic parameters can be determined directly from the TGA thermograms obtained at multiple heating rates.

The TGA thermograms of PPSX (Phillips PR09) were collected at variable heating rates of 3 to 15 °C/min at temperatures from 70 to 450 °C in both helium and air. The combined TGA thermograms of PPSX in helium are presented in Figure 52 with the first

derivative plots in Figure 53. The calculated Arrhenius plot trimmed of extraneous data is presented in Figure 54 with the residual weight fractions drawn in Figure 55. In Figure 55, the solid lines represent residual weight fractions from 0.98 to 0.90, which best fit the sloping peaks in the kinetic plot in Figure 54. This 0-10 % weight loss also best fits the required small change in repeat unit concentration. Analysis of the residual weight fraction slopes produced an average activation energy (E_a) of 31 +/- 3 kcal/mol (He). A similar kinetic analysis of the TGA PPSX decomposition in air produced almost identical results: E_a of 32 +/- 6 kcal/mol (Air). These related thermograms and plots are presented in Appendix C for brevity. These activation energies appear reasonable both in terms of the absolute values and their relative equivalence in air and helium based on the decomposition temperatures of 334 and 342 °C, respectively.

The extension of the kinetic analysis to the determination of the decomposition reaction order (n) and the frequency factor (A) was not successful. The second kinetic plots, derived from Equation 12 above, had negative slopes indicating a negative reaction order, which has no meaning. This difficulty is not wholly unexpected when a likely decomposition mechanism of SO group reactions is considered. The Friedman method is best applied to depolymerization decompositions [199, 200]. These calculations combined with the prior TGA and pyr-GC/MS results demonstrated the relative applicability of the Friedman method to the partial determination of kinetic parameters for the thermal decomposition of PPSX in air and helium.

As a final thermal characterization, DSC thermal analysis was conducted on PPSX (Phillips E2080). The thermogram presented in Figure 56 was clearly absent of either a melt or glass transition. The previously defined decomposition produced a fairly sharp exothermic peak with an onset temperature of 348 °C. The DSC analysis indicated that PPSX is an amorphous polymer lacking a glass transition temperature above 65 °C.

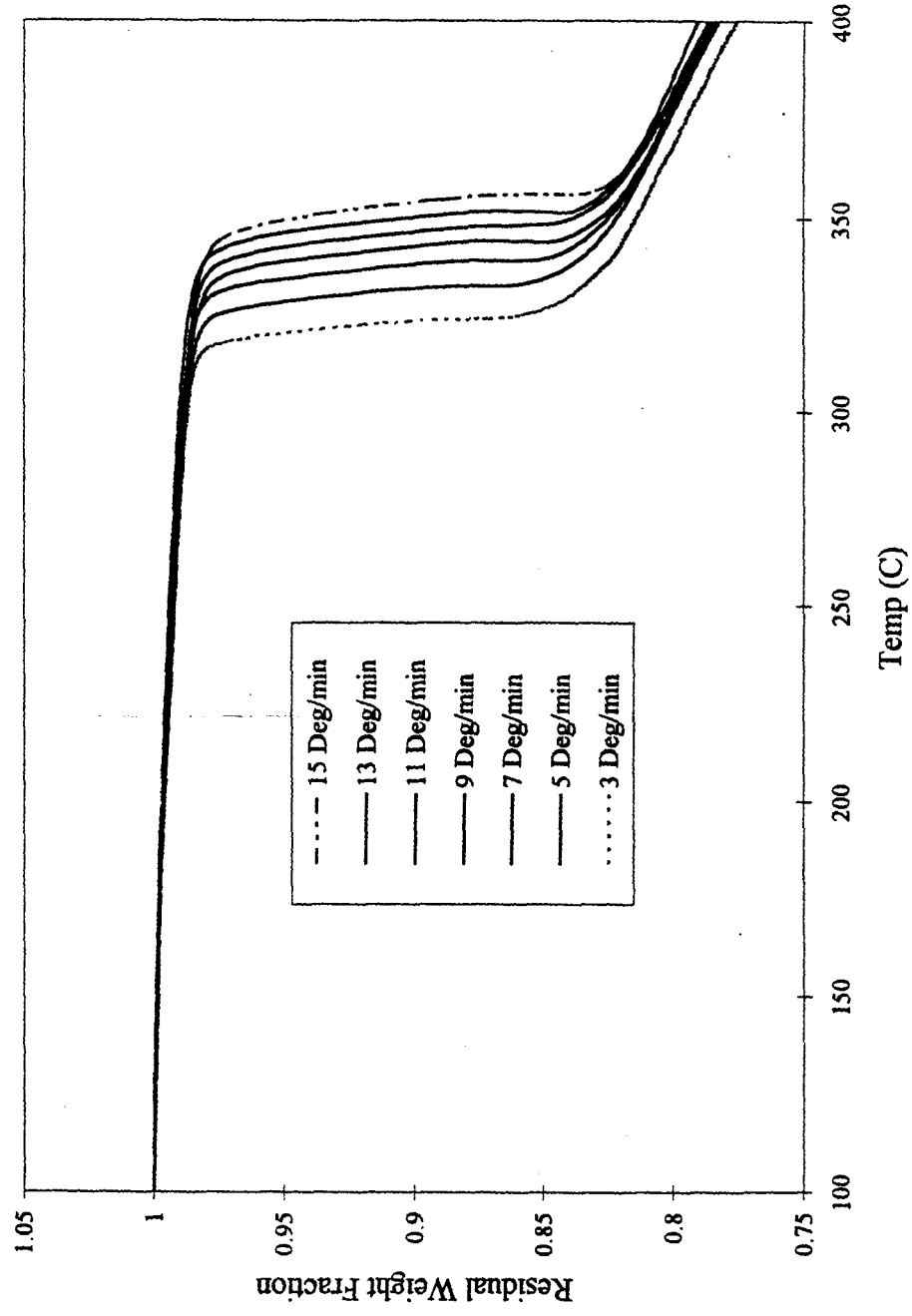

Figure 52 PPSX TGA Varied Rate Decomposition in Helium

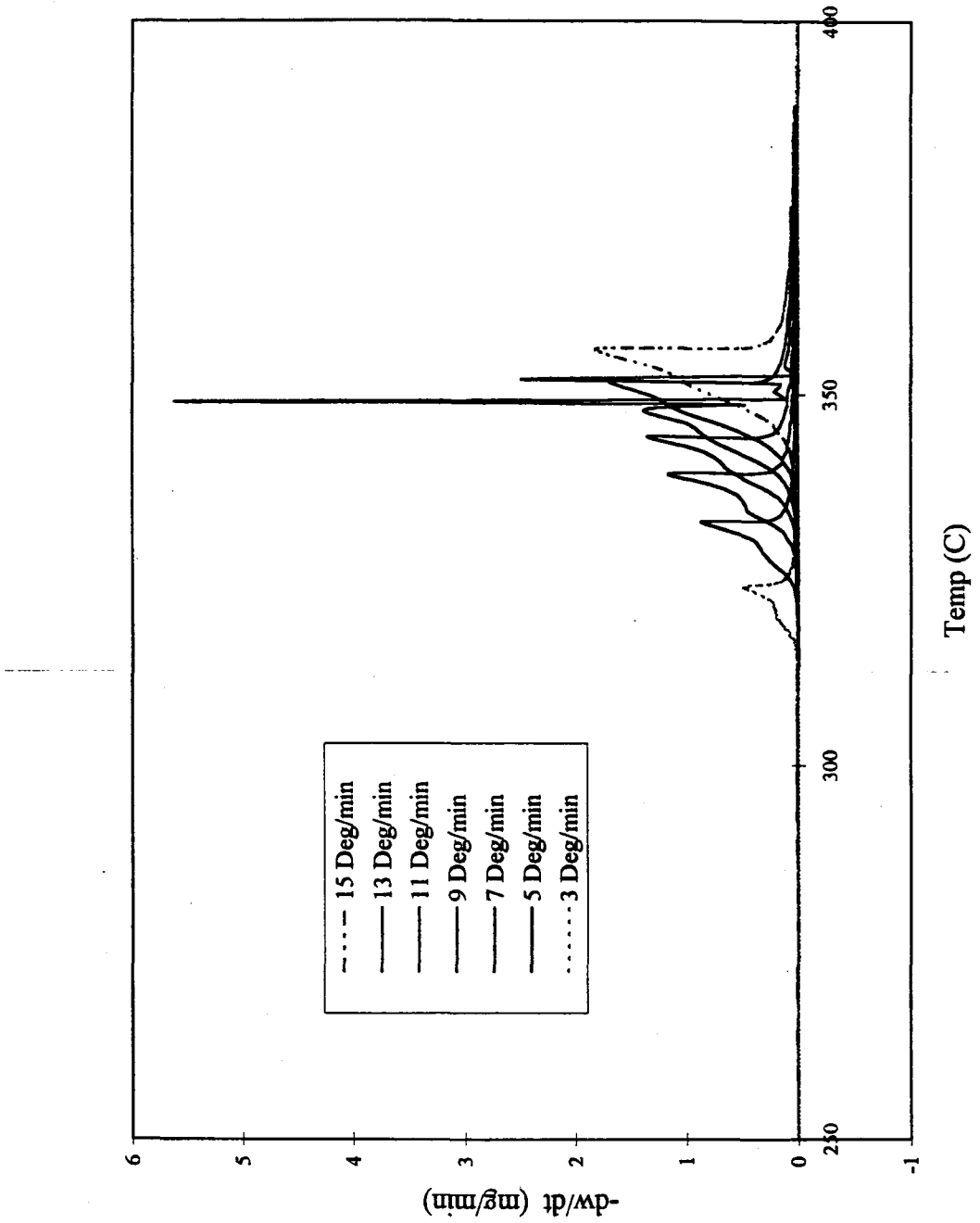

Figure 53 First Derivative of PPSX TGA Varied Rate Decomposition in Helium

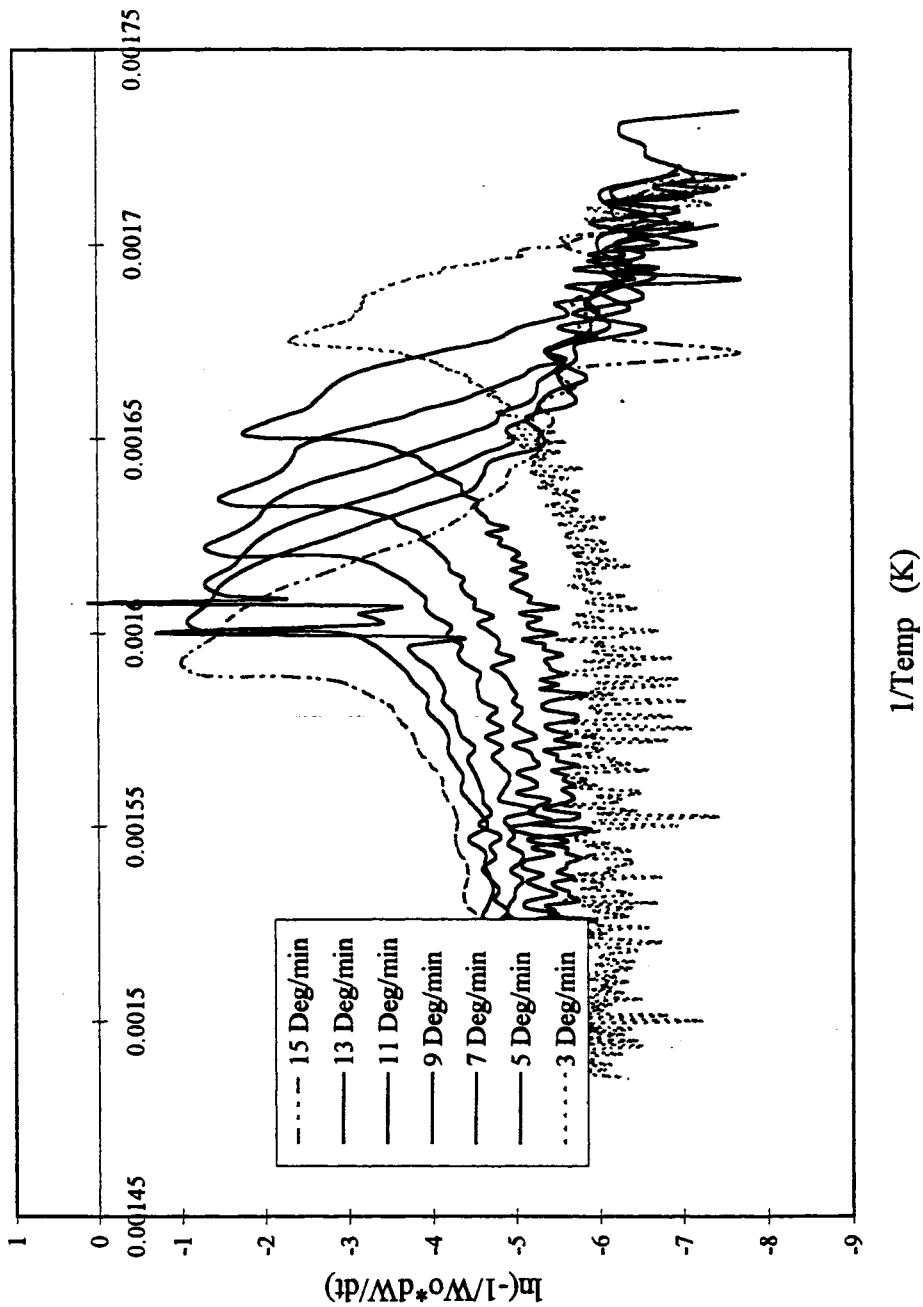

Figure 54 Arrhenius Plot of PPSX TGA Varied Rate Decomposition in Helium

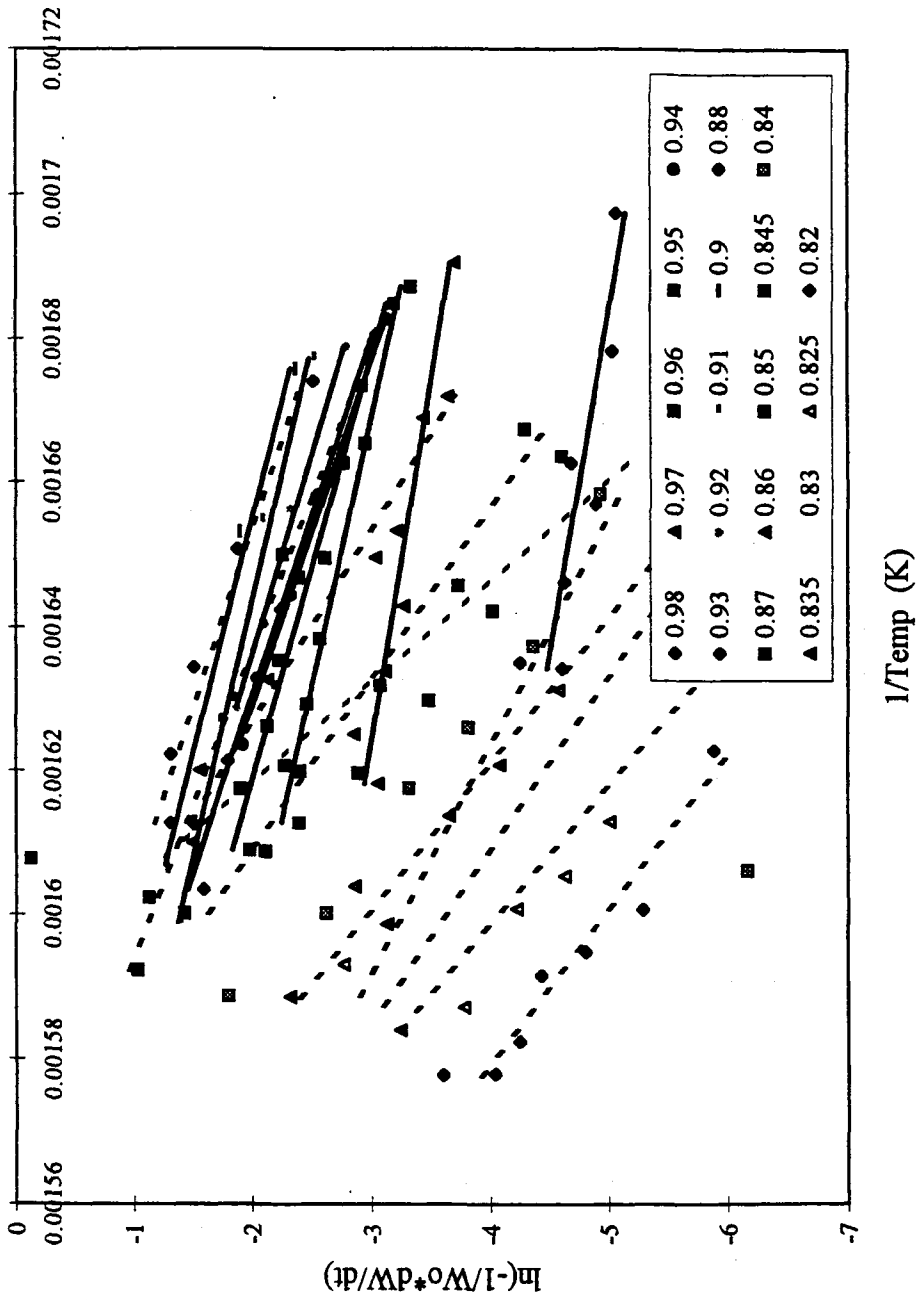

Figure 55 Residual Weight Fraction-Arrhenius Plot of PPSX TGA in Helium

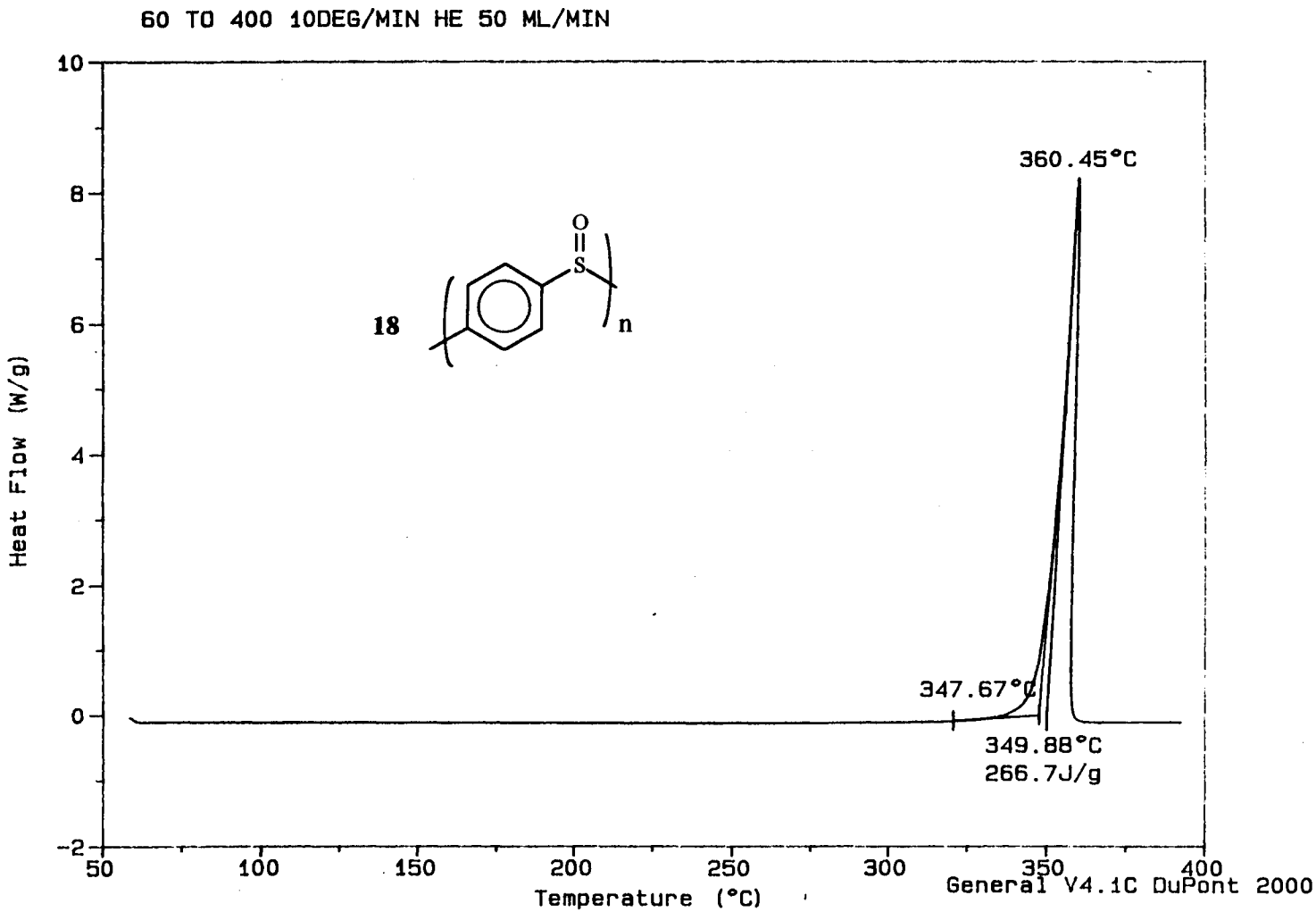

Figure 56 DSC of PPSX

4.4 Model compounds and mechanistic studies

The exclusive oxidation of PPS to PPSX with no apparent nitration seemed to be a rather odd result for a nitric acid reaction. Several experiments were conducted to better understand this reaction and to explore its mechanistic roots. To that end, several model compounds were treated according to the standard fuming nitric acid reaction conditions. Some of the model compounds were commercially available while several others were synthesized. The model compounds are illustrated in Figure 57.

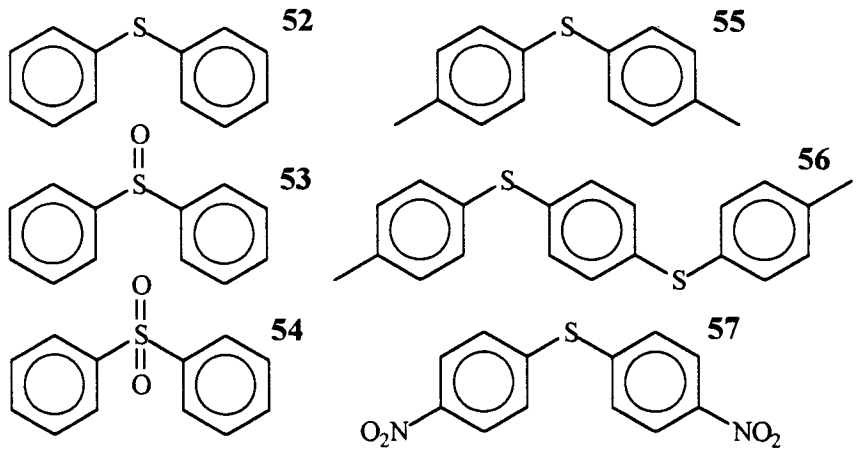

Figure 57 PPSX Model Compounds

The first model compounds treated according to the fuming nitric acid reaction were the diphenyl sulfide derivatives. The products from the reaction of fuming nitric acid with commercially available diphenyl sulfide (**52**) and diphenyl sulfoxide (**53**) appeared quite complex but completely identical by proton NMR. After a considerable effort, the reaction products were identified. The results are illustrated in Figure 58. The absolutely identical composition of the products from the two reactions fairly definitively confirmed that the oxidation of the sulfide to the sulfoxide occurred first in the reaction sequence.

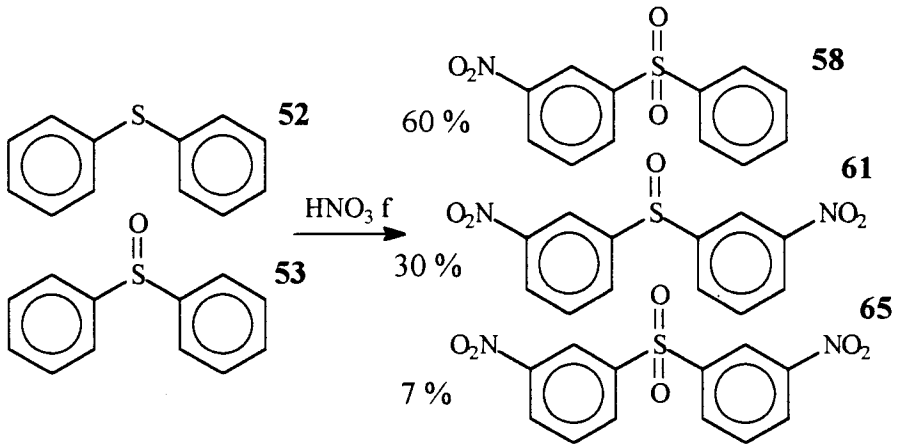

Figure 58 Diphenyl sulfide and sulfoxide Reaction with Fuming HNO_3

As illustrated in Figure 59, the reaction of fuming nitric acid with diphenyl sulfone (**54**) produced a significantly different mixture of products. While the major product *m*-nitrophenyl phenyl sulfone (**58**) was present in all of the diphenyl sulfide derivative reactions, the differing yields of the dinitrated species **61** and **65** indicated that the second nitration and second oxidation likely compete significantly.

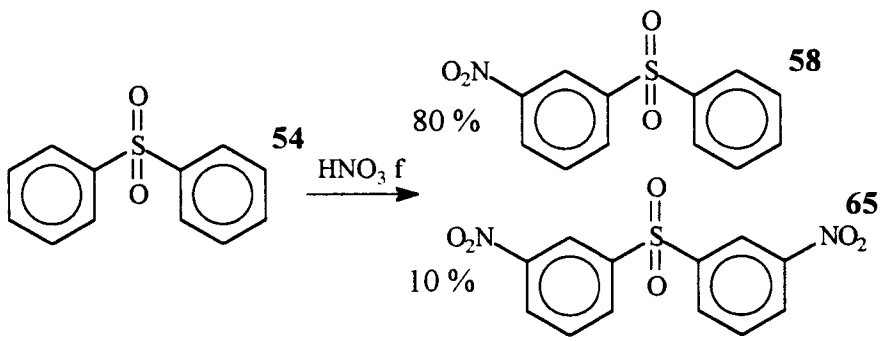

Figure 59 Diphenyl sulfone Reaction with Fuming HNO_3

As the initial identification of the diphenyl thioether derivative reactions was quite difficult and the applicability of the compounds to the PPS/PPSX/PPSO system was less

than ideal, several other compounds were synthesized as more appropriate models. The synthesis of compounds **55**, **56**, and **57** are reported in the Experimental section and documented in literature [201-204]. The reaction products formed from the reaction of **55** with fuming nitric acid are illustrated in Figure 60. In the case of bis(*p*-methylphenyl) sulfide (**55**), the reaction with fuming nitric acid cleanly produced a mixture of the dinitrated sulfoxide and sulfone in a ratio of 2:1. The *para* substitution definitely made identification of the products easier, but this model compound was still not completely similar to the PPS/PPSX/PPSO system.

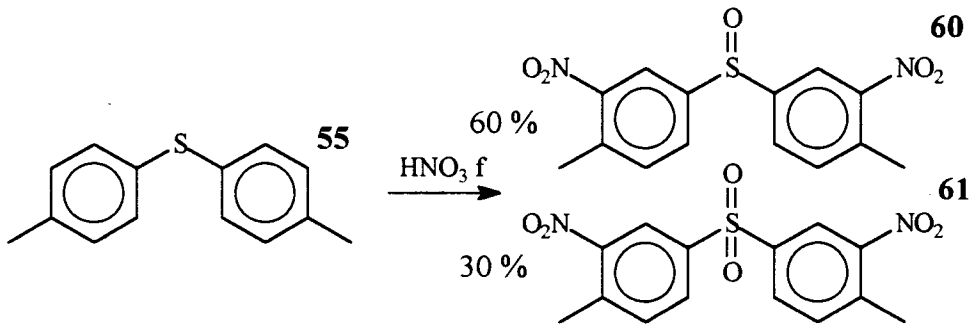

Figure 60 Bis(*p*-methylphenyl) sulfide Reaction with Fuming HNO_3

The three-ring model compound *p*-bis(*p*-methylthiophenoxy)benzene (**56**) contained at least one benzene ring that closely matched the PPS structure and electronics. On reacting with fuming nitric acid, **56** yielded only one product *p*-bis(*p*-methyl-*m*-nitro-thiophenoxy)benzene (**62**), as illustrated in Figure 61. The middle benzene ring closely represented the PPS environment, and as such was not nitrated by reaction with fuming nitric acid. The final model compound bis(*p*-nitrophenyl) sulfide (**57**) was synthesized with the intent of best matching the outer ring electronics and the expected sulfur linker

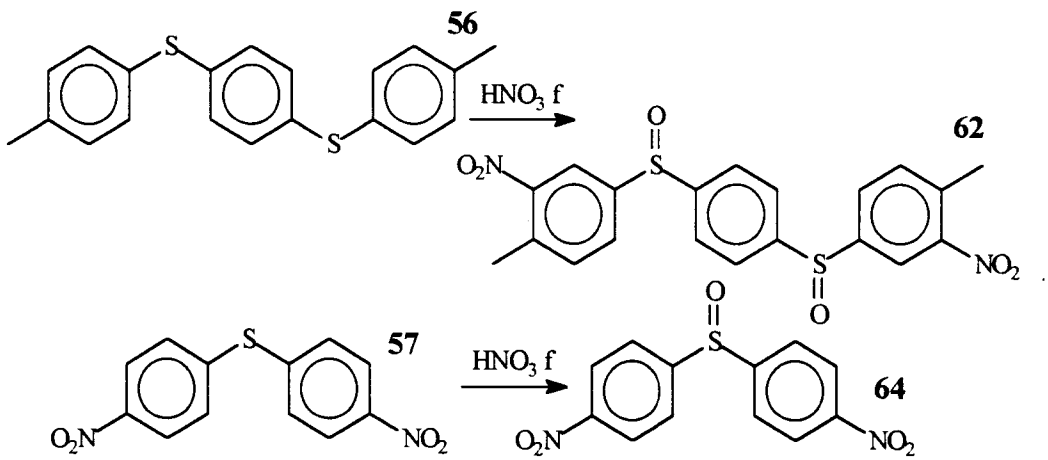

Figure 61 Reaction of **56** and **57** with Fuming HNO_3

environment to the PPSX structure. As also illustrated in Figure 61, compound **57** on reaction with fuming nitric acid produced only one compound bis(*p*-nitrophenyl) sulfoxide **64**. The *para* nitro groups of **57** closely match the electronic environment of the *para* sulfoxide groups of PPSX. An enormous effort to synthesize the three-ring equivalent of **57** proved to be repeatedly unsuccessful despite patent literature precedent [205]. With the inner ring of compound **56** being the best model for the PPS/PPSX aromatic moieties and the sulfur moiety of compound **57** being the best model for the PPS/PPSX sulfur/sulfoxide moieties, the model compounds clearly confirmed the PPS/PPSX reactivity on a small molecule scale.

From the experiences with the varied attempts at synthesizing PPSX, it was clear that solvation was very important to the first complete oxidation of PPS to PPSX. The reagents and solvents that poorly solvated PPSX, such as concentrated nitric acid alone and the mixed acid system with acetic and fuming nitric acid, gave significant amounts of underoxidized product. While the reagents and solvents that well solvated PPSX gave

either PPSX or the overoxidized sulfone. A more challenging issue is found in the explanation as to the selective production of PPSX without observed overoxidation when using fuming nitric acid compared to the mixed acid systems with sulfuric and concentrated nitric acid or the alternative oxidants such as pTFA or hypochlorite. While the latter alternative oxidant results may be argued on the basis of a greater oxidizing potential, the mixed acid system of sulfuric and concentrated nitric acid requires greater elaboration. This is particularly true in light of the absence of overoxidation when using the mixed acid system of TFA and concentrated nitric acid. The obvious differences in these two mixed acid systems are the relative acidity of the acid solvents and the demonstrated ability to form sulfoxide adducts.

The potential importance of adduct formation in the prevention of overoxidation and in the initial solvation-dependent underoxidation was addressed by reacting PPS with concentrated nitric acid and a stoichiometric amount of TFA. The resultant heterogenous products matched the underoxidized concentrated nitric acid reaction with no significant differences. This reaction demonstrated that adduct formation with TFA was most likely not the solitary basis for the controlled oxidation.

The reaction of PPS with fuming nitric acid clearly produced a large amount of gaseous NO_2 as a nitrogen oxide byproduct. This byproduct production was actually employed as a novel laboratory based synthesis of nitrogen tetroxide in other experiments in our laboratory. It was hypothesized that these nitrogen oxide byproducts or other NO_x intermediates may be providing the selective oxidation protection. A reaction of PPSX with white fuming nitric acid confirmed this hypothesis. White fuming nitric acid is

prepared by adding excess urea to fuming nitric acid. The resultant solution is clear and colorless unlike normal fuming nitric acid which retains an orange-red color from the dissolved NO_2 species [206]. The urea acts as a scavenger of nitrous acid and nitrogen dioxide, which decolorizes the solution [207]. Fuming nitric acid itself can be synthesized from the distillation of pure HNO_3 from a mixed acid solution of concentrated sulfuric and concentrated nitric acids [208]. The initially colorless distillate eventually develops its characteristic color after sitting at room temperature. The reaction of white fuming nitric acid with PPS produced a PPSX product with 10 % overoxidation. Clearly the NO_2 gas or an earlier reaction intermediate was providing the overoxidation protection. This conclusion is also supported by several prior reports of the similar selective synthesis of sulfoxides by reactions directly with nitrogen tetroxide N_2O_4, the dimer of NO_2 and with nitronium salts (NO_2^+) [209-212]. The reaction mechanism reported by Olah for the selective oxidation of sulfide to sulfoxide is shown in Figure 62.

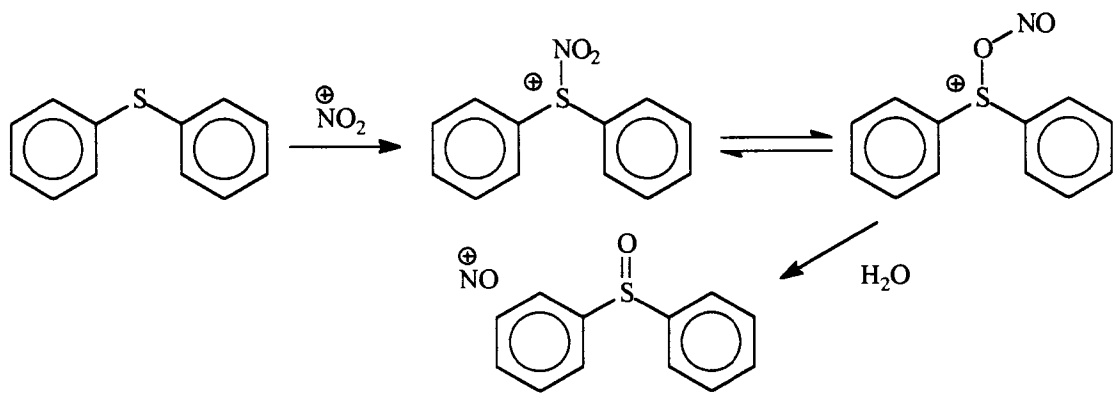

Figure 62 Nitronium Salt Reaction with Aryl Sulfides

The formation of the S-nitrito onium ion provided a protection from overoxidation even in the face of excess amounts of the vigorously oxidizing nitronium salt. The isolated

sulfoxides subsequently were easily oxidized to the sulfone using the same nitronium salt.

The potential importance of the acid-base properties of sulfoxides has also been previously hypothesized as a explanation for the selective oxidation of aryl sulfide to sulfoxides [213-215]. All of these reports discussed the potential protecting effect of the protonation of the sulfoxide in the acidic media, as illustrated in Figure 63. This protonated species would be less likely to be further oxidized to the corresponding

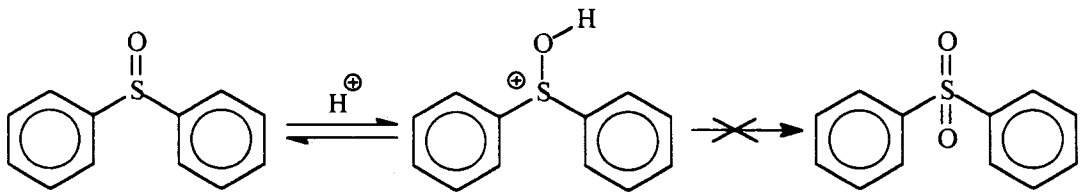

Figure 63 Protonation Based Selective Oxidation

sulfone. The exclusive importance of this mechanism seemed less likely particularly when considering the protective effects of the S-nitrito onium species and the overoxidation of PPSX in white fuming nitric acid and the mixed concentrated sulfuric/nitric acids. In these latter cases the same or even higher acidity failed to protect the sulfoxide from overoxidation. As a final note, it should be noted that the protective effect of any specific species in the oxidation of PPS was eventually overcome by mild heating to 54 °C where some overoxidation was seen even in fuming nitric acid.

As previously mentioned PPSX reacted with sulfuric acid after about an hour of sitting in solution. A green precipitate formed matching a previously documented reaction of aryl sulfoxides with sulfuric acid [216, 217]. The likely reaction of PPSX with sulfuric

acid is illustrated in Figure 64. This reaction is fully reversible and the starting sulfoxide can be recovered by quenching with water.

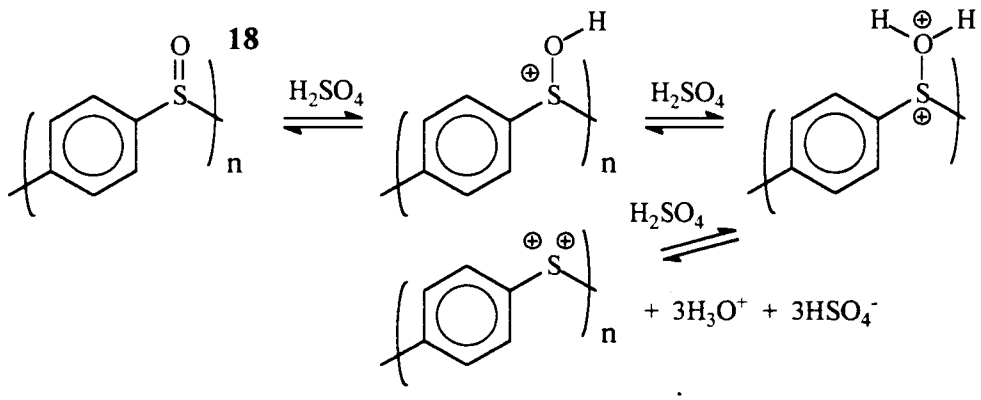

Figure 64 PPSX Reaction with Sulfuric Acid

In a related reaction, hydrobromic acid was reacted with PPSX also producing a precipitate which was orange-red, rather than green. The product from the reaction of HBr with PPSX was identified as PPS, and the orange-red color was due to the byproduct bromine. This reaction, which matched several previously reported sulfoxide reactions, is illustrated in Figure 65 [218-220]. The reaction with hydrobromic acid is fully reversible.

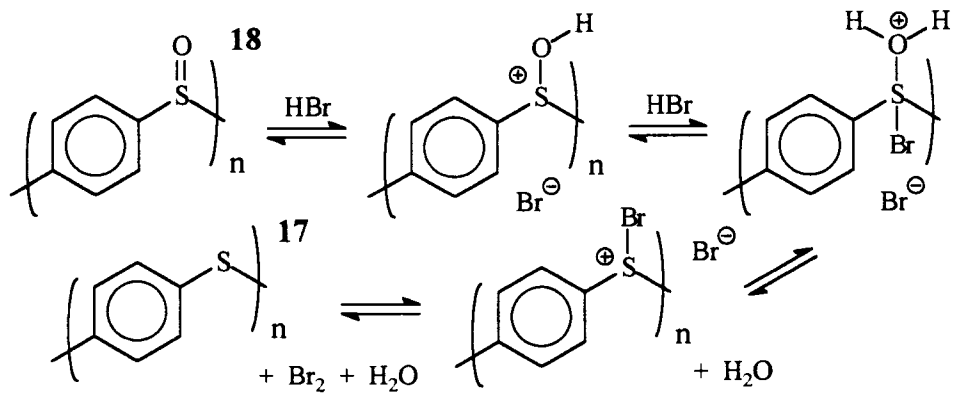

Figure 65 PPSX Reaction with HBr Forming PPS

Figure 66 shows the progressive growth of the PPS band in the UV-VIS spectrum during the reaction with HBr in TFA.

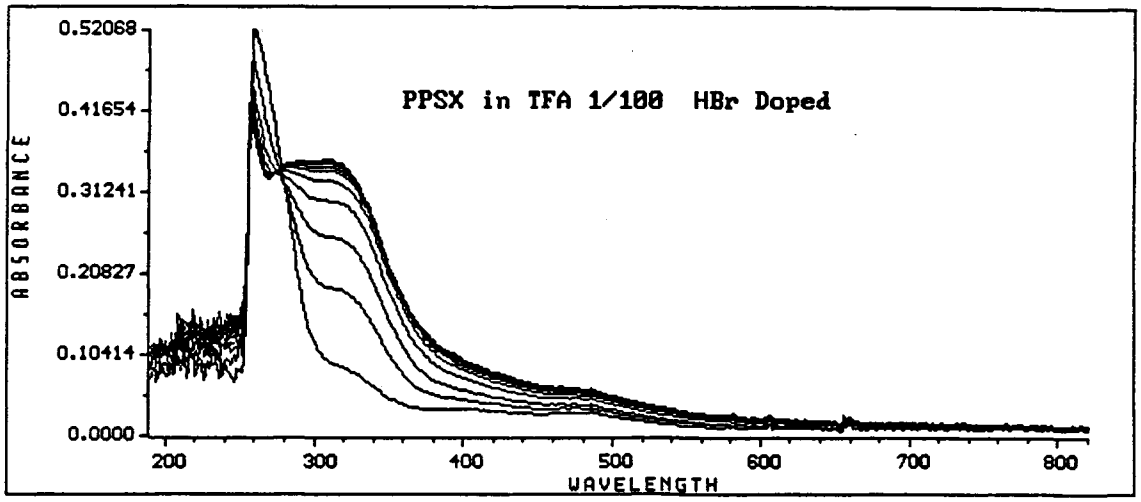

Figure 66 UV-VIS Monitoring of PPSX Reaction of HBr Forming PPS

Another researcher has conducted an extensive investigation into the kinetics of the oxidation of sulfides to sulfoxides with nitric acid [207]. The stoichiometry of the reaction was confirmed as being one mole of nitric acid to one mole of sulfide producing one mole of nitrous acid and one mole of sulfoxide. The rate law for the oxidation of sulfides to sulfoxides with concentrated nitric acid in acetic acid was determined as shown in Equation 13.

$$v = k\,[ArSAr]\,[HNO_3]\,[HNO_2] \qquad (13)$$

The reaction demonstrated an autocatalytic effect as the product nitrous acid impacted the reaction rate. A similar autocatalytic effect was grossly noted in our laboratory with the oxidation of PPS. There was a significant delay (5 minutes) in the solvation during the

stoichiometric nitric acid, white fuming nitric acid, and mixed sulfuric/nitric acid reactions. These authors concluded that a protonated N_2O_4 was the most likely reacting species.

In final consideration of the experimental results from the varied synthetic approaches to PPSX, the model compound reactions and prior literature, it seemed most likely that the selective oxidation of PPS with nitric acid was most strongly influenced by the electronic effects of neighboring sulfoxide deactivation and the direct interactions of a nitrogen oxide product with the sulfoxide moieties. The specific importance of the protonation based deactivation of PPSX was not supported by this work, but rather directly contradicted. While there are several documented nitrogen oxide adducts of sulfoxides, a specific conclusion as to the relevant species cannot be made based on these results. The model compounds clearly demonstrated the similar selective oxidation effects. The proposed electronic deactivation of the neighboring sulfoxides could not alone explain the selective oxidation, as this effect was present in the white fuming nitric acid reaction which also demonstrated overoxidation. This electronic deactivation by the sulfoxides does likely limit nitration of the PPSX aryl moieties . These results and the related work of Olah solidly support the determination that a nitrogen oxide product interaction provided the most vital selective oxidation contribution.

4.5 Metal chelation application

There are an enormous variety of metal complexes with sulfoxides [192, 221-223]. Typically these complexes contain the ubiquitous dimethyl sulfoxide or less commonly diphenyl sulfoxide. There have also been a few macrocyclic polythioether sulfoxides

reported as crown ether like complexing agents [192, 224]. The versatility of the sulfoxide group as a metal coordinator can be attributed to its ambidentate donor character. Metals can coordinate at either the hard oxygen or the softer sulfur. This diversity explains why sulfoxide complexes of virtually every family in the periodic table have been characterized.

A significant area of potential utility for PPSX has its roots in this diverse coordination capability. Several non-polymeric sulfoxides have been investigated for their ability to extract and isolate a variety of metal ions including iron, zirconium, cobalt, chromium, nickel, copper, zinc, aluminum, manganese, calcium, sodium, europium, americium, thulium, plutonium, and uranium [225-233]. As all of these studies focused on metal extraction and isolation using solvated sulfoxides, their most relevant application would be to industrial isolation processes where the use of the organic solvents would be acceptable.

An even more important potential application for which PPSX is ideally suited is metal extraction from aqueous media, hydrometallurgy. A fairly wide variety of functionalized polymers have been used or studied as metal extraction compounds [234-241]. They typically contain carboxylic acid, amide, amine, or amidoxime derivatives of vinyl polymers or functionalized poly(styrenes). They have been used to isolate a large selection of metals: Na, Mg, K, Ca, Ti, V, Cr, Mn, Fe, Co, Ni, Cu, Ag, Au, Zn, Cd, Hg, Cd, Pb. There has been particular interest in the extraction of uranium from seawater as a source of nuclear reactor fuel [242-249]. The uranium concentration in seawater is 3 μg/L with an estimated global total quantity of 5×10^9 tons [248]. The difficult task is

isolation of the uranium from the seawater in an energy efficient manner. More recently, the experiences from the isolation and separation of the uranyl oxocations is being extended to the waste treatment and removal of radioactive elements from contaminated nuclear facilities [250].

With the prior successes of the small molecule sulfoxides in separating and isolating a wide variety of metals and the parallel successes of other polymer based separation techniques, the exploration of PPSX as a possible metal chelating polymer seemed well grounded. For this effort, metals were selected based on available Flame Atomic Absorption Spectroscopy (FAAS) lamps and the uniform availability of the perchlorate salts. The hydrated perchlorate salts were selected based on their relatively poor coordinating ability [206]. The test metals were cadmium, copper, iron, zinc, chromium, nickel, mercury, lead, and lanthanum. The analyte concentrations and instrument parameters were selected based on optimum FAAS working ranges [251]. There were four different separation methods designed to test PPSX. Method I involved simply stirring the loose PPSX powder in an aqueous metal salt solution for 1.5 hours. The slurry was filtered through glass wool and directly analyzed. Method II involved the same procedure as Method I except that nitric acid was added to the solution (1.4 M). Method III was designed as a mimic of the prior biphasic industrial procedures. A solution of PPSX in *m*-cresol was stirred with the aqueous metal salt solution. After stirring for 1.5 hours the aqueous layer was removed and analyzed directly. Method IV was designed to most closely approximate a column extraction technique. The aqueous metal salt solution was percolated through a Pasteur filter pipette which was packed with powdered PPSX

supported by glass wool. Only cadmium, copper, iron, mercury, and zinc were tested using all four methods. The additional metals, nickel, chromium, lanthanum, and lead were tested only using Method I. The results of the metal extraction are presented in Tables 8 and 9.

Table 8. PPSX metal chelation results given by Method I-IV in percent extracted

Metal	Conc*	I	II	III	IV	r^{2***}
Cd^{2+}	5.1	94	-37	93	96	0.98
Cu^{2+}	5.0	86	-38	80	86	0.99
$Fe^{3+/2+}$	5.1	92	-28	69	88	0.99
Hg^{2+**}	250.	25	14	79	31	0.998
Zn^{2+}	5.1	108	-79	112	104	0.97

* Conc in ppm
** Also 0.64 M HNO_3 required for solvation
*** Correlation Coefficient for FAAS standards

Table 9. Further PPSX metal chelation results by Method I in percent extracted

Metal	Conc*	I	r^{2**}
Cr^{3+}	10.0	101	0.998
La^{3+***}	250.	-142	0.84
Ni^{2+}	10.0	107	0.99
Pb^{2+}	20.4	179	0.46

* Conc in ppm
** Correlation Coefficient for FAAS standards
*** $La(NO_3)_3$

These results strongly supported the potential utility of PPSX as a metal chelating polymeric material. The best overall results were obtained using Method I, but the column

percolation Method IV produced comparable results. Method II was designed to indicate the acid removal capability of the polymer-metal complexes. Most of the other polymeric metal chelators release the chelated metals upon acid treatment. Method II clearly indicated that strong acid significantly inhibits PPSX's ability to chelate metals. The generally poor response of mercury was due to the acidification required to dissolve the mercury salts at the concentration detectable by FAAS. The same was true for lanthanum. The lead experiment had rather poor standardization ($r^2 = 0.46$). Another instrumental method is clearly indicated for mercury, lanthanum, and lead [251]. The negative values in Method II likely resulted from the liberation of the test metals which had been previously chelated to the PPSX during synthesis and isolation. The other metals demonstrated excellent separation and chelation by PPSX using either Method I or IV, and fair separation using the biphasic Method III. The two softest metals, zinc and mercury, actually produced the best separation using Method III.

An additional metal chelation experiment was conducted to assess the loading capacity of PPSX. The loading capacity study was a duplication of the Method I experiment with iron except variable amounts of PPSX were used to change the PPSX repeat unit to iron ratio. As expected, the extraction percentage decreased with a decreasing PPSX:Fe ratio. As the metal chelation is also presumably an interfacial reaction/adsorption, the particle size of the PPSX should also have a significant impact. There are a variety of strategies that might improve the PPSX:Fe ratio such as swelling the PPSX in a water immiscible solvent. The results of the loading capacity study are presented in Figure 67.

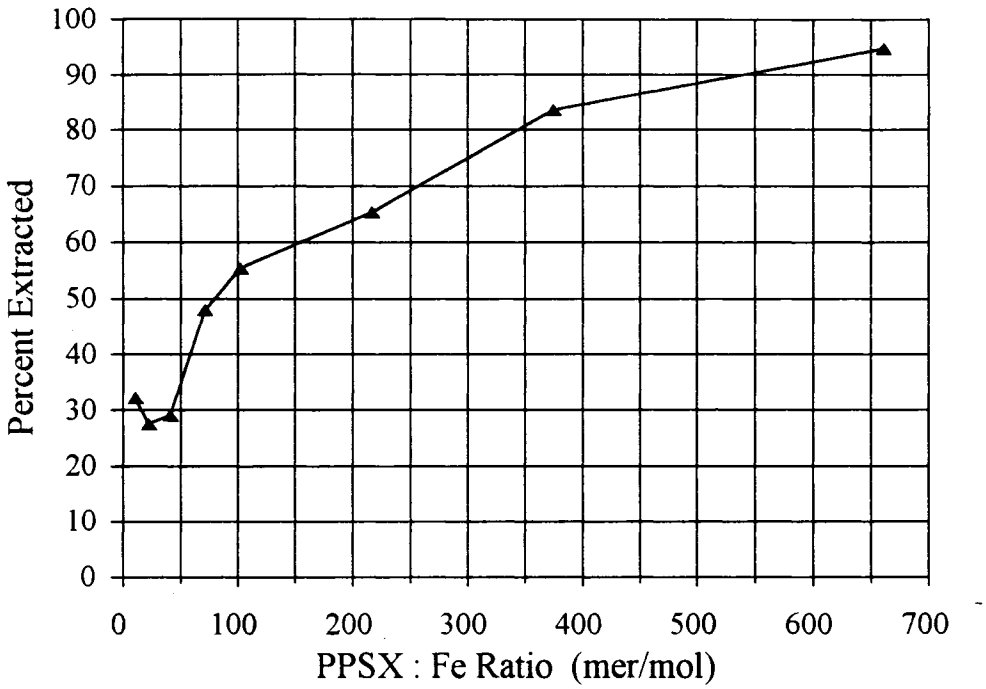

Figure 67 PPSX Metal Chelation Loading Capacity with Iron

4.6 Summary and Conclusions

The polymer poly(*p*-phenylene sulfoxide) (PPSX) **18** was synthesized by a novel, simple, homogenous oxidation of poly(*p*-phenylene sulfide) **17** with fuming nitric acid in high yields. Two other homogenous reactions using limited quantities of fuming or concentrated nitric acid in a trifluoroacetic acid solvent produced equally excellent yields at a significantly lower cost. No overoxidation of PPSX to the sulfone equivalent polymer PPSO was found in the three novel nitric acid oxidations at room temperature. Several other oxidant and solvent systems were investigated, but they generally failed to produce the PPSX polymer in significant yields without underoxidizing or overoxidizing it in the reaction. The underoxidation demonstrated in these other reagent/solvent systems

is best attributed to the lack of solubility of PPSX, while the absence of overoxidation in the novel nitric acid systems is best attributed to the unique nitric acid oxidation environment.

Several model compounds were synthesized to explore the mechanistic foundations of the fuming nitric acid oxidation of PPSX. The results of the fuming nitric acid oxidation of these model compounds as well as the previous results from the alternative oxidant and solvent systems indicated that the most likely explanation for the selective oxidation of PPS to PPSX without overoxidation to PPSO is the formation of a nitrogen oxide adduct with the PPSX during the oxidation. There are most likely contributing electronic influences from both the neighboring sulfoxide groups and protonation of the sulfoxide moieties. However, an increase in the reaction media acidity actually had a detrimental effect causing significant overoxidation of the PPSX. Hence, contrary to prior literature, the protonation of the sulfoxide moieties is not likely to be an important protective mechanism that caused the selective oxidation in nitric acid.

PPSX was characterized by a wide variety of instrumental and polymer specific techniques. The proton NMR, carbon NMR, IR, and UV-VIS spectra of PPSX matched expected and typical values for aryl sulfoxides. The elemental analysis fell somewhat short of the theoretical values, but these results may have been particularly susceptible to problems unique to the macromolecular nature of PPSX. GPC analysis was successfully used to assess the molecular weight distributions of several different PPSX samples derived from different source PPS's. The results matched the reported molecular weight profiles of the original PPS samples. A precipitation/solvation method was developed that

successfully isolated the highest molecular weight PPSX currently identified (Mw 84,000 and Mn 30,800). Extensive viscometry analysis was performed on PPSX, confirming the expected relationship between inherent viscosity and molecular weight as well as identifying PPSX's intrinsic viscosity as 0.274.

Several binary solvent systems were found that greatly assisted in the characterization of PPSX and enhanced its potential for commercial use. The lessons learned from these solvation studies permitted the effective casting of several high quality PPSX films with plasticizer enhancement from unitary and binary solvents.

Several involved thermal analysis techniques were applied to PPSX. The DSC analysis identified PPSX as a completely amorphous polymer lacking a glass transition temperature above 65 °C. PPSX was identified as a highly thermally stabile polymer with decomposition temperatures of 334 °C in air and 342 °C in helium. The weight loss at decomposition exhibited a unique dependence on sample mass possibly indicating a potentially useful cure reaction. The TGA determined weight loss of PPSX in air varied from 16 to 42 %. The activation energies of the thermal decomposition of PPSX in air and helium were determined by the Friedman method to be 32 +/- 6 and 31 +/- 3 kcal/mol, respectively. The other kinetic parameters, reaction order and frequency factor could not be determined.

A potential application of PPSX as a metal chelating polymer was studied using four different separation methods. PPSX effectively chelated all of the tested metals at neutral pH. The two techniques using PPSX as a solid resin in a slurry or in a packed column proved effective at chelating iron, cadmium, copper, and zinc. Nickel and chromium were

also effectively chelated with the slurry technique. The wide variety of known metal sulfoxide coordination complexes and the ambidentate nature of the sulfoxide ligand strongly support a future application of PPSX as a novel metal chelating resin.

While not specifically investigated in this work, any soluble conjugated organic polymer has a potential for electronic applications. This work has demonstrated that PPSX can be selectively oxidized or reduced by approximately 5-10 % and still remain soluble. This partial oxidation or reduction of PPSX may provide the ability to tune the electronic properties of a future electronic device. Furthermore, PPSX's demonstrated metal chelating ability and reactivity to sulfuric acid may provide an additional method of modifying the conductive and electrical properties of PPSX in films or solution. Clearly, PPSX has many possible future applications with few currently defined limitations.

4.7 Experimental

General Methods. All starting materials and solvents were acquired commercially and used without further purification unless stated otherwise. **New Compounds** are marked by an asterisk * in their experimental section. All instrumentation, hardware, and software employed for this research are detailed in Appendix D.

Poly(*p*-phenylene sulfoxide) (PPSX) (18) from fuming nitric acid. The starting material poly(*p*-phenylene sulfide), **17** (5.03 g, 46.5 mmol), was placed in a 250 mL Erlenmeyer flask with a stir bar. Fuming nitric acid (100 mL) was added dropwise to the flask. A brown-orange gas (NO_2) evolved from the flask during the addition. A homogeneous solution eventually resulted within 5-10 minutes of stirring. The solution

was stirred at room temperature for a total of 30 minutes. The final reaction solution was poured into water (300 mL) producing a crude yellow solid. The crude product was isolated by vacuum filtration and washed with two portions of water (100 mL each). The solid was vacuum dried overnight. This crude dried product was re-dissolved in a minimal amount of trifluoroacetic acid (50 mL) and re-precipitated by dropwise addition to vigorously stirring water (300 mL). This re-precipitated product was isolated by vacuum filtration and vacuum dried overnight. This purified dried solid was further dried by stirring in acetone (75 mL) and vacuum filtered with two additional acetone washes (75 mL each). This acetone-dried, purified, pale yellow powder was dried for two days in a vacuum oven. The final yield was 5.09 g, 88 %. The product was identified by its characteristic ^{1}H NMR spectrum: (400 MHz, d-TFA) δ 7.90 (s, 1H): ^{13}C NMR (100 MHz, d-TFA, decoupled) δ 148.1, 129.4. IR-film (cm^{-1}, strg, mod, wk) 3074w, 3041w, 3012w, 1650w, 1468w, 1387m, 1287w, 1095s, 1046s, 1008m, 823m, 811m, 620w, 564s, 534m.

Poly(*p*-phenylene sulfoxide) (PPSX) (18) from fuming nitric acid varied time and temperature. The starting material poly(*p*-phenylene sulfide), **17** (100. mg, 0.926 mmol), was placed in a 5 mL conical vial with a spin-vane. Fuming nitric acid (2 mL) was added dropwise to the vial. A brown-orange gas (NO_2) evolved from the vial during the addition. For the varied time reactions, the reaction ran for 30 minutes, 2 hours, 4 hours, 24 hours, and 48 hours. The varied time reactions were conducted at room temperature. The varied temperature reactions were temperature controlled with either a hotplate or ice bath at temperatures of 0, 54, 65, and 83 °C. Following completion of the reactions at the

specified times and temperatures, the reaction mixtures were added to water (30 mL) in a 50 mL beaker. The resultant precipitate was isolated by vacuum filtration and vacuum dried for two to three days. The highest temperature reaction product (83 °C) reaction was not soluble and as such could not be dissolved for NMR analysis. All of the other reaction products were soluble in TFA. All of the varied time reactions produced exclusively PPSX with no indication of overoxidation or underoxidation as determined by proton NMR. The low temperature (0 °C) reaction also produced exclusively PPSX. The higher temperature (54 and 65 °C) reactions produced a product with partial sulfoxide to sulfone oxidation (5.8 % and 6.3 %, respectively) as determined by proton NMR. The sulfone diad produced a distinct double doublet in the proton NMR. One of the doublets overlapped with the main sulfoxide signal but the downfield doublet was 0.25 ppm downfield from the sulfoxide monomer signal: ^{1}H NMR spectrum of downfield doublet (400 MHz, d-TFA) δ 8.15 (d, J = 8 Hz), 7.90 (s).

Poly(*p*-phenylene sulfide) (PPS) (17) reaction in excess concentrated nitric acid. The starting material poly(*p*-phenylene sulfide), **17** (110. mg, 1.02 mmol), was placed in a 10 mL conical vial with a spin-vane. Concentrated nitric acid (2 mL) was added dropwise to the vial. A brown-orange gas (NO_2) evolved from the vial during the addition. A solid material never completely dissolved in the reaction vial after 1.5 hours of reaction. The slurried product was vacuum filtered directly into water (175 mL) resulting in a yellow precipitate. The crude precipitate was isolated by vacuum filtration and vacuum dried overnight. The original insoluble solid was not analyzed further. The soluble precipitate was analyzed by proton NMR. The yield was 40 mg, 32 % based on sulfoxide product.

The soluble precipitate contained some underoxidized sulfide monomers (< 2 %) as determined by proton NMR. The sulfide diad produced a distinct double doublet in the proton NMR. Both doublets were upfield (-0.27 and -0.37 ppm) from the main sulfoxide monomer signal: ^{1}H NMR spectrum (400 MHz, d-TFA) δ 7.90 (s), 7.63 (d, J = 8 Hz), 7.53 (d, J = 8 Hz).

Poly(*p*-phenylene sulfide) (PPS) (17) reaction in excess white fuming nitric acid. The starting material poly(*p*-phenylene sulfide), **17** (1.00 g, 9.26 mmol), was placed in a 50 mL Erlenmeyer flask with a stir bar. White fuming nitric acid (20 mL) was added to the flask. White fuming nitric acid was synthesized by adding urea (3 g) to fuming nitric acid (40 mL). Air was sparged through the reaction solution throughout the reaction. A brown-orange gas (NO_2) evolved from the vial during the addition. After 30 minutes of reaction, the reaction solution was poured into water (100 mL) resulting in a yellow precipitate. The precipitate was isolated by vacuum filtration and vacuum dried overnight. The precipitate contained some overoxidized sulfone monomers (10 %) as determined by proton NMR. The sulfone diad produced a distinct double doublet in the proton NMR. One of the doublets overlapped with the main sulfoxide signal but the downfield doublet was 0.25 ppm downfield from the sulfoxide monomer signal: ^{1}H NMR spectrum of downfield doublet (400 MHz, d-TFA) δ 8.15 (d, J = 8 Hz), 7.90 (s).

Poly(*p*-phenylene sulfide) (PPS) (17) reaction in sulfuric acid with excess concentrated nitric acid. The starting material poly(*p*-phenylene sulfide), **17** (105 mg, 0.972 mmol), was placed in a 5 mL conical vial with a spin-vane. Concentrated nitric acid (1 mL) and concentrated sulfuric acid (3 mL) was added to the vial. A brown-orange gas

(NO_2) evolved from the vial during the addition. The solid material slowly dissolved in the vial after 30 minutes of reaction. The product was poured into water (75 mL) resulting in a yellow precipitate. The precipitate was isolated by vacuum filtration and vacuum dried overnight. The dried precipitate was analyzed by proton NMR. The yield was 86 mg, 71 % based on sulfoxide product. The precipitate contained significant amounts of overoxidized sulfone monomers (3 %) as determined by proton NMR. The sulfone diad produced a distinct double doublet in the proton NMR. One of the doublets overlapped with the main sulfoxide signal but the downfield doublet was 0.25 ppm downfield from the sulfoxide monomer signal: ^{1}H NMR spectrum of downfield doublet (400 MHz, d-TFA) δ 8.15 (d, J = 8 Hz), 7.90 (s).

Poly(*p*-phenylene sulfide) (PPS) (17) reaction in acetic acid with excess fuming nitric acid. The starting material poly(*p*-phenylene sulfide), **17** (100 mg, 0.926 mmol), was placed in a 5 mL conical vial with a spin-vane. Premixed fuming nitric acid (1 mL) and acetic acid (2 mL) was added to the vial. A brown-orange gas (NO_2) evolved from the vial during the addition. The slurried product was vacuum filtered directly into water (75 mL) resulting in a small amount of yellow precipitate. The crude precipitate was isolated by vacuum filtration and vacuum dried overnight. The original insoluble solid was not analyzed further. The soluble precipitate was analyzed by proton NMR. This precipitate contained significant amounts of underoxidized sulfide monomers (5 %) as determined by proton NMR. The sulfide diad produced a distinct double doublet in the proton NMR. Both doublets were upfield (-0.27 and -0.37 ppm) from the sulfoxide monomer signal: ^{1}H NMR spectrum (400 MHz, d-TFA) δ 7.90 (s), 7.63 (d, J = 8 Hz), 7.53 (d, J = 8 Hz).

Poly(*p*-phenylene sulfoxide) (PPSX) (18) from trifluoroacetic acid with excess fuming nitric acid. The starting material poly(*p*-phenylene sulfide), **17** (20.0 g, 0.185 mol), was placed in a 500 mL Erlenmeyer flask with a stir bar. Trifluoroacetic acid (300 mL) was added to the reaction flask. Fuming nitric acid (45.2 g) was added to the flask. A brown-orange gas (NO_2) evolved from the flask during the addition. A homogeneous solution eventually resulted within 5-7 minutes of stirring. The solution was stirred at room temperature for a total of 40 minutes. The final reaction solution was added dropwise into water (1.5 L) over one hour producing a crude yellow solid. The crude product was isolated by vacuum filtration and washed with two portions of water (250 mL each). The solid was redissolved in TFA (500 g) and re-precipitated by dropwise addition to vigorously stirring water (2 L). This re-precipitated product was isolated by vacuum filtration, washed with two portions of water (250 mL each), washed with three portions of acetone (100 mL each), and vacuum dried for three days. The final yield was 21.9 g, 95 %. The product was identified by its characteristic ^{1}H NMR spectrum (400 MHz, d-TFA) δ 7.90 (s, 1H).

Poly(*p*-phenylene sulfoxide) (PPSX) (18) from trifluoroacetic acid with stoichiometric fuming nitric acid. The starting material poly(*p*-phenylene sulfide), **17** (0.541 g, 5.01 mmol, 1 eq), was placed in a 25 mL pear flask with a stir bar. Trifluoroacetic acid (15 mL) was added to the flask. Fuming nitric acid (0.352 g, 5.03 mmol, 1 eq based on 90 % HNO_3), was added dropwise to the flask. A brown-orange gas (NO_2) evolved from the flask during the addition. The solution was stirred at room temperature for a total of 37 minutes. The final reaction solution was poured into water

(500 mL) producing a crude yellow solid. The product was isolated by vacuum filtration and washed with two portions of water (100 mL each). The solid was vacuum dried overnight. The dried product was analyzed by proton NMR. The final yield was 0.64 g, 103 %. The product was identified by its characteristic ^{1}H NMR spectrum (400 MHz, d-TFA) δ 7.90 (s, 1H).

Poly(*p*-phenylene sulfoxide) (PPSX) (18) from trifluoroacetic acid with excess concentrated nitric acid. The starting material poly(*p*-phenylene sulfide), **17** (175 mg, 1.62 mmol), was placed in a 25 mL Erlenmeyer flask with a stir bar. TFA (6 mL) was added to the reaction flask. Concentrated nitric acid 70 % (2 mL) was added to the flask. A brown-orange gas (NO_2) evolved from the flask during the addition. A homogeneous solution eventually resulted within 5-10 minutes of stirring. The solution was stirred at room temperature for a total of 30 minutes. The final reaction solution was added dropwise into water (25 mL) producing a crude yellow solid. The crude product was isolated by vacuum filtration and washed with two portions of water (25 mL each). The solid was redissolved in TFA (5 mL) and re-precipitated by dropwise addition to vigorously stirring water (25 mL). This re-precipitated product was isolated by vacuum filtration, washed with two portions of diethyl ether (50 mL each), and vacuum dried for 2 hours. The product was identified by its characteristic ^{1}H NMR spectrum: (400 MHz, d-TFA) δ 7.90 (s, 1H).

Poly(*p*-phenylene sulfoxide) (PPSX) (18) from concentrated nitric acid with stoichiometric trifluoroacetic acid. The starting material poly(*p*-phenylene sulfide), **17** (200. mg, 1.85 mmol, 1 eq), was placed in a 25 mL pear flask with a stir bar.

Trifluoroacetic acid (213 mg, 1.87 mmol, 1 eq) was added to the flask. Concentrated nitric acid (6 mL) was added to the flask. A brown-orange gas (NO_2) evolved from the flask during the addition. The solution was stirred at room temperature for a total of 30 minutes. A solid material never completely dissolved in the reaction flask. The slurried product was vacuum filtered directly into water (50 mL) resulting in a yellow precipitate. The precipitate was isolated by vacuum filtration, washed with two portions of water (50 mL each), washed with two portions of diethyl ether (50 mL each), and vacuum oven dried overnight. The original insoluble solid (66 mg) was not analyzed further. The soluble precipitate was analyzed by proton NMR. The yield was 112 mg, 49 % based on sulfoxide product. The soluble precipitate contained some underoxidized sulfide monomers (5 %) as determined by proton NMR. The sulfide diad produced a distinct double doublet in the proton NMR. Both doublets were upfield (-0.27 and -0.37 ppm) from the main sulfoxide monomer signal: ^{1}H NMR spectrum (400 MHz, d-TFA) δ 7.90 (s), 7.63 (d, J = 8 Hz), 7.53 (d, J = 8 Hz).

Poly(*p*-phenylene sulfide) (PPS) (17) reaction with peroxytrifluoroacetic acid. TFA (3 mL) was placed in a 5 mL conical vial with a spin-vane. Hydrogen peroxide 30 wt% (1 mL) was added to the vial. This solution was stirred at room temperature for 20 minutes. The starting material poly(*p*-phenylene sulfide), **17** (56 mg, 0.50 mmol), was added to the reaction vial. A solid remained in the reaction vial throughout the reaction. The solid did change from the dark yellow of PPS to a more tan-white. The solution was stirred at room temperature for a total of 3 hours. The final reaction slurry was poured into water (25 mL). This solid product was isolated by vacuum filtration, washed with two portions

of water (25 mL each), and dried in a vacuum oven overnight. The solid was not soluble in TFA, and hence could not be analyzed by proton NMR. IR spectroscopic analysis confirmed the formation of primarily poly(*p*-phenylene sulfone) (PPSO). IR-KBr (cm^{-1}, strg, mod, wk) 3095w, 1650w, 1559w, 1397m, 1323m, 1290m 1163s, 1101m, 1010w, 833m, 746m, 711w, 643s, 579w.

Poly(*p*-phenylene sulfoxide) (PPSX) (18) reaction with peroxytrifluoroacetic acid. TFA (3 mL) was placed in a 10 mL round bottom vial with a stir bar. Hydrogen peroxide 30 wt% (1 mL) was added to the vial. This solution was stirred at room temperature for 15 minutes. The starting material poly(*p*-phenylene sulfoxide), **18** (58 mg, 0.50 mmol), was dissolved in TFA (1 mL), and this solution was added to the reaction vial. A white precipitate immediately began to form in the reaction vial. The slurry was stirred at room temperature for 30 minutes. The final reaction slurry was poured into water (25 mL). This solid product was isolated by vacuum filtration, washed with water (25 mL), washed with two portions of diethyl ether (25 mL each), and dried in a vacuum oven overnight. The solid was not soluble in TFA, and hence could not be analyzed by proton NMR. IR spectroscopic analysis confirmed the formation of primarily poly(*p*-phenylene sulfone) (PPSO). IR-KBr (cm^{-1}, strg, mod, wk) 3095w, 1650w, 1559w, 1397m, 1323m, 1290m 1163s, 1101m, 1010w, 833m, 746m, 711w, 643s, 579w.

Poly(*p*-phenylene sulfoxide) (PPSX) (18) reaction with hydrogen bromide in trifluoroacetic and acetic acids. The starting material poly(*p*-phenylene sulfoxide), **18** (1.07 g, 8.63 mmol, 1 eq), was dissolved in TFA (35 mL) in a 50 mL round bottom flask with a septum and stir bar. Hydrogen bromide 30 wt% in acetic acid (2.6 mL, 13 mmol

HBr, 1.5 eq) was added to the reaction flask. A yellow precipitate immediately began to form in the reaction flask with an orange color change in the solution. The slurry was stirred at room temperature overnight. The final reaction slurry was poured into water (50 mL). This solid product was isolated by vacuum filtration, washed with two portions of water (50 mL), washed with two portions of TFA (25 mL each), and dried in a vacuum oven overnight. The solid was not soluble in TFA, and hence could not be analyzed by proton NMR. IR spectroscopic analysis confirmed the formation of primarily poly(*p*-phenylene sulfide) (PPS). The yield was 1.16 g, 124 %. IR-KBr (cm^{-1}, strg, mod, wk) 3058w, 1684w, 1560m, 1473m, 1387w, 1351w, 1244w, 1158w, 1091m, 1072w, 1009m, 873w, 810s, 782w, 738w, 557w, 484w.

Poly(*p*-phenylene sulfide) (PPS) (17) reaction with sodium hypochlorite. The starting material poly(*p*-phenylene sulfide), **17** (107 mg, 0.991 mmol), was placed in a 25 mL reaction flask with a stir bar. Trifluoroacetic acid (15 mL) was added to the reaction flask. Sodium hypochlorite 5.25 wt% (1.32 g) was added to the reaction vial. A solid material persisted in the reaction flask after 30 minutes of reaction. The slurried product was vacuum filtered directly into water (100 mL) resulting in a yellow-white precipitate (21 mg). The crude precipitate was isolated by vacuum filtration and vacuum dried overnight. The original insoluble solid was not analyzed further. The soluble precipitate was analyzed by proton NMR. The yield was 21 mg, 17 % based on sulfoxide product. The soluble precipitate contained mostly sulfoxide monomers with trace (< 1 %) indications of overoxidation as determined by proton NMR. ^{1}H NMR spectrum (400 MHz, d-TFA) δ 7.90 (s).

Poly(*p*-phenylene sulfide) (PPS) (17) reaction with calcium hypochlorite. The starting material poly(*p*-phenylene sulfide), **17** (100 mg, 0.926 mmol), was placed in a 25 mL reaction flask with a stir bar. Trifluoroacetic acid (3 mL) and methylene chloride (6 mL) was added to the reaction flask. Calcium hypochlorite (69 mg, 0.97 mmol OCl^-, 1.04 eq) was added to the reaction vial. A solid material persisted in the reaction vial after one hour of reaction. The slurried product was vacuum filtered directly into water (100 mL) resulting in a yellow-white precipitate (3 mg). The crude precipitate was isolated by vacuum filtration and vacuum dried overnight. The original insoluble solid was not analyzed further. The soluble precipitate was analyzed by proton NMR. The yield was 3 mg, 3 % based on sulfoxide product. The soluble precipitate contained mostly sulfoxide monomers with trace (< 1 %) indications of overoxidation as determined by proton NMR. ^{1}H NMR spectrum (400 MHz, d-TFA) δ 7.90 (s).

Thermolysis of poly(*p*-phenylene sulfoxide) (PPSX) (18). The starting material poly(*p*-phenylene sulfoxide), **18** (0.606 g, 4.89 mmol), was placed in a vial in a 350 °C oven for 30 minutes. The resultant product was a brittle black carbonaceous solid with a porous, fibrillar, structure. The final weight was 0.361 g giving a 41 % weight loss. In a second experiment **18** (0.433 g, 3.49 mmol), was placed in a vial in a 420 °C oven for 95 minutes The product was similar to the previous experiment with a final weight of 0.202 g giving a 53 % weight loss.

Gel Permeation Chromatography and fractionation of poly(*p*-phenylene sulfoxide) (PPSX) (18). Multiple polymer samples were prepared according to either the **poly(*p*-phenylene sulfoxide) (PPSX) (18) from trifluoroacetic acid with excess fuming nitric**

acid procedure or the **poly(*p*-phenylene sulfoxide) (PPSX) (18) fuming nitric acid** procedure. The PPS samples were obtained from either Phillips Chemical or Aldrich Chemical with molecular weights assigned by meltflow analysis of the PPS: Aldrich samples were identified as Mn 10K, Poise 1400, Poise 500, Poise 275; the Phillips samples were identified as PR09 (Mw 50,000), GR01 (Mw 50,000 but branched), E2080 (Mw 80,000). Fractionation was conducted on the Aldrich Poise 1400 sample. For fractionation PPSX (2.025 g) was dissolved in trifluoroacetic acid (35.67 g). Water was added stepwise in portions (3.300, 3.648, 4.112 g each portion). There was a localized, temporary precipitation on the first two additions, which redissolved with stirring. The third addition of water resulted in large scale permanent precipitation. TFA (17.08 g) and acetonitrile (1.566 g) was added to this slurry which resulted in little visible change after stirring for 4 hours. The slurry was vacuum filtered into water (100 mL) resulting in the precipitation of the lowest molecular weight fraction from the filtrate (Lowest, 0.081 g). TFA (10 mL) was added to the larger precipitated fraction, and this slurry was stirred overnight. The slurry was vacuum filtered resulting in the highest molecular weight fraction (Highest, 0.468 g) from the precipitate. TFA (30 mL) was added to the filtrate which resulted in a homogenous solution. Acetonitrile was added in 0.5 mL aliquots until the precipitation was permanent. After stirring for 3 hours, this slurry was vacuum filtered into water (100 mL) resulting in a larger medium molecular weight fraction from the slurry precipitate (Medium, 1.082 g) and a smaller lower molecular weight fraction from the filtrate (Low, 0.030 g). Each of these four fractionation portions were redissolved in TFA and reprecipitated into water for purification. The fractions were identified as Highest,

Medium, Low, and Lowest molecular weight (0.468 g, 1.082 g, 0.030 g, 0.081 g, respectively). All of the primary samples and the fractionated samples were analyzed using GPC. GPC was run in a binary solvent system of *m*-cresol and chlorobenzene (1:10, wt:wt) at 1.0 mL/min flow rate with 100 µl injections. Samples were prepared by dissolving the PPSX (20 mg) in *m*-cresol (1.0 g) with stirring and mild heating to 50 °C. After complete solvation, chlorobenzene (10 g) was added with stirring to match the GPC eluent concentration. Molecular weights were calculated relative to poly(styrene) standards. GPC relative to PS std (r^2 = 0.9992): Aldrich Mn10K-- Mw 22,600, Mn 9,750 PD 2.32; Aldrich Mn10K (rerun)-- Mw 23,100, Mn 11,300 PD 2.04; Aldrich Poise 1400-- Mw 51,000, Mn 13,900 PD 3.67; Aldrich Poise 1400 (rerun)-- Mw 32,900, Mn 11,900 PD 2.77; Aldrich Poise 500-- Mw 42,000, Mn 14,700 PD 2.86; Aldrich Poise 275-- Mw 39,100, Mn 14,700 PD 2.66; Phillips PR09-- Mw 30,800, Mn 12,500 PD 2.46. Second series GPC relative to PS std (r^2 = 0.9987): Aldrich Mn10K-- Mw 24,100, Mn 10,400 PD 2.32; Aldrich Poise 1400-- Mw 68,700, Mn 19,800 PD 3.47; Phillips GR01-- Mw 56,900, Mn 18,600 PD 3.07; Phillips E2080-- Mw 63,200, Mn 16,000 PD 3.95; Fractionated Poise 1400---Highest-- Mw 84,000, Mn 30,800 PD 2.72; Medium-- Mw 73,000, Mn 27,300 PD 2.67; Low-- Mw 26,600, Mn 5,300 PD 5.04; Lowest-- Mw 24,500, Mn 5,900 PD 4.17;

Bis(*p*-methylphenyl) sulfide (55). The starting material, *p*-thiocresol (1.89 g, 152 mmol, 1.25 eq), was placed in a 25 mL pear flask with a stir bar and a Hickman still. The solvent, N-methyl-2-pyrrolidone (12 mL) was added with solid potassium hydroxide (1.02 g, 155 mmol, 1.25 eq) to the reaction flask. The solution was heated at 150 °C while

watching for the complete removal of water (about 0.75 mL in one hour). After complete water removal, the still was removed and the solution was heated to reflux solvent. After the still removal, *p*-bromotoluene (1.91 g, 11.2 mmol, 1 eq) was added to the reaction flask. The reaction solution was stirred at 170-180 °C for 15 hours. The condenser was removed, and the solvent was boiled-off at reflux to the consistency of a thick oil. The reaction oil was poured into benzene (45 mL). The homogenous organic layer was washed with two portions of water (75 mL each), dried over anhydrous magnesium sulfate, filtered, and rotary evaporated. The crude product, a brown liquid, was isolated in 2.16 g actual and 84 % yield based on *p*-bromotoluene. The crude product was dissolved in methylene chloride (30 mL), stirred with decolorizing carbon (3g), filtered through silica and anhydrous sodium sulfate, and rotary evaporated. The final yield of bis(*p*-methylphenyl) sulfide **55** was 1.96 g actual and 76 %. mp 49-51 °C (lit 56.8-57.2 °C); ^{1}H NMR (400 MHz, $CDCl_3$) δ 7.23 (d, 2H, J = 8 Hz), 7.10 (d, 2H, J = 8 Hz), 2.32 (s, 3H); MS-DIP 70 eV for $C_{14}H_{14}S$-214, m/e (rel intensity) 216 (3, M+2), 215 (11, M+1), 214 (100, M+), 199 (34), 197 (13), 184 (25), 182 (3), 181 (12), 166 (4), 165 (12), 152 (3), 123(3) 121 (10), 115 (4), 106 (6), 105 (24), 97 (4), 92 (4), 91 (7).

***p*-Bis(*p*-methylthiophenoxy)benzene (56).** The starting material, *p*-thiocresol (5.43 g, 43.7 mmol, 2.2 eq), was placed in a 25 mL Erlenmeyer flask with a stir bar and a Hickman still. The solvent, N-methyl-2-pyrrolidone (20 mL) was added with solid potassium hydroxide (3.3 g, 59 mmol, 3 eq) to the reaction vial. The solution was heated at 150 °C while watching for the complete removal of water (about 2 hours). After complete water removal, the still was removed and the solution was decreased to 120-130 °C. After the

temperature decreased, *p*-dichlorobenzene (2.96 g, 19.6 mmol, 1 eq) was added to the reaction vial. The reaction solution was stirred at 125 °C for 15 hours and 180 °C for 6 hours. The condenser was removed, and the solvent was boiled-off at reflux to the consistency of a thick oil. The reaction oil was poured into benzene (100 mL). The homogenous organic layer was washed with three portions of water (100 mL each), dried over anhydrous magnesium sulfate, filtered, and rotary evaporated. The desired product *p*-bis(*p*-methylthiophenoxy)benzene **56** was isolated in 5.14 g actual and 79 % yield based on *p*-dichlorobenzene. mp 92-93 °C; ^{1}H NMR (400 MHz, $CDCl_3$) δ 7.29 (d, 2H, J = 8 Hz), 7.14 (s, 2H), 7.13 (d, 2H, J = 8 Hz), 2.34 (s, 3H); ^{1}H NMR (400 MHz, C_6D_6) δ 7.26 (d, 2H, J = 8 Hz), 7.15 (s, 2H), 6.78 (d, 2H, J = 8 Hz), 1.97 (s, 3H); MS-DIP 70 eV for $C_{20}H_{18}S_2$-322, m/e (rel intensity) 324 (3, M+2), 323 (10, M+1), 322 (100, M+), 199 (35), 197 (13), 184 (16), 166 (3), 165 (5), 121 (3), 91 (7); IR-KBr (cm^{-1}, strg, mod, wk) 3020w, 2950w, 1491m, 1473m, 1102w, 1085m, 1010m, 819m, 805s, 557w, 498m, 481m.

Bis(*p*-nitrophenyl) sulfide(57). The starting material, *p*-nitrothiophenol (0.797 g, 5.14 mmol, 1.25 eq), was placed in a 10 mL round bottom vial with a stir bar and a Hickman still. The solvent, N-methyl-2-pyrrolidone (5 mL) was added with solid potassium hydroxide (0.379 g, 6.75 mmol, 1.7 eq) to the reaction vial. The solution was heated at 150 °C while watching for the complete removal of water (about 0.25 mL in one hour). After complete water removal, the still was removed and the solution was heated at 120-130 °C. After the still removal, 1-chloro-4-nitrobenzene (0.628 g, 3.99 mmol, 1 eq) was added to the reaction vial. The reaction solution was stirred at 120-130 °C for 15 hours. The condenser was removed, and the solvent was boiled-off at reflux to the consistency of

a thick oil. The reaction oil was poured into benzene (100 mL). The homogenous organic layer was washed with six portions of water (100 mL each), dried over anhydrous sodium sulfate, decolorized over carbon (10 g), filtered, and rotary evaporated. The product, a yellow solid, was isolated in 0.41 g actual and 37 % yield based on 1-chloro-4-nitrobenzene. The crude product was dissolved in methylene chloride (80 mL), stirred with potassium carbonate, filtered through anhydrous sodium sulfate, and rotary evaporated. The final yield of bis(*p*-nitrophenyl) sulfide (**57**) was 0.39 g actual and 35 %. ^{1}H NMR (400 MHz, $CDCl_3$) δ 8.20 (d, 1H, J = 9 Hz), 7.49 (d, 1H, J = 9 Hz); MS-DIP 12 eV for $C_{12}H_8N_2O_4S$-276, m/e (rel intensity) 277 (4, M+1), 276 (100, M+), 265 (6), 247 (5), 246 (62), 231 (11), 216 (37), 201 (31), 200 (23), 184 (8), 152 (29).

Model compound reaction with excess fuming nitric acid. The model compounds (100 mg) were placed in a 5 mL conical vial with a spin-vane. Fuming nitric acid (4 mL) was added dropwise to the vial. A brown-orange gas (NO_2) evolved from the vial during the addition. A homogeneous solution resulted within minutes of stirring. The solution was stirred at room temperature for a total of 30 minutes. The final reaction solution was poured into water (50 mL) producing a solid. The product was isolated by vacuum filtration and washed with two portions of water (25 mL each). The solid was vacuum dried overnight. The products were then analyzed by proton NMR.

Diphenyl sulfide (52). Compound **52** was treated according to the above procedure The product was a fairly complex mixture as determined by proton NMR. The principle component (60 %) was *m*-nitrophenyl phenyl sulfone **58** with a second component (30 %) bis(*m*-nitrophenyl) sulfoxide **61** and a small amount if a third component (7 %) bis(*m*-

nitrophenyl) sulfone **65**. No product separation was attempted. **58*:** ^{1}H NMR (400 MHz, $CDCl_3$) δ 8.75 (s, 1H), 8.40 (d, J = 8 Hz, 1H), 8.26 (d, J = 8 Hz, 1H), 7.95 (m, 2H), 7.72 (t, J = 8 Hz, 1H), 7.62 (m, 1H), 7.52 (m 2H); GC-MS for $C_{12}H_9NO_4S$-263, m/e (rel intensity) 263 (M+), 170, 152, 125, 77 (100), 76, 51, 50; **61*:** ^{1}H NMR (400 MHz, $CDCl_3$) δ 8.55 (s, 1H), 8.35 (m, 2H), 7.90 (dd, J = 8, 7 Hz, 1H). **65*:** ^{1}H NMR (400 MHz, $CDCl_3$) δ 8.80 (s, 1H), 8.48 (d, J = 8 Hz, 1H), 8.35 (d, J = 8 Hz, 1H), 7.78 (t, J = 8 Hz, 1H).

Diphenyl sulfoxide (53). Compound **53** was treated according to the above procedure. The product was a fairly complex mixture and overlaid exactly with the above reaction of **52** as determined by proton NMR. The principle component (60 %) was *m*-nitrophenyl phenyl sulfone **58** with a second component (30 %) bis(*m*-nitrophenyl) sulfoxide **61** and small amount if a third component (7 %) bis(*m*-nitrophenyl) sulfone **65**. No product separation was attempted. **58*:** ^{1}H NMR (400 MHz, $CDCl_3$) δ 8.75 (s, 1H), 8.40 (d, J = 8 Hz, 1H), 8.26 (d, J = 8 Hz, 1H), 7.95 (m, 2H), 7.72 (t, J = 8 Hz, 1H), 7.62 (m, 1H), 7.52 (m 2H); GC-MS for $C_{12}H_9NO_4S$-263, m/e (rel intensity) 263 (M+), 170, 152, 125, 77 (100), 76, 51, 50; **61*:** ^{1}H NMR (400 MHz, $CDCl_3$) δ 8.55 (s, 1H), 8.35 (m, 2H), 7.90 (dd, J = 8, 7 Hz, 1H). **65*:** ^{1}H NMR (400 MHz, $CDCl_3$) δ 8.80 (s, 1H), 8.48 (d, J = 8 Hz, 1H), 8.35 (d, J = 8 Hz, 1H), 7.78 (t, J = 8 Hz, 1H).

Diphenyl sulfone (54). Compound **54** was treated according to the above procedure. The product was a fairly complex mixture and could not be overlaid exactly with the above reactions of **52** and **53** as determined by proton NMR. The main component (80 %) was *m*-nitrophenyl phenyl sulfone **58** with a second component (10 %) bis(*m*-nitrophenyl)

sulfone **65**. No product separation was attempted. The components **58** and **65** were identified by proton NMR. **58*:** ^{1}H NMR (400 MHz, $CDCl_3$) δ 8.75 (s, 1H), 8.40 (d, J = 8 Hz, 1H), 8.26 (d, J = 8 Hz, 1H), 7.95 (m, 2H), 7.72 (t, J = 8 Hz, 1H), 7.62 (m, 1H), 7.52 (m 2H); **65*:** ^{1}H NMR (400 MHz, $CDCl_3$) δ 8.79 (s, 1H), 8.47 (d, J = 8 Hz, 1H), 8.35 (d, J = 8 Hz, 1H), 7.77 (t, J = 8 Hz, 1H).

Bis(*p*-methylphenyl) sulfide (55). Compound **55** was treated according to the above procedure. The resulting product consisted of two compounds as determined by proton NMR. No product separation was attempted. The compounds bis(*p*-methyl-*m*-nitro-phenyl) sulfoxide **60** and bis(*p*-methyl-*m*-nitro-phenyl) sulfone **61** were produced in relative yields of 68 % and 32 %, respectively. **60*:** ^{1}H NMR (400 MHz, $CDCl_3$) δ 8.25 (d, J = 2 Hz, 1H), 7.80 (dd, J = 8, 2, 1H), 7.51 (d, J = 8 Hz, 1H), 2.63 (s, 3H); **61*:** ^{1}H NMR (400 MHz, $CDCl_3$) δ 8.51 (d, J = 2 Hz, 1H), 8.07 (dd, J = 8, 2, 1H), 7.56 (d, J = 8 Hz, 1H), 2.67 (s, 3H).

***p*-Bis(*p*-methylthiophenoxy)benzene (56).** Compound **56** was treated according to the above procedure. A nitro sulfoxide product was cleanly produced as determined by proton NMR. The compound *p*-bis(*p*-methyl-*m*-nitro-phenylsulfinyl)benzene **62** was also identified by mass. **62*:** ^{1}H NMR (400 MHz, dTFA) δ 8.59 (s, 1H), 8.16 (s, 2H), 8.07 (d, J = 8 Hz, 1H), 7.82 (d, J = 8Hz, 1H), 2.86 (s, 3H); MS-DIP 70 eV for $C_{20}H_{16}N_2O_6S_2$-444, m/e (rel intensity) 444 (28, M+), 228 (100), 121 (79), 89 (88), 78 (25), 77 (33), 65 (14), 63 (60);

Bis(*p*-nitrophenyl) sulfide (57). Compound **57** was treated according to the above procedure. The resulting product consisted of one compound as determined by proton

NMR and mass spectroscopy. The compound bis(*p*-nitro-phenyl) sulfoxide **64** was produced in 70 % yield. **64*:** ^{1}H NMR (400 MHz, $CDCl_3$) δ 8.35 (d, J = 9 Hz, 1H), 7.89 (d, J = 9 Hz, 1H); MS-DIP 12 eV for $C_{12}H_8N_2O_5S$-292, m/e (rel intensity) 293 (5, M+1), 292 (100, M+), 244 (17), 170 (9), 154 (16), 138 (14), 124 (6), 110 (10), 108 (8).

Model compound reaction with peroxytrifluoroacetic acid. Trifluoroacetic acid (3 mL) was mixed with hydrogen peroxide 30 wt% (1 mL) in a 5 mL conical vial with a spin-vane. The reaction solution was stirred at room temperature for 20 minutes. The model compounds (100 mg) were added to the reaction vial. A homogeneous solution resulted within minutes of addition. The solution was stirred at room temperature for 30 minutes. The final reaction solution was poured into water (50 mL) producing a solid. The product was isolated by vacuum filtration and washed with two portions of water (25 mL each). The solid was vacuum dried overnight. The products were then analyzed by proton NMR.

Diphenyl sulfide (52). Compound **52** was treated according to the above procedure. The product was cleanly produced the expected product sulfone as determined by proton NMR. The compound diphenyl sulfone **54** was also identified by mass spectroscopy. **54:** ^{1}H NMR (400 MHz, $CDCl_3$) δ 7.95 (m, 2H), 7.52 (m, 3H); MS-DIP 70 eV for $C_{12}H_{10}O_2S$-218, m/e (rel intensity) 219 (3, M+1), 218 (55, M+), 149 (12), 125 (100), 97 (21), 77 (59), 51(31).

***p*-Bis(*p*-methylthiophenoxy)benzene (56).** Compound **56** was treated according to the above procedure. The expected sulfone product was cleanly produced as determined by proton NMR. The compound *p*-bis(*p*-methylphenylsulfonyl)benzene **63** was also identified by mass spectroscopy. **63*:** ^{1}H NMR (400 MHz, dTFA) δ 8.40 (s, 2H), 8.11 (d, J = 8

Hz, 2H), 7.67 (d, J = 8Hz, 2H), 2.68 (s, 3H); GC-MS for $C_{20}H_{18}O_4S_2$-386, m/e (rel intensity) 268, 266, 159, 139, 111 (100), 91.

Film casting and solubility of poly(*p*-phenylene sulfoxide) (PPSX) (18). The polymer PPSX (Phillips E2080, 1.00 g) was dissolved in *m*-cresol (25.0 mL) with stirring and mild heating (50 °C). The PPSX must be free of residual nitric (or nitrous acid) to avoid darkening of the *m*-cresol. This PPSX stock solution (3.22 M) was used to prepare all of the subsequent film solutions. Varied concentration solutions were tested by sequentially diluting this stock solution (3.22, 0.805, 0.322, 0.160 M). Binary solvent films were assessed by mixing the stock solution (0.5 mL) with varied second solvent (1.5 mL). The tested solvent systems are listed below. Additionally, two film plasticizers (tritolyl phosphate or propylene carbonate) were added to the film solutions in varying dropwise amounts to semi-quantitatively assess their effect on film properties. For a single standard film, 2.0 mL of solution was pipetted onto a glass slide. The solution was allowed to expand to its normal surface tension limit without any additional tilting, spreading, etc. The solvent was allowed to evaporate (2 weeks) at ambient temperatures. The films were removed by placing the glass slide with its attached film in water. The solvent systems were assessed based on visual turbidity as clear, hazy, light precipitate, or heavy precipitate. Only clear (dissolved), binary solvents were cast into films. The dried cast films were characterized grossly as excellent, good, fair, bad, or very bad based on flexibility and integrity: a very flexible, durable, free standing film was excellent; flexible, freestanding film was good; a brittle free standing film was fair; a fractured non-free standing film was bad.. **Varied Concentrations:** 3.22 M--fair, 0.805 M--bad, 0.322 M--

very bad, 0.160 M--no film. **Binary Films:** methylene chloride– clear, fair; chlorobenzene– clear, good; benzene– clear, bad; chloroform– clear, good; 1,2-dichloroethane– clear, bad; dimethyl phthalate– lt prec; decalin– clear, bad; nitrobenzene– clear, fair; dimethyl sulfoxide– hv prec; pyridine– hv prec; 1,4-dioxane– hv prec; ethylene glycol– hv prec; xylenes– clear, fair; mesitylene– clear, fair; ethylene glycol dimethyl ether– hv prec; N-methyl-2-pyrrolidone– lt precip; trifluoroacetic acid– clear, very bad; cumene– clear, good; bromonaphthalene– clear, bad; lutidine– hv prec; collidine– hv prec; *n*-propyl benzene–clear, good, very transparent film; tritolyl phosphate–hv prec; propylene carbonate–hv precip; **Plasticizer:** stock solution with 4 drops tritolyl phosphate-- clear, good, but still brittle; binary with cumene and 2 drops propylene carbonate– clear, good; binary with cumene and 10 drops propylene carbonate– clear, very bad; stock solution with 4 drops propylene carbonate– clear, excellent, film curls in response to moisture.

Metal chelation studies of poly(*p*-phenylene sulfoxide) (PPSX) (18). Four different metal chelation/extraction procedures were conducted on PPSX using a variety of metals. The powdered polymer PPSX (Aldrich Poise 1400) was used for all of the metal chelation studies. **Method I:** loose PPSX powder (200-250 mg) was stirred for 1.5 hours in the metal test solution (5 mL) at room temperature. After stirring, the slurry was filtered through glass wool through a Pasteur filter pipette. The filtrate was analyzed by flame atomic absorption spectroscopy (FAAS). **Method II:** Concentrated nitric acid (0.5 mL) was added to the stirring solution identical to Method I. The filtration and analysis was also identical to Method I. **Method III:** PPSX powder (200-250 mg) was dissolved in *m*-cresol (5 mL). The metal test solution (5 mL) was stirred for 1.5 hours in a biphasic

mixture. After stirring, the aqueous layer was pipetted and directly analyzed by FAAS. **Method IV:** The metal test solution (5 mL) was percolated through a Pasteur filter pipette which was packed with powdered PPSX (200-250 mg) supported by glass wool. The filtrate was directly analyzed by FAAS. **Metal Test Solutions:** The metal solutions were prepared in nitric acid washed volumetric glassware from hydrated metal perchlorate salts (except for lanthanum). The test solution concentrations were selected based on optimum FAAS lamp response at specific wavelengths. Standard solutions of at least five different concentrations bracketing the test concentration were used to standardize the FAAS technique. **Analytes:** metal test (5 ppm) with standards (100, 10, 5, 1, 0.5, 0 ppm) Cadmium $Cd(ClO_4)_2 \cdot 6H_20$, Copper $Cu(ClO_4)_2 \cdot 6H_20$, Iron $Fe(ClO_4)_2 \cdot 6H_20$, Zinc $Zn(ClO_4)_2 \cdot 6H_20$; metal test (10 ppm) with standards (200, 20, 10, 2, 1, 0 ppm) Chromium $Cr(ClO_4)_3 \cdot 6H_20$, Nickel $Ni(ClO_4)_2 \cdot 6H_20$; metal test (20 ppm) with standards (400, 40, 20, 4, 2, 0 ppm) lead $Pb(ClO_4)_2 \cdot 3H_20$; metal test (250 ppm) with standards (5000, 500, 250, 50, 25, 0 ppm) mercury $Hg(ClO_4)_2 \cdot 3H_20$, lanthanum $La(NO_3)_3$. **Loading Capacity Study:** an iron test solution (100 ppm) with standards (100, 10, 5, 1, 0.5, 0 ppm) was treated according to the Method I procedure except varying amounts of PPSX were used (0.747, 0.424, 0.245, 0.116, 0.0806, 0.0467, 0.0253, 0.0122 g) giving varied, approximate sulfoxide to iron ratios (672, 381, 220, 104, 72.5, 42.0, 22.8, 11.0 mol SO/mol Fe).

UV/VIS study of poly(*p*-phenylene sulfoxide) (PPSX) (18) with partial HBr reduction. The PPSX polymer (Phillips E2080, 3.9 mg) was dissolved in trifluoroacetic acid (10.0 mL). This solution was diluted to 1/100th its concentration using volumetric

glassware (1 mL volumetric pipette into 100 mL volumetric flask). The final solution was analyzed using UV/VIS spectroscopy. The PPSX was partially reduced to PPS using HBr 40 wt% in water. Two drops of the HBr was added directly with brisk agitation to the UV/VIS cuvette. Spectra were taken at one minute intervals for 10 minutes to visualize the changes. The maximum wavelength for the PPSX spectrum in TFA was 262 nm, while the new PPS moieties have a maximum wavelength at 316 nm.

Bibliography

1. Pellegrin, M.M., *Rec. Trav. Chim. Pays-Bas*, **1899**. *18*, 457.
2. Luttringhaus, A. and Gralheer, H., *Liebigs Ann. Chem.*, **1942**. *550*, 67.
3. Luttringhaus, A. and Gralheer, H., *Liebigs Ann. Chem.*, **1945**. *557*, 108.
4. Luttringhaus, A. and Eyring, G., *Liebigs Ann. Chem.*, **1957**. *604*, 111.
5. Eliel, E.L. and Wilen, S.H., *Stereochemistry of Organic Compounds*. **1994**, New York, NY: Wiley and Sons, Inc.
6. Baker, W., Banks, D.R., Lyon, D.R., and Mann, F.G., *J. Chem. Soc.*, **1945**, 27.
7. Brown, C.J. and Farthing, A.C., *Nature (London)*, **1949**. *164*, 915.
8. Cram, D.J. and Steinberg, H., *J. Am. Chem. Soc.*, **1951**. *73*, 5691.
9. Tsuji, T., Ohkita, M., Konno, T., and Nishida, S., *J. Am. Chem. Soc.*, **1997**. *119*, 8425-8431.
10. Tsuji, T., Kawai, H., Suzuki, T., and Ohkita, M., *Angew. Chem. Int. Ed.*, **1998**. *37*, 817-819.
11. Diederich, F., *Cyclophanes*. Monographs in Supramolecular Chemistry, ed. Stoddart, J.F. Vol. 2. **1991**, Cambridge, UK: Royal Society of Chemistry.
12. Dunitz, J.D., Hafner, K., Ito, S., Lehn, J.M., Raymond, K.N., Rees, C.W., Thiem, J., and Vogtle, F., eds. *Cyclophanes*. Topics in Current Chemistry. Vol. 172. **1994**, Springer-Verlag: New York, NY.
13. Vogtle, F., *Cyclophane Chemistry*. **1993**, New York, NY: John Wiley and Sons.
14. Keehn, P.M. and Rosenfield, S.M., eds. *Cyclophanes*. Organic Chemistry, a Series of Monographs. Vol. 45. **1983**, Academic Press, Inc.: New York, NY.
15. Cram, D.J. and Abell, J., *J. Am. Chem. Soc.*, **1955**. *77*, 1179-1186.
16. Schubert, W.M., Sweeney, W.A., and Latourette, H.K., *J. Am. Chem. Soc.*, **1954**. *76*, 5462-5466.
17. Staab, H.A. and Haffner, H., *Chem. Ber.*, **1977**. *110*, 3358-3365.
18. Longone, D.T. and Chow, H.S., *J. Am. Chem. Soc.*, **1970**. *92*, 994-998.
19. Hopf, H., Grahn, W., Barrett, D.G., Gerdes, A., Hilmer, J., Hucker, J., Okamoto, Y., and Kaida, Y., *Chem. Ber.*, **1990**. *123*, 841.
20. Vetter, A.H. and Berkessel, A., *Tetrahedron Lett.*, **1998**. *39*, 1741-1744.
21. Pietzsch, M., Pamperin, D., Hopf, H., and Syldatk, C., *Tetrahedron: Asymmetry*, **1997**. *8*, 319-325.
22. Belokon, Y., Rozenburg, V., Kharitonov, V., Antonov, D., Sergeeva, E., Aleshkin, A., Ikonnikov, N., and Orlova, S., *Angew. Chem. Int. Ed. Engl.*, **1994**. *33*, 91-92.
23. Cram, D.J., Hornby, R.B., Truesdale, E.A., Reich, H.J., Delton, M.H., and Cram, J.M., *Tetrahedron*, **1974**. *30*, 1757-1768.
24. Masterson, D.S., Hobbs, T.L., and Glatzhofer, D.T., *J.Mol.Cat.A:Chem.*, **1996**. *In Press*.
25. Morvant, M.C., *Synthesis, Properties, and Applications of Polynitro- and Polyamino[2.2]paracyclophanes*, in *Chemistry and Biochemistry*. **1996**, University of Oklahoma, Norman, OK.

26. Reich, H.J. and Cram, D.J., *J. Am. Chem. Soc.*, **1969**. *91*, 3505-3516.
27. Cooper, P.W., *Explosives Engineering*. **1996**, New York, NY: VCH Publishers, Inc.
28. Cooper, P.W. and Kurowski, S.R., *Introduction to the Technology of Explosives*. **1996**, New York, NY: VCH Publishers, Inc.
29. Olah, G.A. and Squire, D.R., eds. *Chemistry of Energetic Materials*. . **1991**, Academic Press, Inc.: New York, NY.
30. Suceska, M., *Test Methods for Explosives*. **1995**, New York, NY: Springer-Verlag.
31. DeptArmy, *Military Explosives TM 9-1300-2124*. **1984**, Washington, DC: Dept. of Army.
32. Brill, T.B. and James, K.J., *Chem. Rev.*, **1993**. *93*, 2667-2692.
33. Marchand, A.P., *Tetrahedron*, **1988**. *44*, 2377-2395.
34. Eaton, P.E., Xiong, Y., and Gilardi, R., *J. Am. Chem. Soc.*, **1993**. *115*, 10195-10202.
35. George, C. and Gilardi, R., *Acta Cryst.*, **1984**. *C40*, 674-676.
36. Maier, W.F. and Schleyer, P.R., *J. Am. Chem. Soc.*, **1981**. *103*, 1891-1900.
37. Cram, D.J. and Allinger, N.L., *J. Am. Chem. Soc.*, **1955**. *77*, 6289.
38. Cram, D.J., Bauer, R.H., Allinger, N.L., Reeves, R.A., Wechter, W.J., and Heilbronner, E., *J. Am. Chem. Soc.*, **1959**. *81*, 5977-5983.
39. Cram, D.J., Alleiger, H., Siegel, M.G., Helgeson, R.C., and Schmidt, E., *J. Am. Chem. Soc.*, **1975**. *97*, 3782-3789.
40. Urbanski, T., *Chap. 14 Explosive Polymers*, in *Chemistry and Technology of Explosives*. **1984**, Pergamon Press, Inc.: New York, NY. 404-421.
41. Glatzhofer, D.T., Personal Communication. **1997**.
42. Iwatsuki, S., *Polymerization of Quinodimethane*, in *Polymerization Reactions*. **1984**, Springer-Verlag: New York, NY. 93-120.
43. Gorham, W.F., *J. Poly. Sci. A-1*, **1966**. *4*, 3027-3039.
44. Raschke, C.R. and Nowlin, T.E., *J. Appl. Poly. Sci.*, **1980**. *25*, 1639-1644.
45. Joesten, B.L., *J. Appl. Poly. Sci.*, **1974**. *18*, 439-448.
46. Vogtle, F. and Neumann, P., *The Sythesis of [2.2]Phanes. Synthesis*, **1973**, 85.
47. Boekelheide, V., *Sythesis and Properties of the [2n] Cyclophanes*, in *Topics in Current Chemistry*. **1983**. 87.
48. Cram, D.J. and Bauer, R.H., *Substituted Stilebenes. J. Am. Chem. Soc.*, **1959**. *81*, 5983.
49. Tabushi, I., Yamada, H., and Kuroda, Y., *J. Org. Chem.*, **1975**. *40*(13), 1946.
50. Winberg, H.E. and Fawcett, F.S., in *Organic Synthesis*, Baumgarten, H.E., Editor. **1973**, Wiley and Sons, Inc.: New York, NY. 883.
51. Brink, M., *Synthesis*, **1975**, 807.
52. Hopf, H., Bohm, I., and Kleinschroth, J., in *Organic Synthesis*, Baumgarten, H.E., Editor. **1990**, Wiley and Sons, Inc.: New York, NY. 485.

53. Icke, R.N., Redemann, C.E., Wisegarver, B.B., and Alles, G., A,, in *Organic Synthesis*, Horning, E.C., Editor. **1955**, Wiley and Sons, Inc.: New, York, NY. 644.
54. Gattermann, L., *Liebigs Ann. Chem.*, **1906**. *347*, 347.
55. Lukasiewicz, A., *Tetrahedron*, **1963**. *19*, 1789.
56. Leuckart, R., *Ber.*, **1885**. *18*, 2341.
57. Moore, M.L., in *Organic Reactions*. **1949**. 301.
58. Wallach, O., *Ann. Liebigs*, **1892**. *272*, 99.
59. Moodie, R.B., Thomas, P.N., and Schofield, K., *J.C.S. Perkins II*, **1977**, 1693.
60. Hartshorn, S.R., Ridd, J.H., and Ramsay, W., *J.Chem.Soc. (B)*, **1968**, 1068.
61. Brickman, M. and Ridd, J.H., *J.Chem.Soc.*, **1965**, 6845.
62. Emmons, W.D., *J.Am.Chem.Soc.*, **1954**. *76*, 3470.
63. Emmons, W.D. and Ferris, A.F., *J.Am.Chem.Soc.*, **1953**. *75*, 4623.
64. Pagano, A.S. and Emmons, W.D., in *Organic Syntheses*, Baumgarten, H.E., Editor. **1973**, Wiley and Sons, Inc.: New York, NY. 367.
65. Demselben, *Liebigs Ann. Chem.*, **1885**. *228*, 250.
66. Smith, S.C. and Gage, L.D., *J.Chromatogr.*, **1977**. *131*, 425.
67. Johnson, C.D. and Northcott, M.J., *J.Am.Chem.Soc.*, **1967**. *32*, 2029.
68. Dauben, H.J. and McCoy, L.L., *J.Am.Chem.Soc.*, **1959**. *81*, 4863.
69. van der Made, A.W. and can der Made, A.W., *J.Org.Chem.*, **1993**. *58*, 1262.
70. Mitchell, R.H. and Iyer, V.S., *Synlett.*, **1989**, 55.
71. Rahm, A., Guilhemat, R., and Pereyre, M., *Synth.Commun.*, **1982**. *12*, 485.
72. Truce, W.E., in *Organic Reactions*. **1954**, Wiley and Sons, Inc..: New York, NY. 331.
73. Rieche, A., Gross, H., and Hoft, E., in *Organic Syntheses*, Baumgarten, H.E., Editor. **1973**, Wiley and Sons, Inc.: New York, NY. 49.
74. Huang, X., Qu, F., and Li, Z., *J.Fluorine Chem.*, **1988**. *40*, 33.
75. Rossa, L. and Vogtle, F., eds. Topics in Current Chemistry. Vol. 113. **1983**, Springer-Verlag: New York, NY.
76. Musker, W.K. and Stevens, R.R., *J.Am.Chem.Soc*, **1968**. *90*, 3515.
77. Bach, R.D., Bair, K.W., and Andrzejewski, D., *J.C.S.Chem.Comm.*, **1974**, 819
78. Wittig, G. and Polster, R., *Liebigs Ann.Chem.*, **1956**. *599*, 1.
79. Puterbaugh, W.H. and Hauser, C.R., *J.Am.Chem.Soc.*, **1963**. *86*, 1105.
80. Puterbaugh, W.H. and Hauser, C.R., *J.Am.Chem.Soc.*, **1963**. *86*, 1108.
81. Hauser, C.R., Beard, W.Q., and Jones, F.N., *J. Org.Chem*, **1961**. *26*, 4790.
82. Klein, K.P., *J.Org.Chem.*, **1966**. *31*, 4276.
83. Klein, K.P., VanEenam, D.N., and Hauser, C.R., *J.Org.Cem.*, **1967**. *32*, 1155
84. Lepley, A.R. and Becker, R.H., *J.Org.Chem.*, **1965**. *30*, 3888.
85. Klein, K.P. and Hauser, C.R., *J.Org.Chem.*, **1966**. *31*, 4276.
86. Klein, K.P. and Hauser, C.R., *J.Org.Chem.*, **1966**. *31*, 4275.
87. Jones, G.C. and Hauser, C.R., *J.Org.Chem.*, **1962**. *27*, 806.
88. Russell, G.A. and Janzen, E.G., *J.Am.Chem.Soc.*, **1962**. *84*, 4153.

89. Bassani, A., Prato, M., Rampazzo, P., Quintily, U., and Scorrano, G., *J.Org.Chem.*, **1980**. *45*, 2263.
90. Paradisi, C., Quintily, U., and Scorrano, G., *J.Org.Chem*, **1983**. *48*, 3022.
91. Prato, M., Quintily, U., and Scorrano, G., *Gazz.Chim.Ital.*, **1988**. *118*, 421.
92. Prato, M., Quintily, U., Salvagno, S., and Scorrano, G., *Gazz.Chim.Ital.*, **1984**. *114*, 413.
93. Prato, M., Quintily, U., and Scorrano, G., *J.Chem.Soc.Perkin Trans.II*, **1986**, 1419.
94. Prato, M., Quintily, U., Scapol, L., and Scorrano, G., *Bull.Soc.Chim.Fr.*, **1986**, 99.
95. Terrier, F., *Chem.Rev.*, **1982**. *82*, 77.
96. Artamkina, G.A., Egorov, M.P., and Beletskaya, I.P., *Chem.Rev.*, **1982**. *82*, 427.
97. Strauss, M.J., *Chem.Rev.*, **1970**. *70*, 667.
98. Modro, T.A. and Ridd, J.H., *J.Chem.Soc.(B)*, **1968**, 528.
99. Wennerstrom, H. and Wennerstrom, O., **1972**. *26*, 2883.
100. Bacaloglu, R., Bunton, C.A., and Ortega, F., *J.Am.Chem.Soc.*, **1989**. *111*, 1041.
101. Konig, B., Knieriem, B., and Meijere, A., *Chem.Ber.*, **1993**. *126*, 1643.
102. Rozenberg, V., Kharitonov, V., Antonov, D., Sergeeva, E., Aleshkin, A., Ikonnikov, N., Orlova, S., and Belokon, Y., *Angew.Chem.Int.Ed.Engl.*, **1994**. *33*, 91.
103. Rossen, K., Pye, P.J., Maliakal, A., and Volante, R.P., *J.Org.Chem.*, **1997**. *62*, 6462.
104. Reich, H.J. and Cram, D.J., *J.Am.Chem.Soc.*, **1969**. *91*, 3527.
105. Comba, P., Fath, A., Huttner, G., and Zsolnai, L., *Chem.Commun.*, **1996**, 1996.
106. Cipiciani, A., Fringuelli, F., Mancini, V., Piermatti, O., and Pizzo, F., *J.Org.Chem.*, **1997**. *62*, 3744.
107. Lukin, K.A., Li, J., Eaton, P.E., and Gilardi, R., *J.Org.Chem.*, **1997**. *62*, 8490.
108. Tani, K., Lukin, K., and Eaton, P.E., *J.Am.Chem.Soc.*, **1997**. *119*, 1476.
109. Buck, P. and Kobrich, G., *Tetrahedron Lett.*, **1967**, 1563.
110. Bartoli, G., *Acc.Chem.Res.*, **1984**. *17*, 109.
111. Voronkov, M.G., Roman, V.K., and Maletina, E.A., *Synthesis*, **1982**, 277.
112. Kimura, M., Kajita, K., Onoda, N., and Morosawa, S., *J.Org.Chem.*, **1990**. *55*, 4887.
113. Shahi, S.P., Gupta, A., Pitre, S.V., Reddy, V.R., Kumareswaran, R., and Vankar, Y.D., *J.Org.Chem.*, **1999**. *64*, 4509.
114. Schmidt, M. and Schmidbaur, H., *Angew.Chem.*, **1959**. *71*, 220.
115. Horita, H., Sakata, Y., and Misumi, S., *Tetrahedron Lett.*, **1976**, 1509.
116. Yamato, T., Kamimura, H., and Furukawa, T., *J.Org.Chem.*, **1997**. *62*, 7560.
117. Blackstock, D.J., Cretney, J.R., Fischer, A., Hartshorn, M.P., Richards, K.E., Vaughan, J., and Wright, G.J., *Tetrahedron Lett.*, **1970**, 2793.
118. Blackstock, D.J., Fischer, A., Richards, K.E., Vaughan, J., and Wright, G., *Chem.Comm.*, **1970**, 641.
119. Pagoria, P.F., Mitchell, A.R., and Schmidt, R.D., *J.Org.Chem.*, **1996**. *61*, 2934.

120. Mitchell, A.R., Pagoria, P.F., and Schmidt, R.D. Patent. *5,569,783*, **Oct. 29, 1996**.
121. Katritzky, A.R. and Laurenzo, K.S., *J.Org.Chem.*, **1988**. *53*, 3978.
122. Katritzky, A.R. and Laurenzo, K.S., *J.Org.Chem.*, **1986**. *51*, 5039.
123. Makosza, M. and Bialecki, M., *J.Org.Chem.*, **1992**. *57*, 4784.
124. Boyer, J.H., *Chem.Rev.*, **1980**. *80*, 495.
125. Muzart, J., *Synthesis*, **1995**, 1325.
126. McKillop, A. and Tarbin, J.A., *Tetrahedron*, **1987**. *43*, 1753.
127. McKillop, A.M. and Tarbin, J.A., *Tetrahedron Lett.*, **1983**. *24*, 1505.
128. Atta-ur-Rahman, *Nuclear Magnetic Resonance*. **1986**, New York, NY: Spinger-Verlag.
129. Allerhand, A., Gutowsky, H.S., Jonas, J., and Meinzer, R.A., *J.Am.Chem.Soc.*, **1966**. *88*, 3185.
130. Michinori, O., *Recent Advances in Atropisomerism*, in *Topics in Stereochemistry*, Allinger, N.L., Eliel, E.L., and Wilen, S.H., Editors. **1983**, Wiley and Sons, Inc.: New York, NY.
131. Yang, C.S.C. and Liu, R.S.H., *Tetrahedron Lett.*, **1973**, 4811.
132. Kini, A. and Liu, R.S.H., *J.Org.Chem.*, **1979**. *44*, 4725.
133. Ford, W.T., Thompson, T.B., Snoble, K.A.J., and Timko, J.M., *J.Am.Chem.Soc.*, **1975**. *97*, 95.
134. Adams, R., Anderson, A.W., and Miller, M.W., *J.Am.Chem.Soc.*, **1941**. *63*, 1589.
135. Adams, R. and Miller, M.W., *J.Am.Chem.Soc.*, **1940**. *62*, 53.
136. Reicker, A. and Kessler, H., *Tetrahedron Lett.*, **1969**, 1227.
137. Auspos, L.A., Burnam, C.W., Hall, L.A.R., Hubbard, K.W.M., Schaefgen, J.R., and Speck, S.B., *J.Polym.Sci.*, **1955**. *15*, 19.
138. Murthy, N.S. and Kim, H., *Polymer*, **1984**. *25*, 1093.
139. Taylor, L.D. and Kolesinski, H.S., *Polym.Lett.*, **1962**. *1*, 117.
140. Yeh, Y.L. and Gorham, W.F., *J.Org.Chem.*, **1969**. *34*, 2366.
141. Chow, S.W., Loeb, W.E., and White, C.E., *J.Appl.Polym.Sci.*, **1969**. *13*, 2325.
142. Longone, D.T. and Chow, H.S., *J.Am.Chem.Soc.*, **1970**. *92*, 994-998.
143. Schafer, O. and Greiner, A., *Macromolecules*, **1996**. *29*, 6074.
144. Loy, D.A., Assink, R.A., Jamison, G.M., McNamara, W.F., Prabakar, S., and Schneider, D.A., *Macromolecules*, **1995**. *28*, 5799.
145. Auspos, L.A., Burnham, C.W., Luther, A.R., Hall, J.K., Hubbard, W.K., Schaefgen, J.R., and Speck, S.B., *J.Polym.Sci.*, **1955**. *15*, 19.
146. Auspos, L.A., Hall, L.A.R., Hubbard, K.W.M., Schaefgen, J.R., and Speck, S.B., *J.Polym.Sci.*, **1955**. *15*, 9.
147. Itoh, T., Okuoka, S., Kubo, M., and Iwatsuki, S., *J.Polym.Sci.A*, **1995**. *33*, 359.
148. Liu, D., Liu, F.Y., Huang, X.L., Qu, F.Q., and Kao, K.C., *J.Appl.Polym.Sci.*, **1990**. *40*, 1795.
149. Norris, W.P., *J.Org.Chem.*, **1972**. *37*, 147.
150. Kirkpatrick, D.E. and Wunderlich, B., *J.Polym.Sci.B*, **1986**. *24*, 931.
151. Chung, C.I. and Sauer, J.A., *J.Polym.Sci.A-2*, **1971**. *9*, 1097.

152. Gazicki, M., James, W.J., and Yasuda, H.K., *J.Polym.Sci.Poly.Lett.*, **1985**. *23*, 639.
153. Errede, A., *J.Polym.Sci.*, **1961**. *49*, 253.
154. Errede, L.A., *J.Am.Chem.Soc.*, **1961**. *83*, 949.
155. Errede, L.A. and Pearson, W.A., *J.Am.Chem.Soc.*, **1961**. *83*, 954.
156. Nowlin, T.E., Smith, D.F., and Cieloszyk, G.S., *J.Polym.Sci.Polym.Chem.*, **1980**. *18*, 2103.
157. Cassidy, P.E., *Thermally Stable Polymers: Syntheses and Properties*. **1980**, New York, NY: Marcel Dekker, Inc.
158. Seanor, D.A., ed. *Electrical Properties of Polymers*. . **1982**, Academic Press: New York, NY.
159. Smith, H.A., *Poly(arylene sulfides)*, in *Encycl.Polym.Sci.Technol.* **1969**, Intersci. Pub.,Inc.: New York, NY. 653.
160. Carlier, V., Devaux, J., Legras, R., and McGrail, P.T., *Macromolecules*, **1992**. *25*, 6646.
161. Hawkins, R.T., *Macromolcules*, **1976**. *9*, 189.
162. Daoust, D., Godard, P., and Devaux, J. Patent. *WO 91/18041*, **28 Nov 1991**.
163. Sergeev, V.A., Shitikov, V.K., Nedel'kin, V.I., and Korshak, V.V., *Vysokomol.Soedin.,Ser. A*, **1976**. *18*, 533.
164. Udipi, K., *Polym.Prepr.(ACS, Div.Polym.Chem.)*, **1987**. *28*, 217.
165. Frank, G., Schleicher, A., and Kulpe, J. Patent. *DE 4,334,198*, **13 Apr 1995**.
166. Dupree, R.L. Patent. *US 4,383,080*, **10 May 1983**.
167. Brady, D.G. and Blackwell, J.P. Patent. *US 3,948,865*, **9 Mar 1976**.
168. Brady, D.G., Williams, R.P., and Hill, H.W. Patent. *US 4,251,575*, **17 Feb 1981**.
169. Fleischer, D., Strutz, H., Kulpe, J., and Schleicher, A. Patent. *EP 623,639*, **9 Nov 1994**.
170. Fleischer, D., Strutz, H., Kulpe, J., and Schleicher, A. Patent. *US 5,496,917*, **5 Mar 1996**.
171. Kohler, B., Russeler, W., Sarabi, B., Reinking, K., and Jonas, F. Patent. *EP 510,475*, **28 Nov 1992**.
172. Scheckenbach, H., Schleicher, A., Eysmondt, J., and Frank, G. Patent. *5,691,427*, **25 Nov 1997**.
173. Harrison, I.R., Smith, H.A., and Handlovits, C.E. Patent. *US 3,3451,873*, **24 Jun 1969**.
174. Smith, H.A. Patent. *US 3,395,132*, **30 Jul 1968**.
175. Smith, H.A. Patent. *US 3,303,087*, **7 Feb 1967**.
176. Suzuki, A., Umezawa, M., and Imai, S. Patent. *JP 63,196,627 [88,196,627]*, **15 Aug 1988**.
177. Kimura, H. and Shunsuke, F. Patent. *JP 61 47,876 [86 47,876]*, **8 Mar 1986**.
178. Imai, Y., Ueda, M., Kato, A., and Kano, Y., *Kobunshi Ronbunshu*, **1980**. *37*, 445.
179. Fujisawa, T., Kakutani, M., and Kobayashi, N., *Polym.Lett.*, **1971**. *9*, 91.
180. Harris, J.M., Liu, Y., Chai, S., Andrews, M.D., and Vederas, J.C., *J.Org.Chem.*, **1998**. *63*, 2407.

181. Farrall, M.J., Durst, T., and Frechet, M.J., *Tetrahedron Lett.*, **1979**, 203.
182. Davies, J.A. and Sood, A., *Makromol.Chem.Rapid Commun.*, **1983**. *4*, 777.
183. Sirringhaus, H., Tessler, N., and Friend, R.H., *Science*, **1998**. *280*, 1741.
184. Jenekhe, S.A., Cui, Y., and Zhang, X., *Macromolecules*, **1999**. *32*, 3824.
185. Sheats, J.R., Antoniadis, H., Hueschen, M., Leonard, W., Miller, J., Moon, R., Roitman, D., and Stocking, A., *Science*, **1996**. *273*, 884.
186. Zurer, P.S., *Chem.Eng.News*, **1998**(April 13), 41.
187. Duke, C.B., Paton, A., and Salaneck, W.R., *Mol.Cryst.Liq.Cryst.*, **1982**. *83*, 177.
188. Oldham, W.J., Lachicotte, R.J., and Bazan, G.C., *J.Am.Chem.Soc.*, **1998**. *120*, 2987.
189. Wang, F., Rauh, R.D., and Rose, T.L., *J.Am.Chem.Soc.*, **1997**. *119*, 11106.
190. Barbarella, G., Pudova, O., Arbizzani, C., Mastragostino, M., and Bongini, A., *J.Org.Chem.*, **1998**. *63*, 1742.
191. Capozzi, G., Drabowicz, J., Kielbasinski, P., Menichetti, S., Mikolajczyk, M., Nativi, C., Schank, K., Schott, N., and Zoller, U., *The Synthesis of Sulphones, Sulphoxides, and Cyclic Sulfoixides*, ed. Patai, S. and Rapport, R. **1994**, New York, NY: Wiley and Sons, Inc.
192. Patai, S., Rapport, Z., and Stirling, C., eds. *The Chemistry of Sulphones and Sulphoxides*. . **1988**, Wiley and Sons, Inc.: New York, NY.
193. Drabowicz, J. and Mikokajczyk, M., *Org.Prep.Proc.Int.*, **1982**. *14*, 45.
194. Marcker, C., *Liebigs Ann. Chem.*, **1865**. *136*, 891.
195. Lambert, J.B., Shurvell, H.F., Lightner, D.A., and Cooks, R.G., *Introduciton to Organic Spectroscopy*. **1987**, New York, NY: Macmillan Publishing Co.
196. Sattich, W., Personal Communication. **1998**.
197. Stevens, M.P., *Polymer Chemistry*. 2nd ed. **1990**, New York, NY: Oxford Univ. Press.
198. Port, A.B. and Still, R.H., *Polym.Degradation and Stability*, **1979**. *1*, 193.
199. Christen, G., *The Effects of Silica, Alumina, Silica Alumina, and HZSM-5 Zeolite on the Thermal Decomposition of Poly(ethylene), Poly(propylene), Poly(styrene), and Poly(vinyl chloride)*, in *Chemistry and Biochemistry*. **1993**, Univ. of Oklahoma, Norman, OK.
200. Doyle, C.D., *J.Appl.Polym.Sci.*, **1961**. *5*, 285.
201. Campbell, J.R., *J.Org.Chem.*, **1964**. *29*, 1830.
202. Moskvichev, Y.A., Mironov, G.S., Alov, E.M., Kramerova, S.K., Grigor'yants, I.K., Bolotina, L.M., Lyubomilov, V.L., Esipov, G.V., and Durneva, V.F., *Otkrytiya Izobret., Prom. Obraztsy, Tovarnue, Znaki*, **1980**. *18*, 153.
203. Rush, A.J., in *Chemistry and Biochemistry*. **1999**, Univ. of Oklahoma, Norman, OK.
204. Uffman, E., in *Chemistry and Biochemistry*. **1997**, Univ. of Oklahoma, Norman, OK.
205. Ansong, O. Patent. *US 5,514,770*, **May 7, 1996**.
206. Cotton, F.A. and Wilkinson, G., *Advanced Inorganic Chemistry*. 5th ed. **1988**, New York, NY: Wiley and Sons, Inc.

207. Ogata, Y. and Kamei, T., *Tetrahedron*, **1970**. *26*, 5667.
208. Windholz, M. and Budavari, S., eds. *Merch Index*. 10th ed. . **1983**, Merck and Co., Inc.: New York, NY.
209. Whitaker, R.D. and Sisler, H.H., *J.Org.Chem.*, **1960**. *25*, 1038.
210. Addison, C.C. and Sheldon, J.C., *J.Chem.Soc.*, **1956**, 2705.
211. Olah, G.A. and Gupta, B.G.B., *J.Org.Chem.*, **1983**. *48*, 3585.
212. Olah, G.A., Gupta, B.G.B., and Narang, S.C., *J.Am.Chem.Soc.*, **1979**. *101*, 5317.
213. Bordwell, F.G. and Boutan, P.J., *J.Am.Chem.Soc.*, **1957**. *79*, 717.
214. Marziano, N., Fiandaca, P., Maccarone, E., Romano, U., and Passerini, R., *Tetrahedron Lett.*, **1967**, 4785.
215. Marziano, N.C., Maccarone, E., Cimino, G.M., and Passerini, R.C., *J.Org.Chem.*, **1974**. *39*, 1098.
216. Szmant, H.H. and Lapinski, R.L., *J.Am.Chem.Soc.*, **1952**. *74*, 4395.
217. Gillespie, R.J. and Passerini, R.C., *J.Chem.Soc.*, **1956**, 3850.
218. Miotti, U., Modena, G., and Sedea, L., *J.Chem.Soc.B*, **1970**, 802.
219. Majetich, G., Hicks, R., and Reister, S., *J.Org.Chem.*, **1997**. *62*, 4321.
220. Mancuso, A.J. and Swern, D., *Synthesis*, **1981**, 165.
221. Cotton, F.A., Francis, R., and Horrocks, W.D., *J. Chem.Soc.*, **1960**. *64*, 1534.
222. Van Leeuwen, P.W.N.M., *Recueil*, **1967**. *86*, 201.
223. Van Leeuwen, P.W.N.M. and Groeneveld, W.L., *Recueil*, **1966**. *85*, 1173.
224. Fujihara, H., Imaoka, K., and Furukawa, N., *J.Chem.Soc.Perkin Trans.1*, **1986**, 465.
225. Shukla, J.P. and Subramanian, M.S., *J.Radioanal.Chem.*, **1980**. *60*, 403.
226. Ramakrishna, V.V., Patil, S.K., Reddy, L.K., and Reddy, A.S., *J.Radioanalytical.Chem.*, **1978**. *47*, 57.
227. McDowell, W.J. and Harmon, H.D., *J.Inorg.Nucl.Chem.*, **1971**. *33*, 3107.
228. Misra, B.B. and Mohanty, S.R., *Aust.J.Chem.*, **1977**. *30*, 2297.
229. Chakrabortty, M. and Mohanty, S.R., *Radiochem.Radioanal.Lett.*, **1979**. *37*, 33.
230. Goryachev, A.A. and Kopkova, E.K., *Zh.Neorg.Khim.*, **1980**. *25*, 1347.
231. Kolosnitsyn, V.S., *Issled.Obl.Khim.Vysokomol.Soedin.Neftekhim.*, **1977**, 41.
232. Afzaletdinova, N.G., *Issled.Obl.Khim.Vysokomol.Soedin.Neftekhim.*, **1977**, 42.
233. Murinov, Y.I., Nikitin, Y.E., Kuvatov, Y.G., Rozen, A.M., Spirikhin, L.V., and Zaev, E.E., *Radiokhimiya*, **1981**. *23*, 33.
234. Sherrington, D.C. and Hodge, P., *Syntheses an d Separations Using Functional Polymers*. **1988**, New York, NY: Wiley and Sons, Inc.
235. Egawa, H., Kuroda, T., and Shiraishi, N., *Bull.Chem.Soc.Jpn.*, **1982**, 685.
236. Katoh, S., Sugasaka, K., Sakane, K., Takai, N., Takahashi, H., Umezawa, Y., and Itagaki, K., *Bull.Chem.Soc.Jpn.*, **1982**, 1449.
237. Egawa, H., Jogo, Y., and Maeda, H., *Bull.Chem.Soc.Jpn.*, **1979**, 1760.
238. Colella, M.B., Siggia, S., and Barnes, R.M., *Anal.Chem.*, **1980**. *52*, 2347.
239. Marton-Schmidt, E., Inczedy, J., Laki, Z., and Szabadka, O., *J.Chromatogr.*, **1980**. *201*, 73.
240. Colella, M.B., Siggia, S., and Barnes, R.M., *Anal.Chem.*, **1980**. *52*, 967.

241. Yamada, M., Takagi, M., and Ueno, K., *J.Coord.Chem.*, **1980**. *10*, 257.
242. Egawa, H., Harada, H., and Nonaka, T., *Bull.Chem.Soc.Jpn.*, **1980**, 1767.
243. Egawa, H., Harada, H., and Shuto, T., *Bull.Chem.Soc.Jpn.*, **1980**, 1773.
244. Katoh, S., Sugasaka, K., Sakane, K., Takai, N., Takahashi, H., Umezawa, Y., and Itagaki, K., *Bull.Chem.Soc.Jpn.*, **1982**, 1455.
245. Astheimer, L., Schenk, H.J., Witte, E.G., and Schwochau, K., *Separation Sci.Technol.*, **1983**. *18*, 307.
246. Sugasaka, K., Katoh, S., Takai, N., Takahashi, H., and Umezawa, Y., *Separation Sci.Technol.*, **1981**. *16*, 971.
247. Kanno, M., *Separation Sci.Technol.*, **1981**. *16*, 999.
248. Vernon, F. and Shah, T., *Reactive Polym.*, **1983**. *1*, 301.
249. Kelmers, A.D., *Separation Sci.Technol.*, **1981**. *16*, 1019.
250. Johnson, J., *Chem.Eng.News.*, **1999**(June 7), 8.
251. Dean, J.A., *Analytical Chemistry Handbook*. **1995**, New York, NY: McGraw-Hill, Inc.
252. Lin, R., *Catalytic Cracking of Poly(ethylene) and Poly(styrene) by Silica-Alumina, HZSM-5 Zeolite, and Sulfated Zirconia*, in *Chemistry and Biochemistry*. **1996**, Univ. of Oklahoma, Norman, OK.

Appendices

Appendix A–Polynitro[2.2]paracyclophanes Spectra

Appendix B–Poly(2,6-dimethyl-*p*-xylylene) (21) Spectra

Appendix C–Poly(*p*-phenylene sulfoxide) (18) Spectra

Appendix D–Instrumentation, Software, and Hardware

Appendix E–X-ray Data for N,N,N-trimethyl(3-bromo-2,4,6-trimethyl-5-nitrobenzyl)ammonium nitrate (26)

Appendix F– Chemical Abbreviations

Appendix A–Polynitro[2.2]paracyclophanes Spectra

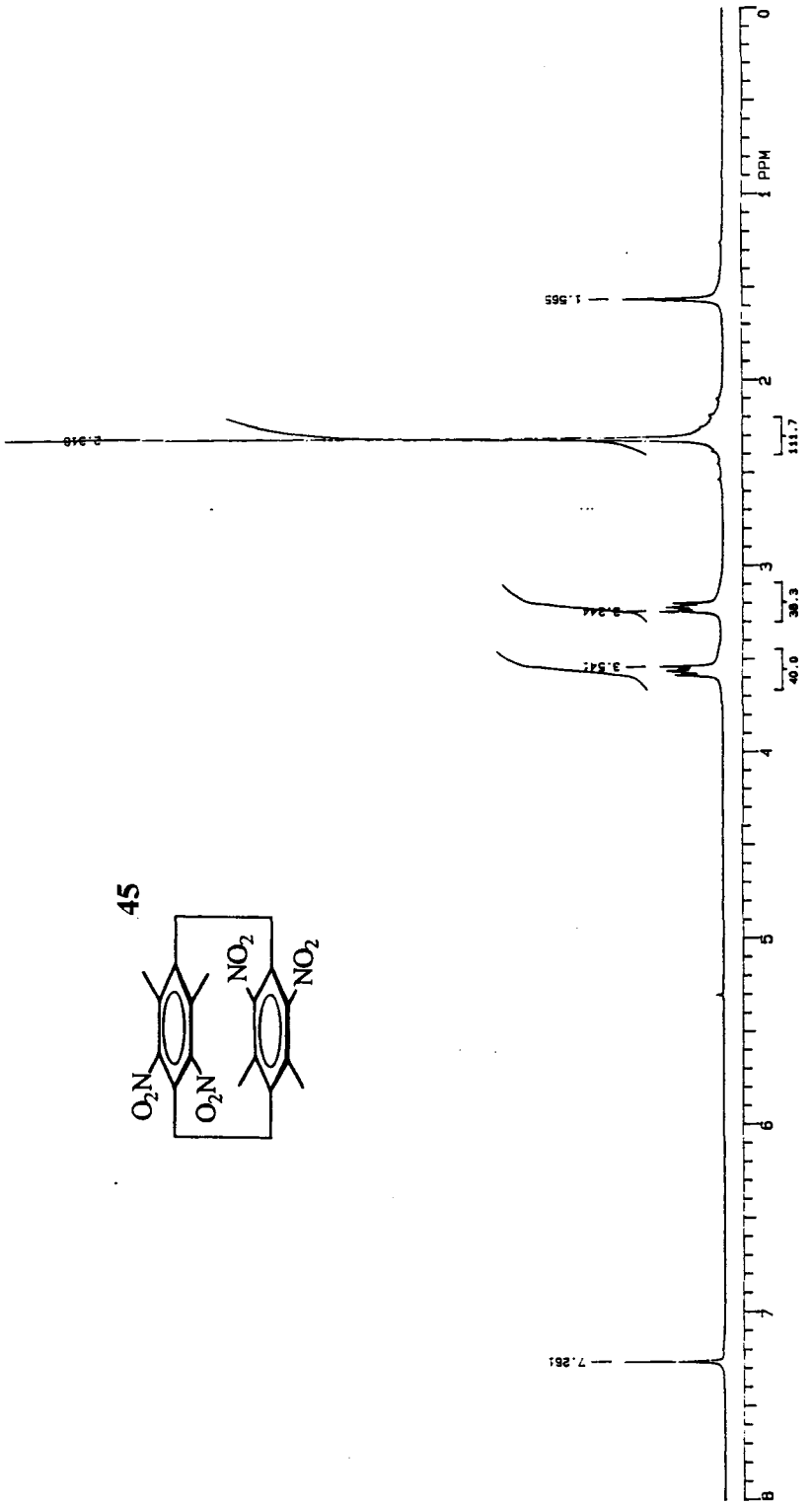

A-1 Proton NMR of **45**

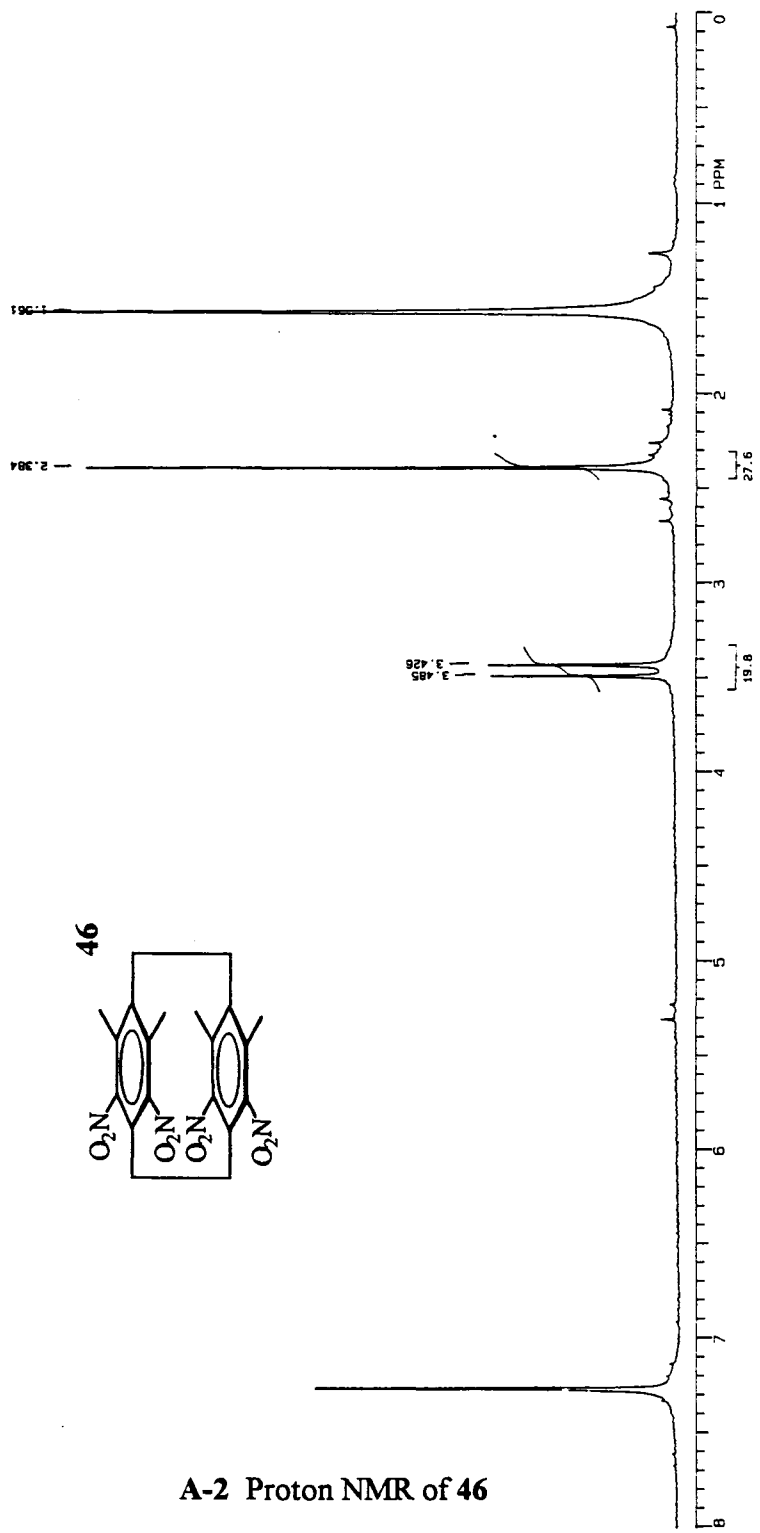

A-2 Proton NMR of **46**

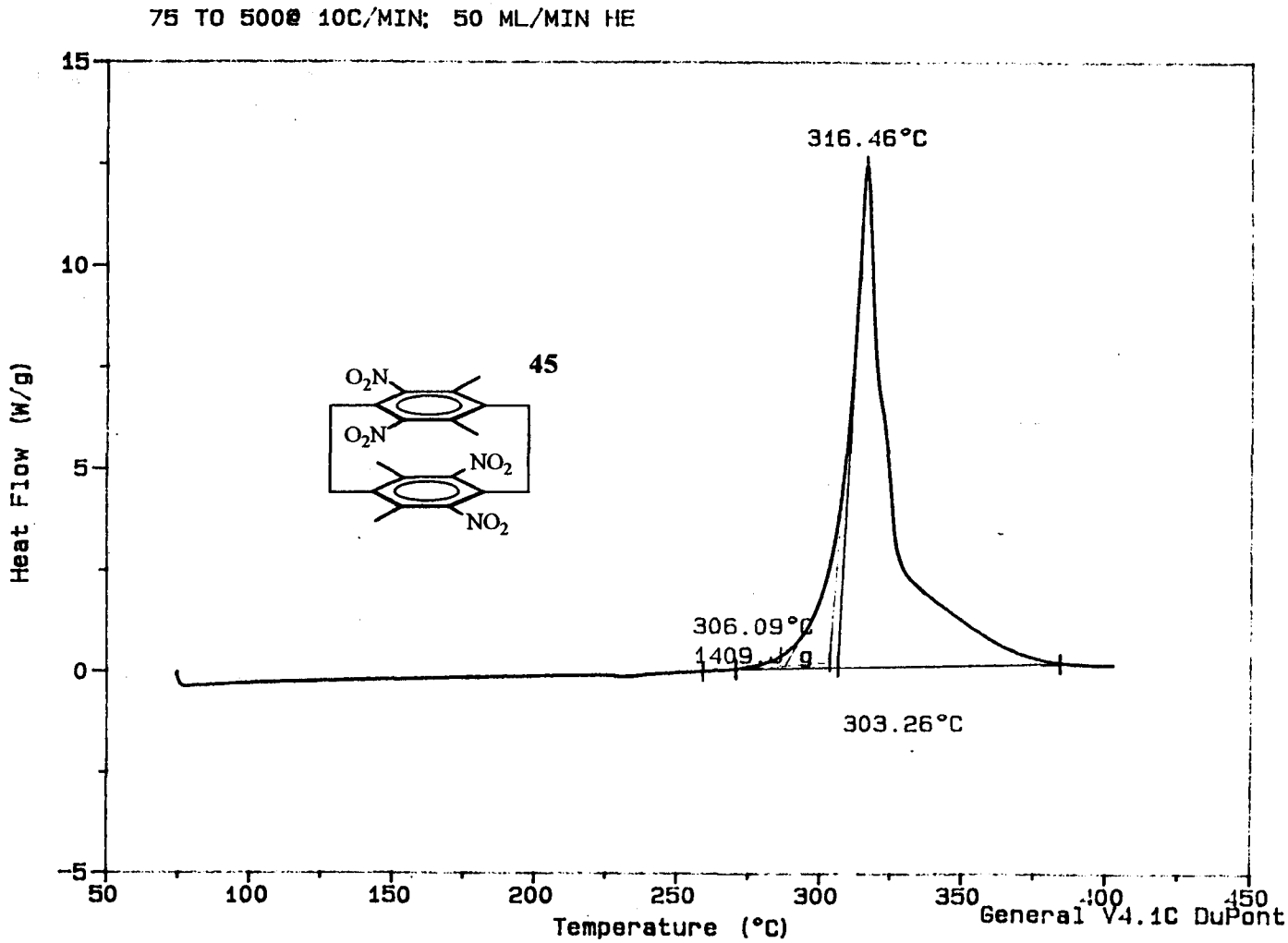
75 TO 500@ 10C/MIN; 50 ML/MIN HE
316.46°C
45
O_2N
O_2N
NO_2
NO_2
306.09°C
1409 J/g
303.26°C
Heat Flow (W/g)
Temperature (°C)
General V4.1C DuPont

A-3 DSC of **45**

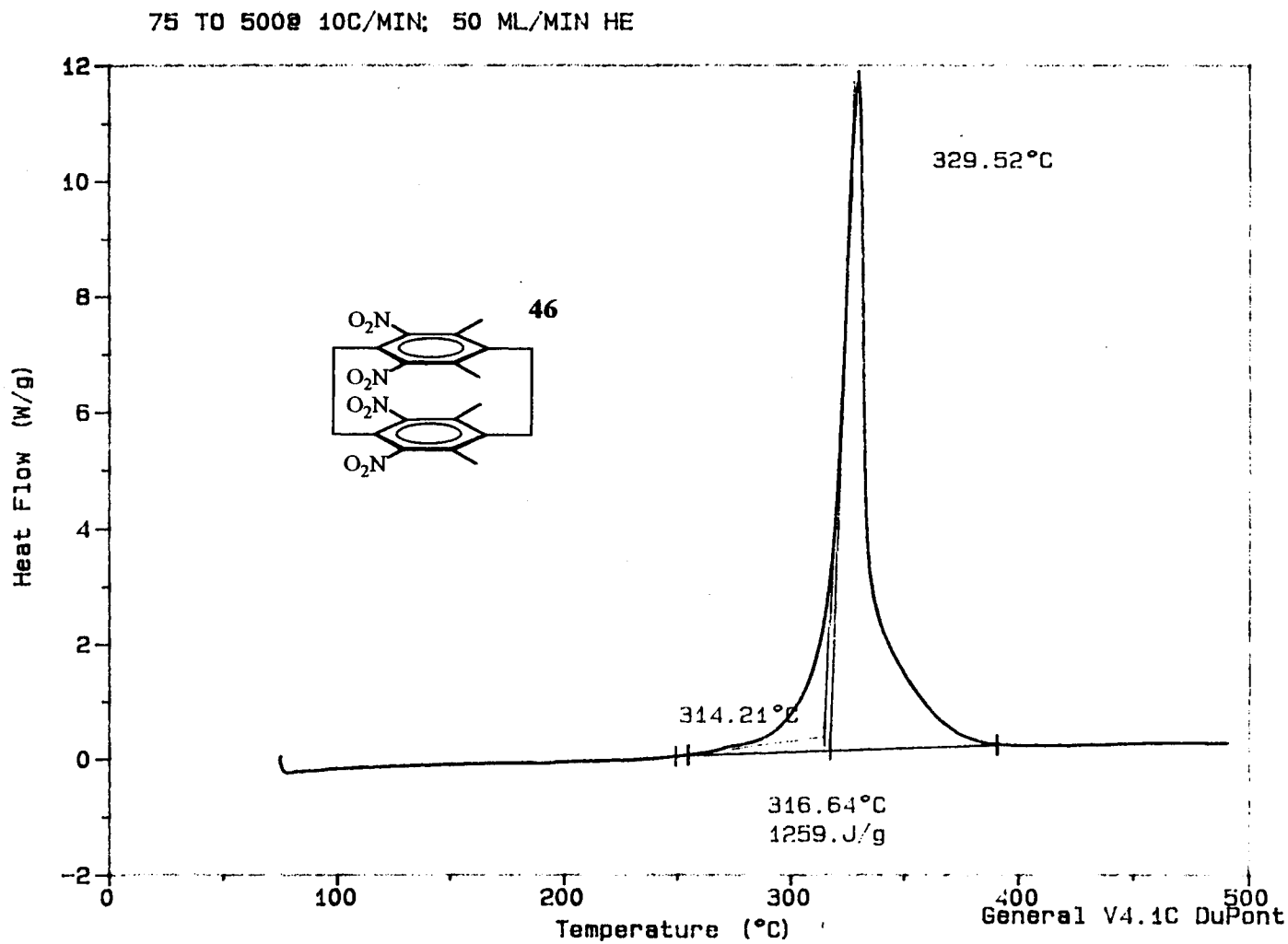
75 TO 500@ 10C/MIN; 50 ML/MIN HE
Heat Flow (W/g)
12
10
8
6
4
2
0
-2
0
100
200
300
400
500
Temperature (°C)
General V4.1C DuPont
329.52°C
314.21°C
316.64°C
1259.J/g
46
O_2N
O_2N
O_2N
O_2N

A-4 DSC of **46**

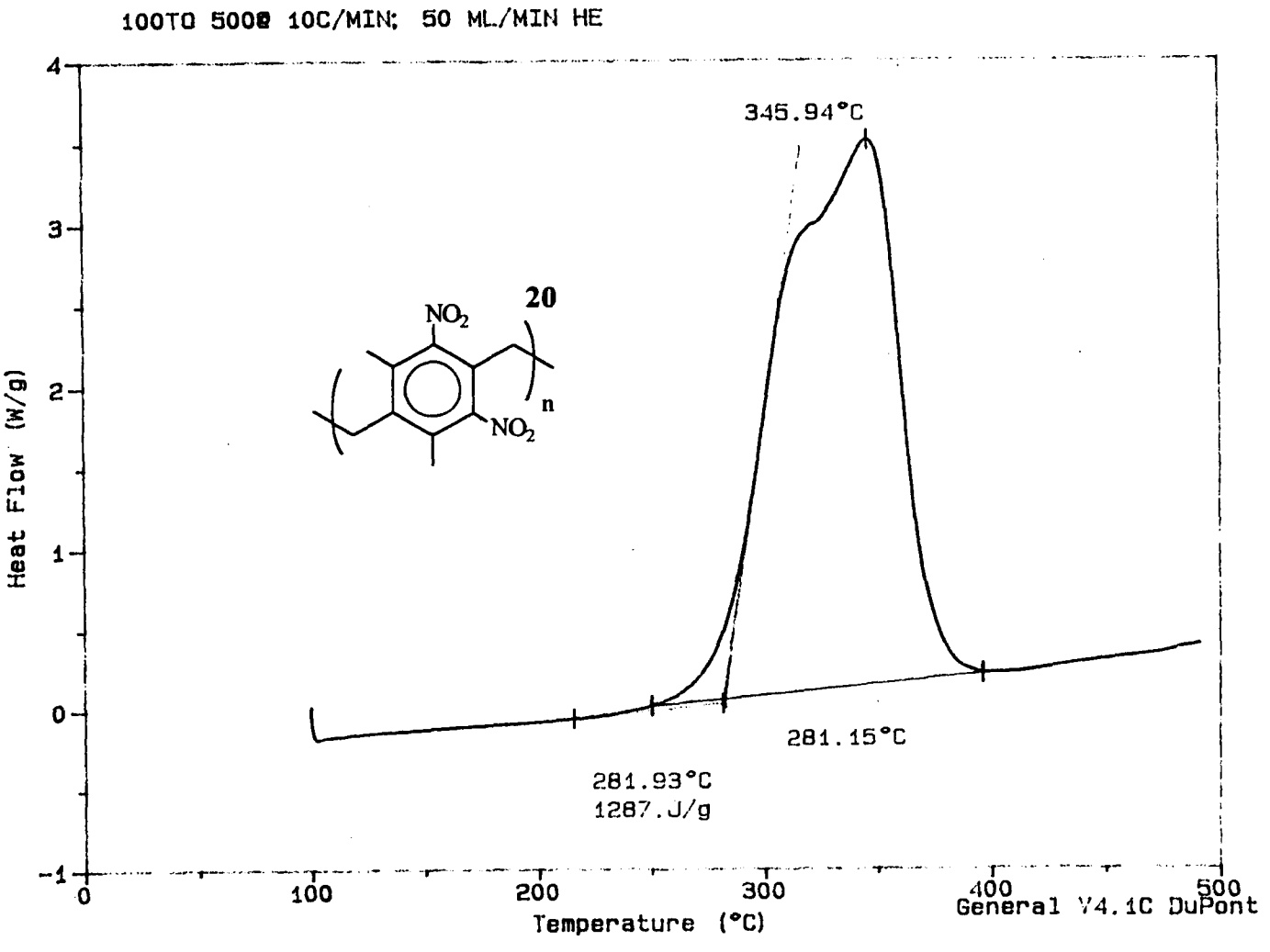
100TO 500@ 10C/MIN; 50 ML/MIN HE
345.94°C
20
NO2
NO2
n
281.15°C
281.93°C
1287.J/g
Heat Flow (W/g)
Temperature (°C)
General V4.1C DuPont

A-5 DSC of **20**

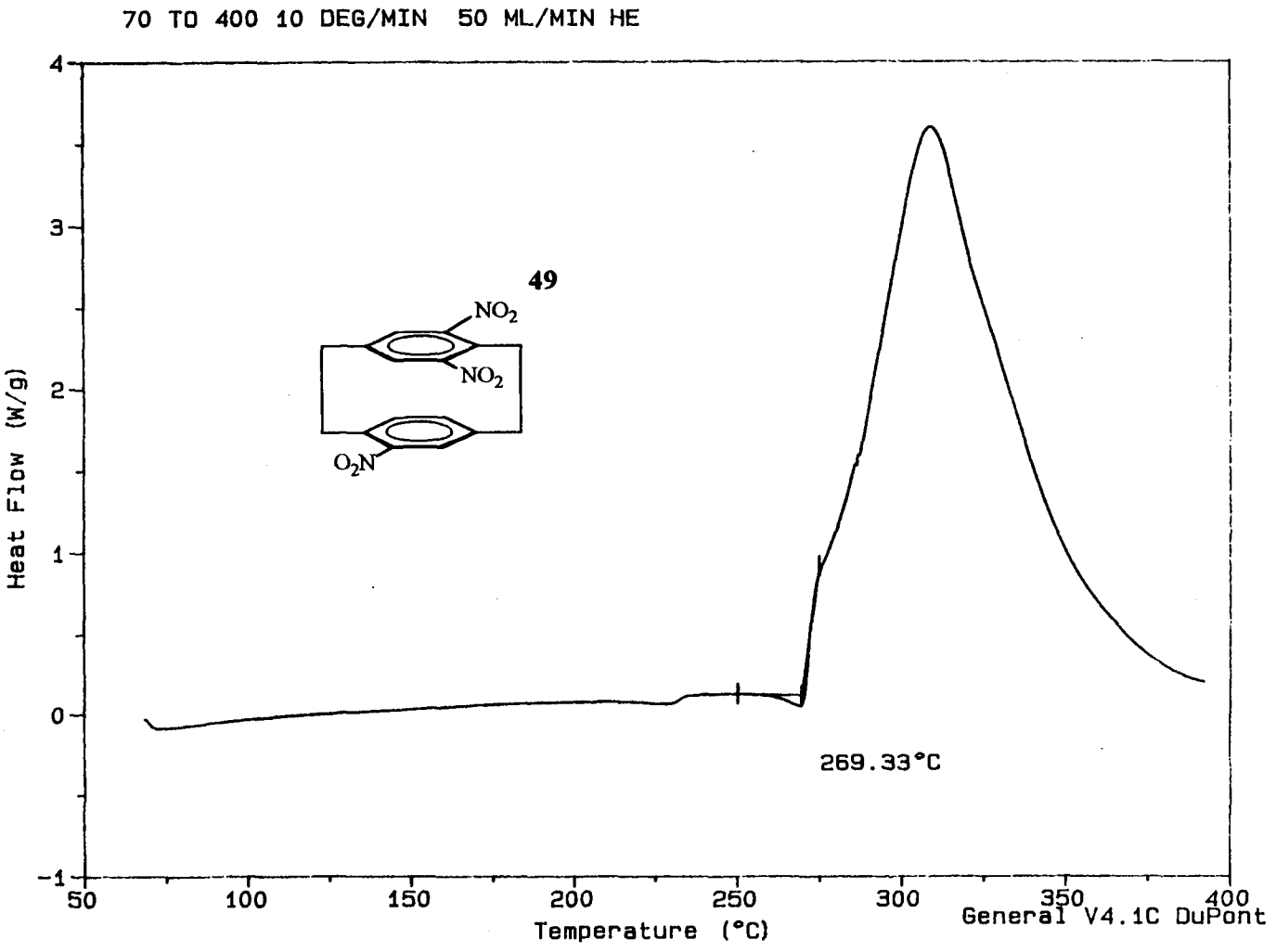
70 TO 400 10 DEG/MIN 50 ML/MIN HE
Heat Flow (W/g)
4
3
2
1
0
-1
50
100
150
200
250
300
350
400
Temperature (°C)
General V4.1C DuPont
269.33°C
49
NO2
NO2
O2N

A-6 DSC of **49**

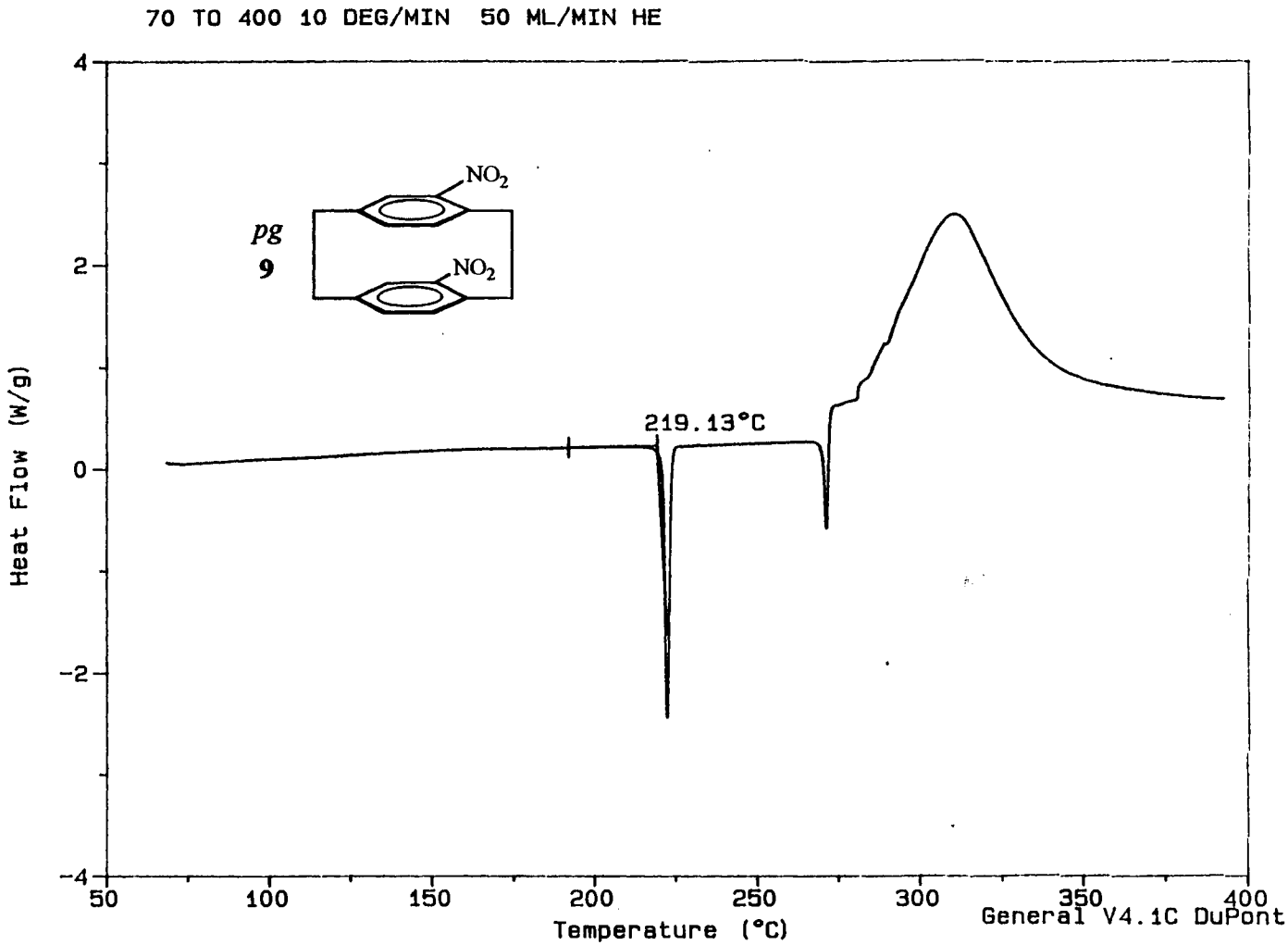

A-7 DSC of *pg*-dinitro[2.2]PCP

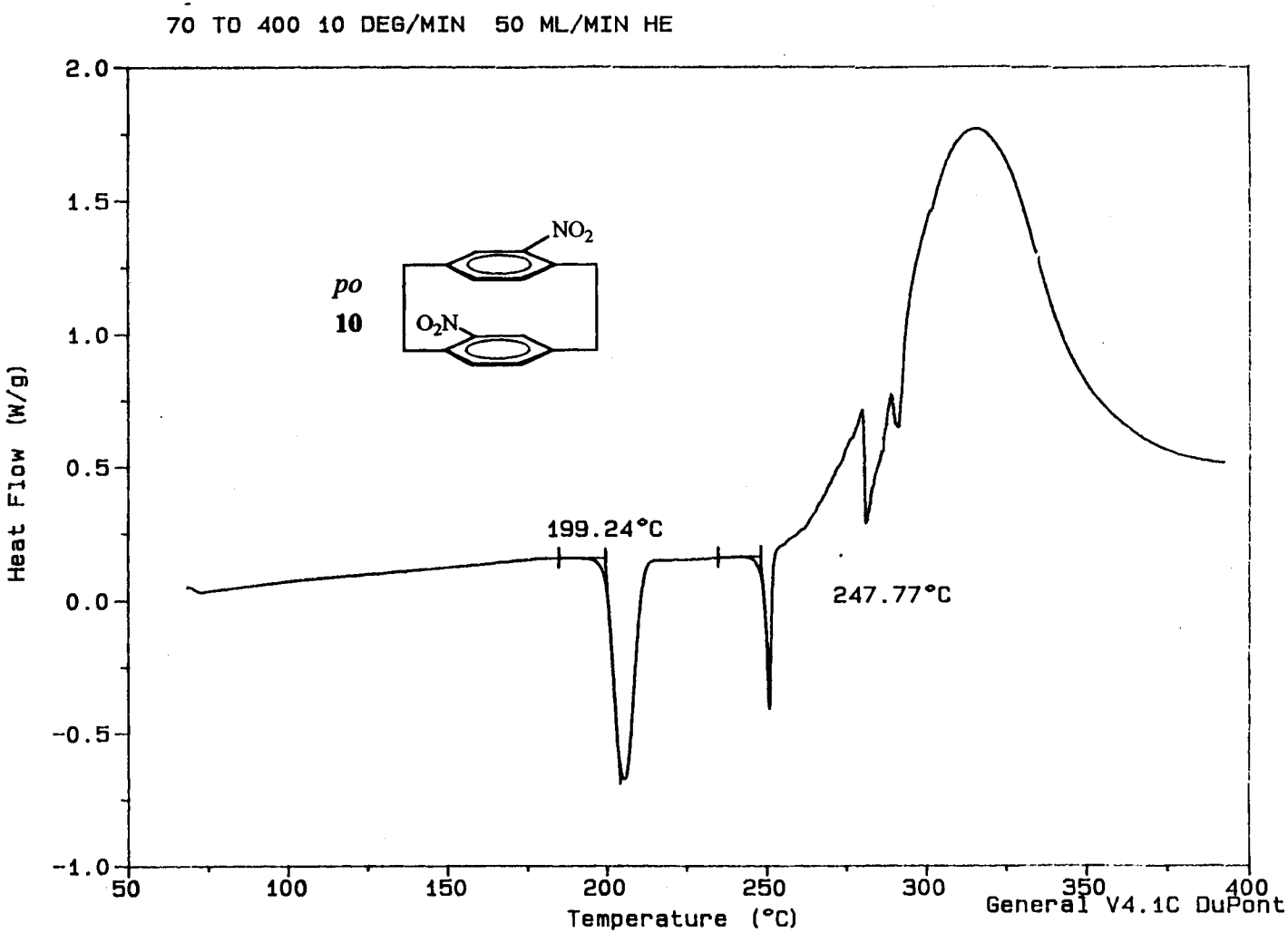

A-8 DSC of *po*-dinitro[2.2]PCP

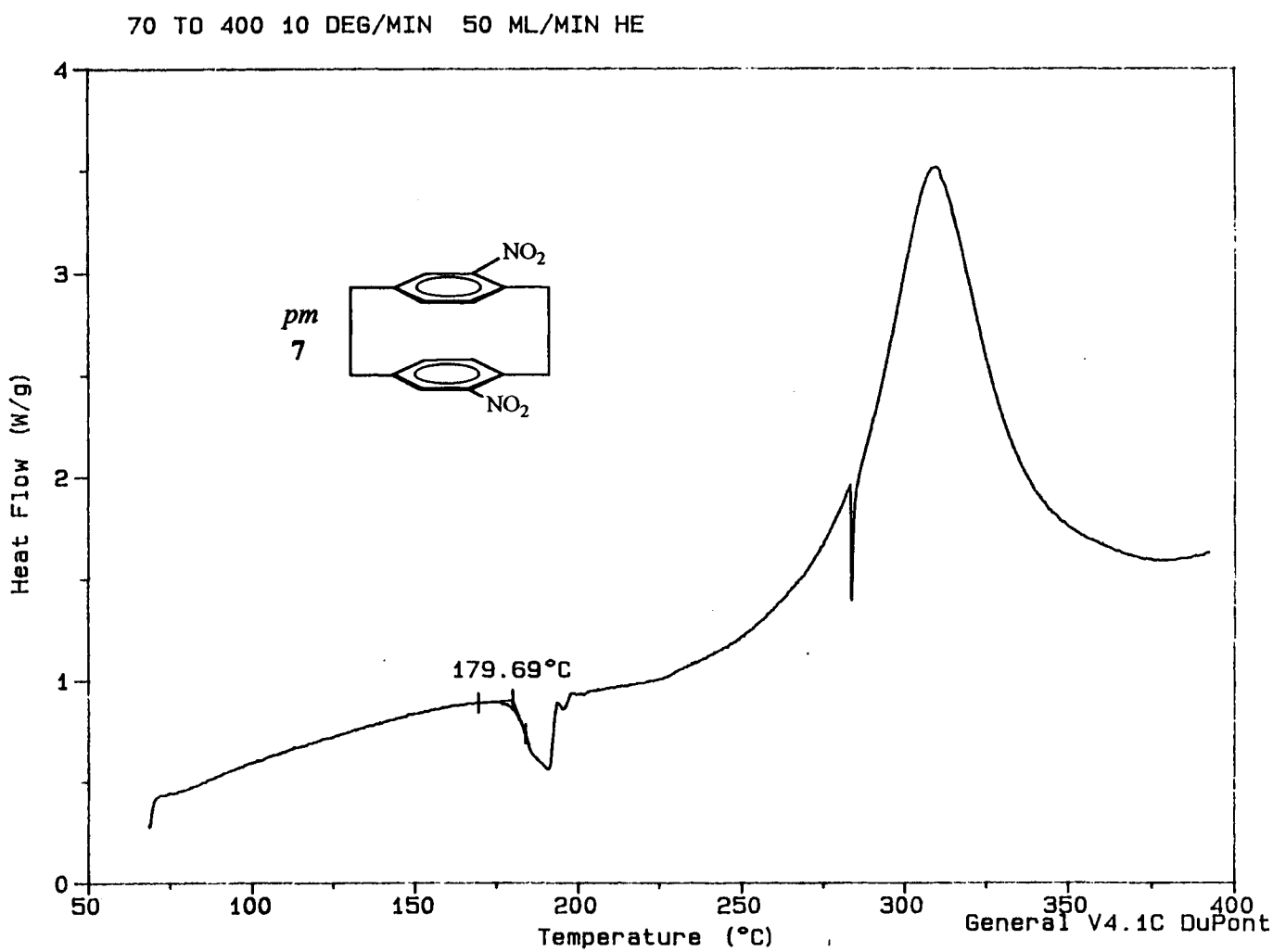

A-9 DSC of *pm*-dinitro[2.2]PCP

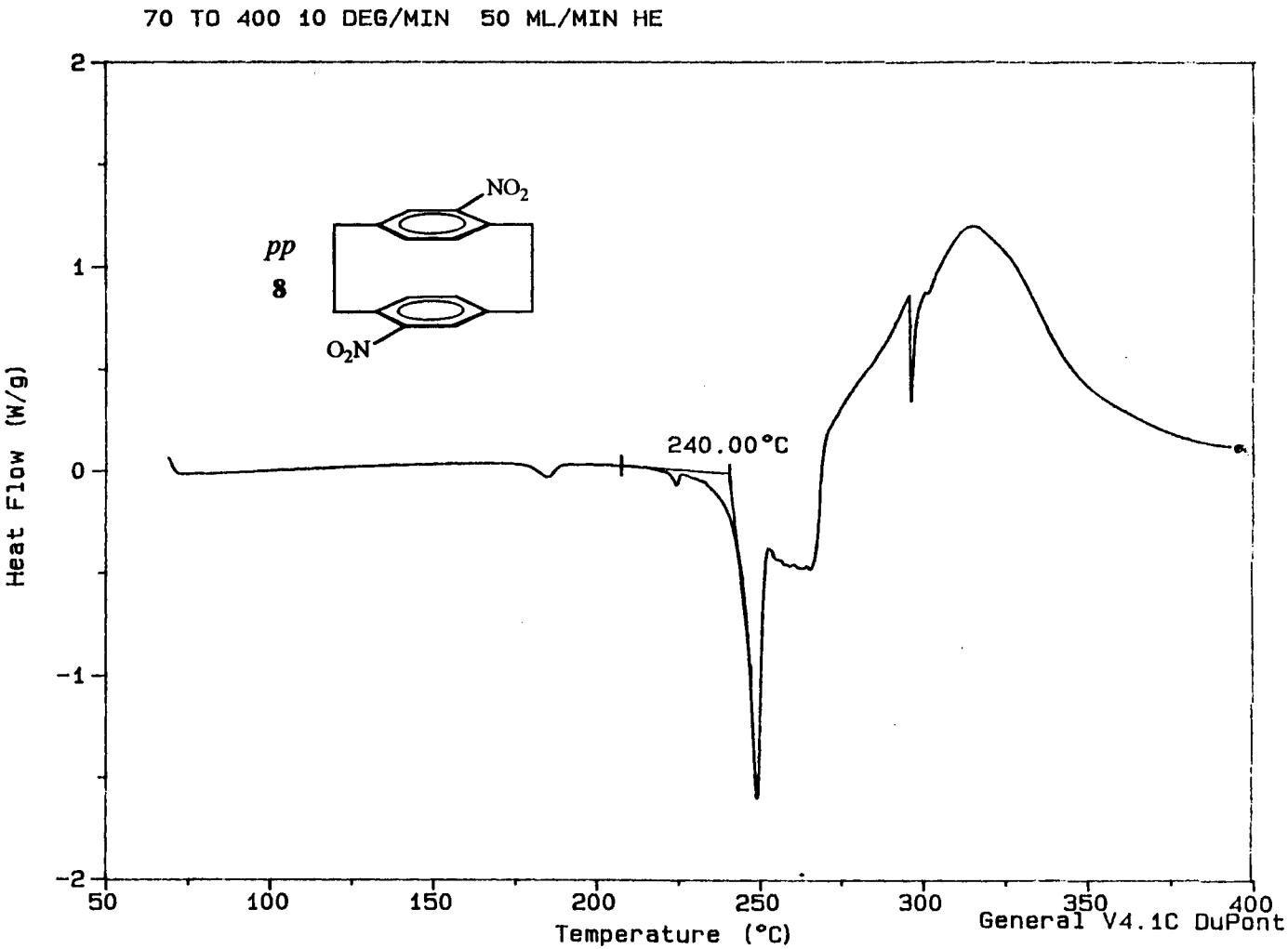

A-10 DSC of *pp*-dinitro[2.2]PCP

Appendix B–Poly(2,6-dimethyl-*p*-xylylene) (21) Spectra

B-1 Proton NMR of **21**

B-2 Carbon-13 NMR of **21**

B-3 IR Spectrum of **21**

B-4 TGA of **21** in Helium

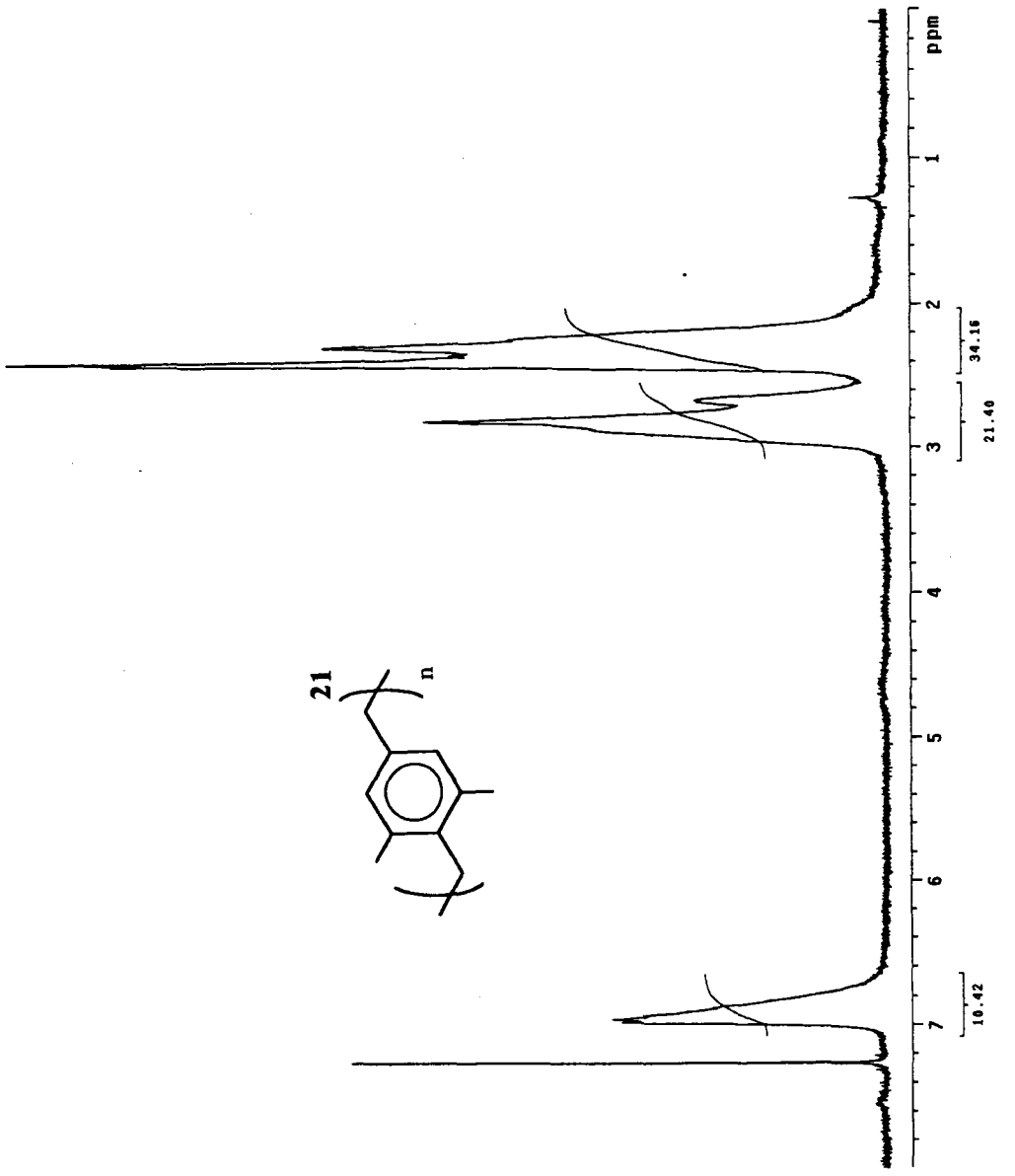

B-1 Proton NMR of **21**

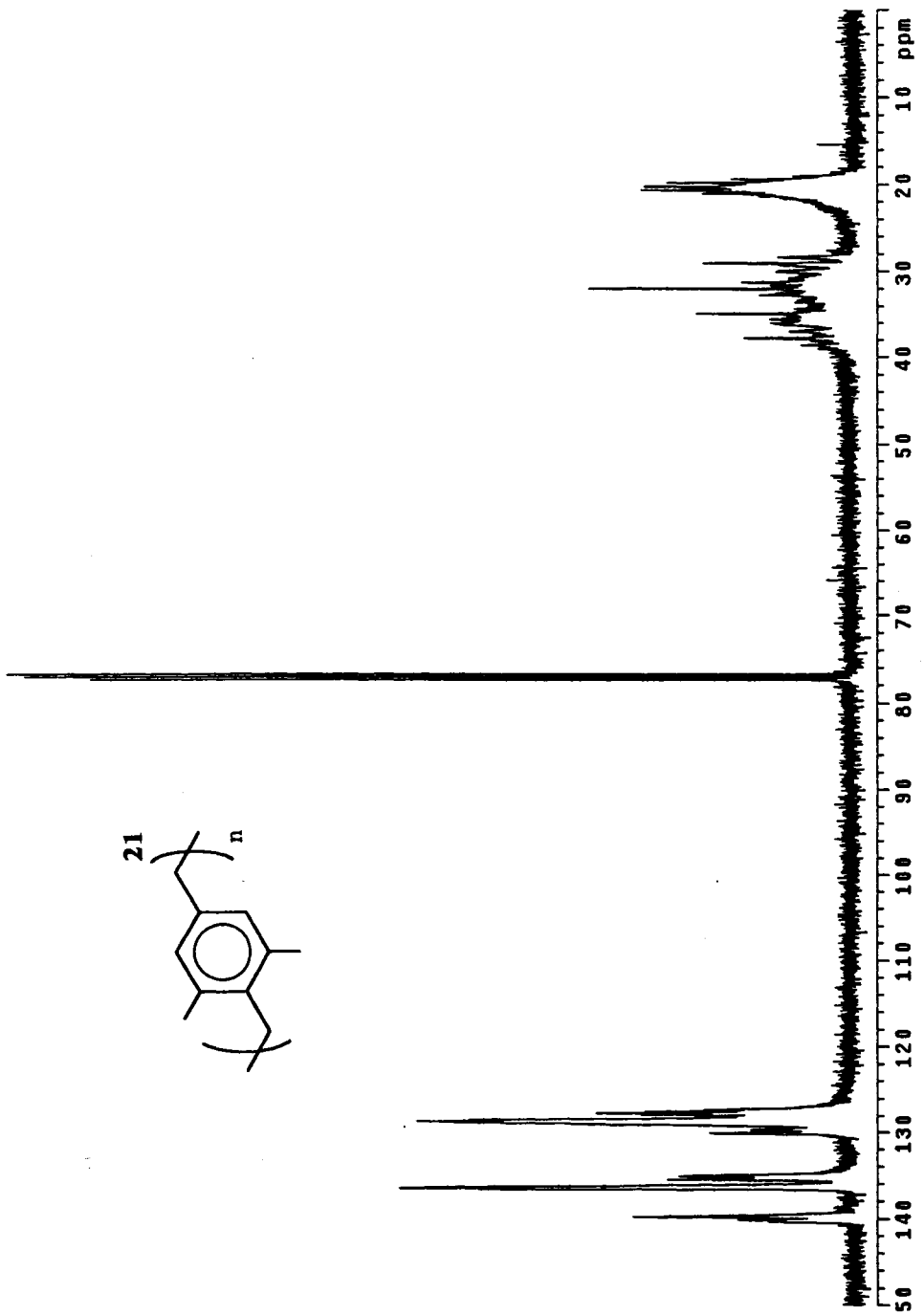

B-2 Carbon-13 NMR of **21**

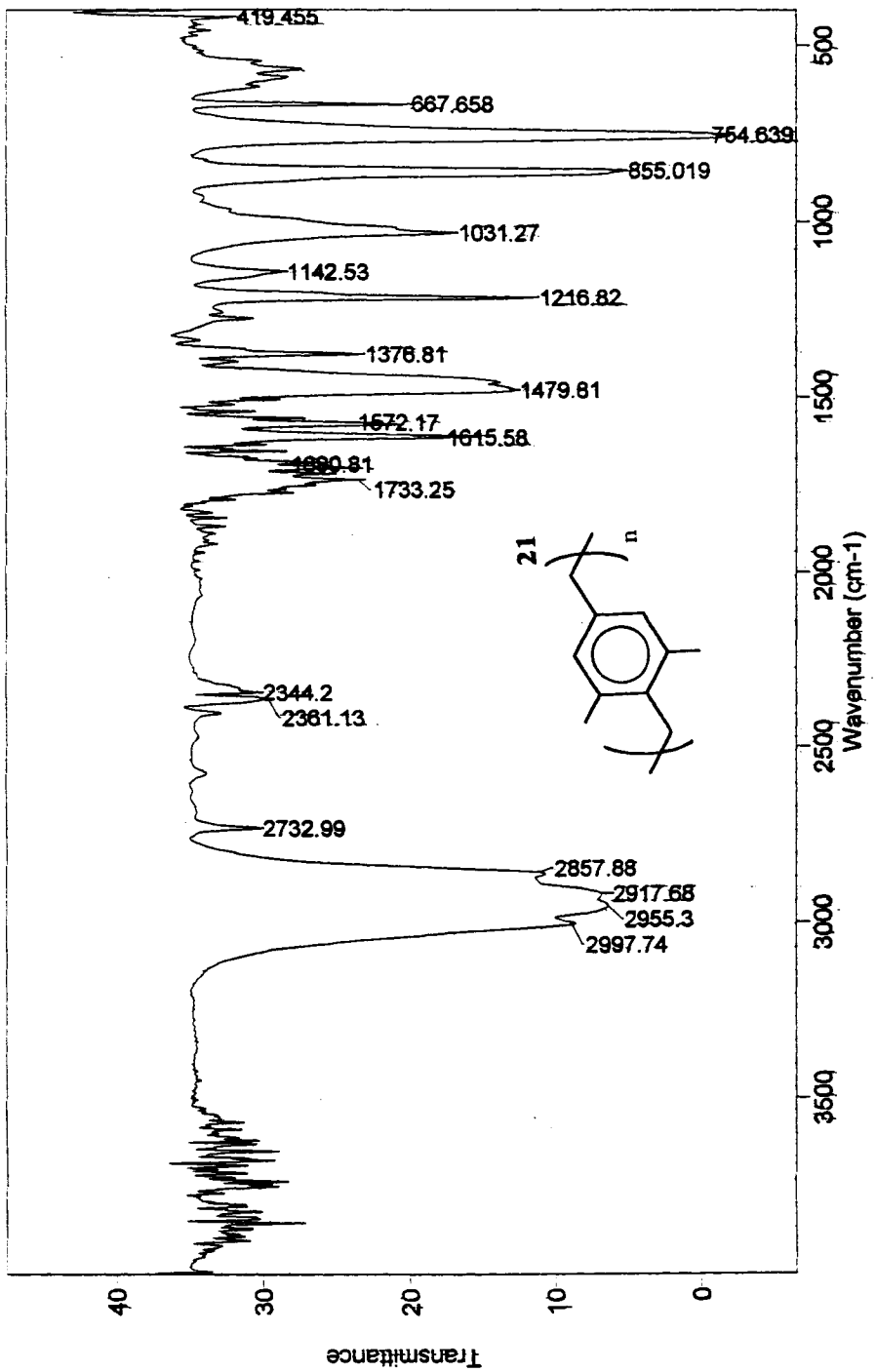

B-3 IR Spectrum of **21**

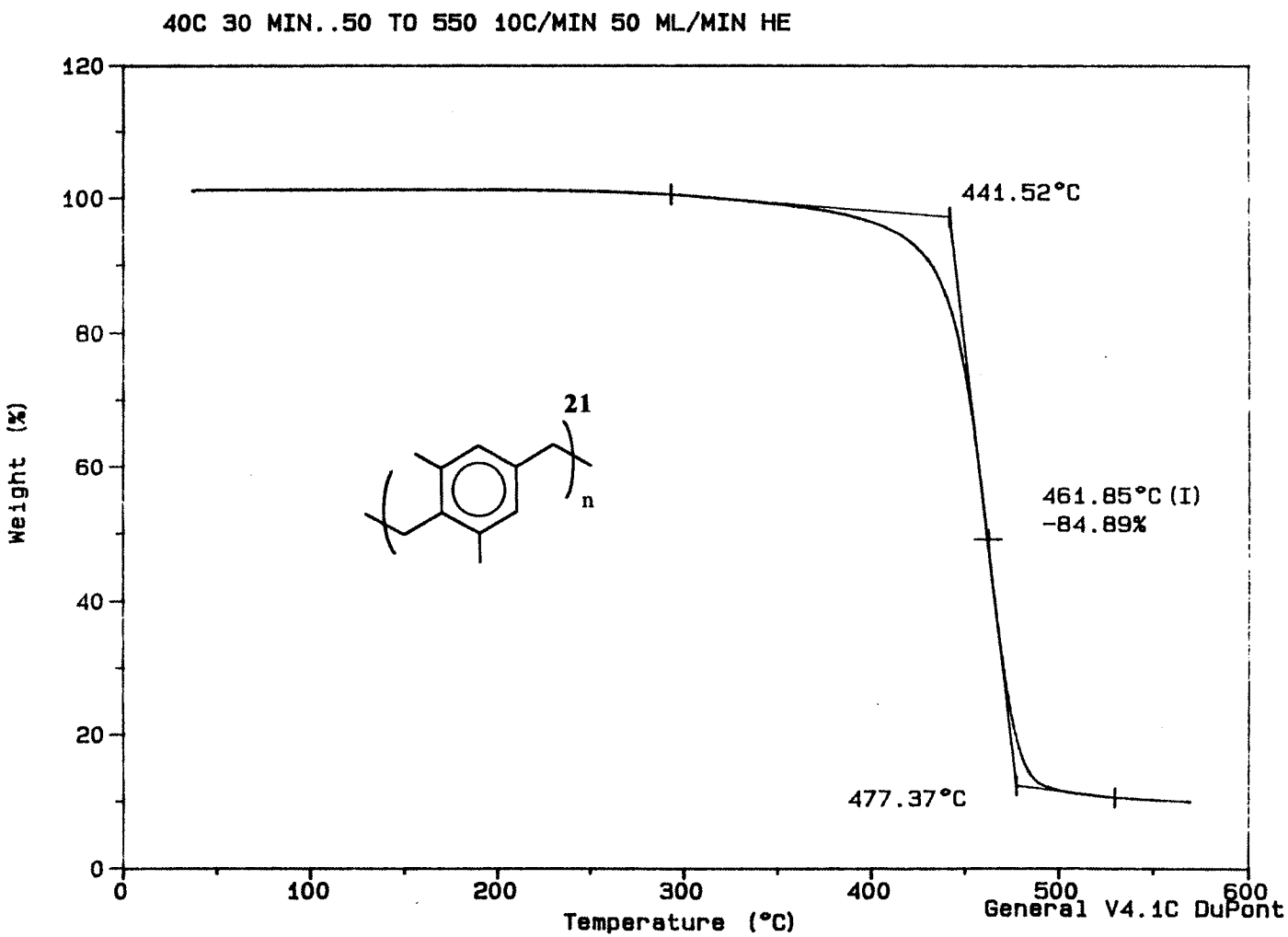

B-4 TGA of **21** in Helium

Appendix C–Poly(*p*-phenylene sulfoxide) (18) Spectra

C-1 PPSX Varied Rate TGA Decomposition in Air

C-2 PPSX First Derivative of PPSX Varied Rate TGA Decomposition in Air

C-3 Arrhenius Plot of PPSX Varied Rate TGA Decomposition in Air

C-4 Residual Weight Fraction-Arrhenius Plot of PPSX TGA Decomposition in Air

C-5 IR Spectrum of PPS

C-6 IR Spectrum of PPSX

C-7 IR Spectrum of PPSO

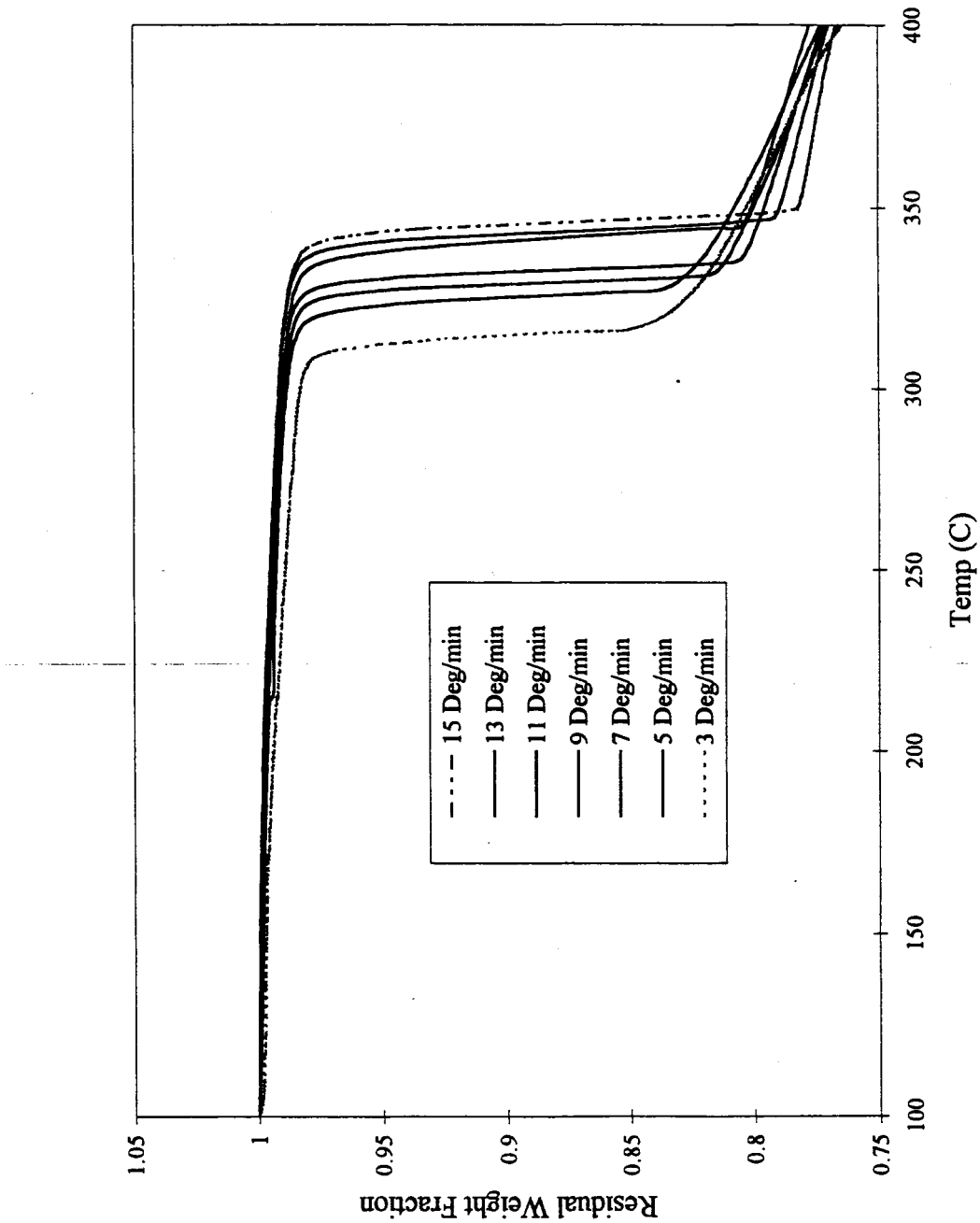

C-1 PPSX Varied Rate TGA Decomposition in Air

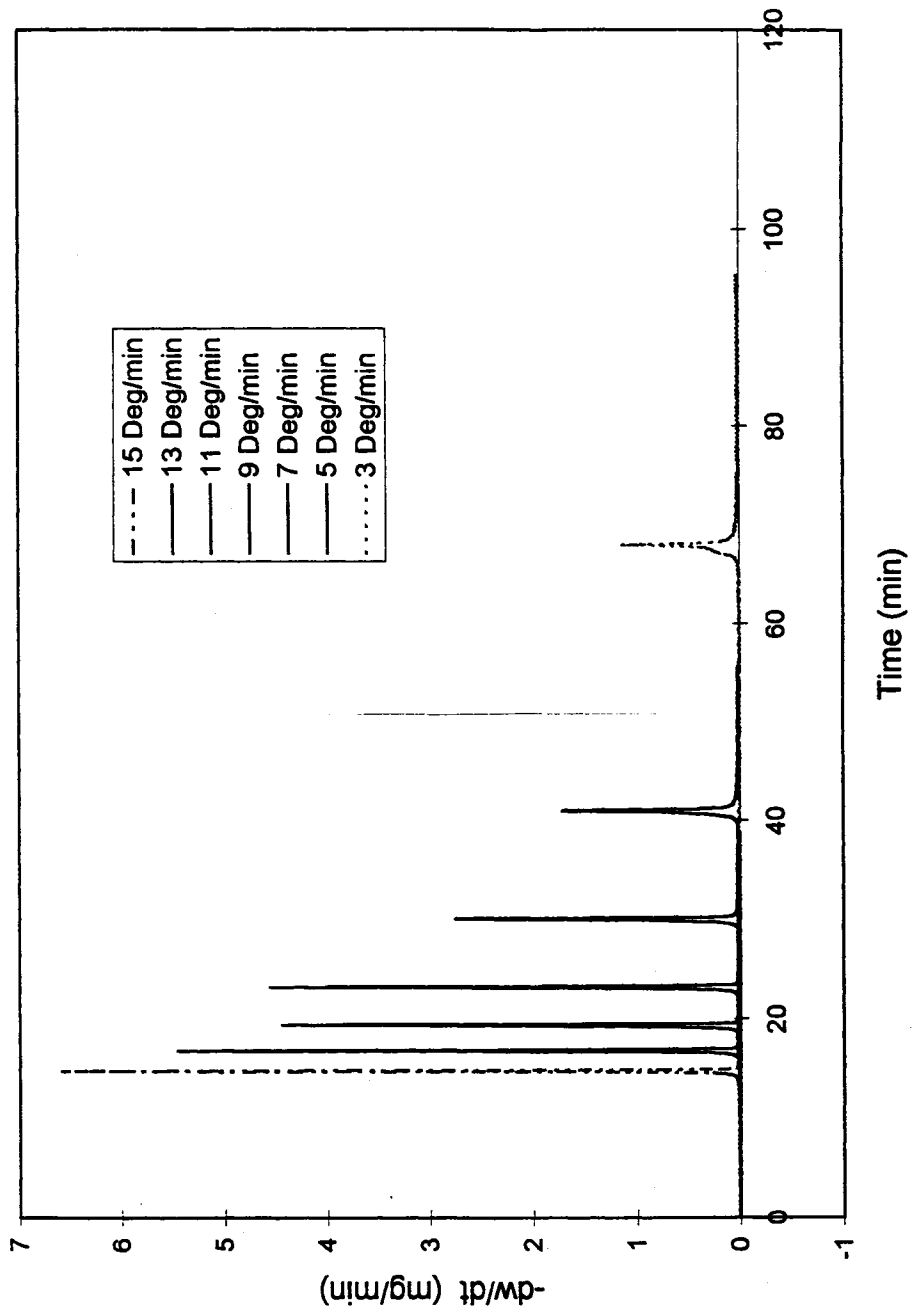

C-2 PPSX First Derivative of PPSX Varied Rate TGA Decomposition in Air

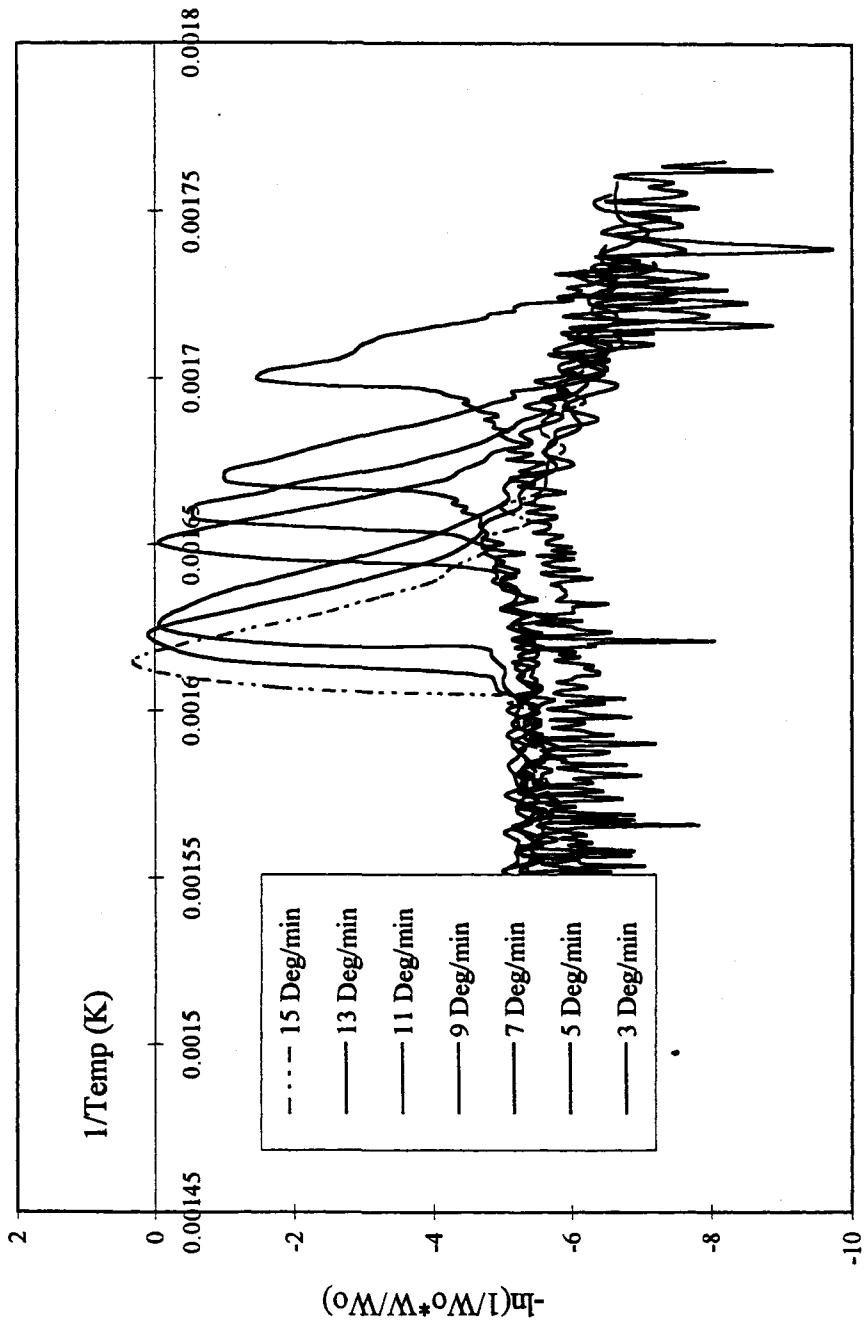

C-3 Arrhenius Plot of PPSX Varied Rate TGA Decomposition in Air

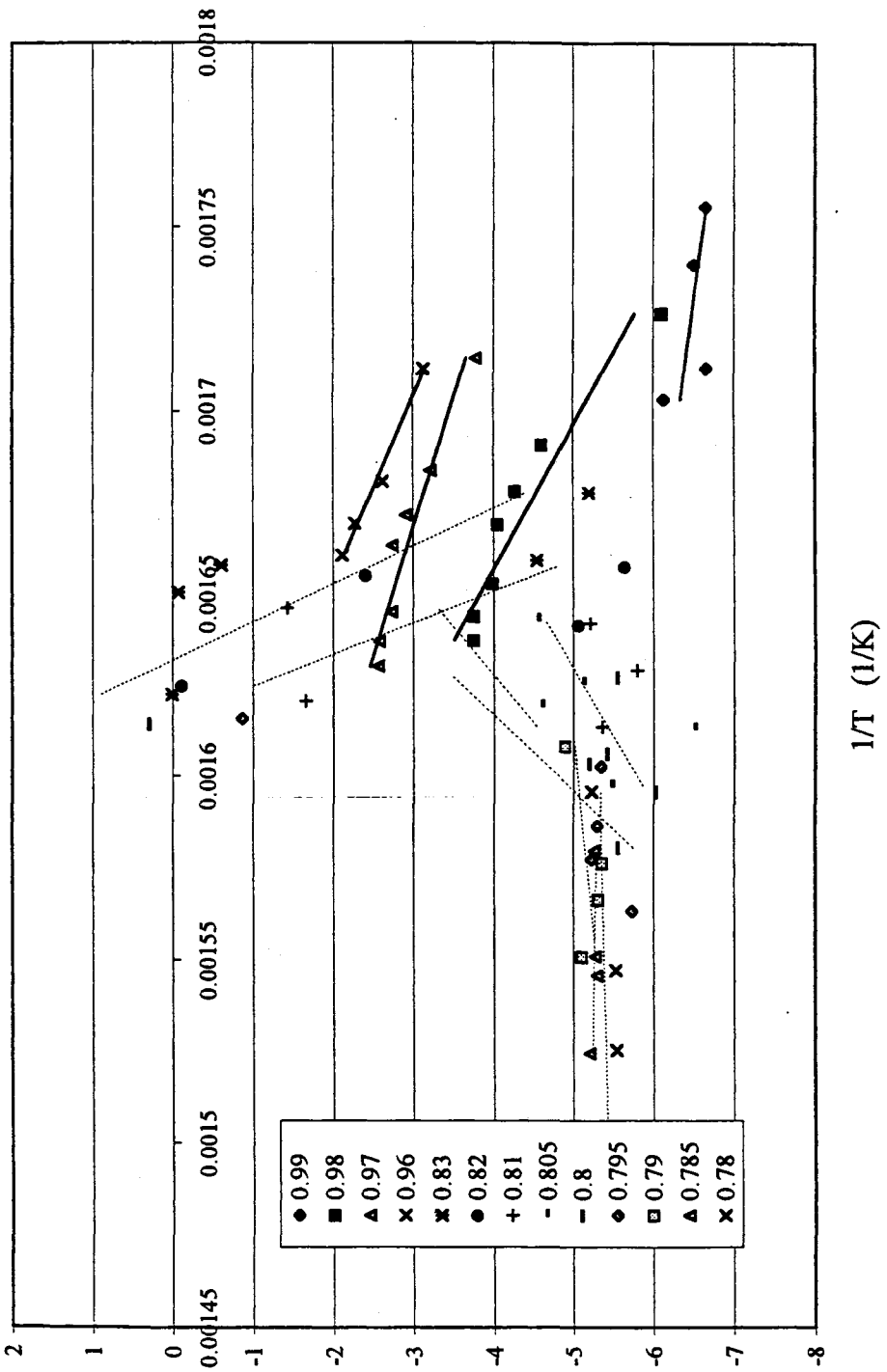

C-4 Residual Weight Fraction-Arrhenius Plot of PPSX TGA Decomposition in Air

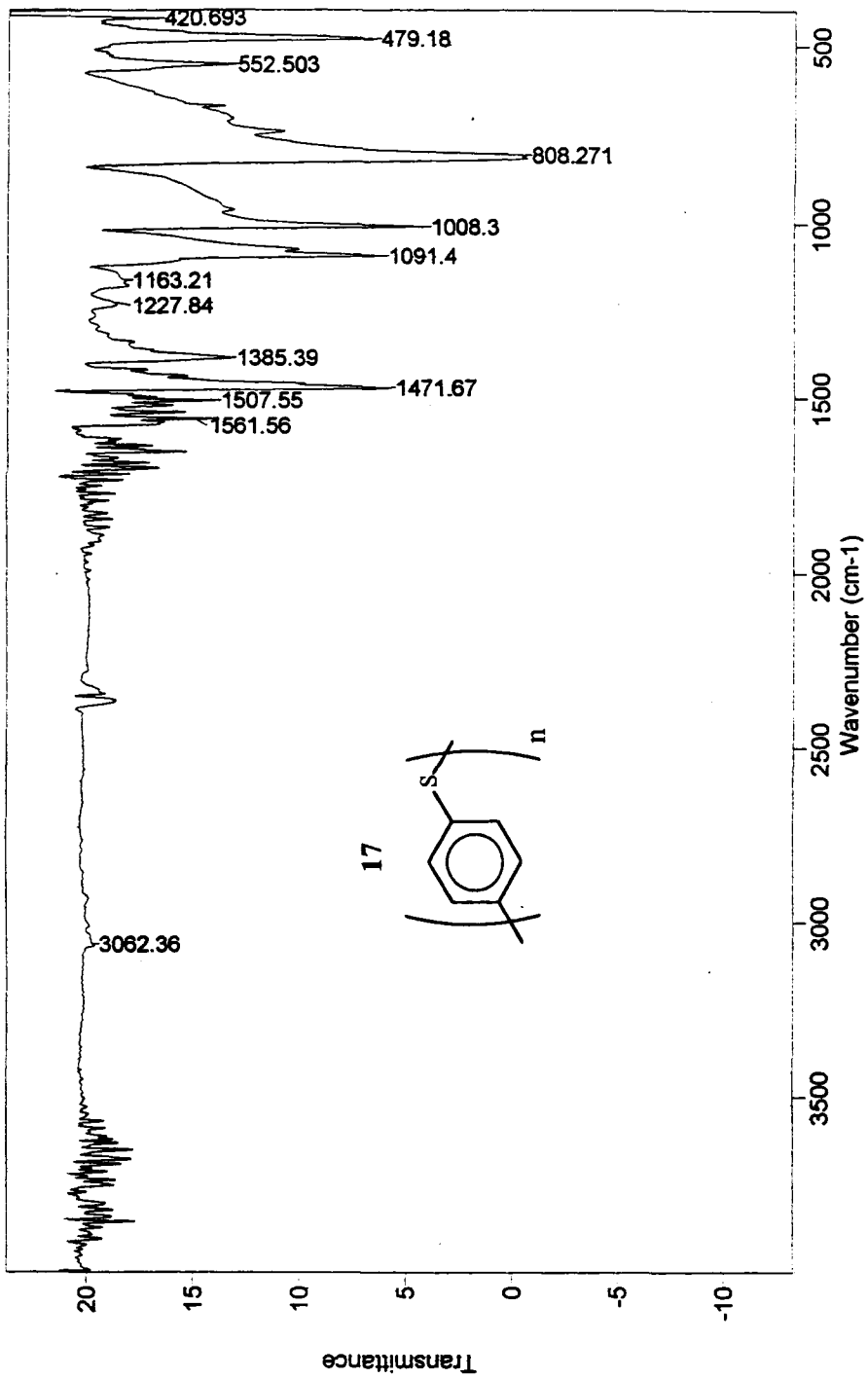

C-5 IR Spectrum of PPS

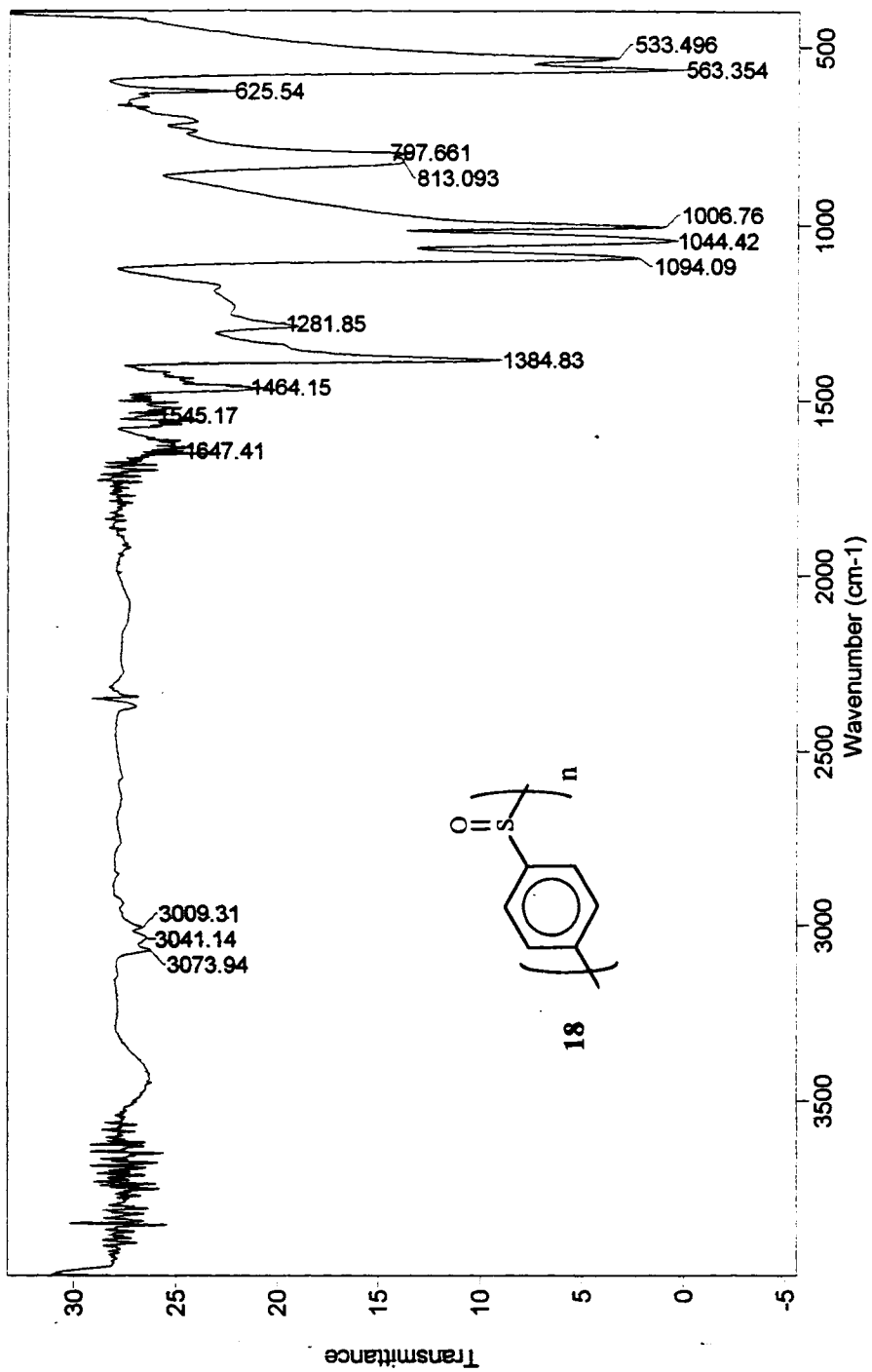

C-6 IR Spectrum of PPSX

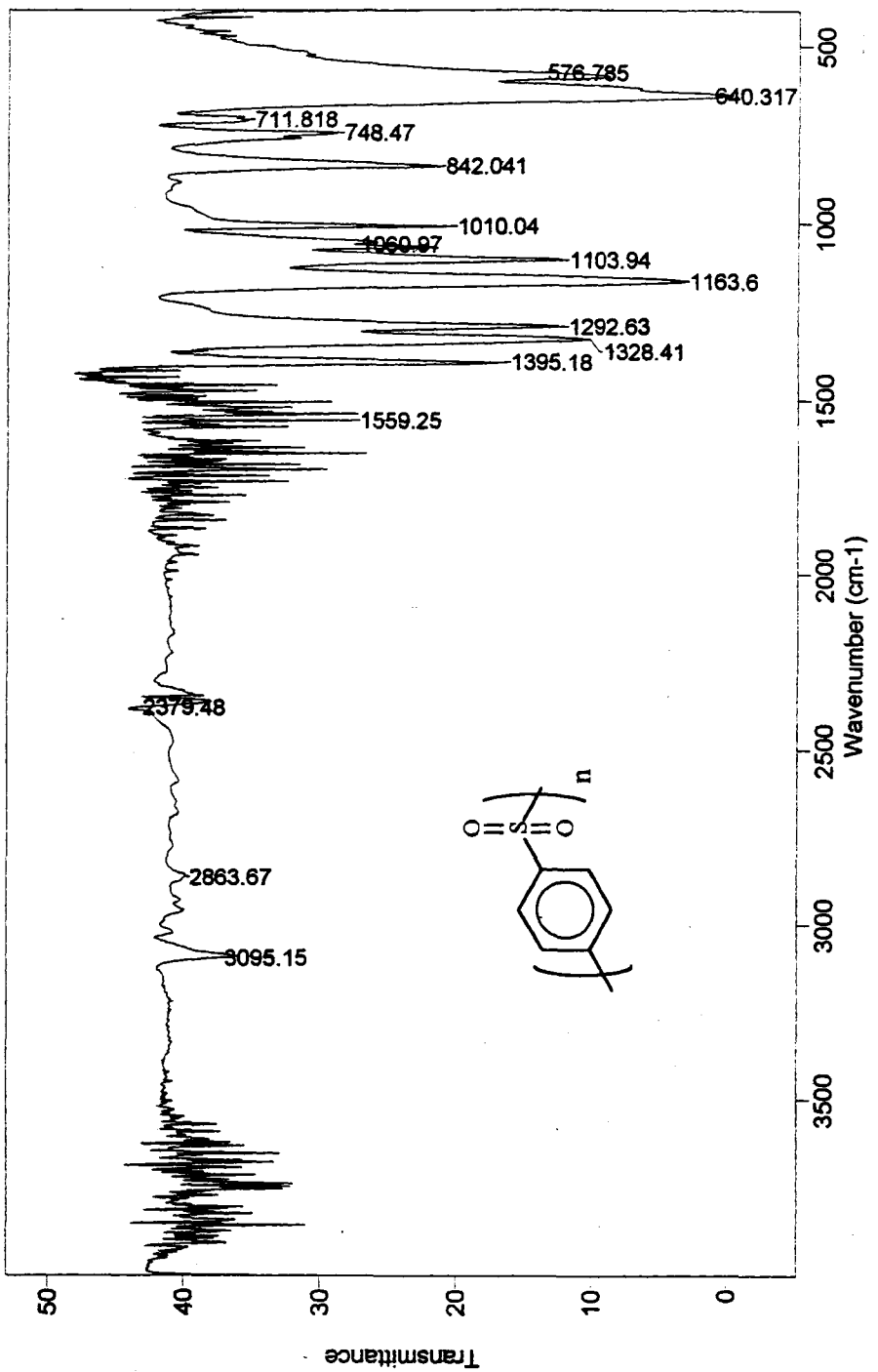

C-7 IR Spectrum of PPSO

Appendix D–Instrumentation, Software, and Hardware

New Compounds are marked by an asterisk * in their experimental section.

Nuclear Magnetic Resonance spectroscopy was conducted on three instruments:

Varian XL-300 NMR Spectrometer using a proprietary operating system and software, XL-200 NMR Operating System Rev G.1. The probes were a Nuclear Cryogenics Corp. D300-5 probe with proton channel, carbon channel, and deuterium lock channel and a Varian Instrument's 30-122 MHz channel (carbon) with a proton channel and deuterium lock channel, and a Varian Instruments 300 MHz 1H/19F 2 channel probe.

Varian Unity plus Spectrometer with an Oxford 400 magnet using Varian VNMR 5.1 software, copyright 1995. The probes were a 4-Nucleus AutoNMR probe with a 13C/31P channel, 1H/19F channel, and a deuterium lock channel, and a Nuclear Cryogenics Corp. H, F (BB) G400-5HT probe with 2 channels. All variably temperature experiments were performed on this instrument.

Varian VXR 500S Spectrometer using Varian VNMR 5.2 software, copyright 1996. The probe was a Nuclear Cryogenics Corp. ID-500-5 probe Varian Instrument's 3 Channel (H, C, D).

Infrared Spectroscopy was conducted on a BioRad FTS 135 FT-IR Spectrometer using Win-IR Foundation Ver 3.04 Level II, by Galactic Industries, Corp, copyright 1991-1994.

Ultraviolet-Visible Spectroscopy was conducted on a Hewlett-Packard HP8452A Diode Array Spectrometer using HP 89532 A UV-VIS Software Rev. A .00.00, Hewlett-Packard, copyright 1986-1991. A standard 10 x 10 x 45 mm quartz cuvette was used for analysis.

High Pressure Liquid Chromatography and Gel Permeation Chromatography were conducted using the same detector and pump system with varying columns. The pump was a Scientific Systems Inc. SSI 222C HPLC Pump with a Shodex RI-71 Refractive Index Detector. HPLC analysis was performed using a SpherisORB S5W bonded silica column with a solvent flow rate of 2-3mL/min. All solvents were filtered and degassed by passing through a Teflon membrane filter. GPC was performed using a Polymer Laboratories PL Gel (39-MIX 50-10E5A 5U) 7.5 x 300 mm column with PL pre-column with a solvent flow rate of 1.0 mL/min. Data was collected using Data Logger Ver. 4.5.9r software by Center for Science and Mathematics Teaching, copyright 1985-1995, through a Vernier Serial Box Interface on a Macintosh platform. GPC data was transferred for regression analysis using Corel Quattro Pro Ver. 8.0.0.470. Polystyrene standards of Mw = 670,000, 184,200, 32,600, 4,075 were run before and after each GPC run, and averaged for final analysis.

Mass Spectrometry was conducted using three instruments. GC-MS was performed on a Hewlett-Packard HP 5890 Series II GC with a HP 5971 Series Mass Selective Detector. The column was an HP-5MS Crosslinked 5 % PhMe Silicon 30 m x 0.25 mm x 0.25 μm. The software was Hewlett-Packard's HP Chem Station Ver.

B.02.02, copyright 1989-1992. MS-DIP was performed on a Hewlett-Packard HP 5985 GC-MS. MS-FAB was performed on a VG Analytical ZAB E/SE instrument.

Flame Atomic Absorption Spectroscopy was conducted on a Varian Spectr AA20 using Flame Program software by Varian Analytical Instrumentation, copyright 1986. All glassware was washed with nitric acid (1N). Data regression was conducted using Corel Quattro Pro Ver. 8.0.0.470. Oxygen and acetylene at 3.5 and 1.5 L/min, respectively, were used for all metals except lanthanum for which nitrous oxide and acetylene was used at 3.5 and 4.5 L/min. All absorbance readings were taken as the average of three, three second collections with intervening three second delays. Observation wavelengths for the metals and the slit width are given in nm (λ/slit): Cd 228.8/0.5, Cu 324.8/0.5, Fe 248.3/0.2, Zn 213.9/1.0, Hg 253.7/0.5, Ni 352.5/0.5, Cr 357.9/0.2, Pb 217.0/1.0, La 403.7/0.5.

Thermal analysis (TGA and DSC) was conducted on a Du Pont Instrument's Thermal Analyst 2000 System with a proprietary operating system and software, TA Operating System 2000 Version 8.1G, copyright 1987 by E.I. Du Pont de Nemours and Co., Inc. DSC was conducted on a 910 Differential Scanning Calorimetry module. The DSC module was standardized to temperature and heat flow using an indium sample. Thermogravimetric analysis was conducted on a 951 Thermogravimetric Analyzer module. Constant temperature thermolysis was conducted in a Blue M. Electric Co. Lab Heat Muffle Furnace. Kinetic analysis of the TGA data was conducted using Microsoft Excel 97-SR1 and Corel Quattro Pro Ver. 8.0.0.470. Pyrolysis-Gas Chromatography-Mass Spectroscopy was conducted

on a modified Hewlett-Packard HP5890 Series II GC with a HP 5988A Mass Selective Detector using Teknivent Vector/one system options Rev. 3.01, copyright 1988. The instrument is detailed in a dissertation from the University of Oklahoma [252]. Heats of combustion and formation for compound **19** (0.8267 g) were determined on a Parr Instrument Co. 1261 Calorimeter standardized with benzoic acid x4 using installed software Rev. 61.3.

Viscometry was conducted with a Cannon-Ubbelohde Dilution Viscometer in a Cannon Instrument Co., Model M-1 Constant Temperature Bath at 30 °C. At least three runs were performed at each concentration. The data was analyzed using Corel Quattro Pro Ver. 8.0.0.470.

Melting Point analysis was conducted on a Mel-Temp apparatus by Laboratory Devices.

Semi-Empirical calculations were performed using the PM3 Hamiltonian with Hyperchem by HyperCube. The PolakRibiere optimizer was used with a convergence limit of 0.001 for geometry optimization. RMS gradient criterion was 0.0005 kcal/(A mol) and UHF was used.

Appendix E–X-ray Data for N,N,N-trimethyl(3-bromo-2,4,6-trimethyl-5-nitrobenzyl)ammonium nitrate (26)

Experimental The data were collected at -110 °C on a Siemens P4 diffractometer using MOKα (λ = 0.71073 Å) radiation. The data were corrected for Lorentz and polarization effect; and an analytical absorption correction was applied. The structure was solved by direct method using SHELXTL (Siemens) system, and refined by full-matrix least-squares on F^2 using all reflections. Hydrogen atoms were included in the refinement with idealized parameters. Final R = 0.0595 is based on 1956 observed reflections [I > 26 (I)]. Details of the crystal data and refinement are given below. Figures are drawn with 50 % thermal ellipsoids.

Crystal data and structure refinement for 26

Identification code	dg819c	
Empirical formula	C13 H20 Br N3 O5	
Formula weight	378.23	
Temperature	293(2) K	
Wavelength	0.71073 A	
Crystal system	Monoclinic	
Space group	P2(1)/c	
Unit cell dimensions	a = 16.688(2) A	alpha = 90 deg.
	b = 5.6280(10) A	beta = 99.340(10) deg.
	c = 16.835(2) A	gamma = 90 deg.
Volume, Z	1560.2(4) A^3, 4	
Density (calculated)	1.610 Mg/m^3	
Absorption coefficient	2.662 mm^{-1}	
F(000)	776	
Crystal size	0.06 x 0.40 x 0.30 mm	
Theta range for data collection	2.45 to 25.00 deg.	
Limiting indices	-5<=h<=19, -6<=k<=6, -20<=l<=19	
Reflections collected	2790	
Independent reflections	2694 [R(int) = 0.0314]	
Absorption correction	Integration	
Max. and min. transmission	0.8540 and 0.4821	

Refinement method	Full-matrix least-squares on F^2
Data / restraints / parameters	2692 / 0 / 206
Goodness-of-fit on F^2	1.080
Final R indices [I>2sigma(I)]	R1 = 0.0595, wR2 = 0.1417
R indices (all data)	R1 = 0.0950, wR2 = 0.1739
Extinction coefficient	0.0000(7)
Largest diff. peak and hole	0.839 and -0.559 $e.A^{-3}$

Atomic coordinates (x 10^4) and equivalent isotropic displacement parameters (A^2 x 10^3). U(eq) is defined as one third of the trace of the orthogonalized Uij tensor.

	x	y	z	U(eq)
Br(1)	3876(1)	1815(2)	8201(1)	33(1)
O(1)	4570(4)	-2428(11)	5209(3)	42(2)
O(2)	3716(3)	223(11)	4750(3)	40(1)
O(3)	1144(4)	2327(10)	4624(3)	41(1)
O(4)	1306(4)	2434(10)	3377(3)	42(1)
O(5)	905(4)	-775(10)	3885(3)	46(2)
N(1)	1095(3)	-3809(9)	6432(3)	17(1)
N(2)	4013(4)	-1159(10)	5232(3)	22(1)
N(3)	1136(3)	1341(10)	3965(3)	22(1)
C(1)	3525(4)	-169(12)	7294(4)	19(1)
C(2)	2934(4)	-1890(12)	7351(3)	19(1)
C(3)	2648(4)	-3230(12)	6668(4)	20(1)
C(4)	3013(4)	-3044(13)	5972(3)	20(1)
C(5)	3618(4)	-1367(12)	5987(4)	21(1)
C(6)	3883(4)	174(12)	6610(4)	21(1)
C(7)	2663(4)	-2253(13)	8154(4)	27(2)
C(8)	1946(4)	-4933(11)	6668(4)	19(1)
C(9)	931(4)	-2034(12)	7035(4)	23(1)
C(10)	493(4)	-5806(13)	6413(4)	27(2)
C(11)	1005(4)	-2656(12)	5628(4)	24(2)
C(12)	2799(5)	-4577(15)	5230(4)	33(2)
C(13)	4543(4)	1979(14)	6567(4)	28(2)

Bond lengths [A] and angles [deg].

Br(1)-C(1)	1.905(6)	O(1)-N(2)	1.178(8)
O(2)-N(2)	1.174(7)	O(3)-N(3)	1.238(7)
O(4)-N(3)	1.238(8)	O(5)-N(3)	1.252(8)
N(1)-C(9)	1.481(8)	N(1)-C(11)	1.487(8)
N(1)-C(10)	1.504(8	N(1)-C(8)	1.547(8)
N(2)-C(5)	1.528(8)	C(1)-C(6)	1.395(9)
C(1)-C(2)	1.398(9)	C(2)-C(3)	1.394(9)
C(2)-C(7)	1.506(9)	C(3)-C(4)	1.409(8)

C(3)-C(8)	1.514(9)	C(4)-C(5)	1.380(9)
C(4)-C(12)	1.512(9)	C(5)-C(6)	1.378(9)
C(6)-C(13)	1.508(10)	C(9)-N(1)-C(11)	109.1(5)
C(9)-N(1)-C(10)	108.8(5)	C(11)-N(1)-C(10)	109.8(5)
C(9)-N(1)-C(8)	111.3(5)	C(11)-N(1)-C(8)	111.4(5)
C(10)-N(1)-C(8)	106.4(5)	O(2)-N(2)-O(1)	128.7(6)
O(2)-N(2)-C(5)	115.7(6)	O(1)-N(2)-C(5)	115.5(5)
O(3)-N(3)-O(4)	121.6(6)	O(3)-N(3)-O(5)	118.8(6)
O(4)-N(3)-O(5)	119.6(6)	C(6)-C(1)-C(2)	123.7(6)
C(6)-C(1)-Br(1)	117.7(5)	C(2)-C(1)-Br(1)	118.6(4)
C(3)-C(2)-C(1)	117.9(5)	C(3)-C(2)-C(7)	123.7(6)
C(1)-C(2)-C(7)	118.3(6)	C(2)-C(3)-C(4)	120.7(6)
C(2)-C(3)-C(8)	120.2(6)	C(4)-C(3)-C(8)	119.1(6)
C(5)-C(4)-C(3)	116.7(6)	C(5)-C(4)-C(12)	118.7(6)
C(3)-C(4)-C(12)	124.6(6)	C(6)-C(5)-C(4)	126.0(6)
C(6)-C(5)-N(2)	117.2(6)	C(4)-C(5)-N(2)	116.8(5)
C(5)-C(6)-C(1)	114.5(6)	C(5)-C(6)-C(13)	122.3(6)
C(1)-C(6)-C(13)	123.1(6)	C(3)-C(8)-N(1)	114.8(5)

Symmetry transformations used to generate equivalent atoms:

Hydrogen coordinates (x 10^4) and isotropic displacement parameters (A^2 x 10^3).

	x	y	z	U(eq)
H(7A)	2332(25)	-3654(51)	8133(10)	40
H(7B)	2355(25)	-901(41)	8276(14)	40
H(7C)	3131(5)	-2437(88)	8564(6)	40
H(8A)	1983(4)	-5619(11)	7201(4)	23
H(8B)	2001(4)	-6218(11)	6296(4)	23
H(9A)	404(12)	-1350(59)	6869(14)	34
H(9B)	1335(17)	-806(45)	7079(20)	34
H(9C)	949(28)	-2796(21)	7548(7)	34
H(10A)	-49(4)	-5180(17)	6296(28)	40
H(10B)	568(19)	-6584(54)	6927(10)	40
H(10C)	575(19)	-6927(45)	6004(20)	40
H(11A)	487(13)	-1878(71)	5515(13)	36
H(11B)	1041(28)	-3840(17)	5224(5)	36
H(11C)	1430(17)	-1507(60)	5625(9)	36
H(12A)	3271(9)	-4789(78)	4979(18)	49
H(12B)	2379(23)	-3818(47)	4859(14)	49
H(12C)	2610(31)	-6097(36)	5381(6)	49
H(13A)	4659(21)	2048(63)	6027(8)	42
H(13B)	5024(10)	1527(47)	6928(22)	42
H(13C)	4365(12)	3512(21)	6718(28)	42

Selected torsion angles [deg].

-4.41 (0.99) C6 - C1 - C2 - C3	176.20 (0.48) Br1 - C1 - C2 - C3
173.41 (0.61) C6 - C1 - C2 - C7	-5.98 (0.81) Br1 - C1 - C2 - C7
7.25 (0.96) C1 - C2 - C3 - C4	-170.43 (0.60) C7 - C2 - C3 - C4
-173.48 (0.57) C1 - C2 - C3 - C8	8.84 (0.98) C7 - C2 - C3 - C8
-4.42 (0.95) C2 - C3 - C4 - C5	176.30 (0.59) C8 - C3 - C4 - C5
174.18 (0.66) C2 - C3 - C4 - C12	-5.10 (0.99) C8 - C3 - C4 - C12
-1.69 (1.02) C3 - C4 - C5 - C6	179.62 (0.67) C12 - C4 - C5 - C6
-179.91 (0.56) C3 - C4 - C5 - N2	1.40 (0.92) C12 - C4 - C5 - N2
-87.02 (0.75) O2 - N2 - C5 - C6	93.75 (0.74) O1 - N2 - C5 - C6
91.36 (0.73) O2 - N2 - C5 - C4	-87.86 (0.75) O1 - N2 - C5 - C4
4.39 (1.00) C4 - C5 - C6 - C1	-177.39 (0.55) N2 - C5 - C6 - C1
-179.04 (0.65) C4 - C5 - C6 - C13	-0.83 (0.95) N2 - C5 - C6 - C13
-1.20 (0.96) C2 - C1 - C6 - C5	178.20 (0.48) Br1 - C1 - C6 - C5
-177.73 (0.64) C2 - C1 - C6 - C13	1.67 (0.88) Br1 - C1 - C6 - C13
86.75 (0.73) C2 - C3 - C8 - N1	-93.97 (0.70) C4 - C3 - C8 - N1
-65.47 (0.67) C9 - N1 - C8 - C3	56.59 (0.68) C11 - N1 - C8 - C3
176.20 (0.52) C10 - N1 - C8 - C3	

Appendix F– Chemical Abbreviations

AIBN	2,2'-azobisisobutyronitrile
ATAZ	4-amino-1,2,4-triazole
BPO	benzoyl peroxide
DMF	N,N-dimethylformamide
DMSO	dimethyl sulfoxide
HMX	cyclo-1,3,5,7-tetramethylene-2,4,6,8-tetranitramine
IER	ion-exchange resin
NBS	N-bromosuccinimide
NG	nitroglycerin
PCP	[2.2]paracyclophane
PEG	poly(ethylene glycol)
PETN	pentaerythritol tetranitrate
PPO	poly(*p*-phenylene sulfone)
PPPX	poly(phenyl-*p*-xylylene)
PPS	poly(*p*-phenylene sulfide)
PPSX	poly(*p*-phenylene sulfoxide)
PPX	poly(*p*-xylylene)
PS	poly(styrene) or polystyrene
pTFA	peroxytrifluoroacetic acid
PVN	poly(vinyl nitrate)
RDX	cyclo-1,3,5,7-trimethylene-2,4,6,8-trinitramine
SPB	sodium perborate
TATB	1,3,5-triamino-2,4,6-trinitrobenzene
TBDMS	*t*-butyldimethylsilyl
TBDMSN	*t*-butyldimethylsilyl nitrate
TCE	1,2-dichloro-ethane
TCNQ	7,7,8,8-tetracyano-*p*-quinodimethane
TFA	trifluoroacetic acid
THF	tetrahydrofuran
TMEDA	N,N,N',N'-tetramethylethylenediamine
TMHI	trimethylhydrazinium iodide
TMS	tetramethylsilane
TMSCl	trimethylsilyl chloride
TMSN	trimethylsilyl nitrate
TNT	2,4,6-trinitrotoluene